DURABILITY OF SHEET MOLDING COMPOUND/METAL ADHESIVE BONDS

by

Ionel M. Spinu

Dissertation submitted to the Faculty of the Virginia Polytechnic Institute and State University in partial fulfillment of the requirements for the degree of:

DOCTOR OF PHILOSOPHY

in

Materials Engineering Science

APPROVED:

J. G. Dillard, Chairman

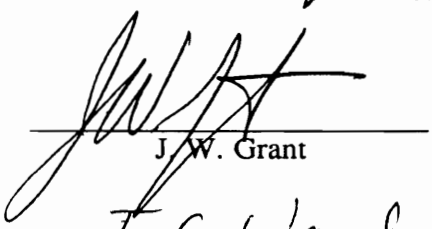

J. W. Grant

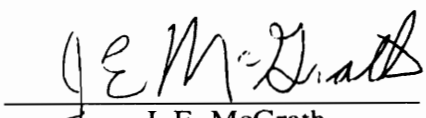

J. E. McGrath

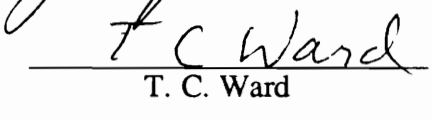

T. C. Ward

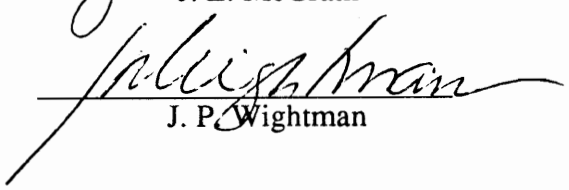

J. P. Wightman

September, 1991

Blacksburg, Virginia

Durability of Sheet Molding Compound/Metal Adhesive Bonds

by

Ionel M. Spinu

Committee Chairman: John G. Dillard

Materials Engineering Science

(Abstract)

Durability of a variety of sheet molding componds (SMC)/ adhesive /metal systems involving steel, aluminum, phase α-SMC, Budd SMC, and polyurea adherends and polyurethane and epoxy adhesives has been investigated. Three specimen geometries with different modes of stress were employed: lap shear, wedge, and butt torsion. Specimens were exposed to an environmental cycle or to fixed conditions of temperature and humidity with or without load.

For phase α-SMC/urethane/ELPO steel adhesive bonds, all visually determined adhesive failure occurs at the SMC/adhesive interface, and it is in reality a mixture of interfacial failure and near surface SMC debonding. The near surface SMC material and the thin layer of primer on the SMC surface are the weak links in the bond. An improvement in durability of phase α-SMC/urethane/ELPO steel adhesive bonds requires an increase in the strength of the outer layer of the SMC material.

The metal surface preatreatment proved to be very important for the durability of phase α-SMC /urethane/aluminum adhesive bonds. The adhesive bonds prepared with solvent cleaned aluminum primed with epoxy or phenolic primer displayed poor durability. This is attributed to the contaminants on the aluminum surface after solvent cleaning which hinder the interactions of aluminum surface species with primers. The use of alkaline cleaned aluminum primed with diisocyanate primer improved durability only in dry air conditions. This can be explained by the high susceptibility of the NCO functionality to

water, which can rapidly weaken the primer/aluminum bonds. Priming alkaline cleaned aluminum adherends with phenolic or epoxy primers improved dramatically the adhesive bond durability under all testing conditions. Enhanced durability is attributed to chemical and hydrogen bonds established between components of phenolic and epoxy primers and aluminum surface species. Reflection absorption FTIR studies of the interactions between identical or similar compounds that exist in the primers, e.g. diglycidyl ether of bisphenol A, phenol, and methylene diphenyl diisocyanate, and alkaline cleaned aluminum surface species indicated chemical processes.

Exposure of bonded samples at 60°C for up to seven days did not reduce the residual strength. Some loaded samples failed during durability tests, indicating that loading is a significant factor in durability. Butt torsion samples proved to be much more sensitive to stress and temperature than the lap shear and wedge samples, showing the important role of the mode of stress in durability. Humidity had a detrimental effect on durability for all systems investigated. For the system Budd SMC/adhesive/ELPO steel an epoxy adhesive exhibited better durability than a polyurethane adhesive. Enhanced durability is explained by higher cohesive strength, a lower moisture absorption rate and higher resistance to hydrolysis of the epoxy adhesive. An increase in bondline thickness proved to be beneficial for adhesive durability, a fact attributed to a more uniform stress distribution in thicker bonds.

To Oana

ACKNOWLEDGMENTS

This dissertation was completed with the help of many people and organizations. I wish to acknowledge these people and express my gratitude for their efforts.

I would first like to thank my advisor Dr. J. G. Dillard for his encouragement, scientific guidance, support and patience and for providing the opportunities to attend meetings and meet fellow scientists.

I would like to thank my committee members Dr. J. W. Grant, Dr. J. E. McGrath, Dr. T. C. Ward, and Dr. J. P. Wightman for serving on my committee and for helpful suggestions.

I would also like to thank Frank Cromer for teaching me how to operate the various surface analitycal instruments, and for his constant help and useful suggestions.

I would like to thank Larry Jackson in the Electronics Shop and Fred Blair, Melvin Shaver, and John Miller in the Physics Shop for their constant support of many projects involved in this research.

I also extend thanks to Francis Webster for his constant and patient help with FTIR experiments and for many useful discussions and suggestions.

I would also like to extend thanks to Daniel Reed for provision of testing fixtures, to Stephen Liptak for provision of the purified DGEBA, to Dr. Wae Waehamad for provision of the purified MDI, to Wanda Ritter, Virginia Keller, Katy Hatfield and Kim Linkous for help with my duties as a CASS fellow, to Paul Veil and Dr. Jean Gorce for teaching me how to operate various instruments in Dr. Ward's laboratories, and to my research group for many helpful discussions.

I would like to thank the Center for Adhesive and Sealant Science for providing graduate fellowships, funds for attending meetings, and for providing an an arena of interactions with scientists of other disciplines.

I would like to thank General Motors Co., Ashland Chemical Co., Alcoa, and NSF Science and Technology Center which also provided funding for my project and the Virginia Center for Inovative Technology for its funding of some of the instrumentation used in this research.

I would like to thank Jeff Saracsan and James Jen from Ashland Chemical Co. and Allen Madura from Lord Corporation for provision of various materials used in my research.

Finally I would like to thank my wife, Maria and my daughter, Oana for their support and understanding throughout graduate school.

TABLE OF CONTENTS

LIST OF FIGURES

LIST OF TABLES

1. INTRODUCTION

1.1. General comments

The use of composite materials is becoming increasingly important in the automotive industry. This is due to the advantages offered by composites over traditional materials (metals): reduced weight, cost, and the number of components needed. Composites are also corrosion resistant. A good example of the extensive use of composites in car manufacturing is General Motors' all purpose van, which has composite panels which are adhesively bonded to a steel subframe [1]. These metal-composite structures allow the optimum use of the properties of both materials. The steel is strong and tough and takes the stresses; the composite is compliant, corrosion- and dent-resistant, and can be molded into complex shapes. To reduce weight, other metals, including aluminum, are likely to be used as alternatives to steel for manufacturing of the subframe [1].

It is of special interest that adhesively bonded metal-composite structures maintain their performance during the service life of the automobile. Adhesively bonded structures may rapidly lose strength under normal operating conditions [2]. The durability problem in adhesively bonded polymeric composites is complicated by the viscoelastic behavior of composites due to the polymeric nature of the matrix. The adhesives, being polymeric materials, also have a viscoelastic behavior. So, there is a potential for viscoelastic failure for both the adhesive and the composite adherend; thus the bonded composite structure is a dual viscoelastic problem [3]. To determine durability, a number of test methods have been developed. Most attention has focused on the bonding of metals; fewer studies have been concerned with other structurally bonded systems [4].

1.2. Objectives of the present research

At the initiation of this research (1987), limited published data on durability of metal-composite bonded structures used in the automotive industry were available. To fully exploit the potential of these structures, a detailed investigation of their durability is necessary. The general objective of this study was to develop a fundamental understanding of durability in structures in which SMC (sheet molding compound) was adhesively bonded to metals. The following program objectives were identified:

- establish experimental conditions that will be valuable for accelerated durability evaluations of SMC/metal adhesive bonds, by exploring different limits of temperature, humidity, and stress level

- study three test specimen geometries (lap shear, wedge, and butt torsion) to assess the mechanical factors involved in bond failure

- use surface analysis techniques to better understand the failure mechanism

- investigate the effect of metal surface pretreatment on the durability of SMC / adhesive/metal adhesive bonds

- explore the metal/primer interfacial interactions and the role of the interfacial region or interphase in determining the durability performance

- investigate other factors which affect durability: adhesive type, bondline thickness, and adherend thickness

- recommend procedures and material selection (primers, adhesives) and modification of the adherend that will enhance durability of SMC/adhesive/metal structures.

The successful conclusion of such a research program will give the designers and manufacturers in the automotive industry: a better characterization of their products, and guidelines for selection of materials, modification of the existing materials, introduction of

new materials and design of bond configurations to obtain more durable adhesively bonded structures.

The approach used accelerated laboratory tests, and it was designed to include a combination of harsh environmental conditions (elevated temperatures, high relative humidity) and analysis of failed test specimens. To achieve a fundamental understanding of principal stresses that cause failure, three specimen geometries with different modes of stress were employed: lap shear which has a mixed mode of stress (shear and tensile), wedge which is loaded almost exclusively in tensile, and butt torsion which has almost a pure shear mode of stress.

The influence of various factors which affect the durability of the phase α-SMC/urethane/ELPO steel adhesive bonds was investigated first. Next, the influence of the adhesive type on the durability for the system Budd SMC/adhesive/ELPO steel was studied. Finally, the durability of the phase α-SMC/urethane/aluminum system in correlation with the type of aluminum surface pretreatment was investigated. The aluminum/primer interfacial interactions were studied, and their role in determining the durability performance of phase α-SMC/urethane/aluminum was addressed.

2. LITERATURE REVIEW

2.1. Sheet molding compound (SMC)

2.1.1. Formulation and chemistry

Sheet molding compounds are highly filled, glass fiber-reinforced thermosetting, unsaturated polyester resins. They are used to make automobile body panels [5]. The advantages of SMC for automotive applications are the flexibility in formulation and properties: excellent mechanical and electrical properties, good thermal resistance and stability, rapid cure times, low mold shrinkage and low cost [6]. A typical sheet molding compound formulation is given in Table 1 [7]. Unsaturated polyester resins result from the reaction of mixtures of saturated and unsaturated dicarboxylic acids (or their anhydrides) with glycols. Most of general purpose resins used for molding compositions are based on phthalic anhydride, maleic anhydride and propylene glycol. For improved and specialized properties, other raw materials may be used, allowing an enormous flexibility by variation in type and quality of the components. A schematic representation of the polyesterification reaction is given below.

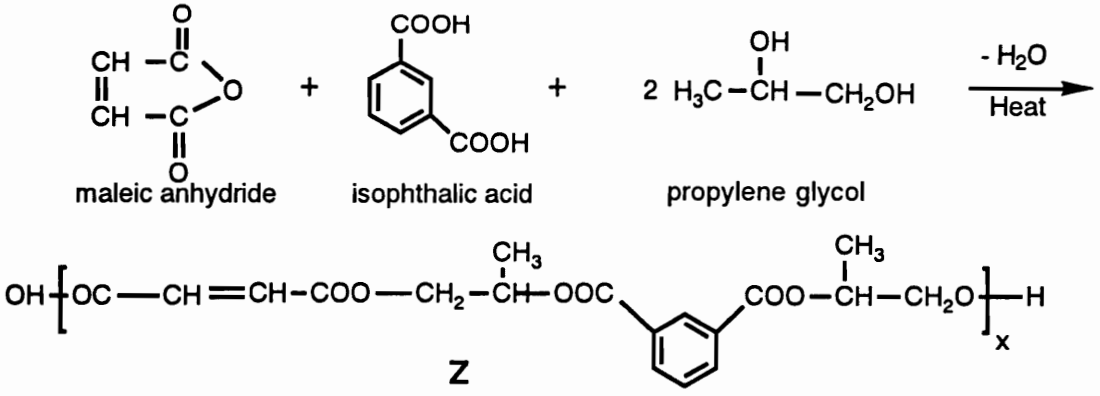

The unsaturated polyester resins formed in this way have low molecular weights, the number-average molecular weight ranging between 1800 and 2500 [8]. They are dissolved

Table 1.
Typical Sheet Molding Compound Formulation [7]

Component	% (by weight)
unsaturated polyester resin	10.50
low shrink additive	3.45
styrene monomer	13.40
initiator	0.25
calcium carbonate	40.70
lubricant (zinc stearate)	1.00
thickener (MgO)	0.70
glass fibers	30.00
	100.00

in unsaturated monomers, usually styrene. During the molding process, the unsaturated polyester is crosslinked by reaction with styrene via peroxide initiation, forming a three-dimensional network which constitutes the matrix of SMC. The crosslinking reaction is represented below:

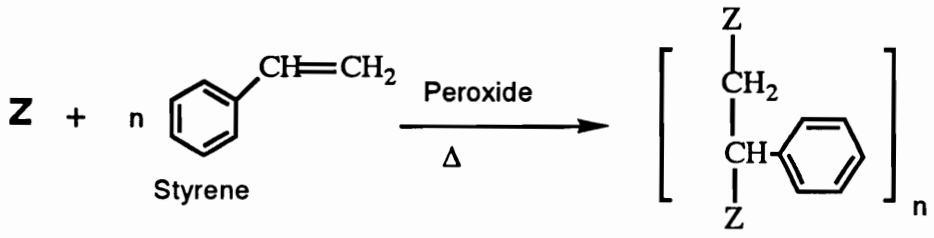

Unmodified, cured, unsaturated polyester resins have poor mechanical properties [8]. For SMC manufacturing, glass fibers are used as reinforcement because of their unique strength to weight characteristics and their high moduli. The glass fibers can be chopped rovings or chopped strand mat. Particulate minerals are used as fillers in SMC formulations, especially for modification of viscosity and rheology and lowering of the cost. The role of the thickening agent, such as magnesium oxide, is to increase the viscosity of sheet molding compounds after preparation to a dry putty consistency suitable for compression molding. Thermoplastic polymers are introduced in the SMC formulation to reduce the shrinkage and improve the surface appearance. Some of these materials eg. polyvinyl acetate, polystyrene, and polymethyl methacrylate are considered true low-profile additives because of the zero shrinkage and good surface appearance [9]. Initiators are introduced in the SMC formulations to decompose and produce free radicals upon heating, thus initiating a controlled crosslinking reaction during the molding operation. To overcome severe mold sticking during the molding process, internal mold release agents such as zinc stearate are introduced in the formulations.

2.1.2. Fabrication and properties

The fabrication of SMC involves five stages:

a) slurry preparation

b) glass fiber presentation

c) slurry application

d) consolidation

e) maturation

The slurry is prepared in a batch operation for low throughput operations and continuously in large plants. The glass fibers are chopped rovings or chopped strand mat. The slurry is applied to polyethylene sheets, which then sandwich the chopped fiberglass or mat. The SMC is usually compression molded. Parts with complex shapes can be obtained by molding of SMC, and this is an important advantage of SMC use in the automotive industry. Molded SMC articles exhibit good structural properties and are capable of bearing load and carrying long-term stresses [10]

SMC has a complicated phase structure [11], and the near surface composition and morphology are unlike that for the bulk [11-13]. The near surface has a much higher low-profile additive and resin contents than the bulk as shown in Figure 1 [14]. A cross-sectional model of SMC is shown in Figure 2 [12]. The surface layer is porous, contains fine calcium carbonate particles and is about 25 μm thick. Under this is a sublayer about 100 μm thick, consisting of calcium carbonate and glass fibers. The bulk of the composite is composed of 100 μm thick strata of alternating glass bundles and aggregate resin-calcium carbonate particles [12]. The SMC surface composition and morphology play an important role both in adhesive bonding and in painting of SMC.

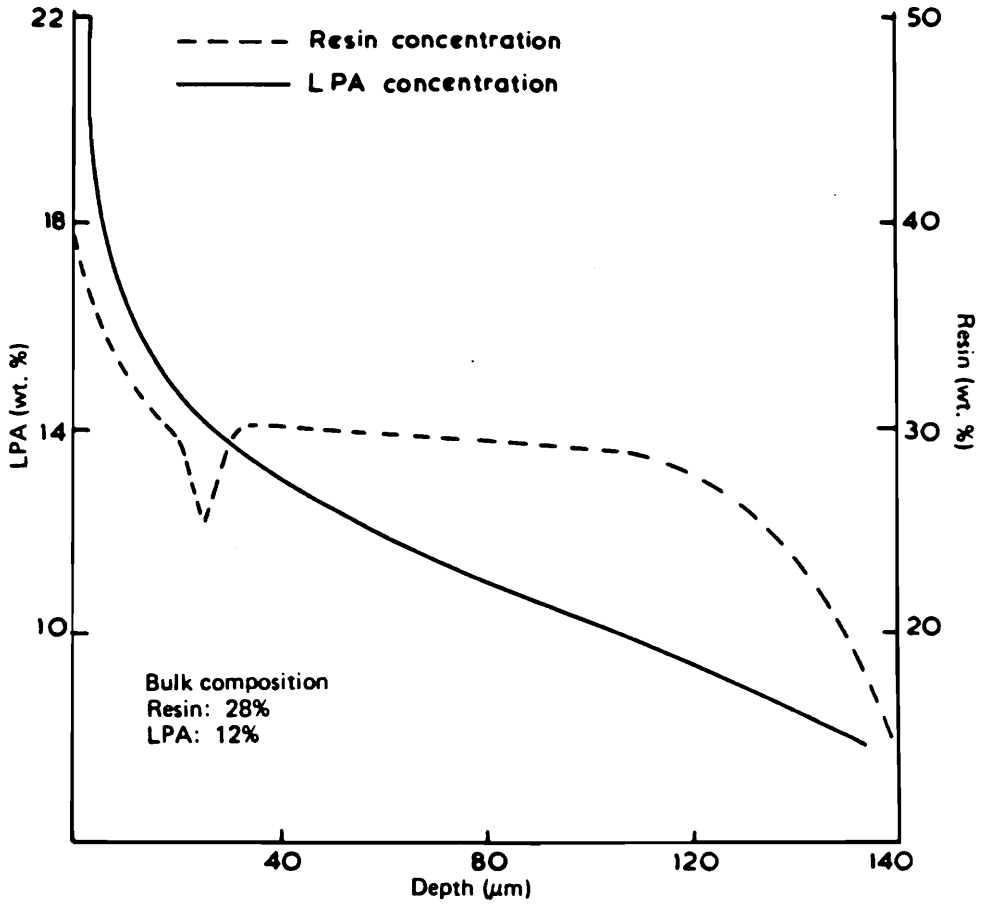

Figure 1. Concentration gradient of resin and low-profile additive from surface to interior of the composite [14].

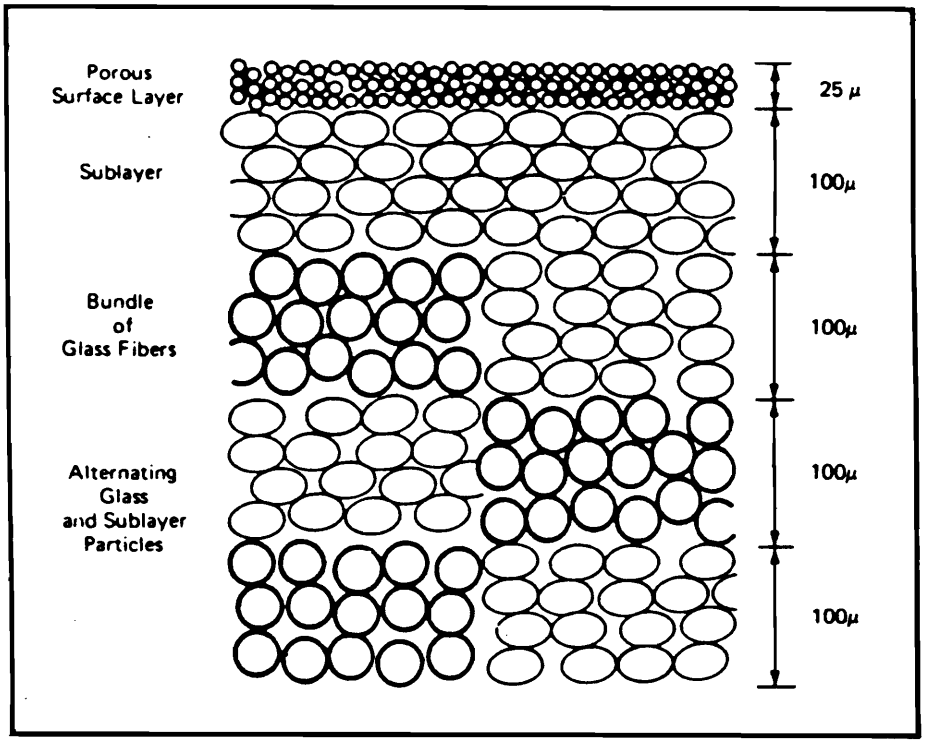

Figure 2. Cross-sectional model of SMC [12].

2.2. Adhesive bonding

2.2.1. General discussion

Composite materials can be joined by adhesive bonding or mechanical fasteners (bolting and riveting). Adhesive bonding is the preferred technique to join composite materials; the advantages it offers over mechanical fastening include [15]:

a) improved stress distribution in the bonded structure which gives a good dynamic-fatigue resistance to the bonded component

b) small weight penalty

c) more convenient and cost-effective, being readily adapted to robotic assembly techniques

There are also some disadvantages associated with adhesive bonding [15]:

a) the bonded structures cannot be disassembled without component damage

b) hostile environments may severely reduce the strength and integrity of adhesively bonded structures.

c) bonding often requires the use of surface pretreatments

d) it is difficult to determine integrity by inspection, the non-destructive test methods for adhesive joints being limited.

The adhesive/adherend interface plays a crucial role in adhesive bond durability which is the concern of this research. The establishment of interfacial molecular contact between the adhesive and adherend by wetting is the first step in the formation of an adhesive bond [16]. The adhesive must be able to be spread over the adherend surface and displace the contaminants on the surface [2].

The attainment of intimate molecular contact at the adhesive/adherend interface is necessary but not a sufficient condition for the formation of strong and stable adhesive bonds. It is also necessary to generate intrinsic adhesive forces between adhesive and

adherend which will prevent their separation under applied load. Four theories have been offered to explain the nature of the intrinsic adhesive forces acting at the adhesive/adherend interface.

2.2.2. Adhesion theories

2.2.2.1. Mechanical interlocking theory

This theory considers that the major source of intrinsic adhesion is due to mechanical keying, or interlocking of the adhesives with irregularities, pores and roughness of the adherend surface. This interlocking prevents direct "pull off" of the adhesive from the adherend surface. For example, mechanical interlocking plays the dominant role in the use of mercury amalgam for filling tooth cavities. Mechanical anchoring is used in metal plating of plastics, in adhesion to surface-treated metals, and in adhesion to porous substrates (paper, leather, and fabric) [17]. For aluminum and titanium, certain etching or anodization pretreatment processes produce porous oxide films on the metal surfaces. The adhesive penetrates into the pores of the oxide layer, mechanically interlocking with the oxide and forming much stronger bonds than if the surface were smooth [18].

However, good bond strengths obtained using smooth surfaces demonstrate that the mechanical interlocking theory is not of wide applicability, and cannot suffice as the sole explanation for the phenomenon of adhesion. It should be mentioned that in specific cases mechanical interlocking has a large contribution to the adhesive bond strength [17].

2.2.2.2. Diffusion theory

The diffusion theory of adhesion suggests that in the case of polymer/polymer bonding, the diffusion of long-chain polymer molecules or segments of these polymers across the interface explains the adhesion. It is necessary that the polymers are compatible,

and that their molecules or chain segments are sufficiently mobile. Voyutskii and coworkers explainied many cases of adhesion by the diffusion theory [19, 20]. It was shown that the bond strengths of pairs of polymers increase significantly with increasing contact time after the interfacial contact was completed. This was attributed to segmental interdiffusion between the two polymers [20]. The bond strengths of polymer pairs increase with increasing bonding temperature [19, 21]. This was associated with the formation of a diffuse interface. The increase in bond strength is accompanied by a change in the mode of failure from interfacial to cohesive.

There is experimental evidence for interdiffusion. Now it is accepted that interdiffusion contributes significantly to the intrinsic adhesion in autohesion (adhesion of a material with itself) of elastomers and in solvent welding of compatible, amorphous plastics [2, 22, 23]. Some critics believe that even when interdiffusion takes place, its contribution to intrinsic adhesion is minimal compared to that from the formation of interfacial secondary bonds. However, when the polymers to be bonded are incompatible or one polymer is crosslinked, crystalline, or below its glass transition, then interdiffusion is not a possible mechanism of adhesion [24].

2.2.2.3. Electronic theory

The principal proponent of this theory is Deryagin [25, 26]. This theory treats the bond as a capacitor which is charged due to the contact of the two different materials (the adhesive and the adherend). The adhesive acts as one plate and the adherend as the other. The separation of these plates requires work done against any electric charge separation. This theory ignores any other contribution to adhesion, and the work of adhesion is considered equal to the energy of the capacitor. It was demonstrated that electrostatic forces are important in adhesion of particles to plane surfaces [27, 28]. In the case of a

typical adhesive/substrate interface, the electronic mechanism of adhesion does not contribute significantly to intrinsic adhesion, and the electrical phenomena observed at joint separation arise from, rather than cause, high joint strength [29, 30]. For example, Roberts [31] concluded that electrostatic forces contribute less than ten percent to the adhesion of a smooth rubber surface to a variety of substrates.

2.2.2.4. Adsorption theory

The adsorption theory is the most widely accepted theory [32] and states that adhesion is due to surface forces acting between atoms and molecules in the surfaces of the adhesive and adherend when there is molecular contact at the interface. These surface forces are varied in nature and can be classified in three groups: van der Waals interactions, acid-base interactions, and primary force interactions. The most common group of forces, van der Waals forces, includes London dispersion forces, dipole-induced dipole interactions, and permanent dipole-dipole interactions. Van der Waals bond strengths are of the order of 0.08 to 20 kJ/mole. The particular chemistry of the system determines the forces which are important. London dispersion forces are universally present and theoretically, high bond strength may result from intrinsic adhesion due only to dispersion forces acting between the adhesive and adherend surfaces. The second group of forces of attraction are donor-acceptor bonds including acid-base interactions and hydrogen bonds. The donor-acceptor interfacial interactions involve redistribution of electrons.

Fowkes and coworkers [33-35] are the chief proponents of the idea that interfacial acid-base bonds between the adhesive and the substrate may play a major role in adhesion. They considered the hydrogen bond a typical acid-base bond. In their opinion, the physical interactions of polymers with neighboring molecules are determined by only two types of interactions: London dispersion forces and acid-base interactions. The interfacial

performance of an adhesive bond is dominated by the dispersion forces and the acid-base interaction and the work of adhesion can be expressed as:

$$W_A = W_A^D + W_A^{A/B}$$

where W_A^D is the dispersion force contribution and $W_A^{A/B}$ is the acid/base contribution.

Sometimes chemical interactions can occur between adhesive and adherend. Primary bonding includes covalent, and ionic bonds at the adhesive/adherend interface. Because of the thinness of the interface, chemical bonding is difficult to detect and studies which directly confirm primary bonding are scarce. However, in some cases, it was shown that primary interfacial bonding occurred and made a significant contribution to adhesive strength [36-38]. Direct evidence for improved adhesion due to interfacial chemical bonding has come from the cases where the introduction of small amounts (0.001-0.1 mole fraction) of reactive functional groups into the adhesive dramatically increased the adhesive strength [36]. Also direct evidence for interfacial chemical bonding was produced using surface analytical techniques [37, 38]. It is believed that the presence of primary bonding not only may increase the bond strength, but may also increase the environmental resistance of bonds [2].

2.2.3. Surface pretreatments

Surface preparation of adherends plays a key role in the performance and reliability of adhesively bonded structures. Although in many cases no adherend surface pretreatment is used before bonding [39], the attainment of maximum performance requires almost always some form of surface preparation for the adherends [39]. Surface pretreatments are used to modify the adherend surface in order to optimize adherend/adhesive interfacial interactions and to produce adhesive joints with higher strength, better reproducibility and improved

durability. The types of pretreatment that are employed both for non-metals (polymeric composites) and metals (steel and aluminum) will be reviewed.

2.2.3.1. Composite adherends

Some polymeric surfaces have poor adhesive properties because of low surface energy incompatibility, chemical inertness, or the presence of contaminants. To promote adhesion, some surface pretreatments are used to modify polymer surfaces, including solvent cleaning, abrading, grit blasting, chemical treatments, electrochemical treatments, photochemical treatments, flame treatments, corona discharge, plasma treatments, and surface grafting [40, 41]. Generally the effects of these treatments are limited to a thin surface layer (100 Å to 100 μm thick), and the bulk properties are not affected.

Many polymeric composites are based on epoxy or polyester resins and their surfaces are more polar than other polymeric resins (i.e., polyolefins) and are more compatible with polar adhesives. Because of this, the surface treatment involves only the removal of contaminants (oils, mold release agents). This is achieved mainly by the peel ply method or abrasion and solvent cleaning [42]. When there is no problem of surface contamination, most new composites can be bonded without surface preparation, especially by toughened acrylic adhesives [43]. For example, Hoa and Feldman [44] found that the pretreatment of SMC (sheet molding compound) by degreasing and abrading did not improve bond strength when an epoxy adhesive was used. In other cases, certain pretreatments applied to SMC increased the adhesive properties. It was shown that plasma treatment of SMC surfaces promoted adhesive bonding when a urethane adhesive was used [45]. It was suggested that the enhanced adhesion was due mainly to the polar group incorporated onto the SMC surface during the plasma treatment. Minford [46] found that abrading SMC produced a higher joint durability than simple alcohol wiping, but the improvement was

modest. The bonds prepared with untreated SMC gave poor durability results. Minford used a variety of room temperature-curing epoxy and reactive acrylic adhesives. Flame treatment of SMC increased the adhesive/adherend interactions when a urethane adhesive was used, but at the same time, produced a structurally weak layer below the oxidized SMC surface which resulted in failure in this region [47]. Infrared laser surface treatments were investigated to promote adhesion for SMC adherends [48, 49]. Laser radiation ablates the surface of SMC, providing a uniform bonding surface which promotes adhesion compared to solvent cleaning followed by abrasion [48]. Although many surface pretreatments were considered for SMC, only solvent-cleaning followed by abrading and priming, usually with isocyanate-based primers, are widely used [48, 50].

Bonazza [51] investigated various treatments for bonding laminates based on polyphenylene sulfide using FM300K adhesive film. For composite surfaces which do not contain residual Teflon® release agent, high strength bonds were produced by wiping the composite surface. However, abrasive surface treatments were necessary to produce high strength bonds on Teflon® contaminated surfaces. Subsequently, flame treatment improved the bond strengths obtained with all surface treatments.

Moyer [52] studied the effect of surface pretreatment on the adhesion properties of carbon fiber-polyimide composites primed with LaRC-TPI (Langley Research Center-Thermoplastic Imide) primer and bonded with LaRC-TPI adhesive tape. Of eight pretreatments used; methanol wash, grit blast, sulfuric acid soak, ammonia plasma, argon plasma, argon plasma followed by ammonia plasma, nitrogen plasma, and oxygen plasma, the oxygen plasma proved to be the best. This was attributed to a decrease in fluorocarbon contamination to trace amounts, and an increase in oxygen surface functionality which causes better wetting of the composite surface and may lead to chemical interaction at the composite/primer interface.

2.2.3.2. Steel adherends

Truly clean metals and metal oxide surfaces generally have high surface free energies and will be readily wetted by organic adhesives giving strong adhesive/metal interfacial secondary force interactions [53]. But there are other factors which complicate the adhesive bonding. In practice, the surfaces of many metal substrates are covered by protective oils, greases or weak corrosion products, and these may act as weak boundary layers in the joint, if not removed before bonding. Truly clean high-energy surfaces will readily absorb atmospheric contamination which may act as a weak boundary layer, if not displaced by the adhesive [54].

The surface pretreatments for metals include: solvent cleaning, mechanical abrasion, chemical treatments and priming. The attainment of good initial strengths requires simple degreasing and possibly mechanical abrasion. Generally, more complex pretreatments are necessary to obtain longer service life in hostile environments [54]. Many times no or a minimum pretreatment is used in bonding steel adherends. Good initial joint strengths are obtained using a combination of degreasing and mechanical abrasion pretreatments. Brockmann [55] investigated the influence of adherend pretreatment on properties of mild steel adherends bonded with epoxy and phenolic adhesives. It was found that treatment of the adherend surfaces by mechanical roughening (grinding, brushing or sandblasting) produced stronger bonds than degreasing or phosphate coating treatments. Also mechanical roughening of surfaces produced bonds with reasonable service life while bonds prepared with degreased steel showed very poor durability. For better durability, chemical pretreatments, or priming may be necessary [56]. For bonding to galvanized steel [57, 58], low strength and poor bond durability were observed for hot dip substrates due to minimum surface roughness and maximum chemical heterogeneity of the surfaces. Higher

strength and better durability were found for electroplated substrates which have rougher and more chemically homogeneous surfaces.

The "clean" metal/adhesive bond has an inherent weakness due to the interface, where a low surface energy organic material (adhesive) is in contact with a high energy metallic oxide. In the presence of moisture, since both metal oxide and water are relatively polar, water will be preferentially absorbed on the oxide surface and may displace the adhesive on the adherend surface [2]. This inherent thermodynamic instability of the metal oxide/adhesive interface in the presence of moisture produces the loss of bond strength during the service life. Because of this problem, as an alternative to bonding directly to cleaned or oiled steel surfaces, the use of ELPO primed steel surfaces has gained wide acceptance in the automotive industry [59].

The ELPO priming process involves first, the deposition of a thin (0.6 μm) layer of zinc phosphate crystals on the ferric oxide surface (Figure 3 [60, 61]) . Then a layer of organic primer is electro-deposited on zinc phosphate. The thickness of the ELPO layer is 10-40 μm. The primer surface prepared in this way is called ELPO primed. ELPO refers to the electrodeposition of the organic primer. Increased strength and durability were observed for bonded ELPO primed steel adherends when compared with clean (degreased) steel [60, 61]. Increase in durability was attributed to more favorable energetics for the adhesive/primer and primer/conversion coating interfaces than for the adhesive/steel interface. The increase in strength was attributed to a different stress distribution in ELPO steel/adhesive joints compared to clean steel/adhesive joints. The presence of ELPO primer reduced stress concentrations and produced a more uniform stress distribution in the joint.

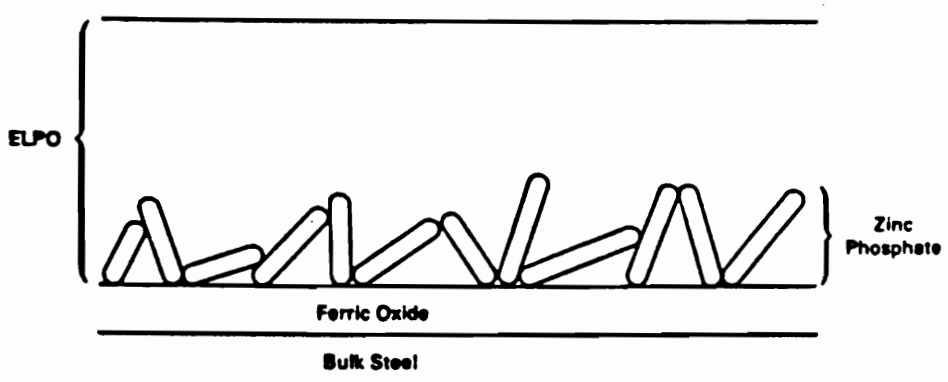

Figure 3. Schematic of ELPO/zinc phosphate/steel interphase bond [60].

2.2.3.3. Aluminum adherends

Many pretreatments are available for aluminum. The most common are degreasing, mechanical abrasion, FPL pretreatment, and acid anodizing. In less demanding applications, no pretreatment or just degreasing or mechanical abrasion is used. However, to obtain joints with high initial strength and good durability, chemical pretreatments must be employed. It was shown that degreasing or grit-blasting pretreatments gave adhesive bonds with markedly inferior initial strength [62, 63] and much less environmental resistance [63, 64] when compared with chemical pretreatments. For mechanical abrasion, the poor adhesive properties are due to surface convulsions and loosely bound detritus which lead to low levels of intimate contact, weak interfacial layers, and stress-cracking of the adherend [63].

Complex chemical pretreatments are in common use in aerospace industries where the attainment of the highest strength and environmental resistance for the adhesive joints is the top priority. The Forest Products Laboratory (FPL) process consists of a number of cleaning, etching, and rinsing steps. The substrate is etched in an aqueous solution of H_2SO_4 and $Na_2Cr_2O_7$. The etch removes the original oxide and a new thin layer of oxide is formed, which thickens during rinsing [65]. The oxide has a cell structure and a high concentration of whiskers that protrude from the surface [66]. The rough morphology of the FPL oxide gives high initial strength of the joint, but the bond durability is determined by the oxide stability. Because the oxide layer formed by etching is thin, it confers low resistance to hydrolytic degradation. To obtain good durability, an anodizing process must be used to increase the thickness of the oxide layer and to give more resistance to hydrolytic degradation [67]. The chromic acid anodizing (CAA) process involves etching in chromic acid and anodizing in a chromic acid solution. This process produces a thick, dense oxide consisting of solid columns which are expected to give good environmental resistance [18].

The oxide produced by the CAA process is more dense and considerably thicker than that produced by FPL or by the PAA (phosphoric acid anodizing) pretreatment, and its surface is less rough than for the other two morphologies [18, 68]. Phosphoric acid anodizing (PAA) consists of chromic acid etching and then anodizing in a solution of orthophosphoric acid in distilled water. This phosphoric acid anodizing produces a thick porous oxide with a columnar-like topography and open pores. The whisker-like protrusions are considerably longer than on the FPL-treated surface [68, 69].

The anodizing processes do not seal the pores of the oxide, so the adhesive or the primer can penetrate the pores and produce a mechanical interlocking between oxide film and the primer or adhesive. Extensive penetration of polymer in the oxide pores will slow the diffusion of moisture to the polymer/oxide interface and will improve environmental resistance to degradation [69].

It is considered that phosphoric acid anodizing produces the most durable bonds [67, 69-71]. The pretreatments discussed previously provide good durability, but there is a need for methods which offer environmental resistance but at the same time are simpler and suitable for other applications involving mass production. One possibility is the use of primers. This was the approach followed in this research for bonding of aluminum to SMC. The treatment applied to aluminum before bonding is minimal: solvent or alkaline cleaning and priming. During the alkaline cleaning, the following processes take place [72]:

a) dissolution of aluminum oxide existing on the surface

$$Al_2O_3 + 2OH^- + 3H_2O \longrightarrow 2\ Al(OH)_4^-$$

b) formation of a new oxide layer

$$2Al + 3\ H_2O \longrightarrow Al_2O_3 + 3H_2 \uparrow$$

2.2.3.4. Metal/polymer interfacial interactions

The importance of adhesive/adherend interfacial interactions in adhesion was shown in 2.2.2.4. Understanding the adherend/adhesive or adherend/primer interactions will aid significantly in explaining existing data and in developing stronger and more reliable bonded systems. The critical importance of the interfacial region or interphase in the performance of adhesives and composites has been widely accepted [73, 74]. A representation of the interphase region in an adhesive bond is shown in Figure 4 [74]. The interphase region comprises the zone where the transition of the local properties from the bulk adherend to the bulk adhesive takes place, while going through the interface.

Metals and alloys of commercial importance (iron, aluminum, copper, zinc, magnesium) are oxidized after exposure to oxygen. In normal conditions, the upper surface oxygens hydrate to form hydroxyl groups. These hydroxyl groups absorb water. A usual metal surface is depicted in Figure 5 [75]. The configuration of the hydroxyls will determine their acidity and reactivity toward the primer or adhesive.

According to Peri's model [76, 77], there are five hydroxyl configurations of an α alumina surface as represented in Figure 6 [77]. The most basic hydroxyls are shown in the top row. They carry a charge of -0.5 and are coordinated to one Al^{IV} or Al^{VI} ion, respectively. The bottom configuration has the most acidic OH group which is linked to three octahedrally coordinated aluminum ions. According to Bolger [75], there are two types of interactions between hydroxyls and organic polar groups:

a) surface interaction with an organic acid

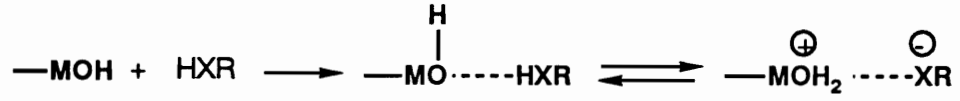

(1)

b) surface interaction with an organic base

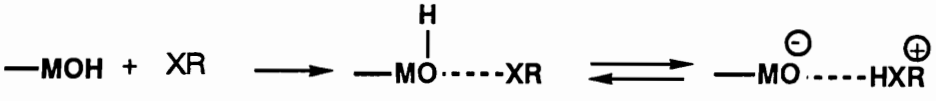

(2)

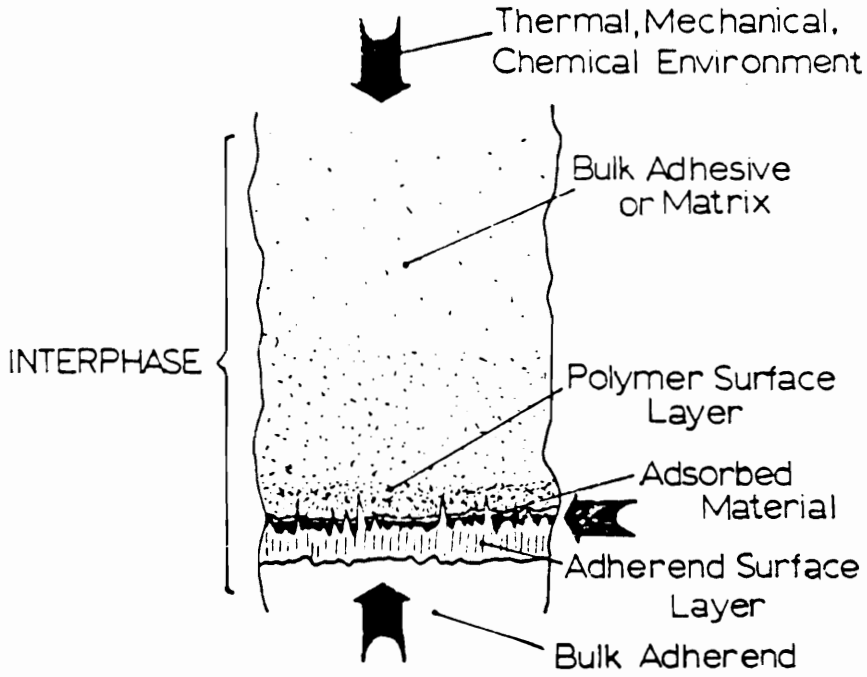

Figure 4. Schematic representation of the adhesive-adherend interphase [74].

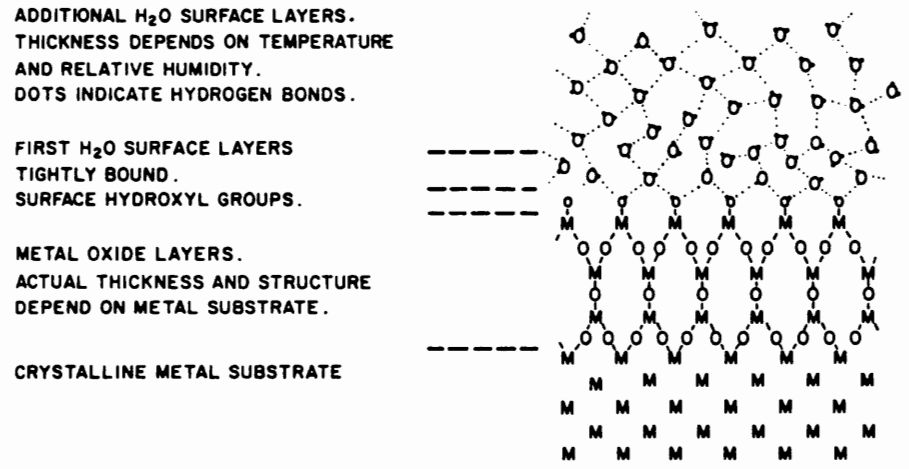

Figure 5. Schematic representation of water and oxide layers on metal surfaces [75].

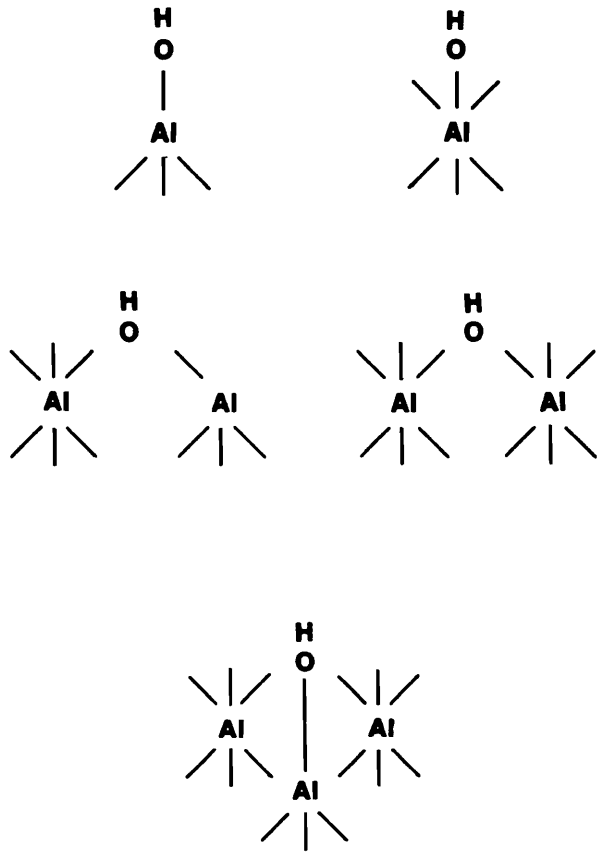

Figure 6. Five coordinations of hydroxyl groups on an aluminum surface [77].

where X in eq. 1 is O, S, or N, and in eq. 2, a halogen. In environmental studies the problem of displacement or interrupting of polymer (HXR or XR)/oxide bonds arises after water permeates through the polymer and reaches the polymer/oxide interface. This can be represented by the following reactions:

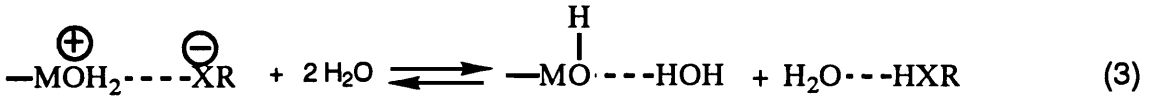

$$-\overset{\oplus}{M}OH_2\cdots\overset{\ominus}{X}R + 2H_2O \rightleftharpoons -M\overset{H}{O}\cdots HOH + H_2O\cdots HXR \quad (3)$$

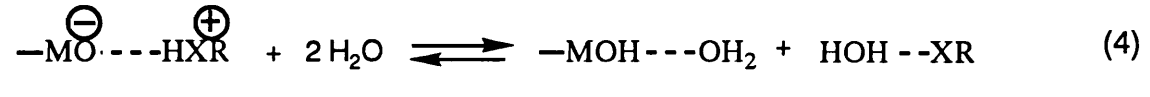

$$-\overset{\ominus}{M}O\cdots H\overset{\oplus}{X}R + 2H_2O \rightleftharpoons -MOH\cdots OH_2 + HOH\cdots XR \quad (4)$$

Only a few polar groups, usually hydroxyl and carboxylic acidic groups actually contribute to bond durability because of the competition with water molecules. Bolger [75] suggested that for the best water resistance there is an optimum concentration of polar groups in the polymer. Too high a polar group concentration increases water permeability and is detrimental for bond durability. It should be mentioned that Bolger's approach was limited to Brönsted acid-base interactions.

Interaction of epoxy resins with metallic substrates is important in adhesive technology considering the wide use of epoxy compounds in bonding and coating of metals. It is known that epoxy groups are reactive with many compounds including hydroxyl groups existing on the metal adherend surfaces [73]. Kollek [78] studied the adsorption of epoxy resin on anodized aluminum surfaces. In his opinion, it seems that the epoxy resin polymerizes on the metal surface after heating and that chemisorption occurs by the epoxy ring opening. Brown et al. [79, 80] investigated the adsorption of a simulated epoxy resin on aluminum oxide surfaces using inelastic electron tunneling spectroscopy (IETS). The model compounds used are shown:

A $H_3C\,CH_2CH_2NHCH_2CH\,(OH)\cdot CH_2CH_3$

B 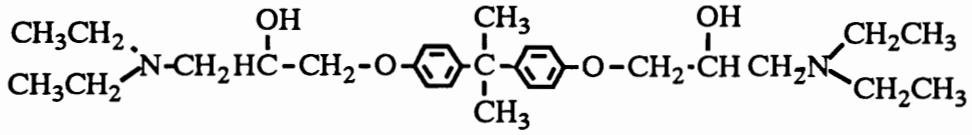

It was observed that compound A reacted strongly with the oxide aluminum surface. The aluminum hydroxyl was almost completely eliminated by the reaction to form alkoxide. There was evidence also that the nitrogen abstracts a proton from the surface. The results are consistent with the adsorbed species being bound to the surface in a chelate-type structure. For compound B, the adsorption was more limited, probably because of the size of compound.

J. Comyn et al. [81] found that curing does not take place for a mixture of epoxy resin and aliphatic amines on aluminum oxide in an IETS junction. It was suggested that the epoxy and/or amine groups are adsorbed on the aluminum oxide surface so that they are prevented from reacting with each other.

FTIR studies of the interaction of epoxy resin with steel [73, 82] showed that upon heating, the epoxy resin interacts chemically with steel surface species causing homopolymerization at the metal surface. It seems that the chemically active species existing on the steel surface are very effective catalysts that produce fast curing even at room temperature. It was observed that epoxy resin without any added catalyst polymerized above 150 °C on copper surfaces [83]. The presence of a very thin layer of polymerized epoxy resin coating on a metal surface may influence the adhesion and mechanical properties of the coating [83].

Phenolic resin/metal interactions play an important role in the use of phenolic primers. Many studies have used model compounds to investigate the interaction of phenol and its

derivates with aluminum oxide surfaces [84-88]. Usually the authors used infrared spectroscopy or inelastic electron spectroscopy techniques to study thin layers of materials deposited on an aluminum oxide surface. Infrared spectroscopic studies [84, 85] showed that phenols are strongly chemisorbed on γ alumina in the form of phenolate structures. The infrared spectrum of chemisorbed phenol differs markedly from that of liquid or physisorbed phenol and is similar to that of aluminum phenolate (KBr disc) [84]. The phenol OH stretching and in-plane vibrations (3350 and 1360 cm^{-1}, respectively) and the phenyl ring vibration (1474 cm^{-1}) which is coupled with the 1360 cm^{-1} OH in-plane vibration disappear upon chemisorption. The C-O stretching mode is shifted from 1259 to 1286 cm^{-1}, indicating some strengthening of the C-O bond [85]. It was suggested that phenol is adsorbed on the Lewis center, formed by dehydroxylation of the aluminum oxide surface [84, 85]. The phenol molecule loses a proton to the surface and the resulting phenoxide ion is chemisorbed on the surface aluminum ion as represented below. The phenol proton combines with a surface hydroxyl forming water which is then desorbed [85]:

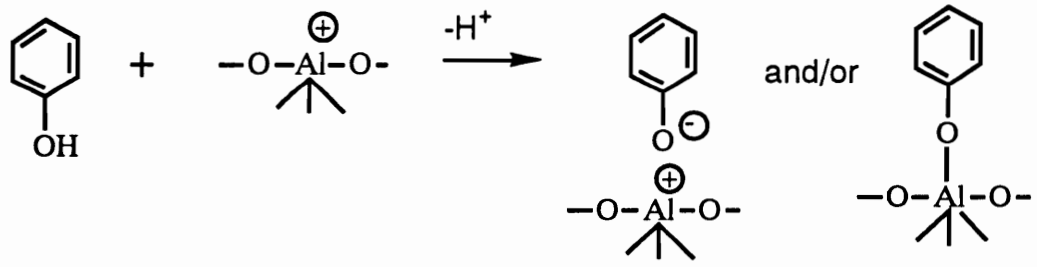

It was suggested that the chemisorbed surface species have considerable ionic character [85] The IETS studies showed that phenol is irreversibly chemisorbed as a phenoxide ion on a thin amorphous film of aluminum oxide [86]. Extensive hydrogen bonding was observed among adsorbates and between adsorbates and the hydroxylated alumina surface. Also the chemisorption of phenol in plasma-grown alumina was

investigated by IETS [87]. The OH groups on the plasma-grown oxide are of a more acidic type with few or possibly no nearest neighbor oxide anions [87]. The spectra of the adsorbed phenol did not show the vibrational modes associated with OH groups of the phenol, indicating the chemical reaction of phenols with surface bound OH (Brönsted acid sites) or with cationic surface aluminum centers (Lewis acid sites). No evidence for surface-bound molecular water was found. The authors concluded that water may be formed by protonation of surface OH groups by the phenolic protons lost at formation of phenolate ions, but it is removed in the vacuum. The phenolate anion is left bound to aluminum cations on the surface. It is also possible for phenol to react directly with surface cations, and the phenolic proton is lost to neighboring anionic oxide centers such as:

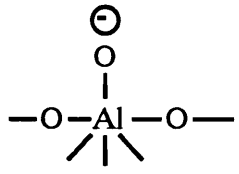

No evidence for hydrogen bond OH groups was found. It was also concluded that the phenolate anions are perpendicular to the oxide surface.

Brown et al. [88] investigated the interaction of phenol- and cresol-formaldehyde model compounds with aluminum oxide using IETS techniques. The molecular structures of the model compounds used are given in Figure 7 [88]. The results indicated that these polyphenolic molecules are chemisorbed at the aluminum oxide surface as phenolate anions. Water formed upon reaction between phenolic and surface hydroxyl is desorbed. The behavior of polyphenolic molecules is similar to that of monofunctional phenols, suggesting that functional groups involved in adsorption act independently. In the case of phenolic-methylol systems, both the phenolic OH and the alkyl OH may interact with the

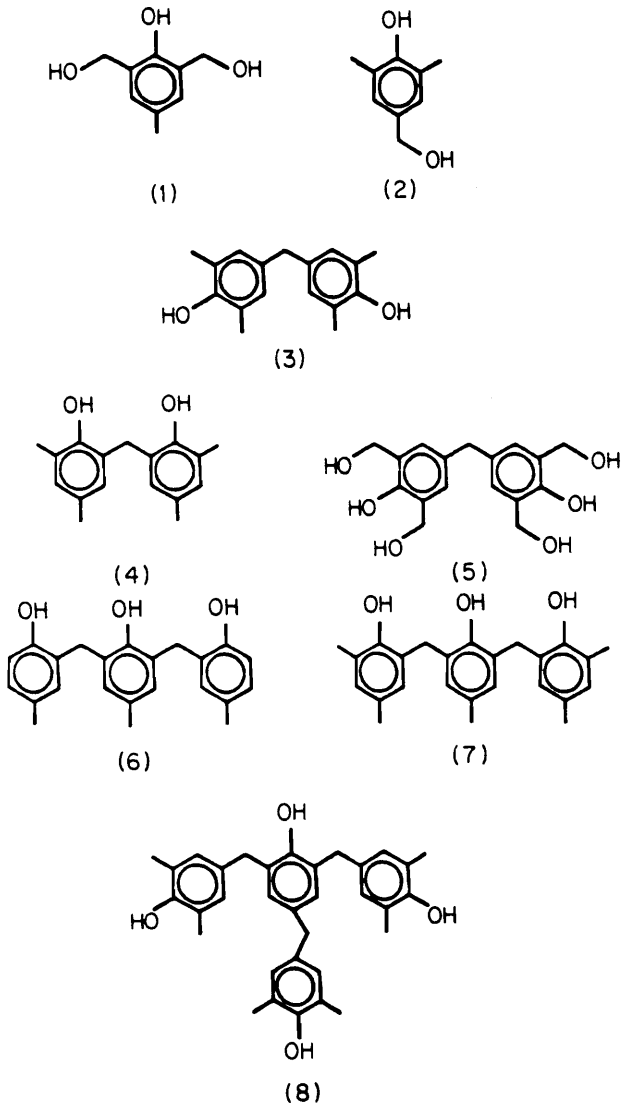

Figure 7. Molecular structure of the model compounds used [88].

oxide surface, as shown in Figure 8 [88]. It is concluded that the strong interaction between phenolate and oxide leads to the observed spectra.

2.2.4. Adhesives

Toughened acrylic and epoxy resins and polyurethane-based adhesives are the most commonly used adhesives for composite bonding. The use of hard and brittle adhesives creates structures prone to damage at shock loading, especially when flexible composites are involved. The distortion of the substrate under load introduces powerful peel and cleavage forces which may break the adhesive. The use of ductile polyurethane adhesives and toughened adhesives reduces the tendency of overloaded bonded structures to fail when distorted.

2.2.4.1. Epoxy adhesives

Epoxy structural adhesives typically contain several components, the most important being the epoxy resin around which the adhesive is formulated. The epoxy resins can be aromatic, aliphatic, cyclic or acyclic with one or more reactive groups. The one feature common to all these resins is the epoxy ring.

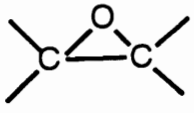

The structure of the resin determines the physical and chemical properties, particularly the reactivity of the epoxy and the other groups present. The most commonly used epoxy resins are those based on bisphenol A-epichlorhydrin codensates which can be described by the general formula:

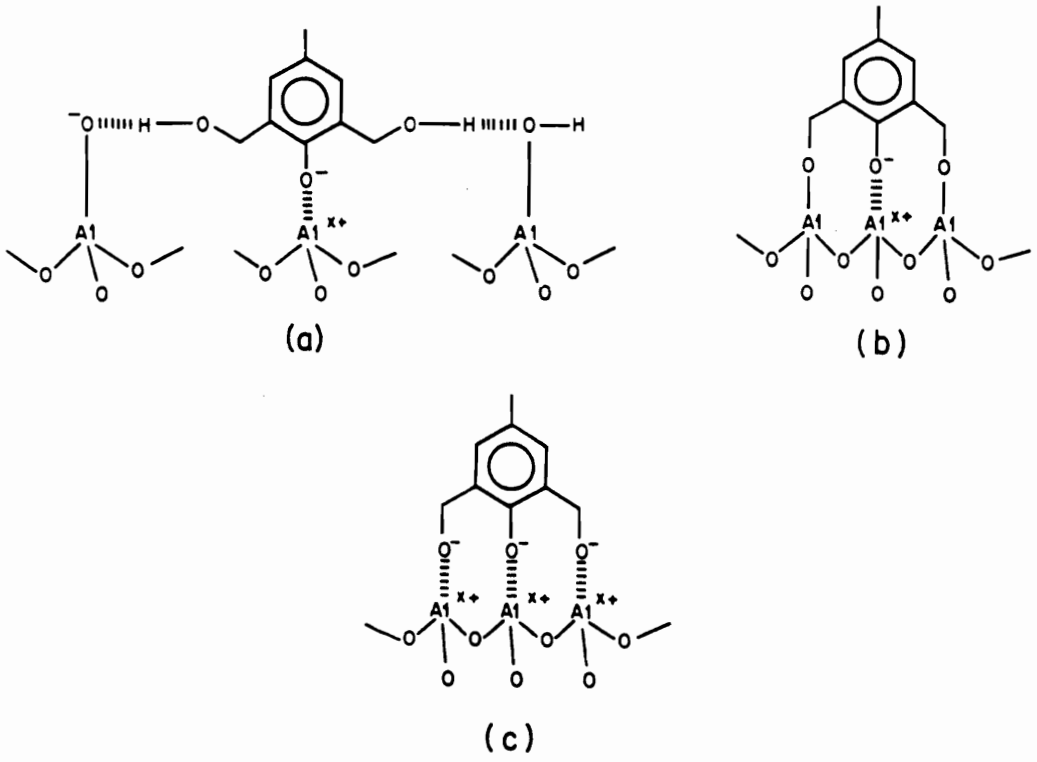

Figure 8. Structures of the possible phenolate interactions with the aluminum oxide surface: (a) ionized phenolic - OH interacting with exposed surface cationic sites and associated alkyl - OH hydrogen-bonding with surface hydroxyl or oxide anionic centers; (b) phenolate interaction as in (a) but with alkyl-OH reacting with the surface hydroxyl to give aluminum alkoxide species; or (c) an electrostatic interaction between ionised phenolic and methylolic-OH with surface aluminum cations [88].

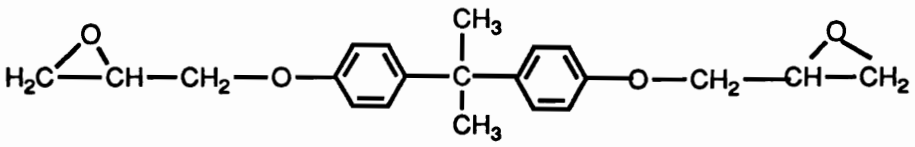

However, a large number of polyglycidyl materials have been synthesized and used in different applications.

The epoxy resins are thermosetting materials; they have the ability to transform readily from the liquid or thermoplastic state to tough, thermoset solids during the curing reactions. The conversion is accomplished by the addition of chemically active compounds known as curing agents (hardeners). Curing agents can be acidic or basic. The basic curing agents employed in epoxy resin technology are Lewis bases, inorganic bases, primary and secondary amines and amides. Among the acid curing agents used in epoxy resin technology are: carboxylic acids, dianhydrides, dibasic organic acids, phenols and Lewis acids. Besides the resins and hardeners, epoxy adhesive formulations include other components: fillers, polymers, rubbers, and co-reacting resins. Of special interest in structural applications are the toughened epoxy adhesives, which have a second phase of dispersed rubbery particles in the thermosetting polymer. When the adhesive bond is overloaded, the energy is dissipated mainly by the plastic shear-yielding in the matrix. Such plastic deformation takes place to a far greater extent for toughened epoxy than for untoughened material due to the interactions between the stress field ahead of the crack and the rubbery particles [89]. Toughened epoxies are considered prime candidates for bonding composites, providing increased peel and impact performances. Also if absolute maximum performance is required, the toughened epoxies are recommended [43].

2.2.4.2. Polyurethane adhesives

A linear polyurethane can be obtained by the reaction of a diol or polyol and a diisocyanate.

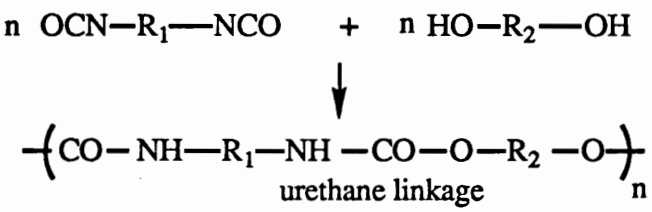

A wide range of technologies is available for polyurethanes. Usually, these adhesives consist of two components: one is a prepolymer terminated in some active group, and the other is a multifunctional isocyanate or an isocyanate terminated low molecular weight polymer. The former can be polyethers, polyesters, amino-polyethers, hydroxy-terminated polydienes. On mixing, the components undergo a rapid addition reaction at room temperature. Normally conversion is 100%. Polyurethane adhesives are strong, resilient and suitable for structural applications. They have enhanced impact and peel resistance [43]. Polyurethane adhesives are resistant to oxidation [90] but not to hydrolysis [43, 90]. Both the raw materials of the adhesives and the crosslinked adhesive itself are sensitive to moisture [43]. The deterioration of polyurethane adhesives exposed to moisture or hot/wet climates is due to hydrolysis [90]. Frequently polyurethane adhesives must be used with primers [43].

2.2.5. Testing of adhesive bonds

2.2.5.1. General considerations

The performance of adhesive joints is assessed usually by destructive mechanical tests. Many tests are used. The standard test methods do not allow the determination of the magnitude of intrinsic adhesion forces acting at the adhesive/adherend interface even when the failure was interfacial. Also most test methods do not permit the measurement of mechanical properties of the adhesive even when the failure mode is cohesive [91]. An adhesive bond is a system consisting of adhesive, adherends, surface treatment, primer,

and interfaces between these components including adhesive/adherend surface interactions [92]. For almost all test methods, the measured strength of the adhesive bonds depends not only on the intrinsic adhesion and the mechanical properties of adhesives, but on all components of the adhesive system, on the testing conditions and the geometry of the joints. In many cases, the state of stress in the adhesive joint is complex, and it is very difficult to obtain useful data for joint design and analysis [92].

The failure mode introduces another complication in the interpretation of results, especially for bonded composites. Often the matrix materials of composite adherends are weaker than the adhesives used to bond them. Thus failure may take place by delamination or interply failure within the composite rather than in the adhesive. In the adhesively bonded structures, there are three basic modes of loading: opening or cleavage is mode I, in-plane-shear or sliding is mode II, and anti-plane shearing or tearing is mode III. These models are shown in Figure 9 [93]. .

2.2.5.2. Single lap shear test

The single lap shear test is the most widely used adhesive test method. ASTM E1002 describes the conditions for this test. The specimen is loaded in tension or in compression. Ideally the adhesive is loaded in shear. The test is a useful screening test for evaluating adhesive joints. This test cannot be used to obtain mechanical data suitable for joint design. This test has several advantages. The test is simple and economical to conduct and can be performed in standard tensile testing equipment. Also it duplicates one of the most common joint geometry employed in industry. The test has also a number of disadvantages. The reported or nominal shear stress does not correspond to any intrinsic adhesive mechanical property. The state of stress in the adhesive is not pure shear. Due to the specimen geometry, the load path through the bond is eccentric, causing bending

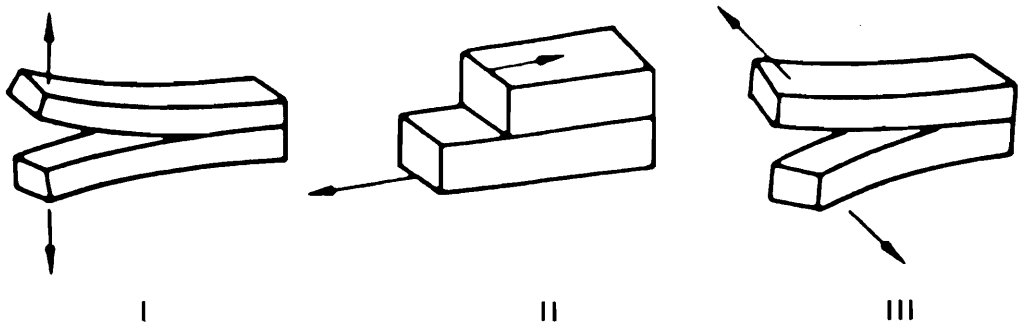

Figure 9. Loading modes. I, Opening (cleavage); II, forward shear (edge sliding); III, sideways shear (tearing) [93].

moments which deform the specimens and tensile forces in the adherends at the end of the bond overlap [92]. The deformation of a single lap shear specimen under load is shown in Figure 10 [94]. The adhesive layer is in a mixed mode of stress: shear and tensile. Figure 11 [95] shows the stress distribution along the mid-plane of the joint in loaded lap shear specimens; p represents the mean stress in the adherends away from the joint, τ_o is the shear stress, σ_o is the normal tensile stress and σ_f is the longitudinal tensile stress. Both shear and transverse tensile stresses occur close to the ends of the overlap and are much greater than the average shear stress. The maximum transverse normal stress occurs at the ends of the overlap. The transverse tensile stress plays an important role in the fracture of single lap joints. Many times it is the cause of joint failure. For metal/metal joints, the transverse tensile stress is frequently higher than the yield stress of the metal substrates and thus causes permanent deformation. For bonded composites, the transverse tensile stress often causes bond failure by delamination of the substrate before the adhesive fails [96]. Besides the intrinsic adhesion and mechanical properties of the adhesive, the results obtained with the lap shear tests depend on the adherend thickness, adhesive thickness and the existence of adhesive fillets.

Volkersen [97] was the first who analyzed the stresses in single lap shear joint. He considered only the differential straining of bonded substrates. Goland and Reissner [95] considered also the tensile stresses due to the eccentricity of the loading path. Later work involved the use of finite element techniques to treat non-linear mechanics and material behavior in real joints, the adhesives being modelled as elastoplastic materials [96, 98, 99]. The viscoelastic and viscoplastic effects are very important, especially at high temperatures and stresses. The distribution of stresses and strain in the adhesive initially change quickly when a load is applied, and this influences adhesive joint strength [99].

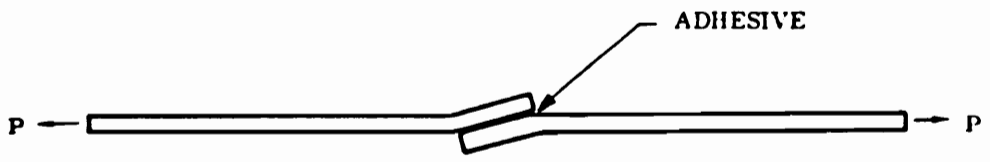

Figure 10. Deformation of a single lap shear specimen [94].

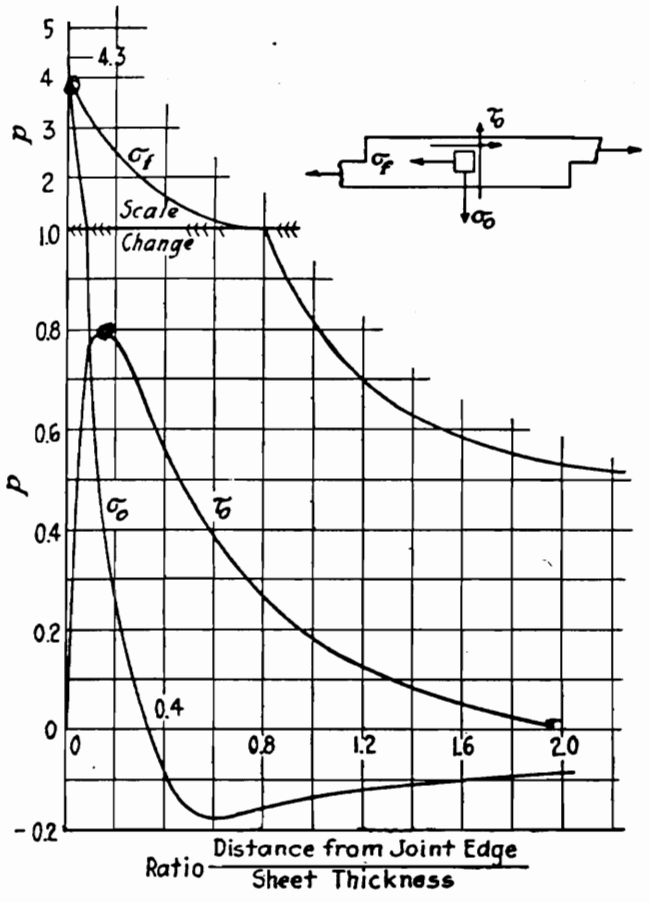

Figure 11. Stress distribution along the shear plane as a function of distance from the edge of the overlap [95].

2.2.5.3. Wedge test

The wedge test specimen or uniform DCB (double cantilever beam) specimen is a simplified variation of the tapered double cantilever beam. The wedge specimen configuration is shown in Figure 12 [2]. For this specimen, the bondline is subjected to mode I loading. The wedge specimen can be loaded under constant stress by applying a normal load on one end or can be loaded under constant displacement by introducing a wedge between the two adherends. If the adherend thickness is sufficient and all strain in the adherends is elastic, then the strain energy created at loading is stored in the sample. If the adherends deform elastically, the strain energy release rate G_I can be calculated for the wedge sample from the expression [100]:

$$G_I = \frac{y^2 E h^3 [3\,(a+0.6h)^2] + h^2}{16[(a + 0.6h)^3 + ah^2]^2} \qquad (1)$$

where y is the displacement at load point or the wedge thickness, E is the adherend modulus, h is the adherend thickness, and a is crack length from the loading point to the crack tip.

The wedge specimen has the advantage that it is simple, can be self-stressed, and placed easily in a variety of environments. In conducting tests, the sample is loaded, and the initial crack is measured. Then it is exposed to the desired environment, and the increase in crack length is measured as a function of time. An assessment of durability can be made based on the rate of crack propagation and on the failure mode. The wedge test is more sensitive to environmental attack than the lap shear sample. It is a useful and quick quality control for assessing the effectiveness of surface pretreatment [101]. It was found that the wedge test can discriminate between adequate, marginal, and inadequate surface

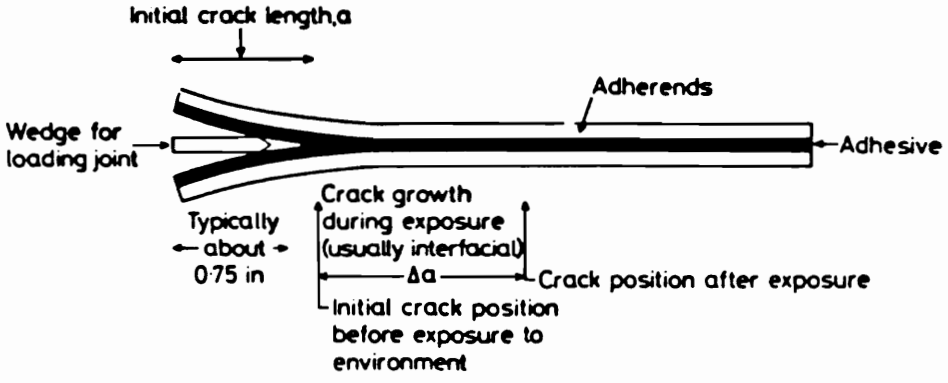

Figure 12. Wedge specimen [2].

preparation [100]. While the wedge specimen was developed specifically as a simple specimen for process control, Cognard used it for basic durability studies [102-104].

2.2.5.4. Butt torsion test

The butt torsion specimen is shown in Figure 13 [105]. Equal and opposite torques are applied to the specimen, and the adhesive is loaded in nearly pure mode III. The shear stress in the adhesive increases linearly from zero at the center to a maximum at the outside of the bond [105]. The shear stress distribution is

$$\tau = \frac{2\,T\,r}{\pi R^4}$$

where τ is the shear stress at radius r, T is the applied torque, and R is the radius of the joint. The shear fracture stress is the maximum stress which occurs at the outer circumference at failure of the specimen:

$$\tau_f = \frac{2T}{\pi R^3}$$

where R is the radius of the bond. The butt torsion sample is useful because the state of stress in the bond is almost pure shear. However, the butt torsion specimen has some disadvantages. It is difficult to make; the bondline thickness, uniformity, and specimen alignment are critical to obtain reliable data. Adhesive fillets should be removed prior to testing because they can increase the joint stiffness and the stress concentrations at the adhesive/adherend interface at the substrate corner.

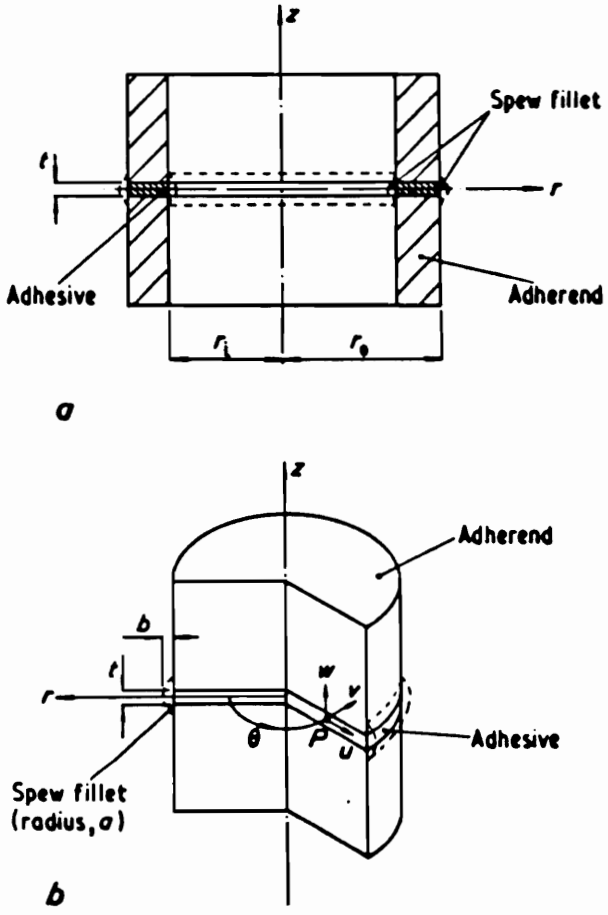

Figure 13. Circular butt joints: (a) annular; (b) solid [105].

2.2.6. Durability of adhesive bonds

2.2.6.1. General discussion

The durability problem is one of the most important in adhesion science and technology. It is required that adhesively bonded structures maintain their performance during their service life. For this, it is necessary that the adhesive bonds retain a significant proportion of their strength under normal operating environmental conditions for the whole period of surface life of the bonded structure. Situations exist where the loss of joint strength during service was so high that joint failure took place prematurely at very low levels of load, long before the expiration of expected service life [106]. While the durability of adhesive bonds is a problem of utmost practical importance, it is a very complex one, because it depends on many factors, some being determined by the operating environment, others by the manufacturer. The most important environmental factors which may reduce durability are: exposure to liquids and their vapors, salts, high temperature, and stress. In many cases, the service conditions for adhesive bonds involve combinations of these factors [70, 107] which can be particularly detrimental to durability [53]. Among the factors controlled by manufacturers are: material selection, treatments, and bond geometry.

The durability problem is complicated by the fact that an adhesive bond is a multicomponent system (adherends, adhesive, surface treatments adhesive/adherend interface, bond geometry). Environmental factors influence every component and may affect the durability of the system. Also every component may pose specific problems upon environmental exposure. For example, while for bonded metals the adhesive/adherend interface is sensitive to water, for bonded composites the adhesive/adherend interface is relatively stable [2, 3]. However, composite adherends have the potential for viscoelastic failure during service life [3].

2.2.6.2. Factors affecting durability of adhesive bonds

2.2.6.2.1. Water

Water is one of the most hostile environments [2, 108] and poses the greatest problem to the environmental stability of adhesive bonds [109], especially in conditions of relatively high stress and temperature [108]. Water may enter the joint by the following processes: absorption of water by the adhesive, wicking or penetration of water along the adhesive/adherend interface, capillary transport through cracks and crazes in the adhesive, and adsorption of water by a permeable adherend (for example, a composite) [109]. Water may weaken the joint by attacking the adhesive/adherend interface (displacing the adhesive), altering the properties of the adhesive reversibly (plasticization) or irreversibly (hydrolysis, cracking, crazing), altering the adherend (hydration of metal oxide surfaces or degrading composite adherends), and introducing swelling stresses in the bond [109, 110].

Gledhill and Kinloch [111] developed thermodynamic considerations to determine the intrinsic stability of the adhesive/adherend interface in the presence of liquids. The work of adhesion W_a in an inert medium and in the absence of chemisorption, mechanical interlocking, and interdiffusion is:

$$W_a = \gamma_S + \gamma_{Ad} - \gamma_{SAd}$$

where γ_S and γ_{Ad} are surface energies of substrate and adhesive, respectively, and γ_{SAd} is the interfacial free energy.

In the presence of a liquid, the work of adhesion W_{AL} is:

$$W_{AL} = \gamma_{SL} + \gamma_{AdL} - \gamma_{SAd}$$

where γ_{SL} and γ_{AdL} are the interfacial free energies between the substrate/liquid and adhesive/liquid interfaces, respectively.

The work of adhesion for an adhesive/substrate interface is, usually, positive. In the presence of a liquid, the work of adhesion W_{AL} may have a negative value showing that

the surface is not thermodynamically stable. The change from a positive to a negative work of adhesion is the driving force for the displacement of adhesive by the liquid. Working with an epoxy/mild steel system, Gledhill and Kinloch [111] calculated the work of adhesion before and after water attack. They predicted the instability of this system in hostile environments using the above-mentioned thermodynamic considerations. The thermodynamic approach shows that water will be preferentially adsorbed on an oxide surface, explaining the difficulties encountered in practice to obtain durable high energy substrate/adhesive interfaces. It is predicted that the composite/adhesive interface is relatively stable [2, 109, 112]. It should be mentioned that the thermodynamic approach ignores the primary bonding and mechanical interlocking.

Water will almost always displace adhesives from metal surfaces if only secondary molecular forces act across the interface [110]. To obtain durable metal/adhesive interfaces, stronger intrinsic adhesion forces are necessary. This was achieved by the establishment of interfacial primary bonds using primers (usually silane-based and phenolic) [2, 112]. Due to their high energy, the chemical bonds across the interface may bring a decisive contribution to interface stability because water will not readily displace a chemisorbed adhesive or primer [112]. The interfacial primary bonds for some systems of interest were discussed in 2.2.3.4. Also mechanical interlocking may have a contribution to increasing the durability of adhesive joints even if it is not a major one [17, 110 112].

Environmental attack on the adherend material may cause a loss in joint strength. Gross substrate corrosion of metal adherends is not usually an operative mechanism in environmental failure. The adherend corrosion occurs generally after the displacement of adhesive on the metal oxide by water [110-113]. If gross corrosion is encountered only in special situations [113], subtle changes in the nature of the oxide may cause a decrease in bond strength. Venables [18] observed that moisture penetration in aluminum bonds

causes the largely amorphous aluminum oxide, formed by pretreatment, to convert to a crystalline hydroxide. This hydroxide is loosely bonded to the underlying oxide and represents a weak bonding layer. However, Kinloch [69] did not observe the hydration of aluminum oxide under an epoxy-phenolic primer in durability studies of bonded aluminum. It was concluded that hydration takes place after failure rather than being the direct cause of environmental failure. Titanium dioxide under severe conditions undergoes a polymorphic transformation [18].

Moisture attack at the adhesive/adherend interface may induce failure modes which are different than under dry conditions. Some aluminum joints failed through the oxide layer after environmental attack while prior to environmental exposure all joints failed cohesively in the adhesive [114]. Cognard in studies of environmental attack on adhesive joints by cleavage fracture [115] found that when an adhesive joint is cleaved in a liquid, the crack is longer than in air, and occurs along the interface from the very beginning instead of progressing inside the adhesive as in air.

It was shown in some cases that the rate of environmental failure is controlled by the diffusion rate of water into the joint [111, 116, 117]. If water penetrates into the joint by diffusion, the water concentration profile within the joint can be calculated by measuring the diffusion coefficients using bulk adhesive films. For other systems, the situation is more complicated. When a silane-base primer is used, the diffusion of water does not control the kinetics of environmental attack [118].

Water adsorption by adhesives and composite adherends may change their properties and reduce the environmental resistance of the bonds. Some of these changes are reversible, and the adhesive bond strength is recovered after drying; others may be irreversible and the loss of strength is not recovered. Adsorption of moisture by the adhesive and the composite matrix tends to accelerate time-dependent properties by

depressing the glass transition temperature and lowering the modulus and strength. Water adsorption produces swelling of the adhesive and composite matrix and differential swelling stresses may develop at the adhesive/composite adherend interface. Both plasticization and swelling are reversible processes.

Attempts have been made to correlate the decrease in Tg with the water content for epoxy adhesives using the Fox equation [119]. For some systems, the authors found an agreement between predicted and experimental values. For other systems, the depression of Tg was lower than predicted; a fact explained by water being clustered instead of being completely dispersed. Unexpectedly, on prolonged exposure to water, Tg increased for all systems studied. This was explained by the formation of additional crosslinks between unreacted groups. This indicates that plasticization is a contributing factor in durability only in some cases. Moisture adsorption also decreases the β–transition temperature for epoxy resins [120]. Mijovic and Lin [121] found, for an epoxy resin, that moisture adsorbed in the initial stage of diffusion enters preferentially the lower crosslink density matrix and affects the β-transition temperature, while moisture adsorbed after a certain moisture content value enters the highly crosslinked structure and depresses Tg.

In addition to plasticization and swelling, water may promote irreversible changes in the adhesive and composite adherend (chemical reactions, cracking and crazing). Antoon and Koenig [122] studied the irreversible effects of moisture exposure at 80°C on an anhydride-crosslinked epoxy resin unreinforced or reinforced with high surface area fumed alumina or powdered E-glass. The short-term effect was hydrolysis and leaching of unreacted anhydride. For the stressed samples, hydrolysis of ester groups was observed. The unstressed samples hydrolyzed much more slowly. The authors concluded that hydrolytic attack on the epoxy resin is a mechanical process accelerated by the presence of E-glass and alumina filler particles. Both the external and internal stresses enhance

hydrolytic degradation. Hydrolytic degradation of the epoxy matrix does not play an important role in the absence of fillers or stresses [122].

Moisture adsorption may produce cracking and crazing of the adhesive or the composite matrix due in part to swelling and shrinkage stresses. Crazing and cracking play a more important role than hydrolysis [109]. The cracks may serve as fracture initiators [3] or may increase the rate of water transport [109]. For composite adherends, the damage in the composite allows direct access of water to the adhesive by capillary wicking [3].

Based on their durability studies on steel bonded with an epoxy adhesive, Gledhill et al. [116] concluded that there must be a critical level of water concentration in the adhesive below which environmental attack does not occur. Comyn et al. [117, 123] reached the same conclusion working with aluminum joints.

2.2.6.2.2. Temperature

Moderate temperatures alone (40-50°C) usually do not affect the durability of adhesive bonds [70]. Cotter [124] maintained aluminum joints prepared with six types of adhesives at a desert location for six years and found that only one adhesive system deteriorated significantly. The combination of high temperatures (100°C) and high humidities (100 %RH) may reduce severely adhesive bond durability [70]. The increase in temperature increases the water uptake rate and accelerates chemical degradation. Gledhill et al. [116] found that increasing temperature increases both the diffusion coefficient and the equilibrium water concentration in an epoxy adhesive exposed to water. Nakamura et al. [125] found that the strength of epoxy/aluminum bonds in an aqueous environment decayed faster with increasing temperature from 65 to 85°C. The diffusion coefficient also increased with increasing temperature.

2.2.6.2.3. Stress

During their service life, adhesive joints may be subjected to stress intermittently or continuously. Stress usually increases the rate of strength loss, especially in combination with high humidity (100%RH) or elevated temperature (>50°C) [70]. Stress may increase the rate of diffusion and the solubility of the diffusing medium in the adhesive. Stress can lower the free energy barrier for destruction of adhesive/adherend interfacial bonds and adhesive and composite matrix cohesive bonds, making them more susceptible to environmental attack [109,126]. The rate of destruction for chemical bonds would be [109]

$$k = A \exp. \left(\frac{- (E_a - \gamma \sigma)}{RT} \right)$$

where k is the degradation rate, A and γ are experimentally determined constants, E_a is the activation energy in the absence of stress, R is the gas constant, T is the temperature, and σ is the applied stress. For the hydrolysis of an anhydride-cured epoxy resin, (a mechanically activated process) in water of pH = 11.9, at 80°C, with an applied stress of 5.4×10^8 dyn/cm^2 the value of $\gamma\sigma$ is about 4 kcal/mol and E_a is about 11 kcal/mol [122]. So the stress significantly (36%) reduces the activation energy for this process. Hydrolytic degradation in the absence of stress is very slow. Minford [127] showed the importance of stress for durability of aluminum bonded with two adhesives: two-part epoxy and one part vinyl-phenolic. For unstressed joints exposed to 51.7 °C and 100% RH the epoxy adhesive gave better joint strength retention. In conditions of applied stress, the joints prepared with vinyl-phenolic adhesive behaved much better than those prepared with epoxy adhesive.

In some cases, the application of load may result in joint strength reduction or rapid joint failure, while in other cases the effect of stress is not significant [128, 129]. Of particular interest related to the influence of stress on durability, is the concept of

endurance limit (stress level below which no attack is observed). Unhappily, there is no generally accepted theory for an endurance limit concept [130 131].

2.2.6.2.4. Adherend surface pretreatment. Primers.

Adherend surface pretreatment is a very important factor in the durability of adhesive joints. As was mentioned in section 2.2.3, for bonding of metals, initial strong joints can be obtained by removing surface contamination and weak oxide layers, but to obtain durable joints it is necessary to form stable oxides and to produce strong and stable adhesive/metal oxide interfacial bonds. The surface pretreatments for the adherends of interest in this research were presented in 2.2.3. Some examples of the effect of surface pretreatments on joint durability will be presented next.

For aluminum joints, there is broad agreement regarding the ranking of pretreatments with respect to durability. The usual order of durability is degreasing < chromic acid etching < chromic acid anodizing < pickling < phosphoric acid anodizing [70]. This is supported by the results obtained by many workers [18, 63, 67, 69, 71, 132]. However, the reasons for such behavior are still subject to speculation. It was suggested that one reason for the better results obtained with the phosphoric acid anodized aluminum is due to the adsorbed phosphate which inhibits the oxide/hydroxide conversion process [18]. Better durability results obtained with pickling and phosphoric acid anodizing pretreatments are also explained by penetration of the adhesive into the depths of the oxide films formed by these treatments, increasing the interface area and eliminating a true planar adhesive/adherend interface. The effect of moisture is delayed due to an increase in the diffusion path. For other treatments, the penetration of adhesive or primer into the oxide is more limited [63, 69, 71].

The durability of bonds made with as received steel (oily) is poor. Removing the oil by degreasing produced only a small improvement in durability. Major improvements in durability were observed only by applying a silane coupling agent or by bonding to a very clean steel surface (alkaline cleaned) [128]. The beneficial effect of ELPO priming on steel durability when compared with base steel was discussed in 2.2.3.2. For stainless steel, treatments in which the reaction of metal with water in the oxidizing solution goes to completion provide good durability, and there is no thermodynamic driving force for further reaction in a humid environment [133]. The surface remains covered with basic OH^- groups which can interact with the adhesive.

Primers are used to improve durability. This is accomplished by establishing strong and moisture-resistant interfacial bonds. Primers also protect the surface of the adherend from corrosion [134]. Silanes represent the most widely used primers. Silanes act as coupling agents between the adherend and the adhesive forming primary bonds with both materials [70, 135, 136]. Phenolic- and epoxy-based primers are also used to increase the durability of adhesive joints. Interfacial interaction of these primers with metal surfaces is discussed in 2.2.3.4. ELPO priming is widely used for steel adherends in the automotive industry.

For polyester fiberglass composites bonded to aluminum and exposed to different environmental conditions, abrading the composite gave somewhat better durability than alcohol wiping [46]. Untreated composites produced poor joint durability.

2.2.6.2.5. Other factors

There are other factors which affect durability of adhesive bonds, including adhesive type, alloy composition, and exposure to salt. The type of adhesive also influences the environmental resistance of the adhesive/adherend interface. Cotter [124] investigated long

term durability of aluminum bonded with six adhesives and exposed to different natural conditions with or without stress. The epoxy novolac and nitrile-phenolic formulations gave the best durability in all climates, while the epoxy-polyamide adhesives showed the lowest environmental resistance due to high level of moisture absorption in humid environments. Minford [46] investigated the durability of polyester fiberglass composites bonded to aluminum using a variety of acrylic and epoxy adhesives. Acrylic type adhesives provided the best environmental resistance. Krause et al. [137] studied the durability SMC bonded with urethane and epoxy adhesives. Monotonic testing showed that epoxy is superior to the urethane adhesive. In fatigue testing, performance of the urethane adhesive was superior. The results obtained in fatigue testing are explained by the lower modulus of the urethane adhesive which reduces the peel stresses generated during fatigue testing.

Alloy composition plays a role in durability of aluminum adherends. For example, Kinloch et al. [138] investigated the effect of surface pretreatment on the durability of different Al-Mg alloy joints. Joint durability decreased as the magnesium content at the aluminum adherend surface increased. However, Pool and Watts, investigating the durability of various bonded aluminum alloys, did not find any significant correlation between chemical composition and durability [139].

Exposure to salt can have a serious effect on durability. The effect of salt spray may be more severe than exposure to high humidity and temperature [70].

2.2.6.3. Durability tests

A number of testing methods have been developed to assess the durability of bonded structures. There are several factors which must be considered in selection of the durability tests. The material and processes employed to prepare the durability specimens must be the

same as those used in production. This includes surface preparation, primer and adhesive application techniques, and bondline edge protection. The specimen geometry and type of loading must be related to those of the joints in service. Usually the variables in durability tests are: time, temperature, exposure media, and stress [140].

The required life of a bonded structure for autos and airplanes is long, so accelerated durability tests are used to reduce the time of testing and to allow new adhesives to be tested and adapted in a reasonable period of time [70]. The acceleration of environmental attack may be accomplished by increasing the temperature, load or humidity over the level experienced by the actual joint during the service life [70]. While the increase in temperature generally accelerates environmental attack, it may also change the mechanism(s) of environmental attack and bond degradation. The introduction of new failure mechanisms not observed during the service life of the bond may give misleading results [141]. It is recommended that only moderate increases above the maximum service temperature be used [70]. The use of much higher loading than that encountered during the service in combination with high temperature and humidity may also change the mechanism of failure leading to creep rupture and misleading results. The level of loading must be similar to that expected during the service life [141].

The best assessment of durability requires a close duplication of the service environmental conditions. This requires a long time. Often long-term outdoor tests are performed in correlation with laboratory accelerated tests [70].

In durability tests, both unstressed and stressed joints are employed. For the unstressed joints, the durability is evaluated by measuring the residual strength after exposure. The testing of unstressed joints is useful as a screening test and for evaluating the susceptibility of the bonded structure to corrosion [70, 140]. For structural applications, it is recommended that stressed joints be tested [70]. The stressed joint may

be evaluated using dynamic or static fatigue tests. In dynamic fatigue tests, a cyclic or sinusoidal load is applied to the bonded joint and the number of cycles to failure is determined. Dynamic fatigue induces failure of adhesive bonds at a lower level of stress than their failure strength under monotonic loading. For the same level of stress, samples tested in dynamic fatigue tests will fail faster than samples tested in static fatigue tests [142]. In static fatigue or creep tests, a constant, sustained load is applied to the joint and the time to failure is determined.

Standard methods for creep testing joints in compression and tension are described in ASTM D2293 and D2294, respectively, and dynamic fatigue tests in ASTM 3166. These methods use the single lap shear specimen. Other samples are also used: thick adherend lap shear specimen, cracked lap shear specimen, tapered double cantilever beam, and thin double cantilever beam specimen (Boeing wedge specimen). Of particular interest in industry for durability tests is the Boeing specimen discussed in 2.2.5.3.

The most important aspect of durability testing is the assessment of results and their correlation with the service life [140]. Gledhill et al. [116] developed a model based on a critical concentration concept to predict joint durability. They used thermodynamic and water diffusion data in combination with a continuum fracture mechanics approach. For an epoxy/mild steel system exposed to water where the mechanism of failure was rupture of interfacial secondary forces and the kinetics of failure were governed by the rate of water diffusion through adhesive, a good agreement was found between predictions and experimental measurements. Predictive models for failure times of adhesive bonds were developed based on reaction rate theory with relative humidity terms included [143]. The independent variables in the equations were humidity, temperature and stress, which were experimentally determined. The approach was empirical; the models have no theoretical basis.

2.3. Analytical techniques

2.3.1. Scanning electron microscopy (SEM)

2.3.1.1. General discussion

Scanning electron microscopy (SEM) is a powerful technique which allows the observation and characterization of materials and surfaces on a micrometer or submicrometer scale. SEM techniques are widely used in adhesion science for surface characterization [66]. Providing large depth of field, good resolution and easily interpreted images, SEM gives important information about rough surfaces in a large range of magnification. The sample is irradiated with a finely focused electron beam and emits secondary electrons, backscattered electrons, Auger electrons, and X-rays. In SEM, the secondary electrons are of primary interest, and are detected. The signal produced in the detector by the secondary electron emission is amplified and forms an image on a CRT (cathode ray tube) screen. The basic components of the SEM are the lens system, electron gun, electron collector, visual and recording cathode tube (CRT's) and associated electronics. Figure 14 [144] shows a schematic drawing of the electron optics of an instrument.

2.3.1.2. Electron optics

The electron optical columns for SEM consist of the electron gun and two or more electron lenses. The electron gun has a source of electrons which is used to form the electron beam. Typically the electrons are obtained from a filament or cathode by thermionic emission. The electron gun contains also a grid cap or Wehnelt cylinder which is negatively biased with respect to the cathode and an anode plate. The electrons emitted by the cathode are accelerated to the anode by a potential between cathode and anode. Because of the grid cap, the electrons are focused to a crossover point below the grid cap.

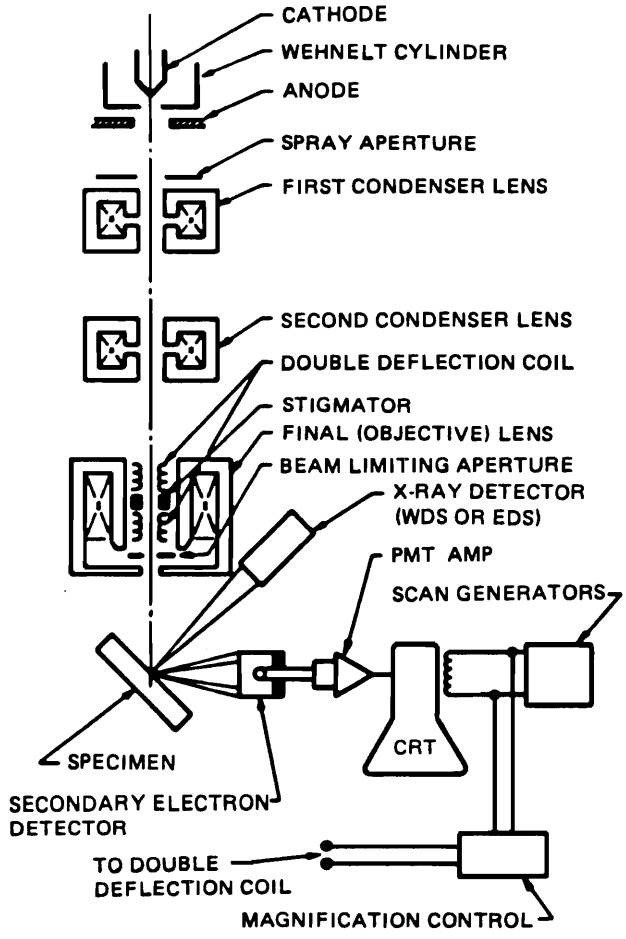

Figure 14. Schematic drawing of the electron and x-ray optics of a combined SEM-EPMA [144].

Electronic lenses demagnify the electron image formed at the crossover (25-100 mm) in the electron gun to the final probe size (50 Å-1mm). The role of the condenser lenses is to determine the beam current which irradiates the sample. The final lens (objective lens) controls the final spot size on the sample. The lenses used are electromagnetic lenses, and the electron beam is controlled by the electromagnetic field of the lenses.

A large depth of field is an important advantage of SEM, and it is defined as the distance above and below the optimum focus (point Q in Figure 15 [145]) the sample surface can be displaced without affecting the performance of the instrument. The depth of field is controlled by the objective lenses. It is a compromise between depth of field and resolution, one may be increased at the expense of the other.

2.3.1.3. Electron beam-specimen interactions

A variety of interactions occur when the electron beam impinges on the sample. They may be classified in two groups: elastic or inelastic. Elastic interactions occur with alterations of the beam electron trajectories but without significant changes in energy. Inelastic interactions occur with transfer of energy to the sample and the decrease in the kinetic energy of the beam electrons. Of inelastic processes, the excitation of conduction electrons leading to emission of secondary electrons is of interest in SEM. The secondary electrons usually have an initial kinetic energy less than or equal to 50 eV [146]. Secondary electrons produced close to the surface and with energies greater than surface barrier energy (2-6 eV) have a high probability of escaping from the surface. Because the electrons are strongly absorbed, those produced 100 Å below the surface have a very small probability of escaping. So almost all secondary electrons which escape through the surface and can be detected originate very close to the surface [147]. Other inelastic processes are: plasma excitation, ionization of inner shells, Bremsstrahlung or continuum

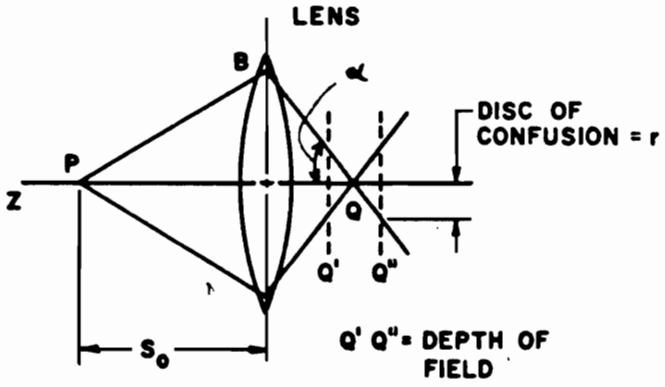

Figure 15. Schematic drawing showing depth of field [145].

X-rays and excitation of phonons [146]. A schematic diagram of various electron-specimen interactions is given in Figure 16 [147].

Interactions between the electron beam and non-conductive specimens cause charging phenomena which result in image distortion and thermal and radiation damage. A thin layer of gold, silver or copper applied on the insulating surfaces aids in eliminating charging problems [148].

2.3.1.4. Image formation

The image system consists of: the scanning system, the signal detector, the amplifiers and the display. The scanning system consists of two sets of electromagnetic scan coils which scan the electron beam in synchronism with the electron beam of a separate CRT, the electromagnetic scan coils of the microscope and of the CRT being driven by the same scan generator. For every beam position on the sample surface, there is a unique position on the CRT. The electron beam will dwell for some fixed time at each point on the sample surface and will interact with the sample. The emitted secondary electrons are collected by a positively biased collector grid. Behind the collector grid, the secondary electrons are accelerated onto the scintillator-multiplier detector, which emits light when struck by high energy electrons. The light goes by total internal reflection to a photomultiplier which amplifies the signal sent to the CRT. So the brightness of every point on the CRT depends on the interaction specimen beam for the corresponding point of the sample. No true image exists in the SEM, the image being produced by the mapping operation. Magnification of the SEM image is the ratio of the area scanned on the CRT to the area scanned on the specimen.

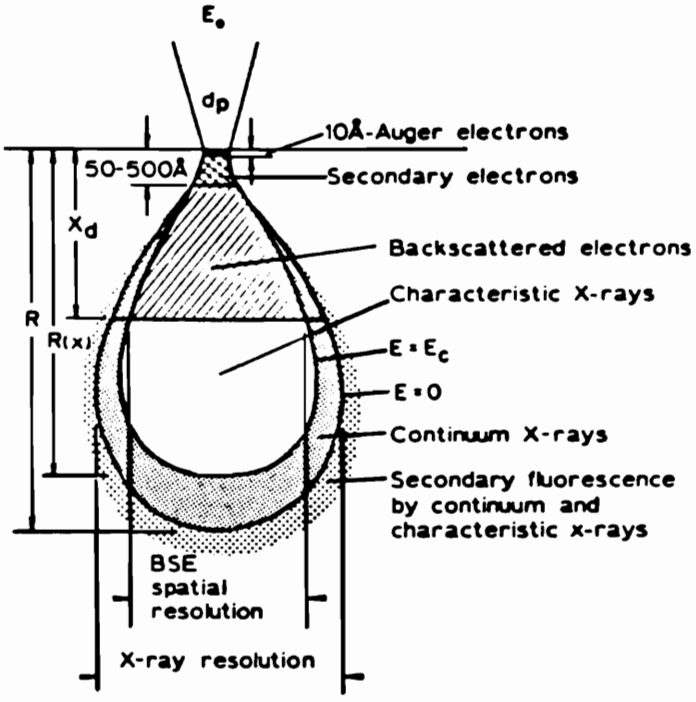

Figure 16. Schematic of electron-beam interactions and the depths to which they occur in the sample [147].

2.3.2. X-ray photoelectron spectroscopy (XPS)

2.3.2.1. General discussion

XPS is a widely used surface technique in adhesion science. XPS involves the bombardment of the sample with X-rays of characteristic energy which causes the ejection of electrons. The process is shown schematically in Figure 17 [149]. The ejected photoelectrons are separated according to their energy and counted. The kinetic energy of ejected photoelectrons depends on their binding energy and the energy of photon source and is characteristic of a specific level of a particular atom. This allows identification of the element ejecting the electrons.

For the X-rays of kilovolt energy used in XPS, the depth of penetration is about 1000 nm [150]. However, the signals observed in XPS originate from very near the surface due to the low value of the escape depth of electrons. The technique probes to a depth of 5-10 nm, depending on the composition of the surface and X-ray energy. For example, the sampling depth (depth from which 95% of the signal is derived) for C 1s electrons in organic materials is 4 nm and 7 nm for magnesium and aluminum sources, respectively [151]. XPS provides good qualitative and quantitative elemental analysis of surfaces. Also it gives information about chemical bonding [66].

An XPS instrument consists of vacuum system, the X-ray source, the energy analyzer, the detector and the data storage and control system. Figure 18 [152] shows a schematic illustrating the basic experimental set-up for XPS. X-rays impinge on the sample which cause photoelectrons to be ejected. The energy analyzer measures the energies (more precisely the velocities) of photoelectrons ejected from the sample surface. After passing through the analyzer, the electrons are detected as discrete events. The number of electrons for a given detection time and energy is stored digitally and recorded.

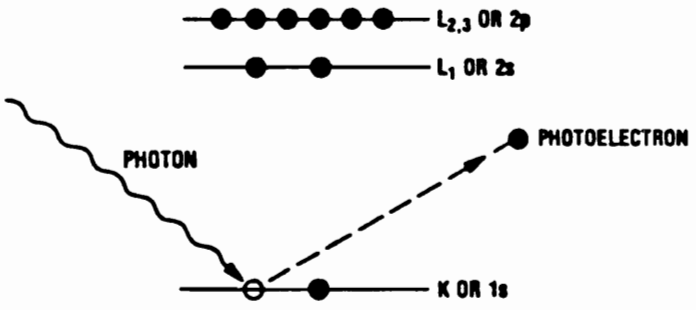

Figure 17. The emission of photoelectrons in the XPS [149].

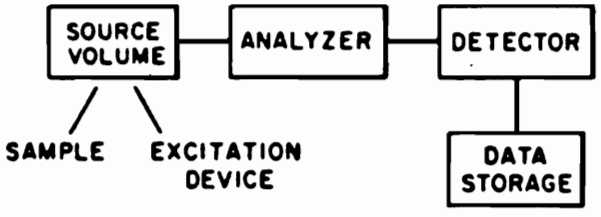

Figure 18. Schematic of general plan of electron spectrometer [152].

2.3.2.2. Qualitative analysis

The elemental identification in XPS is based on the fact that the kinetic energy of the ejected electrons is characteristic of a specific level of a specific atom. According to the Einstein equation governing the interaction of a photon with an electron, the kinetic energy (E_{KE}) of an ejected photoelectron is a function of X-ray energy, hν, the binding energy of the photoelectron, BE, and the work function Φ

$$E_{KE} = h\nu - BE - \Phi \qquad (1)$$

The work function Φ depends on both sample and spectrometer. Equation 1 assumes that the photo-emission process is elastic, no energy being lost by the electron between ejection and detection [153].

Photoelectron binding energies for different levels of most elements are well documented in the literature [154] and serve as a reference for identification of peaks observed in experimental spectra. Besides elemental identification, XPS gives other information due to the fact that non-equivalent atoms of the same element give core-level peaks with different binding energies. The difference in binding energy is called a chemical shift. The non-equivalence of the atoms may have several causes: difference in formal oxidation state, difference in molecular environment, or difference in lattice site. The binding energy of the ejected photo-electrons changes as a function of formal oxidation number of the atom. Usually, for the same oxidation state, the binding energy increases as the electronegativity of the neighboring atoms increases. So this chemical shift offers valuable information on the chemical state of atoms [153].

2.3.2.3. Quantitative analysis

Quantification can be accomplished in three ways: a) use of basic principles, b) use of published data bases, and c) use of locally produced standards. A combination of these three methods may give the best results [150]

A detailed theoretical and experimental study of the application of X-ray photoelectron angular distribution measurements to quantitative XPS was presented by Fadley et al. [155]. Their theoretical model took into account X-ray reflection and refraction, non-uniform X-ray flux, non-uniformity of surface layers, surface roughness and a realistic spectrometer acceptance function. Battistoni et al. [156] determined atomic ratios in a series of pure organic compounds using two methods: first principle method (FPM) and elemental sensitivity factors (ESF) method. Both methods gave results in good agreement with expected values and show similar degrees of accuracy (about 10%)

Powell and Larson [157] used a model for quantitative XPS similar to that of Fadley et al. [155]. They assumed that the sample is homogeneous and smooth. They obtained satisfactory agreements between the predicted and measured intensities.

2.3.2.4. Overlapping spectral features

Frequently an XPS spectrum consists of a number of overlapping peaks, often with different peak shapes and intensities. The overlapping peaks may be chemically shifted peaks, satellites, energy loss features and Auger peaks. Also the peak width of the XPS photopeaks, ΔE, depends on several factors: natural line width of the core level, ΔE_n, the photon source width, ΔE_p, and the analyzer resolution, ΔE_A, according to the equation [153].

$$\Delta E = (\Delta E_n^2 + \Delta E_p^2 + \Delta E_A^2)^{1/2}$$

In the case of overlapping peaks, no spectrum can be unambiguously analyzed [158]. However, two data processing methods are used to improve the quality of information in this situation: deconvolution and curve fitting. The purpose of deconvolution methods is to obtain the "true" spectrum by removing the effects of spectral broadening due to instrumental factors. By deconvolution, the peaks are sharpened, and it is easier to determine the energy position of photopeaks and to detect and identify shoulders on the peaks. Curve fitting is used to separate overlapping peaks. A spectrum is synthesized by summing a series of functions representing individual peaks whose height, width, and binding energy are adjusted to give a synthesized spectrum which closely resembles the experimental spectrum. The most common types of function used for curve fitting are Gaussian and Lorentzian functions. Curve fitting often provides more accurate and reliable chemical information by determination of energy positions, intensity and shifts for the component photopeaks.

2.3.3. Fourier transform infrared (FTIR)

2.3.3.1. Introduction

Infrared (IR) spectroscopy is one of the most widely used analytical techniques. In IR spectroscopy, the molecule is irradiated with infrared radiation and absorbs radiation energy only at certain frequencies which match the natural vibrational frequencies of the molecules. The infrared spectrum is characteristic of the entire molecule. However, certain groups of atoms absorb at or near the same frequency without regard to the structure of the rest of the molecule [159]. A molecule absorbs infrared radiation by increasing its own vibrational energy [160]. There are two types of molecular vibrations: stretching and bending. In infrared only those vibrations that result in a rhythmical change in the dipole moment of the molecule are observed The frequency of the radiation absorbed depends on

the relative masses of the atoms, the force constant and the geometry of the atoms. The stretching frequency can be calculated by applying Hooke's law. For a simple molecule consisting of two atoms, the frequency of oscillation ν (cm^{-1}) is [161]:

$$\bar{\nu} = \frac{1}{2\pi c}\left(\frac{f}{\frac{M_x M_y}{Mx + My}}\right)^{1/2}$$

where: M_x, M_y are atomic masses, c is the velocity of light and f is a force constant.

The instrumentation for IR spectroscopy includes dispersive IR spectrometers and FTIR spectrometers. In a dispersive instrument, the intensity of the transmitted radiation is directly detected as a function of frequency. The FTIR technique is based on the use of a Michelson interferometer, a sensitive infrared detector, and a digital minicomputer [162]. In an FTIR spectrometer, the intensity is detected as a function of the mirror displacement which is translated to a function of time which is converted to wavenumber. FTIR spectrometers have important advantages over the dispersive instruments. The throughput of FTIR spectrometers is high (energy throughput advantage or Jacquinott's advantage) due to elimination of dispersive elements and slits. The entire frequency range can be observed at any time (multiplex advantage or Felgett's advantage). The frequency accuracy is very high (Conne's advantage) due to the use of a He-Ne laser as monitor device for mirror movement.

2.3.3.2. Photoacoustic FTIR (PAS-FTIR)

FTIR-PAS is based on the fact that when modulated IR radiation hits the surface of a sample, it will cause the surface to heat and cool alternately. Cyclic heating and cooling of

the sample produces cyclic variations in the volume of sample. These are transmitted to the coupling gas in the photoacoustic cell, causing the development of a standing sound wave which is detected by a microphone. A schematic diagram of a photoacoustic cell is shown in Figure 19 [163]. Only the absorbed frequencies will heat the sample and will produce sound waves. So the sound waves are used to detect the absorption of infrared radiation in FTIR-PAS [163], the audio response corresponding to the absorption characteristics of the sample [164]. The PAS technique has several advantages including minimal sample preparation and depth profiling capability [165]. Among the disadvantages are: low signal-to-noise ratio, possible light scattering, and depth probing dependence on frequency [163, 165].

2.3.3.3. Reflection-absorption spectroscopy (RAS)

RAS is a method of examining a thin surface layer by reflection of infrared radiation from suitably reflective substrates. With the advent of FTIR spectrometers, a large increase in sensitivity was obtained. RAS can be schematically explained using Figure 20 [164]. Polarized light incident at grazing angle on a highly reflective surface is considered. At nearly normal angle of incidence, the incident and the reflected waves combine to form a standing wave field. This standing wave electric field has a node at the surface of the metal, the amplitude of the standing wave is zero. Therefore, there will be no interaction of the incident radiation with a film deposited on the surface [166]. For the non-normal incidence case (Figure 20 [164]), the phase change of light reflected from a metal depends both upon the angle of incidence and the state of polarization of the light. The phase shift for the component polarized perpendicularly to the incidence plane is close to 180° for all angles of incidence. The electric vectors nearly cancel each other at the metal surface for all

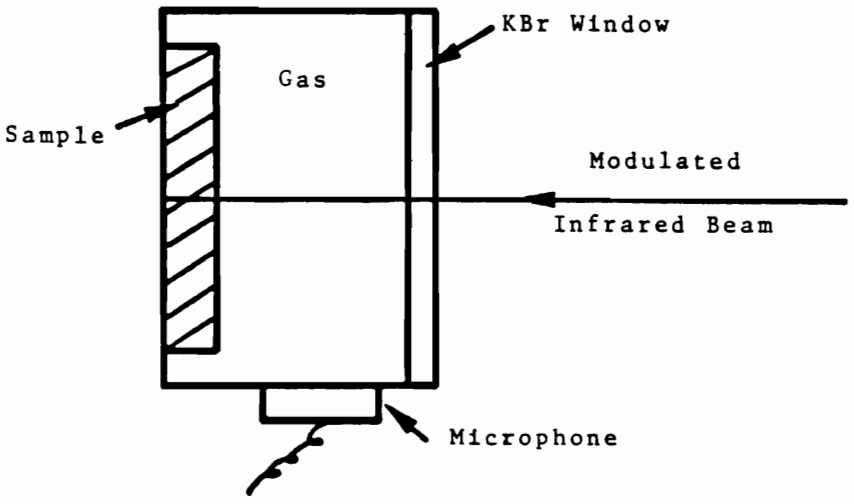

Figure 19. Schematic diagram of photoacoustic cell [163].

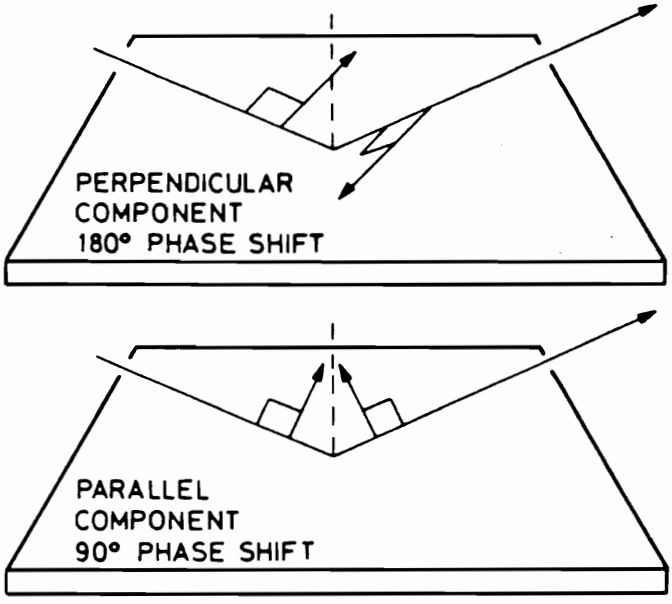

Figure 20. Incident and reflected vector geometries at the metal surface at grazing angles [164].

angles of incidence, the interaction of the incident and reflected light causing a standing wave with a near-zero amplitude. Therefore, little absorption from a layer on the surface is expected. Thus perpendicularly polarized radiation reflected from the surface contains little information about the surface species [164, 166]. When the light is polarized parallel to the plane of incidence, the phase shift changes rapidly at high angles of incidence. The vector sum of the incident and reflected vectors becomes large as the angle of incidence increases, reaching a maximum near 88°. At this angle, the highest sensitivity is obtained. The parallel polarized radiation produces a standing wave with a finite amplitude at the surface of the metal for all angles of incidence except very close to 90°. The electric vector of the standing wave is perpendicular to the metal surface and will interact appreciably only with the dipole moment change of the surface species normal to the metal surface [164, 166].

For this technique, the mathematical calculations have been made using a model consisting of a plane-surfaced material with the optical constants of a metal, covered by a thin isotropic, homogeneous parallel sided layer shown in Figure 21 [166]. The calculations showed that the spectrum obtained depends on the state of polarization of the incident light and optical properties of the materials involved in the model. The adsorbance increases linearly with film thickness (d) up to values of $d/\lambda = 0.0004$, where λ is the light wavelength. The absorbance increases also with increasing extinction coefficients both of the film, k_2, and of the metal, k_3, and decreases with increasing refractive index of the film, n_2. The absorbance is insensitive to the refractive index of the metal, n_3.

Due to peak distortions and peak shifts, there are problems in peak identification and quantitation. Reflectance spectra cannot be compared directly with transmission spectra. Reflectance spectra of layers of different thicknesses may be different in both shape and maximum peak frequency [167]. Most of these effects are due to the anomalous dispersion

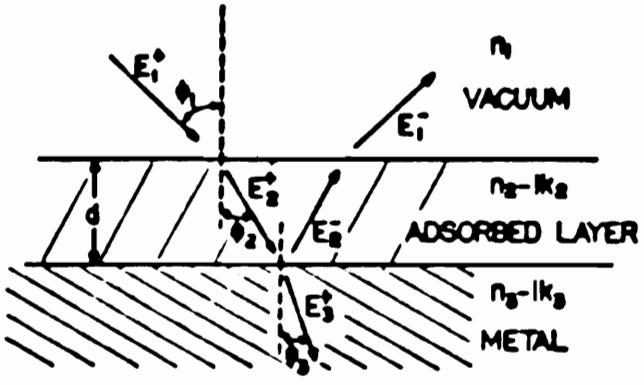

Figure 21. Model of a thin layer on a metal surface used to formulate the reflection problem [166].

of the refractive index of the film in the vicinity of the adsorption band [168]. Calculations showed that while for the moderately strong bands the position in RAS spectra agrees with that in transmission spectra, for very strong bands the variation of refractive index causes important changes when compared with transmission spectra. In monolayer or very thin films, the shift will always be to higher frequencies relative to the transmission spectra. The distortion effects will change more rapidly for the higher frequency band with increasing film thickness [168].

It is hoped that by carrying out this research, a more fundamental understanding of durability in sheet molding compound/adhesive/metal structures, which are increasingly used but not sufficiently studied, will be achieved. This is expected to provide dual benefits. For the automotive industry, the practical aspects of how to obtain more durable and reliable adhesively bonded SMC/metal structures will be of interest. Additionally, it is hoped that the findings of this research will make a contribution to adhesion science, specifically to the important, challanging, and complex field of bonded composites.

3. EXPERIMENTAL

3.1. Materials

The adherends were phase α-SMC (Ashland Chemical Co.), DSM 950B Budd SMC (Budd Co.), aluminum 6061, ELPO steel and Bayflex 150 (a polyurea RIM from Mobay Corporation). Phase α-SMC and DSM 950B Budd SMC are commercial names for crosslinked unsaturated polyesters reinforced with glass fibers, used in the automotive industry. Both SMC materials have proprietary formulations. A typical SMC composition was shown in Table 1. Aluminum 6061 is an alloy which contains Al (98.98%), Si (0.6%), Cu (0.28%), Mg (1.0%) and Cr (0.20%). ELPO steel is a proprietary material. For a description of the ELPO priming process see 2.2.3.2. Bayflex 150 is a proprietary polyurea material obtained by the reaction injection molding (RIM) process from a mixture of diisocyanate and diamine-based compounds. Three types of primers provided by Ashland Chemical Co. were used: one part diisocyanate-based (Pliogrip 6036), one part phenolic-based (Pliogrip 6025), and two-part epoxy-based (Pliogrip 6031/6032) primers. All primers used have proprietary formulations. Pliogrip 6036 contains poly(methylenephenylene) polyisocyanate (~2%) and methylene chloride (~98%). Pliogrip 6025 consists of ~17% phenolic resin, ~3% vinyl polymer, ~3% carbon black, and ~77% various solvents. Pliogrip 6031 contains epoxy resin (~20%), talc (~25%), chromium oxide (~1%) and solvents (~54%). Pliogrip 6032 contains the curing agents (probably an amine ~12% and a cyclic amide ~3%). The adhesives employed were: Pliogrip 6600/6610 (Ashland Chemical Co.), a two-part polyurethane adhesive, and Fusor 320/323 (Lord Corporation), a two part epoxy adhesive. Both adhesives are proprietary materials. Pliogrip 6600 consists of a mixture of polyurethane polymer (~45%), modified methylene diphenyl isocyanate (~22%), poly(methylenephenylene) polyisocyanate (~8%), and talc

(~25%). Pliogrip 6610 contains two polyols (~88%), a polyurethane polymer (3%), piperazine (~3%), and amorphous silica. Fusor 320 is a bisphenol A type epoxy resin (~60%) compounded with reinforcing agents (~40%). Fusor 323 is a polyamide resin (~60%) compounded with reinforcing agents (~40%). Phenol, ACS reagent grade of 99+% purity, purchased from Aldrich, was used as received. Methylene diphenyl diisocyanate (MDI) was obtained from Eastman Kodak and purified by distillation under vacuum at 170°C. Diglycidyl ether of bisphenol A (DGEBA) was received from Dow Chemical. It was purified by recrystallization from 56/44 (v/v) ethoxy ethyl ether and methyl isobutyl ketone followed by washing with methanol and then with hexane. Methylene chloride, ACS reagent grade, purchased from J. T. Baker, was used as received.

3.2. Preparation of samples

Three specimen geometries were used: single lap shear, wedge, and butt torsion (See Figure 22). Sample dimensions are given in Tables 2-4. In order to assure a uniform bondline thickness and good specimen alignment, butt torsion samples were assembled using a special jig shown in Figure 23.

All phase α-SMC/urethane/ELPO steel samples were assembled at the Ashland Laboratory, Ashland, Ohio. The adhesive mixture was prepared using an industrial mixer. All the other samples were assembled at VPI. The adhesive mixture was prepared by placing the two components in plastic bags and kneading the bags until thoroughly mixed, usually 1.5-2 min.

3. 2. 1. SMC/Urethane/ELPO steel samples

SMC adherends were primed with Pliogrip 6036 (a diisocyanate-containing primer)

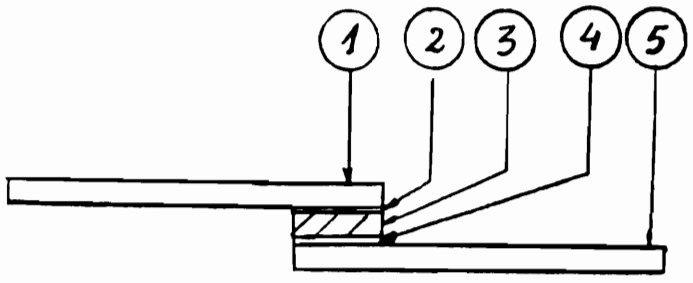

Lap shear

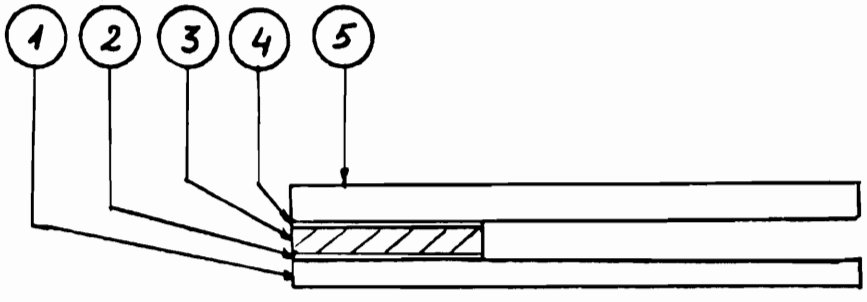

Wedge

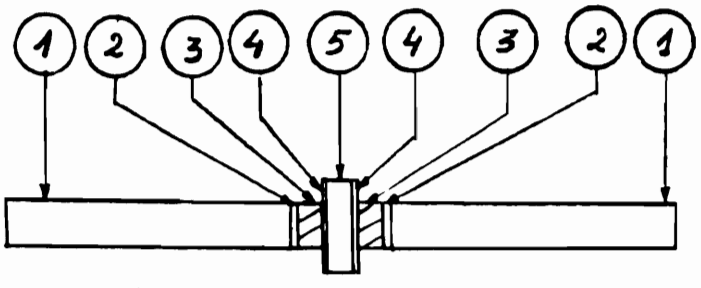

Butt torsion

Figure 22. Specimen geometry:

1. Metal adherend
2. Primer
3. Adhesive
4. Primer
5. SMC adherend

Table 2.

Dimensions of SMC/ELPO Steel Specimens

Specimen Geometry	Dimensions of SMC Adherend	Dimensions of Steel Adherend	Bonded Area	Adhesive Thickness
Lap Shear	1" x 4" x 0.100"	1" x 4" x 0.85"	1 sq. in.	3.5 ± 0.5 mm
Wedge	1" x 6" x 0.200"#	1" x 6" x 0.85"#	2 sq. in.#	3.5 ± 0.5 mm#
	4 "x 6" x 0.200"*	4" x 6"x 0.85"*	8 sq. in.*	3.5 ±0.5 mm*
Butt Torsion	ϕ = 1.25" L = 0.100"	ϕ = 1" L = 6"	0.8 sq. in.	3.5 ± 0.5mm

Only for Budd SMC/ELPO steel samples.

* Only for phase α- SMC/ELPO steel samples.

ϕ= diameter

L = length

Table 3.

Dimensions of Polyurea/ELPO Steel Specimens.

Specimen Geometry	Dimensions of SMC Adherend	Dimensions of Steel Adherend	Bonded Area	Adhesive Thickness
Lap Shear	1" x 4" x 0.14"	1" x 4" x 0.85"	1 sq. in.	3.5 ± 0.5 mm
Butt Torsion	ϕ = 1.25" L = 0.14"	ϕ = 1" L = 6"	0.8 sq. in.	3.5 ± 0.5 mm

ϕ = diameter

L = length

Table 4.

Dimensions of Phase α-SMC/Aluminum Specimens

Specimen Geometry	Dimensions of SMC Adherend*	Dimensions of Aluminum Adherend	Bonded Area	Adhesive** Thickness
Lap Shear	4" x 1" x 0.100" 4" x 1" x 0.200"	4" x 1" x 0.125"	1 sq. in.	3.5 ± 0.5 mm, 1.25 ± 0.25 mm
Wedge	6" x 1" x 0.200"	6" x 1" x 0.190"	2 sq. in.	3.5 ± 0.5 mm, 1.25 ± 0.25mm
Butt Torsion	ϕ = 1.25" L = 0.100"	ϕ = 1" L = 6"	0.8 sq. in.	3.5 ± 0.5mm, 1.25 ± 0.25mm

* The dimensions of the SMC adherend for lap shear samples were 4" x 0.100" if not otherwise mentioned.

**The thickness of the adhesive was 3.5 ± 0.5 mm if not otherwise mentioned.

ϕ = diameter

L = length

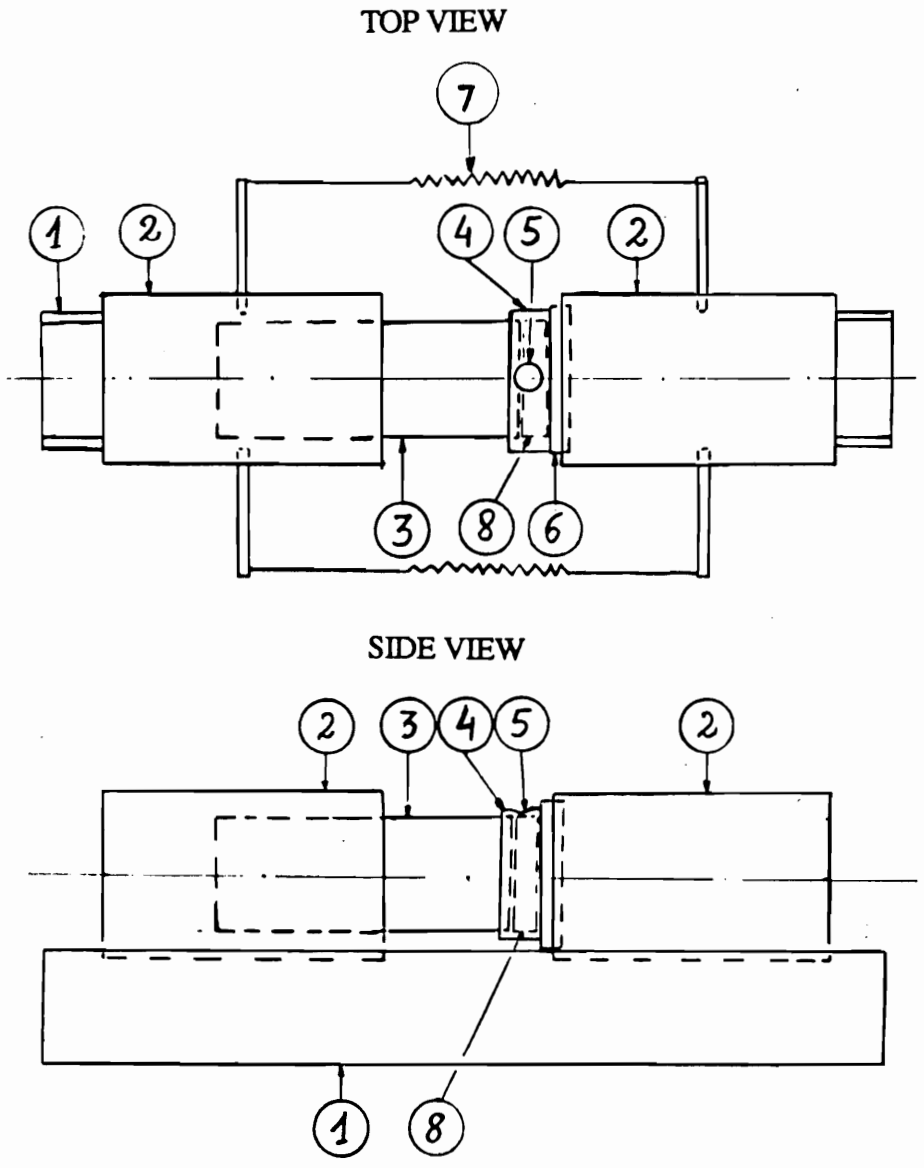

Figure 23. Jig for butt torsion samples preparation.

1. Aluminum channel
2. Aluminum cylinder
3. Metal adherend
4. Teflon cylinder
5. Hole for adhesive
6. SMC disc
7. Extension springs (not shown in the side view)
8. Adhesive

using a Kim-wipe tissue saturated with primer solution. Before the application of the adhesive, the steel adherends were wiped with a dry Kim-wipe-type tissue to remove dust. Bonds were prepared using Pliogrip 6600/6610 adhesive. The bonded specimens were cured at room temperature for about one hour and then additionally cured for 30 min. in a forced air oven maintained at 149°C (300°F).

3.2.2. Phase α-SMC/urethane/phase α-SMC lap shear samples

These samples were prepared following the procedures described for SMC/urethane/ELPO steel specimens, except that both adherends were phase α-SMC material with the dimensions of 1" x 4" x 0.100". The bondline thickness was 3.5 mm.

3.2.3. Polyurea/urethane/ELPO steel samples

These samples were prepared according the the procedures for SMC/urethane/ELPO steel samples with the exception that the polyurea adherends were not primed. The polyurea adherends were wiped with a dry Kim-wipe-type tissue to remove dust.

3.2.4. Budd SMC/epoxy/ELPO steel samples

Before the application of the adhesive, both the SMC and the ELPO treated steel adherends were wiped with a dry Kim-wipe-type tissue to remove dust. Bonds were prepared using Fusor 320/323 adhesive. All bonded specimens were cured 10 min. at 93°C (200°F) followed by a 30 min. postcure at 149°C (300°F).

3.2.5. Phase α-SMC/urethane/aluminum samples

SMC adherends were primed with Pliogrip 6036, a diisocyanate-containing primer.

The aluminum adherends were alkaline cleaned or solvent (CH_2Cl_2) cleaned. For alkaline cleaning the aluminum adherends were treated in a 5% (w/w) aqueous solution of NaOH at 70°C (158°F) for two min.; washed with 50% (w/w) aqueous solution of concentrated HNO_3 at room temperature for one min.; rinsed thoroughly with distilled water and dried 30 min. in an oven at 110°C (230°F). Solvent cleaning consisted of wiping the aluminum adherends with solvent saturated tissues. The diisocyanate primer was applied with a Kim-wipe tissue saturated with primer solution. The primed adherends were dried at room temperature for about 30 min before bonding. Phenolic primer was applied by dipping the aluminum adherends in primer. The primed adherends were dried for about 10 min at room temperature and then heated at 177° C in a forced air oven for 30 min. Before application of the epoxy primer, the two components were mixed in a 1:1 proportion by volume and the mixture was left to prereact at room temperature for one hour. Then the primer was applied by dipping the aluminum adherends in primer. The primed adherends were dried at room temperature for about 10 min and then heated at 82°C for 5 min in a forced air oven. In most cases the cleaned aluminum adherends were primed. All specimens bonded with urethane adhesive were cured at room temperature for about an hour followed by curing at 149°C (300°F) in a forced air oven for 30 min, according to the indications of the manufacturer.

3.3. Durability testing

The experimental matrix for durability testing involves combinations of the following factors:

- sample geometry
- temperature
- humidity

- level of stress

- adhesive type

- adherend type

- adherend surface pretretment

- adherend thickness

- bondline thickness

To determine a reference failure strength, "as prepared" samples (i.e. not exposed to stress and environmental conditioning) were tested in the Instron and their ultimate failure force (moment) was determined. Then the durability tests were initiated. During the durability tests, most of bonded specimens with or without load were tested at fixed conditions of temperature and humidity (static tests). Phase-α-SMC/urethane/ELPO steel samples were exposed also to an environmental cycle. The environmental cycle consisted of the following steps:

16 hrs	97% RH, 38°C (100°F)
2 hrs	RT (~22°C)
2 hrs	dry air, 82°C (180°F)
2 hrs	-30°C (freezer)
2 hrs	5% w/w aqueous NaCl spray

Most of the durability tests were conducted over a seven day period, which was considered a practical and reasonable duration for durability evaluation by short time testing in harsh conditions of temperature and humidity. However, several tests were performed over a longer period of time (14-30 days) in order to determine also the effect of exposure time on durability.

Individual insulated containers with temperature controllers were used to house the samples during the tests. A Fisher brand upright freezer was used to maintain samples at

-30°C. The humidity was measured with an Omega RH-30 humidity indicator which was calibrated with an Omega RH-30-CAL humidity calibration kit.. The samples were maintained under stress using the stressing devices described below.

A cylindrical steel pipe capped with a tension spring and retaining plate and containing a retaining pin at the bottom of the cylinder was used to hold the lap shear sample at a fixed load (see Figure 24). Initially, the ultimate failure force for lap shear samples and the spring constant for every tension spring were determined by Instron testing. Individual lap shear specimens were loaded into the test fixture at room temperature, the tension spring length was adjusted to obtain the selected stress level, and the sample-tension apparatus was placed into the particular environmental container and the test initiated. At appropriate times, the sample-tension holders were transferred to the various environmental containers.

For wedge samples, the displacement of the adherends versus load and and the ultimate failure load were determined by Instron testing. Stress was applied to most wedge samples by driving a wedge between the metal and composite panels to produce a displacement of the adherends corresponding to the desired level of stress in the sample (Figure 25), and then the samples were placed in the environmental chambers. For the wedge experiments this procedure is equivalent to a constant displacement mode. It was noted that during the experiments the 0.200" SMC adherend deflected about ~0.15" at the non-bonded end of the plate. Some wedge samples were tested under constant stress using a device consisting of a wedge, an aluminum channel, two extension springs and two eyebolts (Figure 26). The wedge sample was placed in the aluminum channel and the wedge was inserted between SMC and metal and connected by springs at both ends. All springs were calibrated by hanging weights and measuring the lengths versus load. The length of the springs was adjusted using the eyebolts to obtain the selected stress level, and

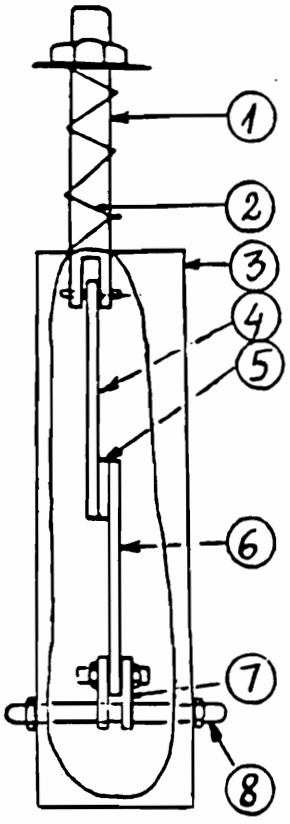

Figure 24. Stressing device for lap shear samples.

1. Threaded rod
2. Compression spring
3. Steel cylinder
4. Metal adherend
5. Adhesive
6. SMC adherend
7. Clamp
8. Pin

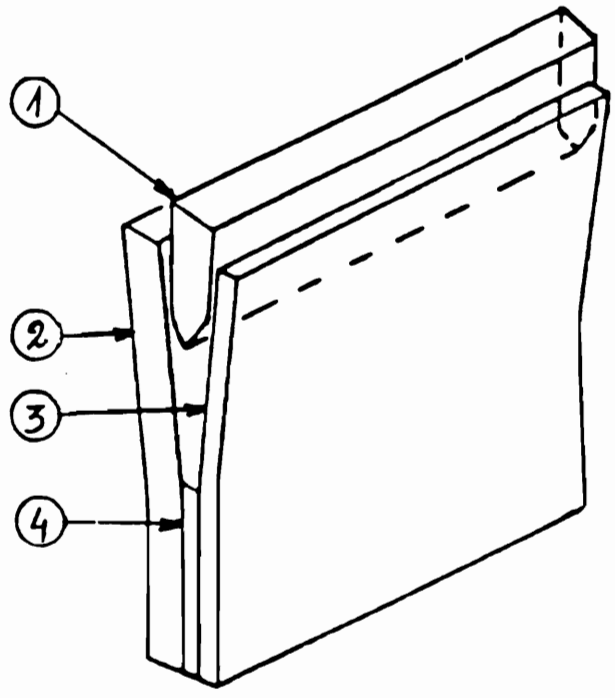

Figure 25. Stressing device for wedge samples (constant displacement).

1. Wedge
2. SMC adherend
3. Metal adherend
4. Adhesive

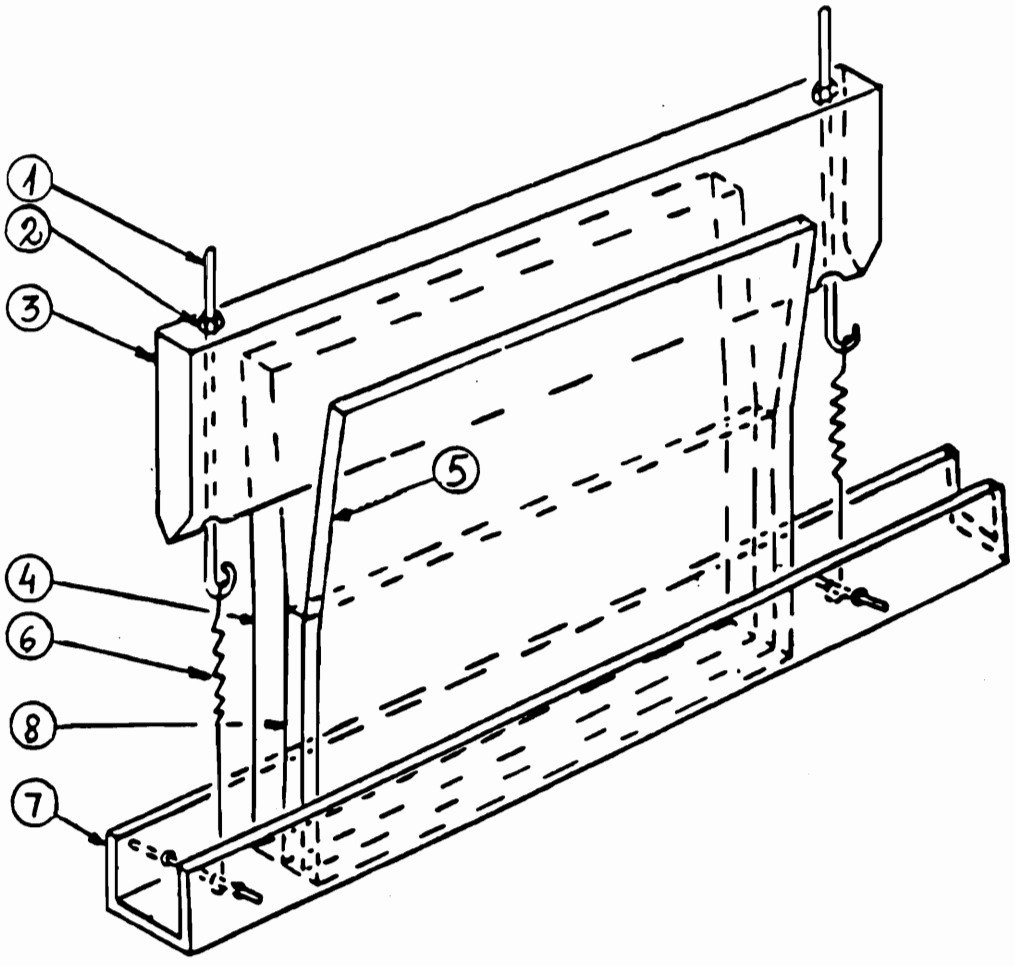

Figure 26. Stressing device for wedge specimens (constant stress).

1. Eye bolt
2. Nut
3. Wedge
4. SMC adherend
5. Metal adherend
6. Extension spring
7. Aluminum channel
8. Adhesive

the samples were placed into the environmental chambers. Because the SMC adherend deformed during the tests, it was necessary periodically to adjust the springs to maintain constant loading. The wedge samples were loaded in the constant displacement mode unless otherwise noted.

The butt torsion samples were maintained under stress using a special apparatus shown in Figure 27. In the test fixture, the samples were placed vertically. Each sample had two holes (one in the upper half, the other in the lower half) through which a rod was inserted. The lower rod was fastened in a fixed position to the apparatus. The upper rod was attached to the apparatus through extension springs (loaded in opposite directions) which produced a torsion moment. All springs were calibrated by hanging weights and measuring length versus load. The length of the springs was adjusted to produce the selected torsion moment and the apparatus was placed into the environmental apparatus.

Some samples failed during the tests and the time to failure was recorded. The samples which did not fail during the exposure scheme were removed and their residual strength was determined using an Instron machine. The residual strength of the exposed samples was compared with the reference strength for that particular type of sample.

At least five measurements were made for each kind of sample. In the tables the data will appear in the form of $\bar{x} \pm s$, where $\bar{x}$ is the average and s is the standard deviation. The $\bar{x}$ and s values were calculated using the following formulae:

$$\bar{x} = \frac{\Sigma x_i}{N} \; ; \; s = \sqrt{\sum_{i=1}^{N} \frac{(x_i - \bar{x})^2}{N - 1}}$$

where, x_i = values of individual measurments, and N = number of measurments.

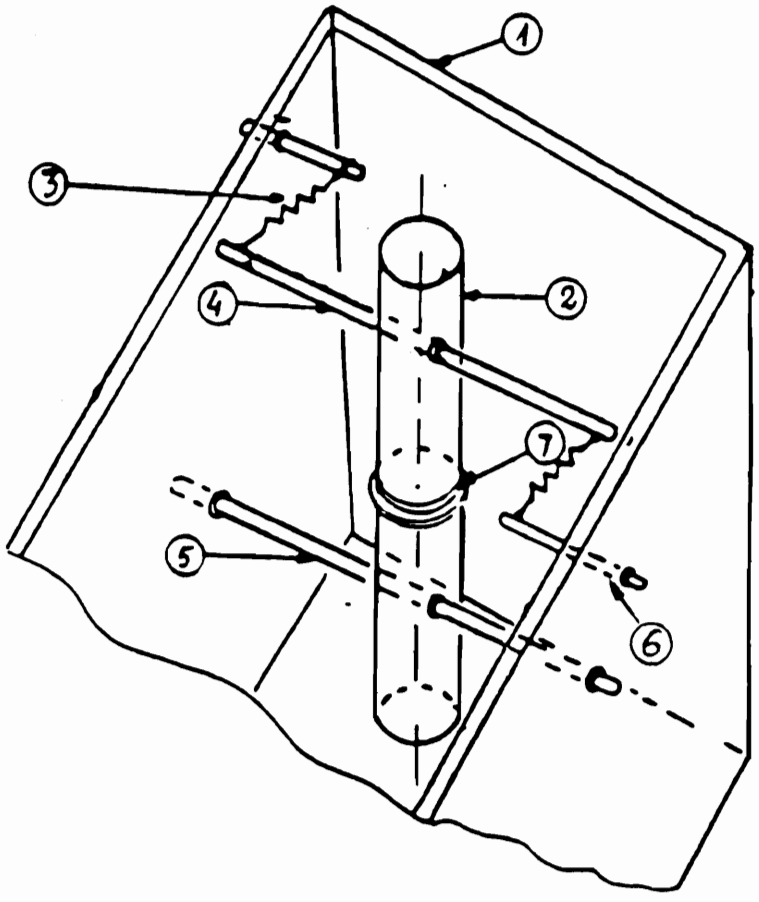

Figure 27. Stressing device for butt torsion samples.

1. Metallic frame
2. Butt torsion sample
3. Extension spring
4. Upper rod
5. Lower rod fastened to the metallic frame
6. Rod fastened to the metallic frame
7. Adhesive

The distribution of failure modes: ie., D, delamination of composite; A, adhesive; C, cohesive was determined by visual inspection of the failed sample surface.

In the failure experiments, two specimens were obtained: one specimen was principally adhesive and the other composite or metal depending on the type of specimen tested. For a better determination of the mode of failure XPS and SEM measurements were carried out for portions of the failed surfaces which exhibited visually determined adhesive failure. For these measurements the side showing bulk adhesive was designated the adhesive side and the other SMC (composite) side or metal side.

3.4. Instrumental techniques

3.4.1. Scanning electron microscopy (SEM)

The topographical analysis of failed surfaces was accomplished using scanning electron microscopy. Generally, the samples analysed by SEM had been previously studied using XPS. Samples were sputter-coated with a thin gold film (~200Å) using an Edwards S150B sputter coater to reduce charging of the sample by the electron beam. Scanning electron micrographs were taken with a ISI SX-40 instrument at a voltage of 10 kV.

3.4.2. X-ray photoelectron spectroscopy (XPS)

XPS was used for surface characterization in all phases of this research. Chemical composition of all adherends was determined before and after various treatments. The failed surfaces were also analyzed by XPS to determine the locus of failure. Sample size was approximately 17 x 15 mm. Samples were cut with a saw, the region to be analyzed was wrapped in aluminum foil to prevent composite dust, produced during cutting operation, from contaminating the surface to be analyzed. Surface chemical analysis was accomplished via X-ray photoelectron spectroscopy with a Perkin-Elmer PHI 5300

photoelectron spectrometer. Photoelectrons, generated using Mg K_α radiation ($h\upsilon$ = 1253.6 eV), were analyzed in a hemispherical analyzer, and detected using a position sensitive detector. The spectra were accumulated under control of a Perkin Elmer Model 7500 computer. In the presentation of the elemental results, photoelectron spectral peak areas were measured and subsequently scaled to account for ionization probability and an instrumental sensitivity factor to yield results which are indicative of surface concentration in atomic percent. The precision and accuracy for the concentration evaluations are about 10% and 15%, respectively.

The binding energy scale was calibrated by setting the CH_n C 1s binding energy at 285.0 eV [169]. Survey scans were taken from 0 to 1100 eV and narrow scans were obtained on the significant peaks in the survey scan spectra. To obtain the distribution of various functional groups, curve fitting of the carbon photopeaks was accomplished for the reference surfaces involved in the adhesive bonds. Based on this, C 1s spectra corresponding to a limited number of combinations from the whole variety of mixed failed surfaces which could result during testing were synthesized. The C 1s spectra of the failed surfaces were compared with the synthesized C 1s spectra and in correlation with the atomic concentration results and the SEM results were used to aid in determining the nature of the failed surfaces. The curve fitting procedure assumed FWHM value of 1.55 ± 0.05eV and peaks of Gaussian shape for carbon. Working with polymethyl methacrylate standards, Burtoff [170] found for the CH_n, -COR, and $-CO_2R$ functionalities FWHM (Full width at half maximum) values of 1.60, 1.55, and 1.55 eV, respectively. The -COR, -NCO, and >C=O, carbon 1s binding energies were set at 286.5 ± 0.05eV, 286.8 ± 0.05eV, and 288.0 ± 0.05 eV [169], respectively. The $-CO_2R$ binding energy was set at 289.1 ± 0.05 eV. For polyalkyl acrylates, Clark [171] observed that the C 1s binding energy corresponding to $-CO_2R$ functionality is shifted ~ 4 eV to a higher binding energy

from that of the CH_n functionality (285.0 eV). For polymethyl methacrylate, Burtoff (170) found the C 1s binding energy for the -CO_2R peak at 4.2 eV higher binding energy than that for the CH_n peak (285.0 eV).

3.4.3. Fourier Transform Infrared Spectroscopy (FTIR)

The PAS-FTIR (photoacoustic FTIR) spectra were obtained using a Nicolet 5DBX FTIR spectrometer and a MTEC, Model 100 photoacoustic cell and detector. The photoacoustic sample chamber was purged with helium for 5 minutes. Samples were in the form of powder (DGEBA and carbon black) or very small crystalls (phenol and MDI). The instrument resolution was 4 cm^{-1}. The spectrum was obtained using a background reference of Norit A alkaline decolorizing carbon black.

Transmission FTIR spectra for DGEBA were obtained using a Nicolet MX1 spectrometer. The as received DGEBA sample was prepared by deposition of several drops of 10g/100ml DGEBA solution in methylene chloride on salt plates and evaporation of the solvent. The thermally heated DGEBA (a viscous liquid) was prepared by deposition of sample on salt plates.

Thin films of primer on metal were studied by reflection absorption FTIR spectrometry using a Nicolet 5DXB spectrometer and a reflection absorption attachment shown in Figure 28. The incidence angle is 85°. A TGS detector was used. A wire grid polarizer polarizes the entering beam before it hits the sample surface. The sample size was 37 x 37 mm. The sample chamber was purged with nitrogen for one hour before a spectrum was obtained. The aluminum substrates were alkaline cleaned following the same procedure used for aluminum adherends (See 3.2.5). The gold substrates (gold mirrors) were cleaned in a hot (~ 125°C) solution 75/25 (v/v) of conc. H_2SO_4 /30% H_2O_2 solution for 30 sec, rinsed with distilled water, washed with methylene chloride and allowed to dry

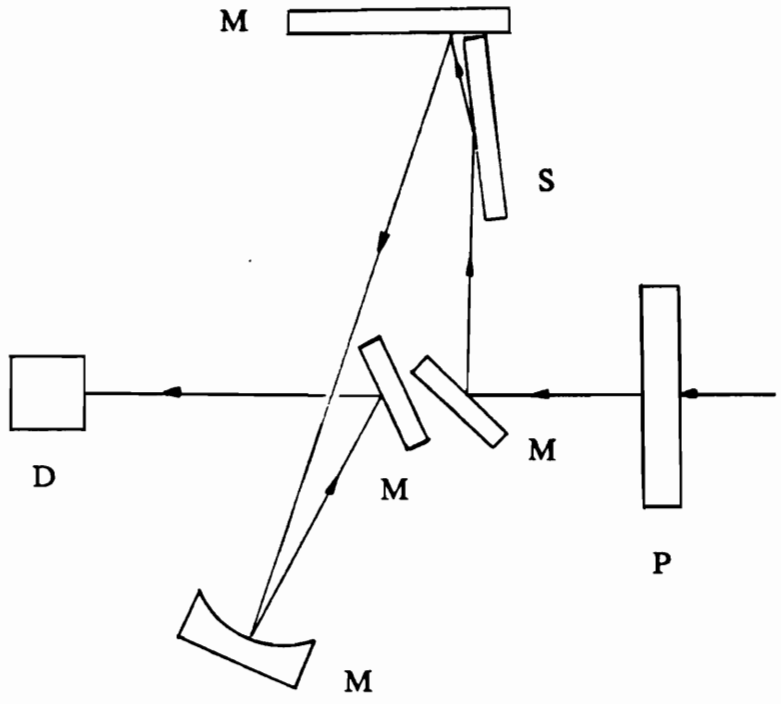

Figure 28. Reflection-absorption attachment
P = polarizer
M = mirror
S = sample
D = detector

at room temperature for several minutes. In measuring the spectra, a background spectrum for the metallic substrate was taken first. Then the metal surface was covered with a thin layer of primer by spin coating using solutions of primers. Methylene chloride was the solvent used for all samples. A spectrum of the primer deposited on metal was obtained. The sample (primer on metal) was heated at 150°C in vacuum (2×10^{-4} torr) for 30 min. to simulate the curing process. A spectrum was taken for the thermally treated sample. Some samples were washed with methylene chloride and again analyzed by FTIR. All sample spectra were ratioed to the background spectrum of the metallic substrate used.

3.4.4. Ellipsometry

The film thicknesses for spin coated samples on gold were determined by ellipsometry using a Gaertner L 116A dual mode automatic ellipsometer. Both linear and circular polarization were employed and a continuous rotating analyzer was used with automatic data sampling at 72 points for each state of polarization. A 1 mW helium-neon laser (632.8 nm) was used as the incident light source and the spot size analyzed was 1 mm^2. The surface films were assumed to be transparent at this wavelength. First, the optical constants for cleaned gold mirrors were measured at an incidence angle of 70°. Then, the film thicknesses were measured at an incidence angle of 70 ° using the values of refractive indexes found in literature: 1.5701 for DGEBA [172], and 1.5408 for phenol [173].

3.4.5. Instron

Failure force was determined using an Instron Model 1123 machine with a thermally controlled chamber, Model 3116. The Instron machine was calibrated electronically. The

lap shear specimens were tested in tension. The failure force for the wedge samples was determined by pushing a wedge between metal and composite panels. A torsional apparatus shown in Figure 29 [174] was used to measure the failure moment for butt torsion samples. The cross-head speed was 1.27 cm/min. (0.5"/min) for lap shear and butt torsion samples and 12.7 cm/min. (5"/min) for wedge samples. Samples were conditioned at the selected testing temperature for 30 min. before testing.

3. 5. Water uptake measurements

Water uptake was measured at 60° C and 85% RH for adhesives and composite materials at conditions where most of the durability tests were performed. The adhesive samples were thin films (100 mm x 100 mm) with thicknesses between 0.32 and 1.1 mm . Diffusion into the edges can be neglected because the thickness is very small compared with the other two dimensions: 0.32 -1.1 mm vs 100 mm. The SMC materials were 75 mm x 75mm x 2.5 mm pieces cut from the as received materials, heated 30 min at 150°C to simulate the effect of the curing process of adhesive bonds. The cut edges of the SMC samples were protected against moisture penetration by painting with nail polish. Samples were placed in environmental chambers at constant temperature and constant humidity and removed periodically and weighed. The humidity was measured with an Omega RH-30 humidity indicator which was calibrated with an Omega RH-30-CAL humidity calibration kit. The equilibrium water uptake, M_{∞},was determined as the weight when there was a change in weight less than 0.02% over a time interval comparable to that required to obtain that value. The equilibrium water concentration, C_{∞}, was calculated by dividing the equilibrium water uptake, M_{∞}, by the initial weight of sample, M_S: $C_{\infty} = M_{\infty}/M_S$ Five measurements were made for each kind of sample. For the adhesive samples the uptake

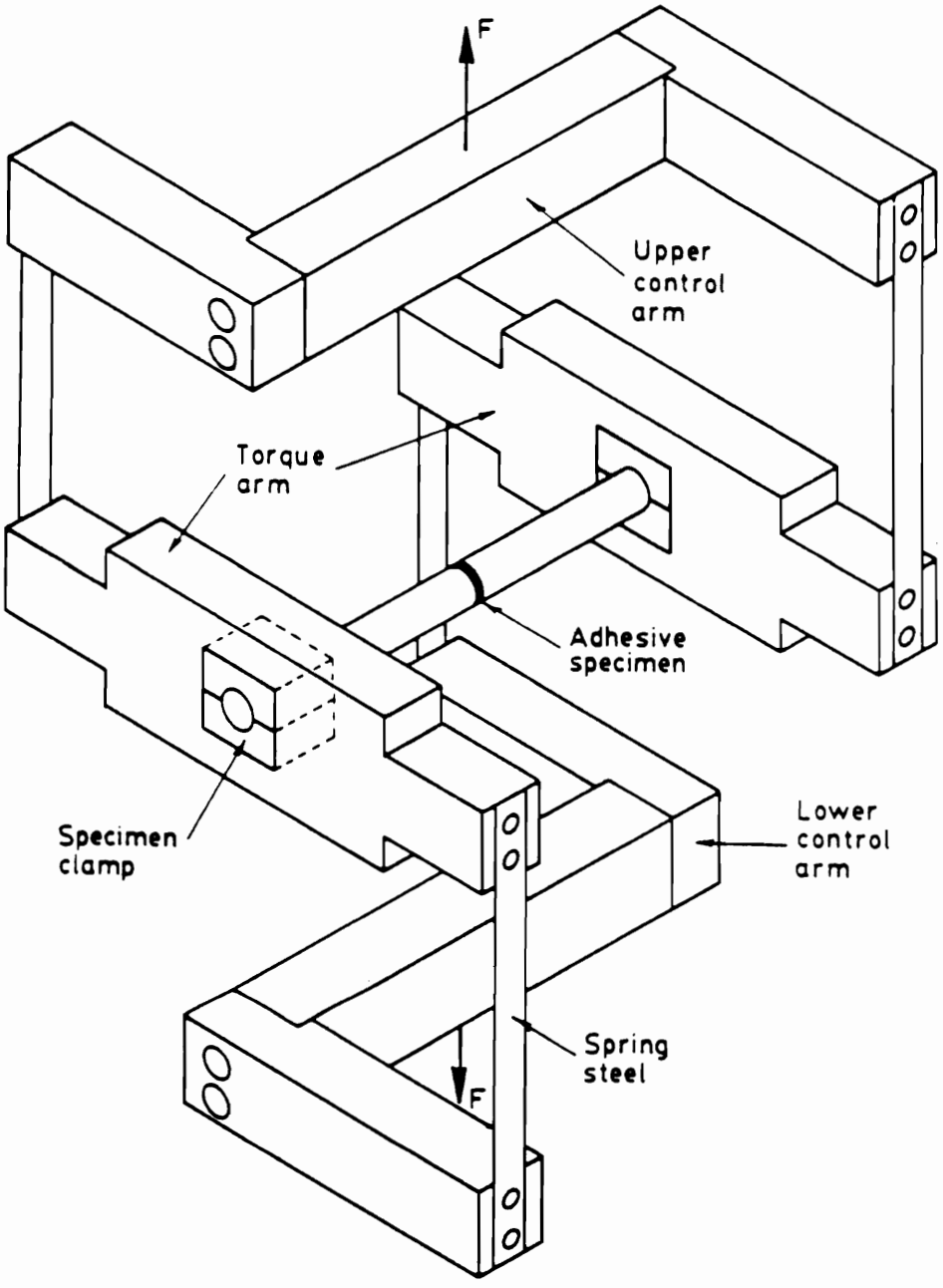

Figure 29. Torsional load apparatus for butt torsion specimens [174].

plots were constructed by plotting the fractional uptake M_t/M_∞ vs $t^{1/2}/l$. M_t is the water uptake at time of exposure and l is half of the film thickness.

4. RESULTS AND DISCUSSION

4.1. Water uptake

The equilibrium water concentrations in adhesives and SMC materials at 60° C and 85% RH are presented in the Table 5. The results show that the polyurethane adhesive absorbs somewhat more water (1.165 ± 0.007%) than the epoxy adhesive (1.060 ± 0.069% at exposure at 60° C in 85% RH. While the equilibrium water concentrations are close for the two adhesives their sorption behavior is different. The water uptake plot for the polyurethane adhesive presented in Figure 30 shows characteristics of Fickian sorption [109] :

a) it is initially linear

b) above the liniar region, the curve is concave against the abscissa

c) the curves for different thicknesses (0.47mm and 1.09mm) coincide

The water uptake plots for epoxy adhesive presented in Figure 31 do not coincide for films of different thicknesses, indicating a non-Fickian behavior. The water uptake plots also show that the rate of moisture absorption for the polyurethane adhesive is higher than that for the epoxy adhesive. The moisture absorption for SMC materials is small: 0.398 ± 0.011% for phase α–SMC, and 0.290% ± 0.017 for Budd SMC. For SMC-25, SMC-65, and SMC-30EA materials exposed at 65°C and 60% RH, Loos et al. [175] found moisture absorptions of 0.50%, 1.25%, and 0.45%, respectively.

4.2. Interactions of aluminum and gold with primers by FTIR

Because of the important role of chemical interfacial interactions in adhesive bonding, it was of interest to study the primer/aluminum interface to determine if chemical interactions between primers and aluminum occur. Reflection absorption FTIR spectroscopy was

Table 5

Moisture Absorption at 60°C and 85% RH

Material	Equilibrium water concentration, C_∞, %
Pliogrip 6600/6610	1.165 ± 0.007
Fusor 330/323	1.060 ± 0.069
Phase α–SMC	0.398 ± 0.011
Budd SMC	0.290 ± 0.017

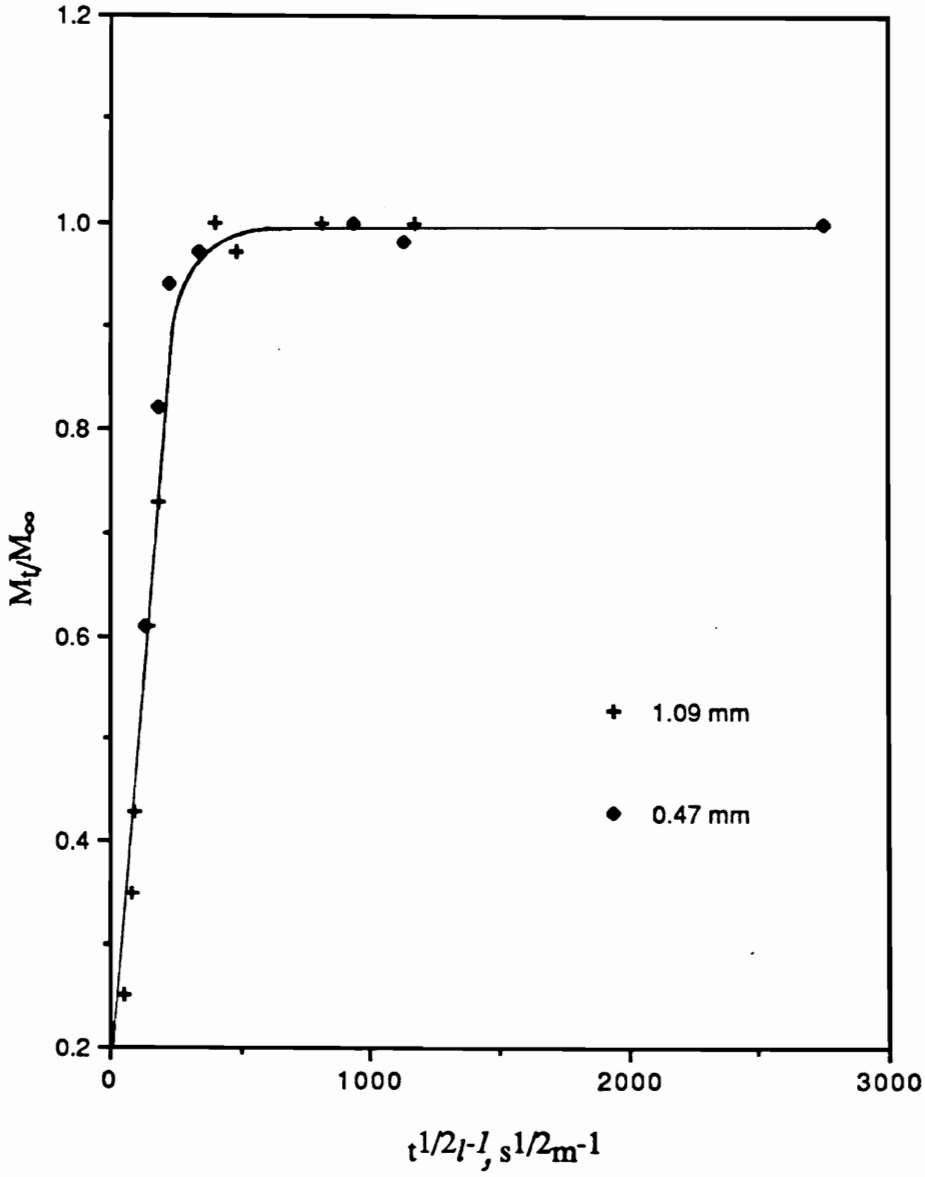

Figure 30. Water uptake plots at 60°C and 85% RH for the Pliogrip 6600/6100 adhesive.

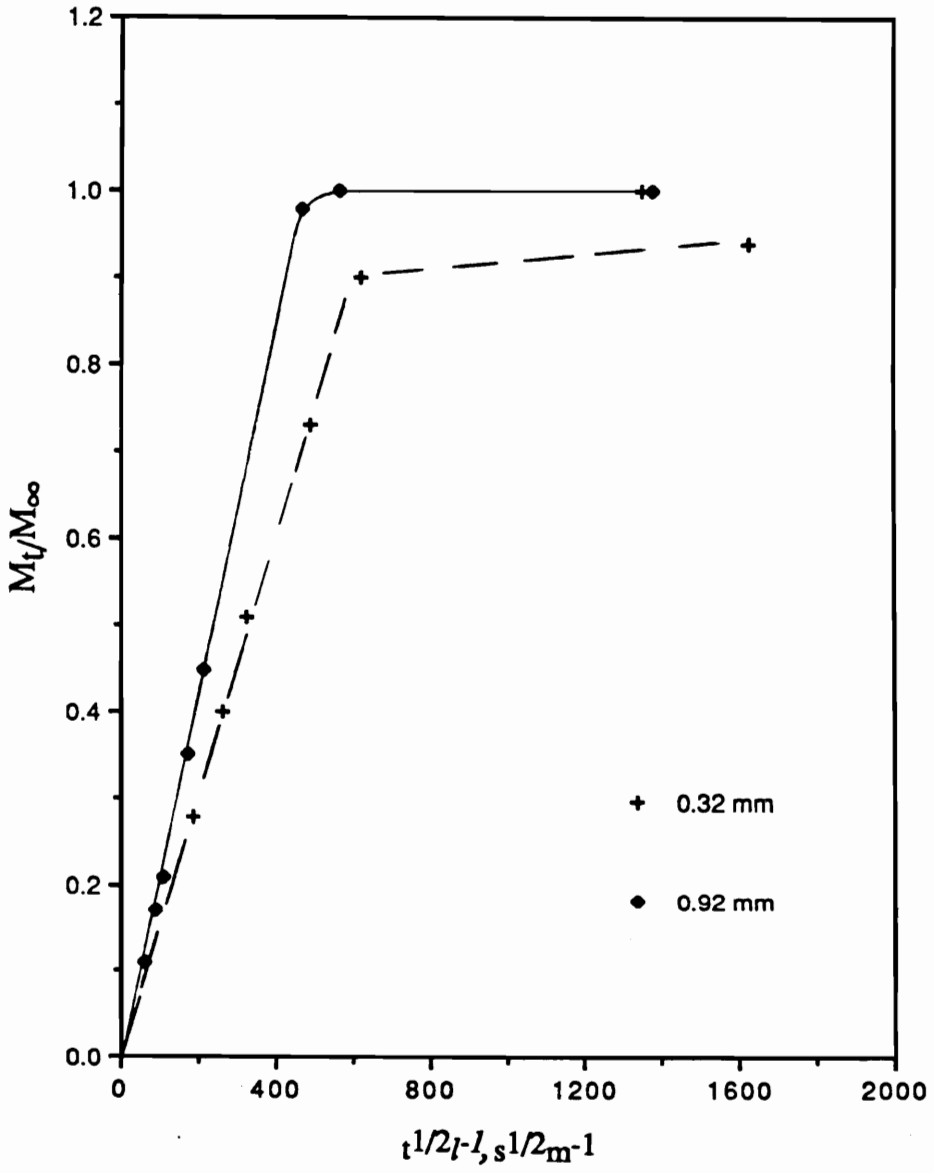

Figure 31. Water uptake plots at 60°C and 85% RH for the Fusor 320/323 adhesive.

selected, because it is an excellent method for studying the chemistry of surfaces (See 2.4.3.3.). The study was conducted using model compounds whose chemical structures are similar or identical with that of the main components of the primers used to prepare adhesive bonds. The chemical structures are given below.

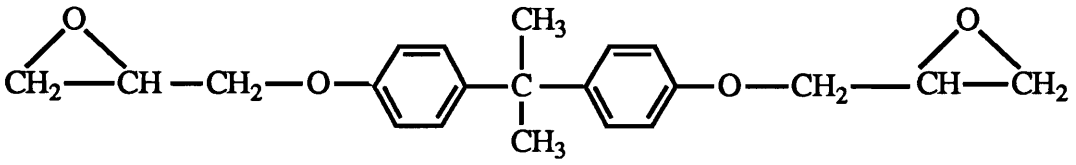

DGEBA (diglycidyl ether of bisphenol A)

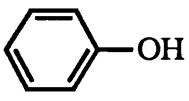

Phenol

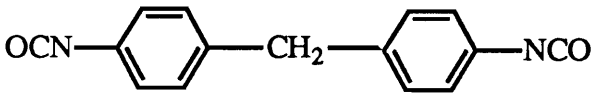

MDI (methylene phenylene diisocyanate)

The primer/gold interfacial interactions were investigated under the same experimental conditions and the results obtained for two systems: primer/ aluminum and primer/gold were compared. Because gold does not have a significant oxidized surface layer [75] it represents a different bonding situation than aluminum. In interpretation of RAS-FTIR data the problems related to peak identification and quantitation mentioned in 2.4.3.3. should be considered.

4.2.1. Epoxy/metal

Figures 32 and 33 present the FTIR spectra for DGEBA films deposited on aluminum from solutions of 0.25 and 10 g/100ml DGEBA/methylene chloride respectively, before and after heating for 30 min at 150° C in vacuum. The peak assignments are given in Table 6 [81, 176]. The thickness of a thin layer of epoxy on

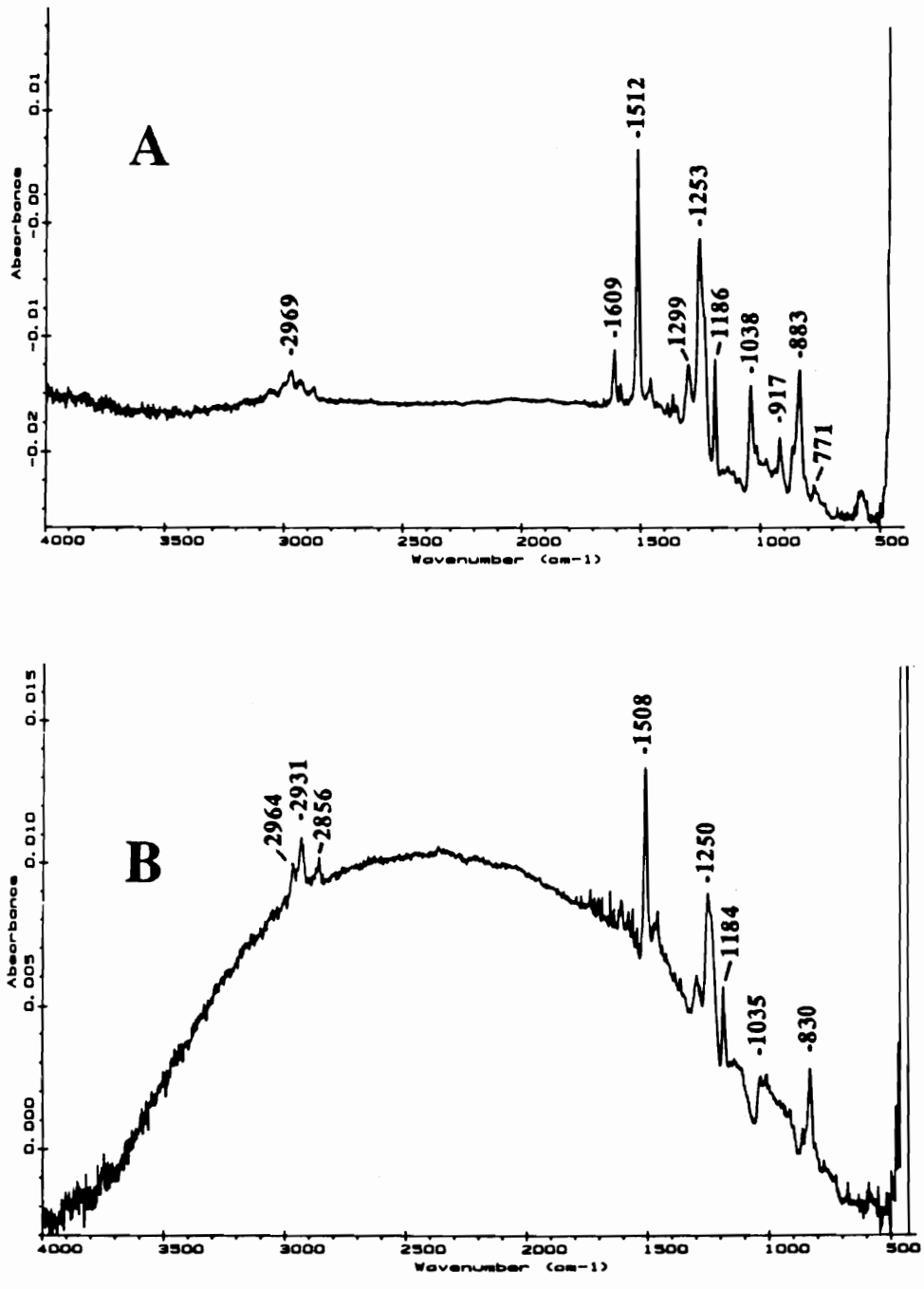

Figure 32. Reflection-absorption spectra of a DGEBA film on aluminum cast from a 0.25 g/100 ml DGEBA/methylene chloride solution.

A. No treatment. Film thickness 8.4 nm.

B. After heating for 30 min at 150°C in vacuum. Film thickness 2.8 nm.

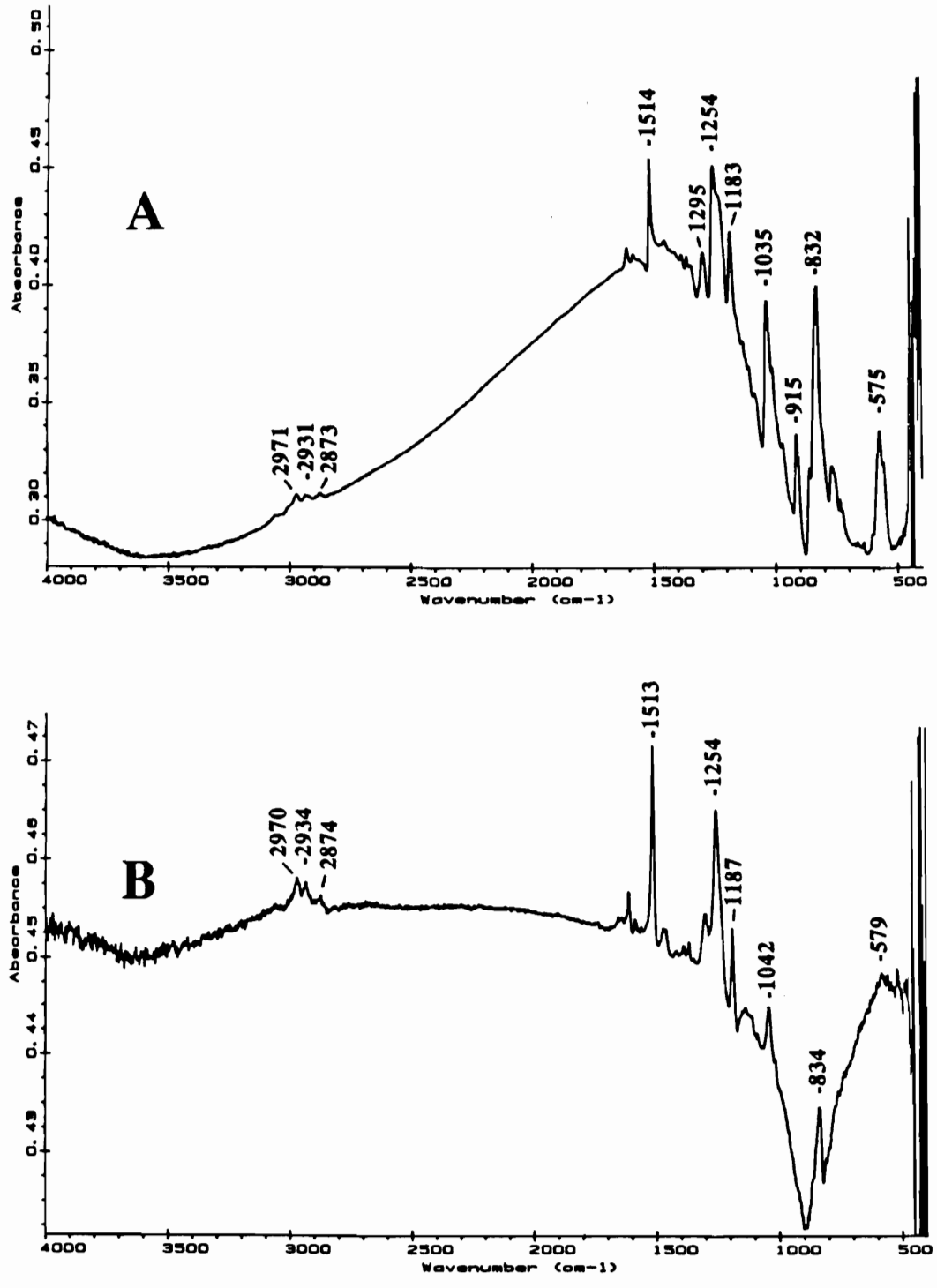

Figure 33. Reflection-absorption spectra of a DGEBA film on aluminum cast from a 10 g/100 ml DGEBA/methylene chloride solution.

A. No treatment. Film thickness 16 nm.

B. After heating for 30 min at 150°C in vacuum. Film thickness 6.8 nm.

Table 6.

Peak assignments for DGEBA

Wavenumber, cm^{-1}	Peak Assignment
3005	C-H asym. str. epoxide
2974	C-H asym. str. CH_3
2930	C-H asym. str. CH_2
2876	C-H sym. str. CH_3
1609	aromatic C-C stretch quadrant str. benzene ring
1512	semicircle str. benzene ring C=C str. benzene ring
1298	- OH in-plane def. CH_2 twisting
1251	aryl - O str. C-O-C asym. str.
1186	C-H in-plane def. C-C str. of Ar-C-Ar
1038	C-O str. C-O-C sym. str.
916	asym. epoxy ring vib.
837	out of plane bending of p-disubstituted benzene ring
770	aromatic C-H out of plane bending
575	not assigned

gold was measured by ellipsometry and used in connection with the 1510 ± 2 cm^{-1} peak absorbance as a reference for film thickness calculation for other samples. The spectra of the two films are similar. For both samples the absorption peak at 916 ± 2 cm^{-1}, characteristic of the epoxy ring, disappears after heating. This indicates that homopolymerization of the epoxy resin takes place at the aluminum surface. The hydroxyl groups existing on the aluminum surface may be involved in this reaction, by initiating the epoxy homopolymerization. Metal oxides and hydroxides are known to catalyze epoxy polymerizations [82, 177]. Figure 34 shows the reflection-absorption spectrum for the alkaline cleaned aluminum. Broad peaks attributed to -OH groups are observed in the 3100 and 3600 cm^{-1} regions indicating the presence of -OH species on the aluminum surface. To determine if the aluminum surface species play a role in the reaction which take place at the aluminum surface additional experiments were conducted.

Bulk DGEBA was heated 30 min at 150°C. Transmission FTIR spectra taken before and after the heating are shown in Figure 35. The absorption peak at 916 cm^{-1} characteristic of the epoxy functionality does not disappear after heating, showing that heating alone does not produce homopolymerization of the epoxy resin. This suggests that the surface species of the aluminum substrate induce homopolymerization of deposited epoxy films upon heating.

Figure 36 shows the spectrum of DGEBA film on aluminum prepared from a 10 g/100ml DGEBA/methylene chloride solution, heated for 30 min at 150°C, before and after washing in methylene chloride for 15 min. A decrease in film thickness from 6.4 nm to 3.6 nm occurred as a result of washing. However the spectrum of the washed specimen is similar to the spectrum taken before washing. This result indicates that most of the epoxy film remains on the aluminum substrate after washing. This suggests a strong bond between the aluminum substrate and the epoxy film, a result of chemical interaction

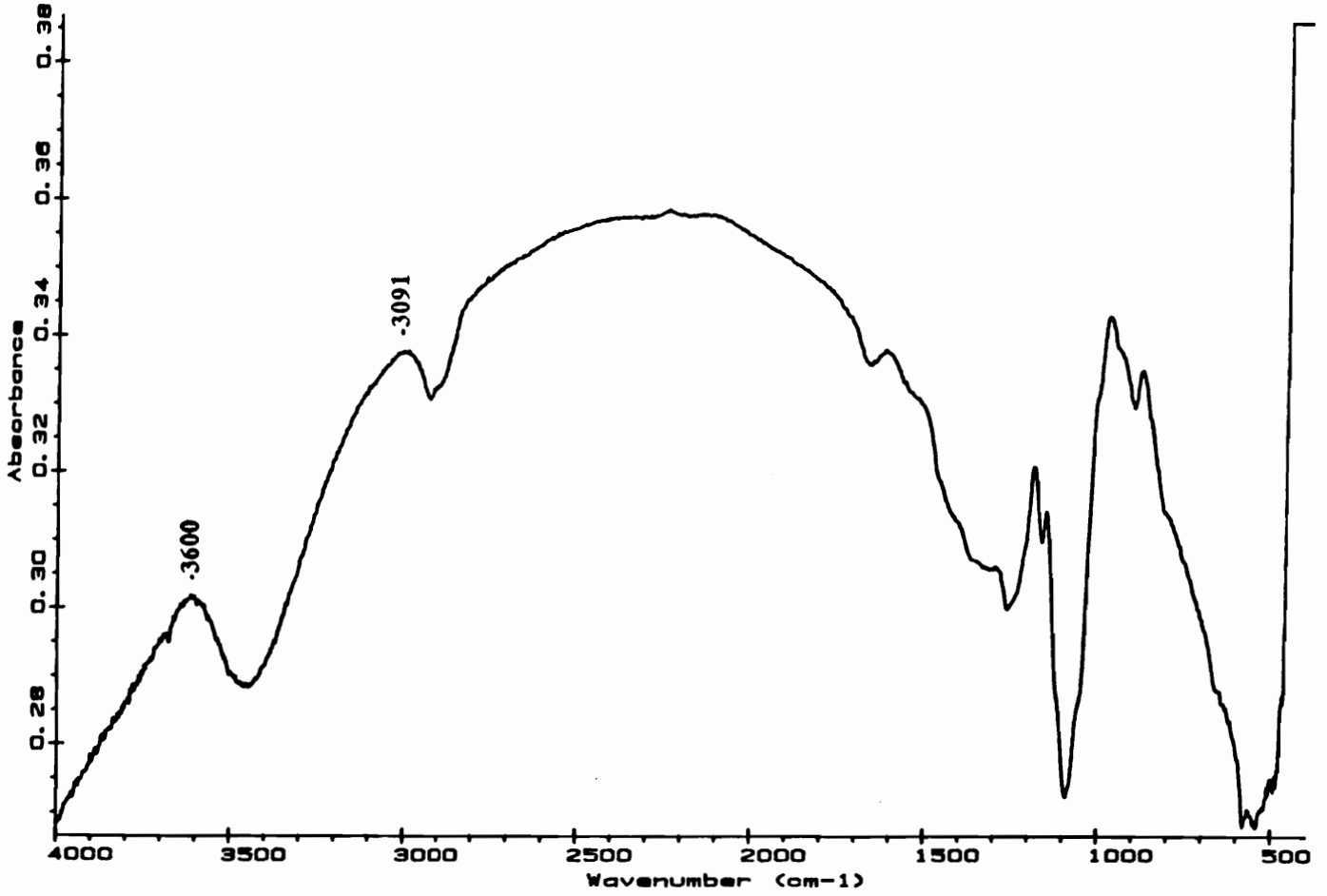

Figure 34. Reflection-absorption spectrum for the alkaline cleaned aluminum.

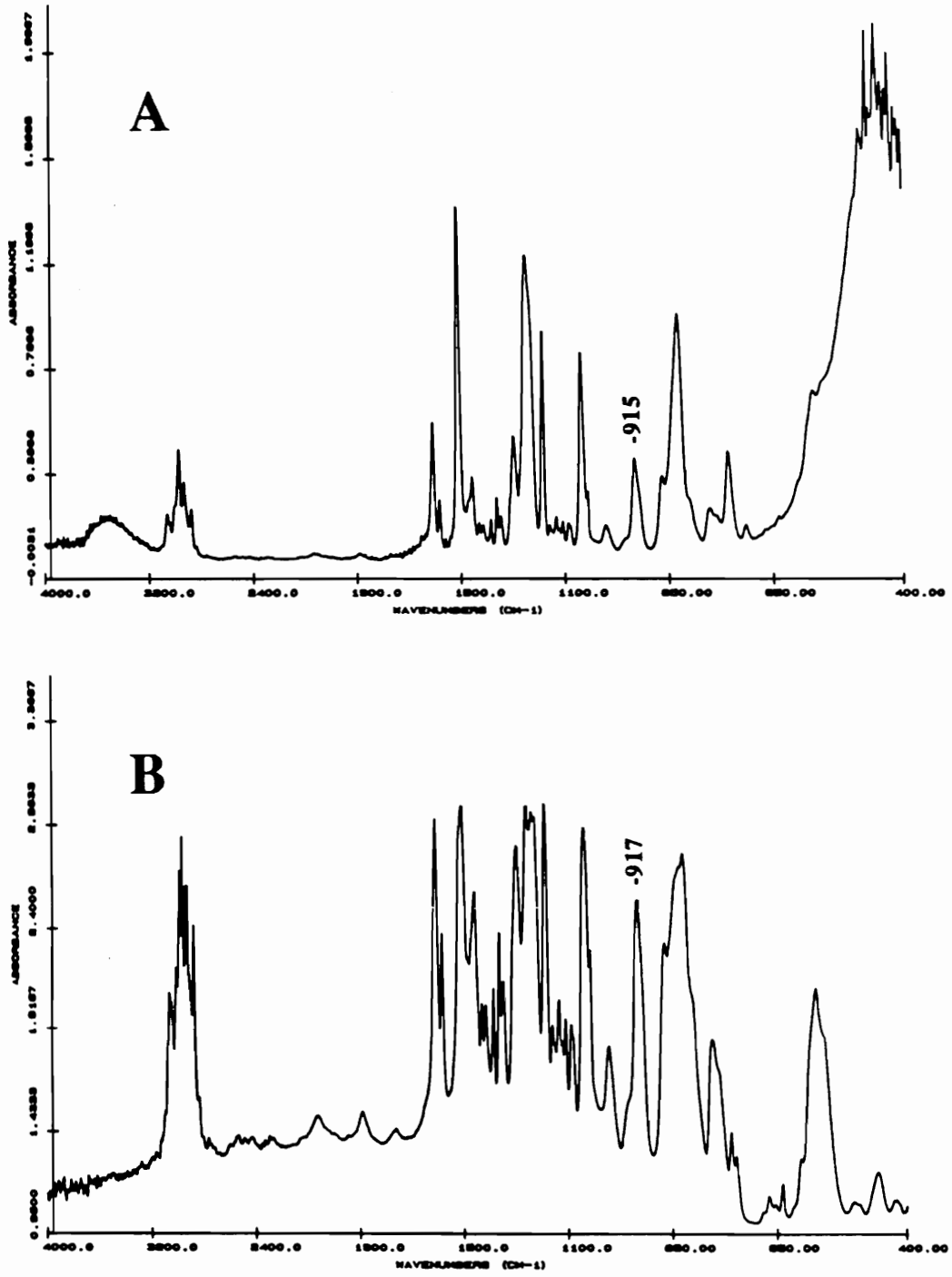

Figure 35. Transmission spectra of DGEBA.
A. No treatment.
B. After heating for 30 min at 150°C.

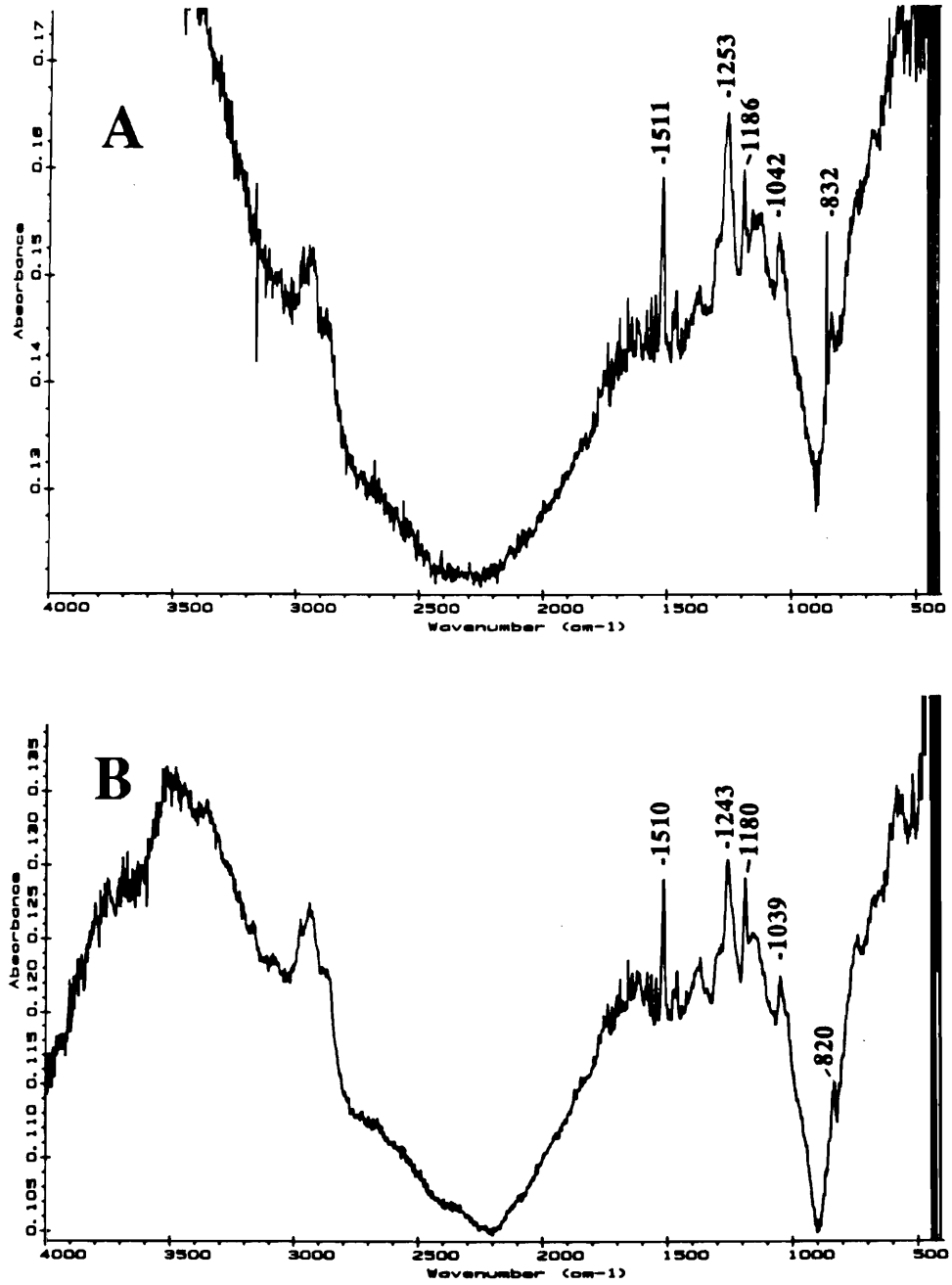

Figure 36. Reflection-absorption spectra of a DGEBA film on aluminum cast from a 10 g/100 ml DGEBA/methylene chloride solution heated for 30 min at 150°C in vacuum.

A. Before washing. Film thickness 6.4 nm.

B. After washing with methylene chloride for 15 min. Film thickness 3.6 nm.

between the active species of the aluminum surface and the epoxy resin at heating. A possible reaction would be:

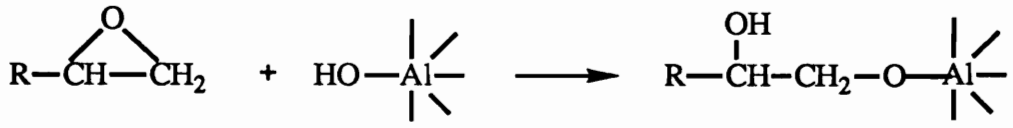

Once the reaction is initiated at the aluminum/epoxy interface, the reaction will self propagate through the epoxy film due to the hydroxyl groups formed on the epoxy resin backbone during the initiation step:

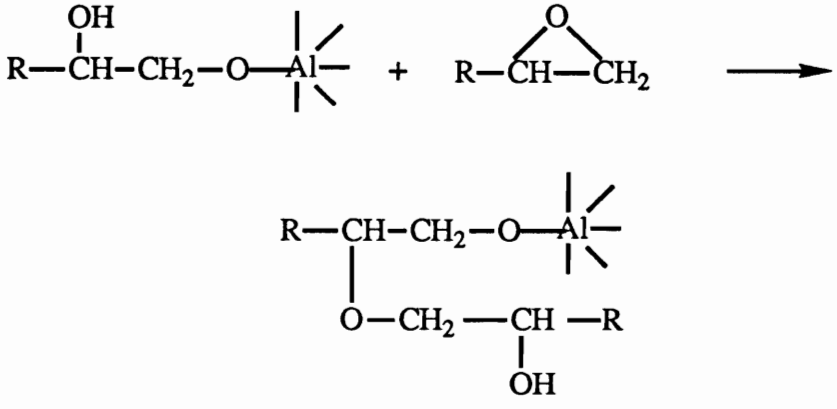

In Figure 37 are presented the FTIR spectra for a DGEBA film on aluminum prepared from a 0.25g/100ml DGEBA solution, before and after washing with methylene chloride for 15 min. The most important changes are the loss of the 916 ± 2 and 1038±2 cm^{-1} peaks. This disappearance may indicate that the epoxy resin was entirely removed from the aluminum surface by washing. However, the presence of absorption peaks at 1510 ± 2, 1251 ± 2, 1186 ± 2, and 835 ± 2 cm^{-1} suggests that some epoxy resin remains on the aluminum substrate after solvent washing. Solvent washing removes most but not all of the uncured epoxy film deposited on aluminum, the film thickness decreases from 10

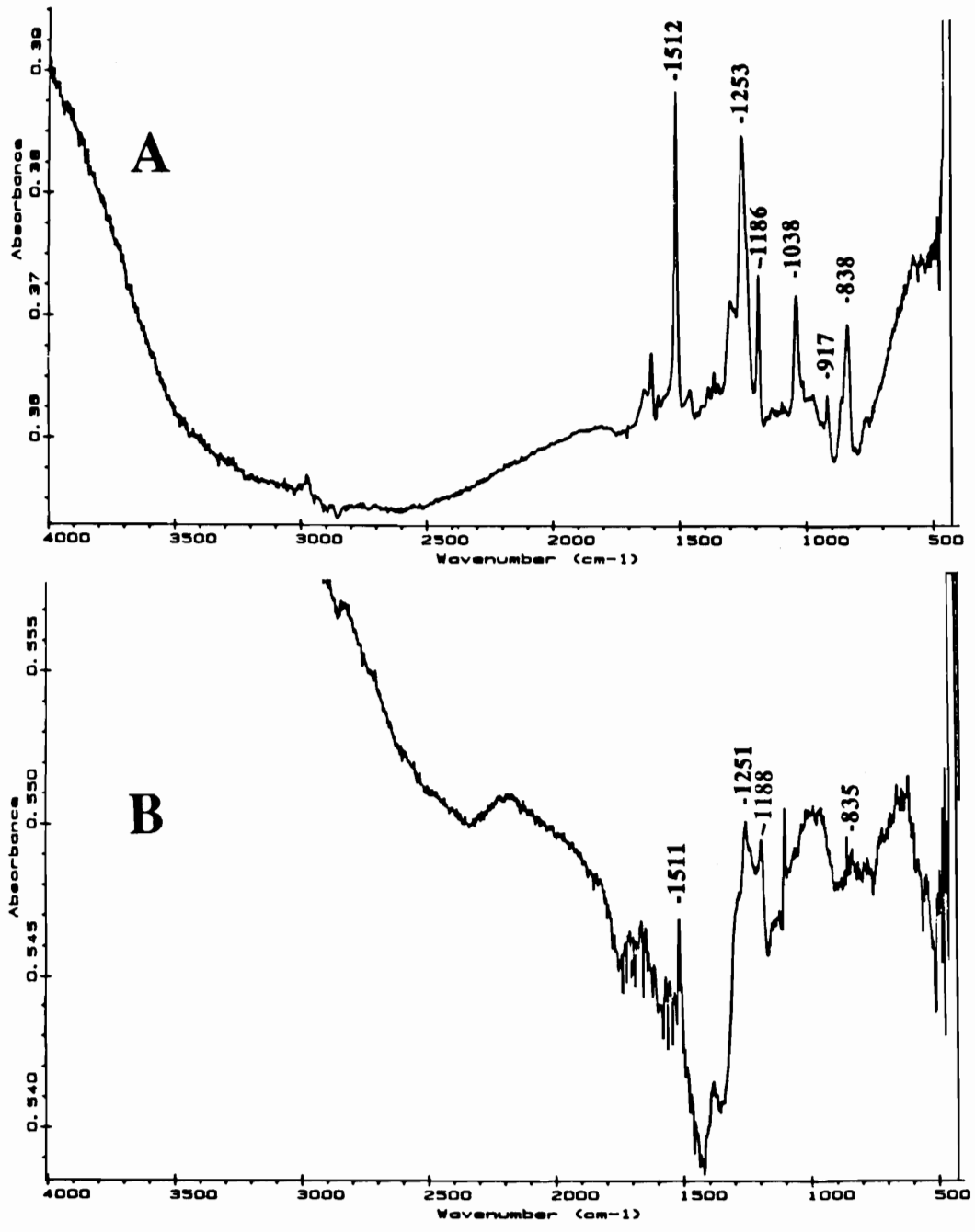

Figure 37. Reflection-absorption spectra of a DGEBA film on aluminum cast from a 0.25 g/100 ml DGEBA/methylene chloride solution.

A. No treatment. Film thickness 10.0 nm.

B. After washing with methylene chloride for 15 min. Film thickness 1.6 nm.

nm to 1.6 nm after washing. The disappearance of the peak associated with epoxy functionality may be due to reaction with the aluminum surface species or to a prefered molecular orientation effect. Such an orientation would be alignment of the C-O dipole moment of the cyclic ether parallel to the aluminum surface. RAS FTIR is not sensitive to functionalities whose dipole moment is aligned parallel to the substrate surface (See 2.3.3.3.). For very thin uncured DGEBA films on aluminum the 916 ± 2 and 1038 ± 2 cm^{-1} do not appear in the spectrum. For example see the spectrum of a 1.0 nm thick uncured DGEBA film on aluminum in Figure 38. The cause for the absence of the peak associated with epoxy functionality in the spectra of thin films of DGEBA on aluminum is not known from the present experiments. Other changes in the spectrum after washing of uncured films may be due to contamination upon exposure to air or subtle changes in substrate which may have an important contribution to the spectrum for such thin films. These results indicate that a strong bond is established between aluminum and the epoxy resin even at room temperature.

Figure 39 shows the FTIR spectra for a DGEBA film on gold prepared from a 0.25 g/100ml DGEBA/methylene chloride solution before and after heating 30 min at 150°C in vacuum. The absorption peak at 916 ± 2 cm^{-1} characteristic to the epoxy ring disappears after heating indicating that homopolymerization of the epoxy resin takes place on the gold surface upon heating. It is likely that residual physisorbed water on the gold surface, initiates the epoxy ring opening. (Recall that the application of DGEBA was not accomplished under absolutely dry conditions). The atomic concentrations for clean gold determined by XPS were: 64.7% Au, 29.4% C, and 5.41% O. The binding energy for the oxygen 1s peak is 533.3 eV. The oxygen photopeak position suggests the presence of water on the cleaned gold surface. Figure 40 presents the spectrum of the DGEBA film on gold prepared from a 0.25 g/100ml DGEBA/methylene chloride solution, heated for 30 min

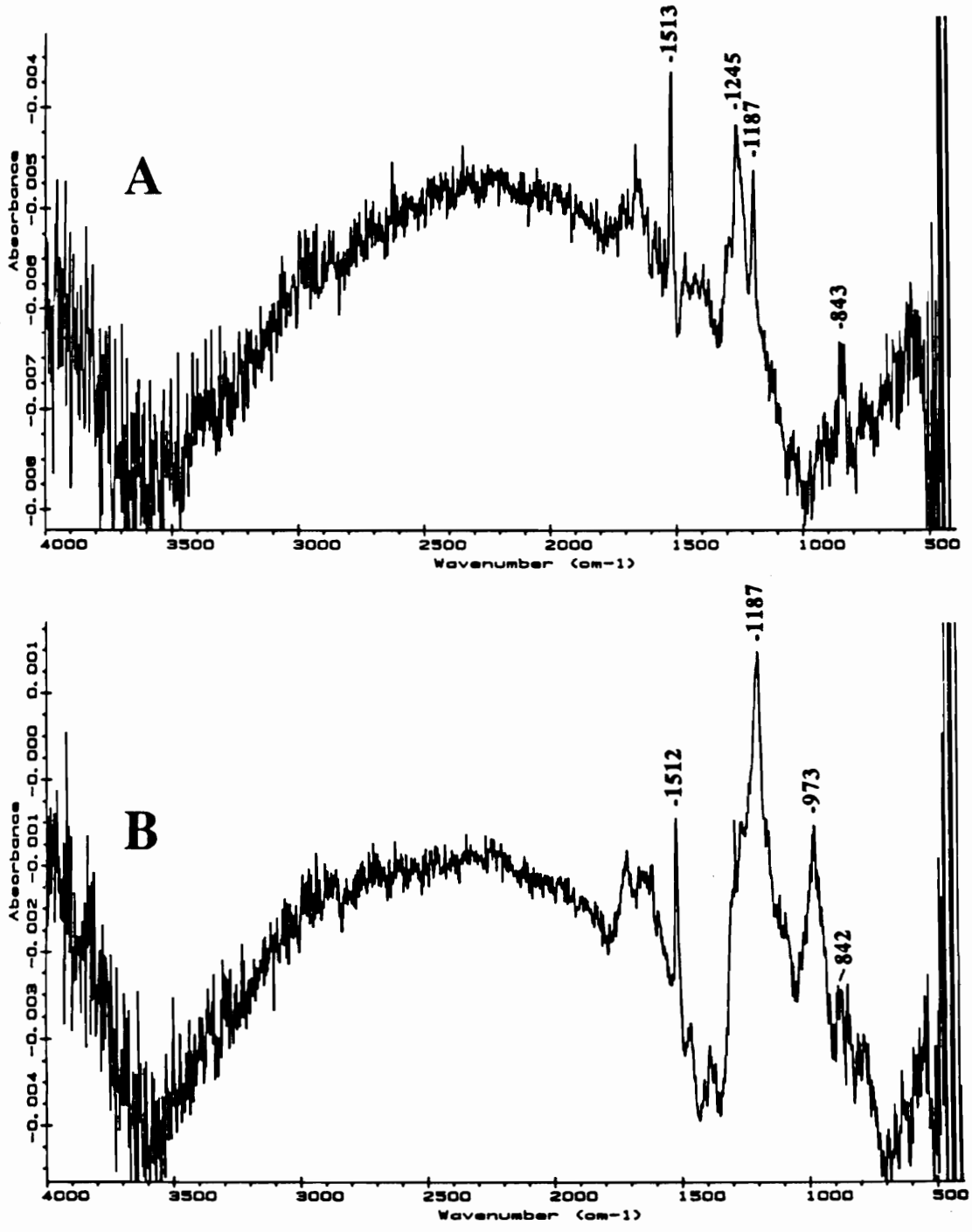

Figure 38. Reflection-absorption spectra of a DGEBA film on aluminum cast from a 0.025 g/100 ml DGEBA/methylene chloride solution.

A. No treatment. Film thickness 1.0 nm.

B. After heating for 30 min at 150°C in vacuum. Film thickness 0.8 nm.

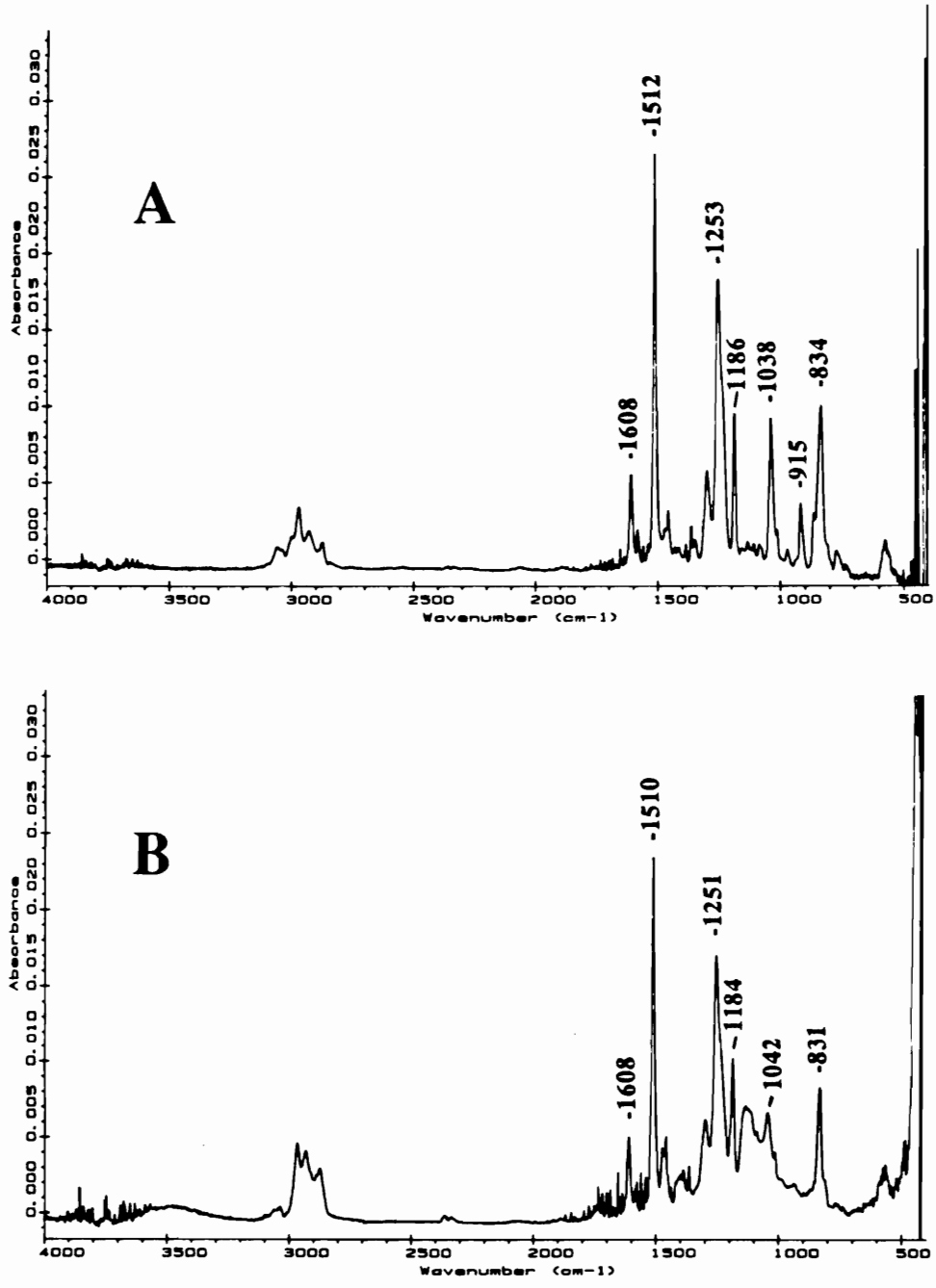

Figure 39. Reflection-absorption spectra of a DGEBA film on gold cast from a 0.25 g/100 ml DGEBA/methylene chloride solution.

A. No treatment. Film thickness 10.4 nm.

B. After heating for 30 min at 150°C in vacuum. Film thickness 8.8 nm.

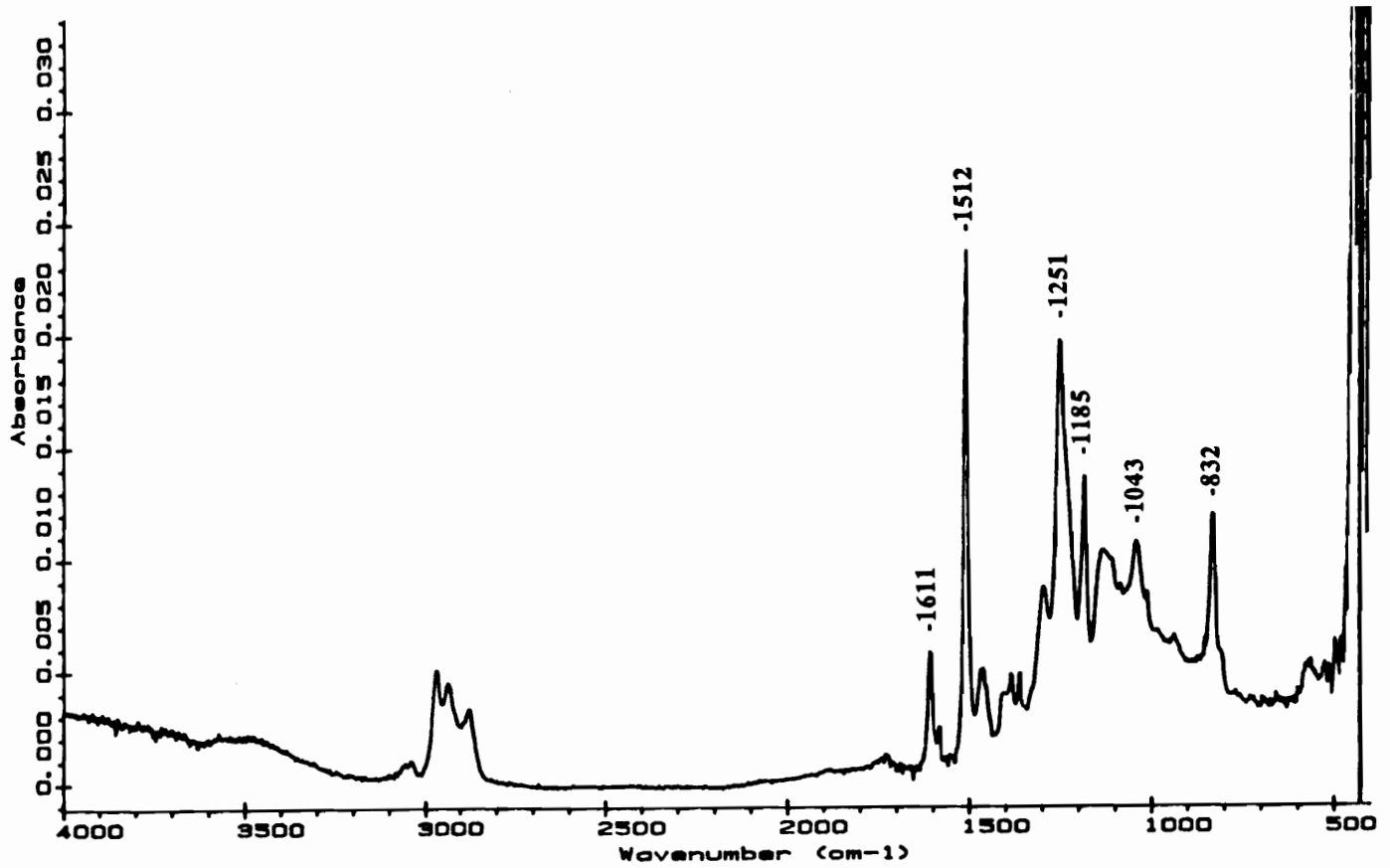

Figure 40. Reflection-absorption spectra of a DGEBA film on gold cast from a 0.25 g/100 ml DGEBA/methylene chloride solution, heated for 30 min at 150°C in vacuum and then washed with methylene chloride for 15 min. Film thickness 8.4 nm.

at 150°C in vacuum and then washed with methylene chloride for 15 min. This spectrum is similar to the spectrum taken before washing (Figure 39), indicating that the epoxy film is not removed from the gold substrate by methylene chloride. Figure 41 presents the FTIR spectra for a DGEBA film on gold prepared from a 0.25 g/100ml DGEBA/methylene chloride solution, before and after washing with methylene chloride for 15 min. The results are similar to those obtained for washed DGEBA film on aluminum shown in Figure 38. After washing, the peak at 916 ± 2 cm^{-1} corresponding to the epoxy functionality is not observed. However, the peaks at 1510 ± 2, 1251 ±2, and 1186 ± 2 cm^{-1} are present indicating that some epoxy resin remains on gold. It is apparent that washing removes most, but not all of the epoxy deposited on gold. As a result of CH_2Cl_2 washing, the film thickness decreases from 9.6 nm to 1.2 nm. It was shown in Figure 37 that for thin films of epoxy on aluminum the 916 ±2 cm^{-1} peak does not appear in the spectrum. The presence of DGEBA on gold surface after washing with methylene chloride suggests that an interaction occurs between gold and uncured resin. The nature of this interaction is not known from the present measurements.

The FTIR results indicate that homopolymerization takes place both at the aluminum and gold surface upon heating. The above results for washed uncured films of DGEBA on metal showed strong aluminum/uncured DGEBA and gold/uncured DGEBA bonds. This indicates that the resin displaces the contamination existing on the metal surface (water, hydrocarbons) by dissolving it and making a direct contact with the metal surface.

The water dissolved in the epoxy resin may initiate the epoxy ring opening upon heating. However, considering the high reactivity of the epoxy resin toward the OH functionality [178] and the intimate epoxy/aluminum contact, it is reasonable to assume that in the case of aluminum/epoxy films, the OH groups existing on the aluminum surface are also involved in the epoxy homopolymerization. In this way chemical bonds are formed

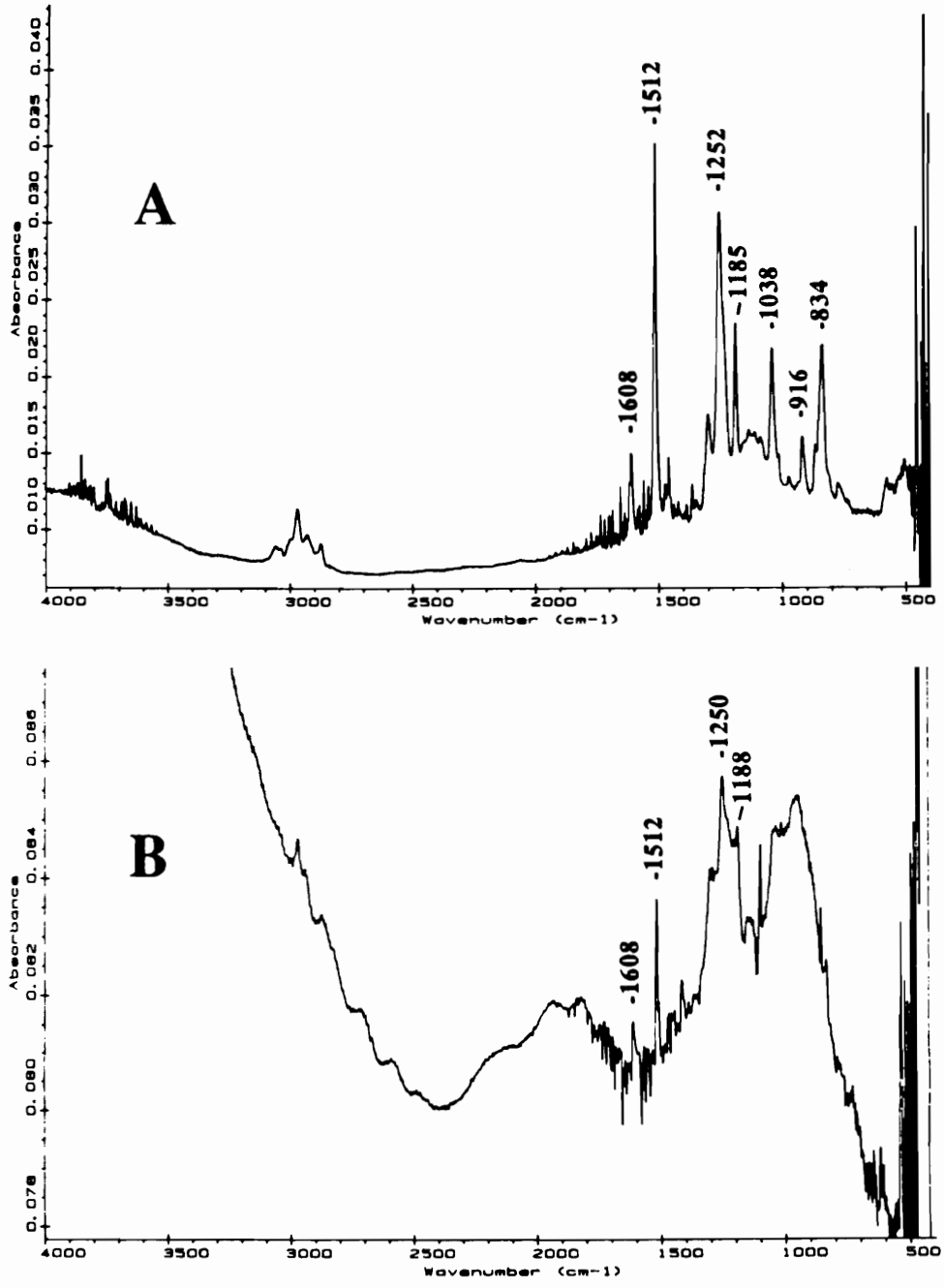

Figure 41. Reflection-absorption spectra of a DGEBA film on gold cast from a 0.25 g/100 ml DGEBA/methylene chloride solution.

A. No treatment. Film thickness 9.6 nm.

B. After washing with methylene chloride for 15 min. Film thickness 1.2 nm.

between the aluminum substrate and the cured epoxy film.

Comparing the results obtained in this research for the alkaline cleaned aluminum/epoxy system with those found in literature regarding different metal/epoxy systems, some important observations can be made.

The results obtained in this study for the alkaline-cleaned aluminum/epoxy system show clearly that homopolymerization of neat epoxy resin takes place at the alkaline-cleaned aluminum surface upon heating. Comyn et al. [81] investigated the aluminum-epoxy interaction by innelastic electron tunneling spectroscopy; however, they did not observe any evidence of chemical reactions at the epoxy/aluminum interface upon heating. Kollek [78], working with a chromic acid anodized aluminum/epoxy system noticed the absence of the epoxide peak in the IR spectra of adsorbed epoxy resin both before and after simulated curing. Kellek assumed that the absence of this adsorption was due to epoxide ring opening but his results do not show unequivocally that the reaction of epoxy resin takes place at the aluminum surface. Additionally, he worked with very thin films of epoxy on aluminum, and the absence of the epoxy peak may also be due to preferential molecular orientation. The results of this study indicate that for very thin films of uncured epoxy on aluminum, the IR spectra do not show the epoxide peak, while for thicker, uncured films the epoxy peak was always present in the spectra and disappears only upon heating. Affrossman et al., [79,80] studied the adsorption of simulated epoxy resin fragments on aluminum. Because the model compounds do not contain epoxy functionalities, the findings of their research are only relevant for the epoxy/aluminum interactions which take place after the epoxide ring is opened during curing.

The present results have more similarities with those obtained by Ishida et al., [73,82] on steel/epoxy and copper/epoxy systems. For example, Ishida observed polymerization of epoxy resin on copper substrates immersed in epoxy baths at elevated

temperatures (>150°C); this observation was supported by the absence of the epoxy band at 915 cm^{-1} in the IR spectrum. These results suggest that metal surface species are involved in the homopolymerization of the epoxy resin. No reaction mechanism was proposed to explain the observed metal/epoxy interfacial interactions. Also for epoxy/steel systems [73,82] it was found that the epoxy resin homopolymerizes at metal surface upon heating. This suggest a chemical interaction between epoxy and steel surface species as in the case of epoxy/alkaline cleaned aluminum system.

It should be mentioned that the results of the present work also indicate a strong bond between alkaline cleaned aluminum and uncured epoxy resin.

4.2.2. Phenol/metal

Figure 42 shows the reflection-absorption FTIR spectrum of a film of phenol deposited on gold from a solution of 10g/100ml phenol/methylene chloride, taken immediately after deposition on the substrate. This spectrum is similar to the transmission FTIR spectrum of a solid film of phenol presented in reference 179. The peak assignments made from the relevant literature are presented in Table 7 [179-181]. Figures 43 and 44 present the FTIR spectra for films of phenol deposited on aluminum substrates from solutions of 1 g/100 ml and 10 g/100 ml phenol/methylene chloride solutions, respectively, before and after heating for 30 min at 150°C in vacuum. The film thickness for the phenol/aluminum samples was estimated using the relative 830 ± 2 cm^{-1} peak intensity from the epoxy/gold reference sample for which the thickness was measured by ellipsometry. The peak assignments are presented in Table 8 [84,179-181]. The absorption peaks associated with the OH group of phenol are absent. A relatively intense peak in the 1108 ± 3 cm^{-1} region, assigned to C-O-Al stretch was observed for all phenol films on aluminum. Filbey [182] also observed an absorption peak at 1094 cm^{-1} in the

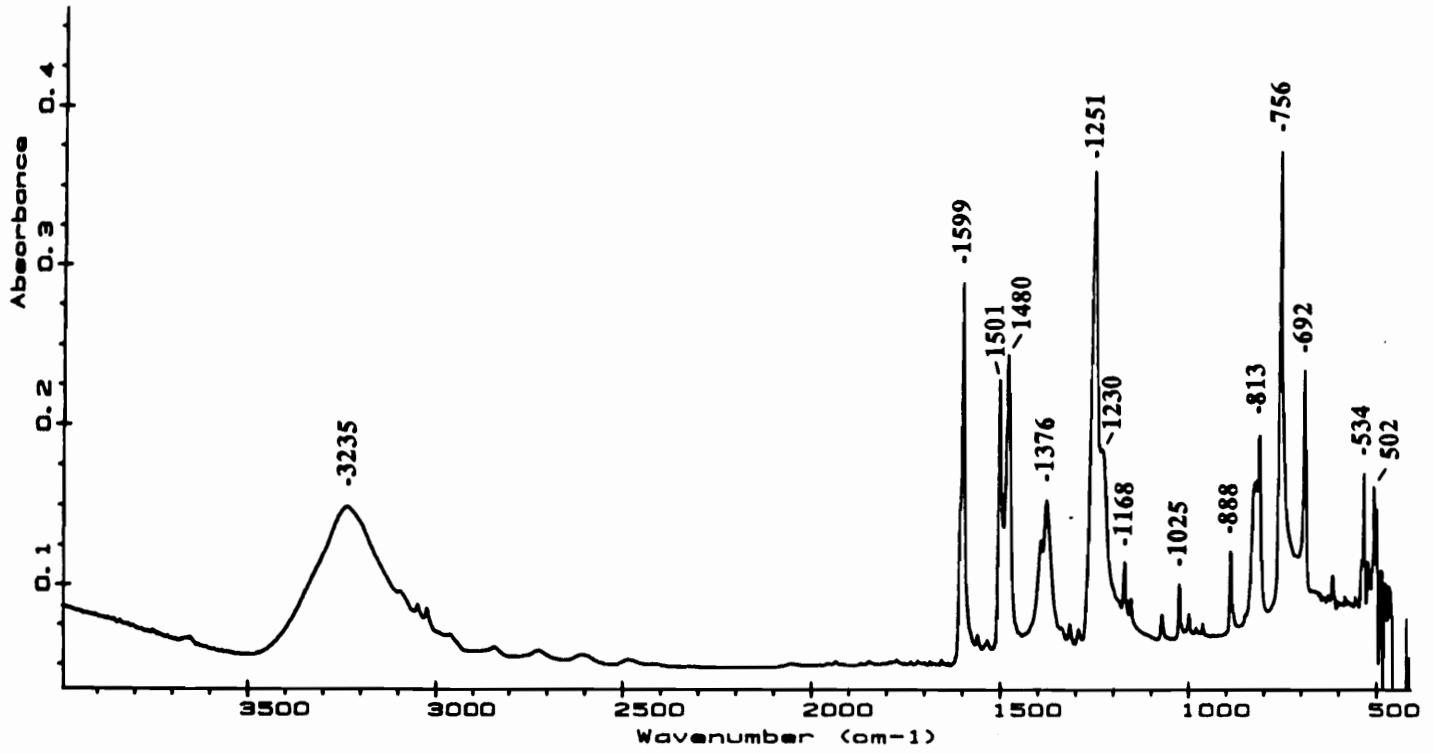

Figure 42. Reflection-absorption spectrum of a phenol film on gold cast from a 10 g/100 ml phenol/methylene chloride solution, measured immediately after film deposition. No treatment. Film thickness 100 nm.

Table 7.

Peak Assignments for Thick Film of Phenol on Gold

Wavenumber, cm^{-1}	Peak Assignment
3225	OH stretch
2839, 2728, 2607, 2482	overtone or combination bands
1599, 1501, 1480	C-C ring stretch
1390, 1346	in plane OH bend
1251	OH sensitive mode
1230	C-O stretch
1169, 1025, 888, 825, 813, 756	CH bend
692	ring C=C bend
534, 502	OH sensitive mode

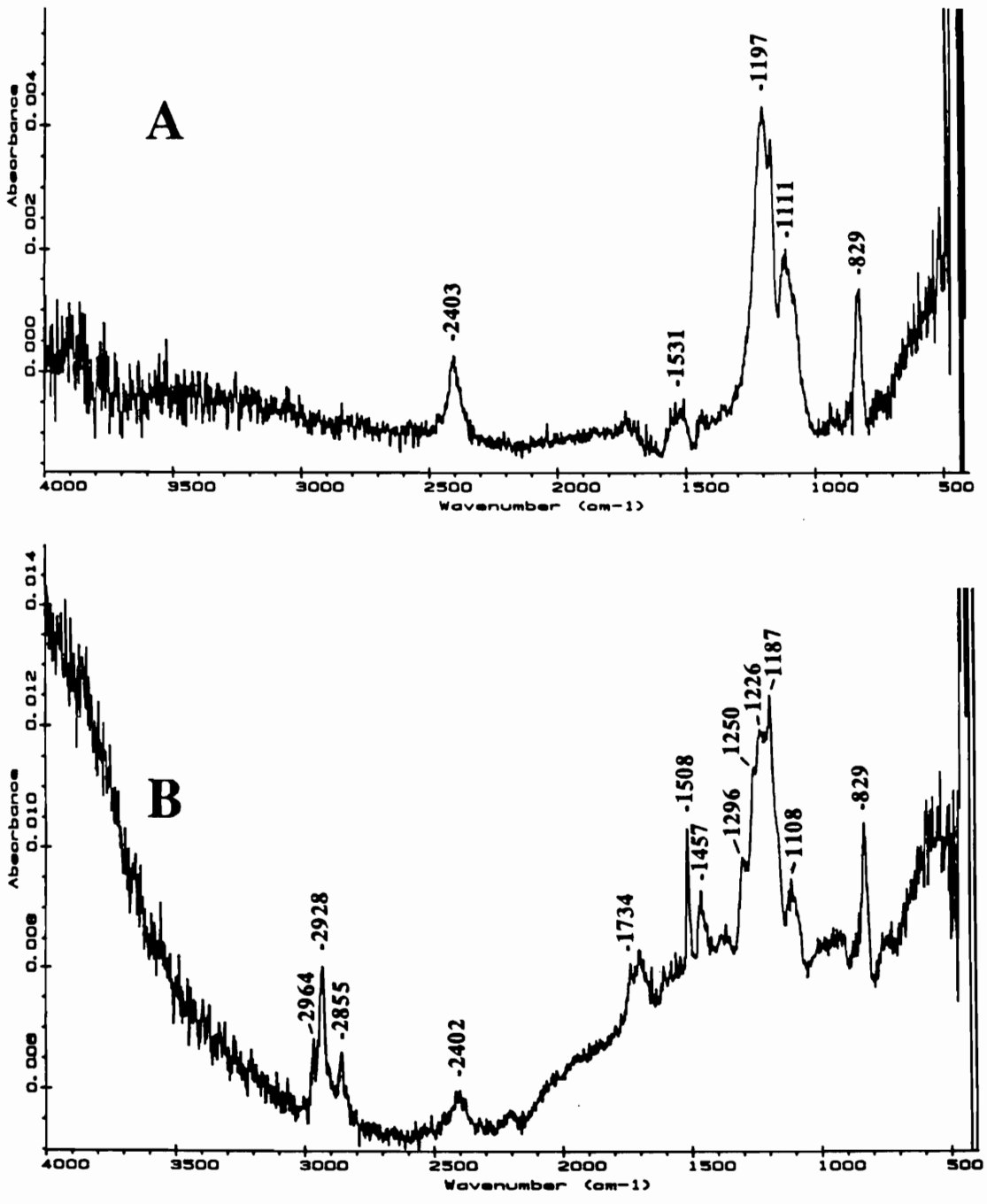

Figure 43. Reflection-absorption spectra of a phenol film on aluminum cast from a 1.0 g/100 ml phenol/methylene chloride solution.

A. No treatment. Film thickness 2.2 nm.

B. After heating for 30 min at 150°C in vacuum. Film thickness 2.2 nm.

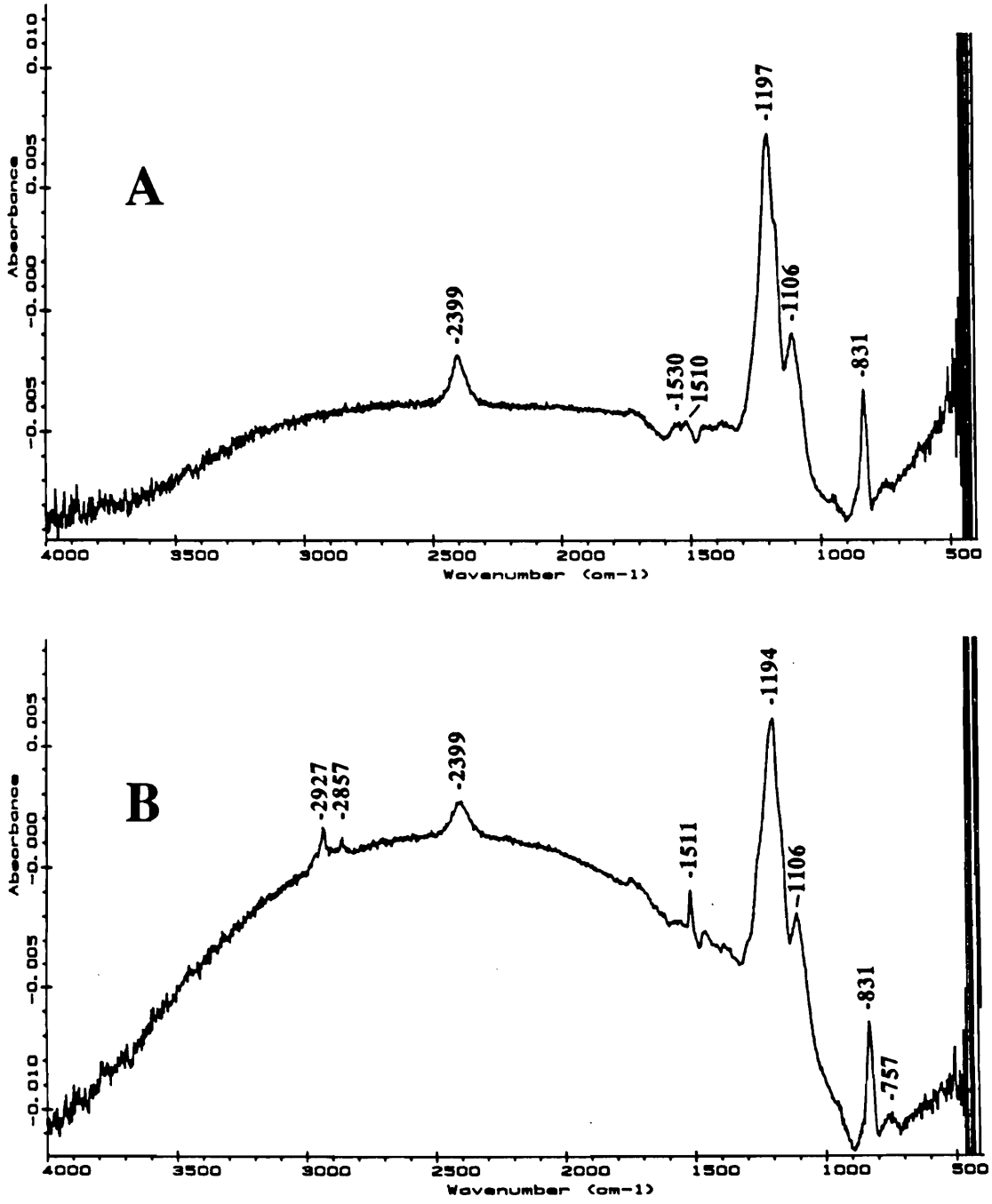

Figure 44. Reflection-absorption spectra of a phenol film on aluminum cast from a 10.0 g/100 ml phenol/methylene chloride solution.

A. No treatment. Film thickness 5.0 nm.

B. After heating for 30 min at 150°C in vacuum. Film thickness 5.0 nm.

Table 8.

Peak Assignments for Thin Film of Phenol on Aluminum

Wavenumber, cm^{-1}	Peak Assignment
2964,2928, 2855	hydrocarbon contamination from the vacuum system
2400	unassigned
1730	combination band
1530, 1510	C-C ring stretch
1457	unassigned
1296, 1256	C-O stretch in phenolate structure
1225	C-O stretch
1186	CH bend
1108	C-O-Al stretch
829	CH bend
754	CH bend

reflection-absorption spectrum of sec-butyl aluminum alkoxide, which was attributed to the C-O-Al stretching. These observations suggest that phenol reacts with aluminum surface species as was previously shown in 2.2.3.4. The spectra of the two samples, taken before heating are similar. The heating produces only slight changes in the spectrum of the sample prepared from 10 g/100 ml phenol/methylene chloride solution. New peaks at 2928 and 2855 cm^{-1} appear due to hydrocarbon contamination from the vacuum system. The 1511 cm^{-1} peak is sharper and more intense for the heated sample. Heating produces more significant changes in the spectrum of the sample prepared from the 1g/100ml phenol/methylene chloride solution. Besides the new peaks at 2964, 2928 and 2855 cm^{-1}, attributted to hydrocarbon contamination from the vacuum system, and an increase in the relative height of 1510 cm^{-1} peak, new peaks at 1226, 1250, and 1296 cm^{-1} superimposed on the 1186 cm^{-1} peak are observed. The peak at 1226 cm^{-1} is assigned to the C-O stretch. The peaks at 1250 and 1296 cm^{-1} may be due to the C-O bond vibration in the phenolate structure. It is reasonable that phenolate is formed when phenol is absorbed on the surface of aluminum oxide. Shabalin et al. [84] found absorption bands at 1256 and 1285 cm^{-1} in the IR spectrum of aluminum phenolate and assigned these bands to the vibrations of the C-O band in a phenolate structure.

To determine the effect of heating, bulk phenol was heated for 30 min at 150° C and FTIR spectra were measured before and after heating. These spectra , presented in Figure 45, are identical indicating that heating at 150° C does not change the chemical structure of phenol. The spectrum of phenol film prepared from 10 g/100 ml phenol/methylene chloride solution, heated for 30 min at 150° C and washed with methylene chloride for 15 min. is similar to that taken before washing (Figure 46). This shows that the phenol film is not removed by solvent washing. The FTIR results suggest a strong phenol/aluminum chemical bond. Possible reactions between phenol and the aluminum surface species are:

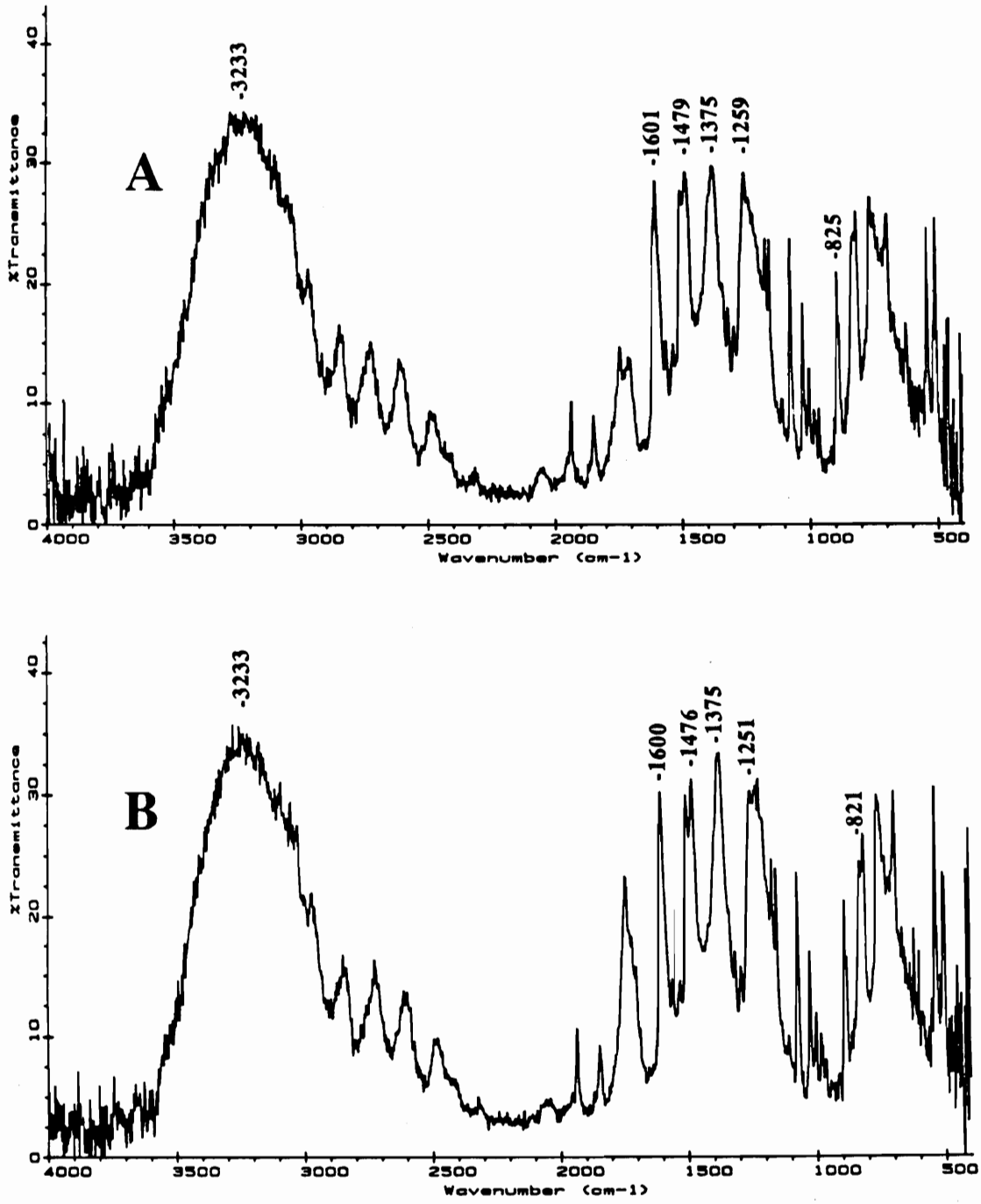

Figure 45. Photoacoustic spectra of phenol.
A. No treatment
B. After heating for 30 min at 150°C.

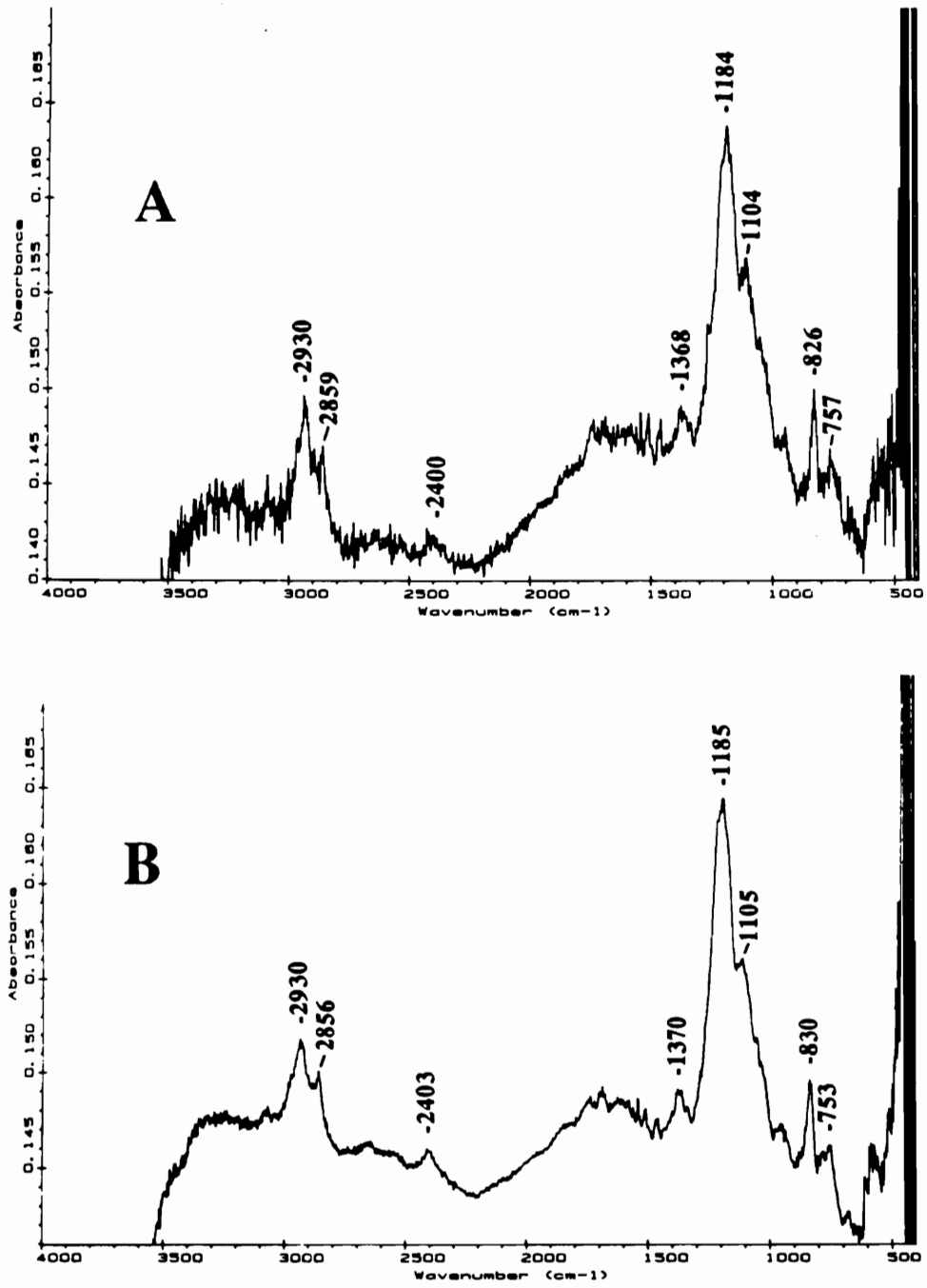

Figure 46. Reflection-absorption spectra of a phenol film on aluminum cast from a 10.0 g/100 ml phenol/methylene chloride solution heated for 30 min at 150°C in vacuum.

A. Before washing. Film thickness 6.0 nm.

B. After washing with methylene chloride for 15 min. Film thickness 5.0 nm.

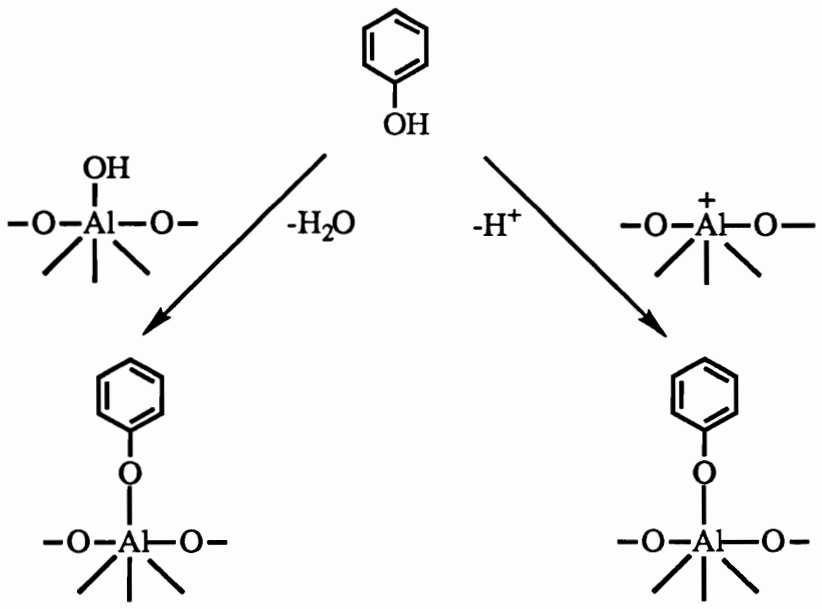

Figure 47 shows the FTIR spectra of a phenol film on aluminum prepared from 10 g/100 ml phenol/methylene chloride solution, before and after washing with methylene chloride for 15 min. The spectrum taken after washing is similar to that taken before washing both in shape and peak intensities. Only a slight decrease in thickness from 7.6 nm to 6.6 nm is observed after washing. Almost all phenol remains on the aluminum after washing, indicating that a strong bond is establish between aluminum and phenol even at room temperature.

Figure 48 shows FTIR spectra for a phenol film on gold prepared from 10 g /100 ml phenol/methylene chloride solution before and after heating for 30 min at 150°C in vacuum. The thickness of the film before heating, measured by ellipsometry was 0.8 nm. The spectrum taken before heating is unlike the spectra of phenol films on aluminum shown in Figures 43 and 44. Also film thickness is much lower 0.8 nm (on gold) vs 5 nm (on aluminum). The spectrum taken before heating has absorption peaks which can be attributed to phenol: 1595, 1502, 1222, and 756 cm^{-1}, indicating that some phenol is adsorbed on gold. However, the absorption peaks associated with the OH group of phenol

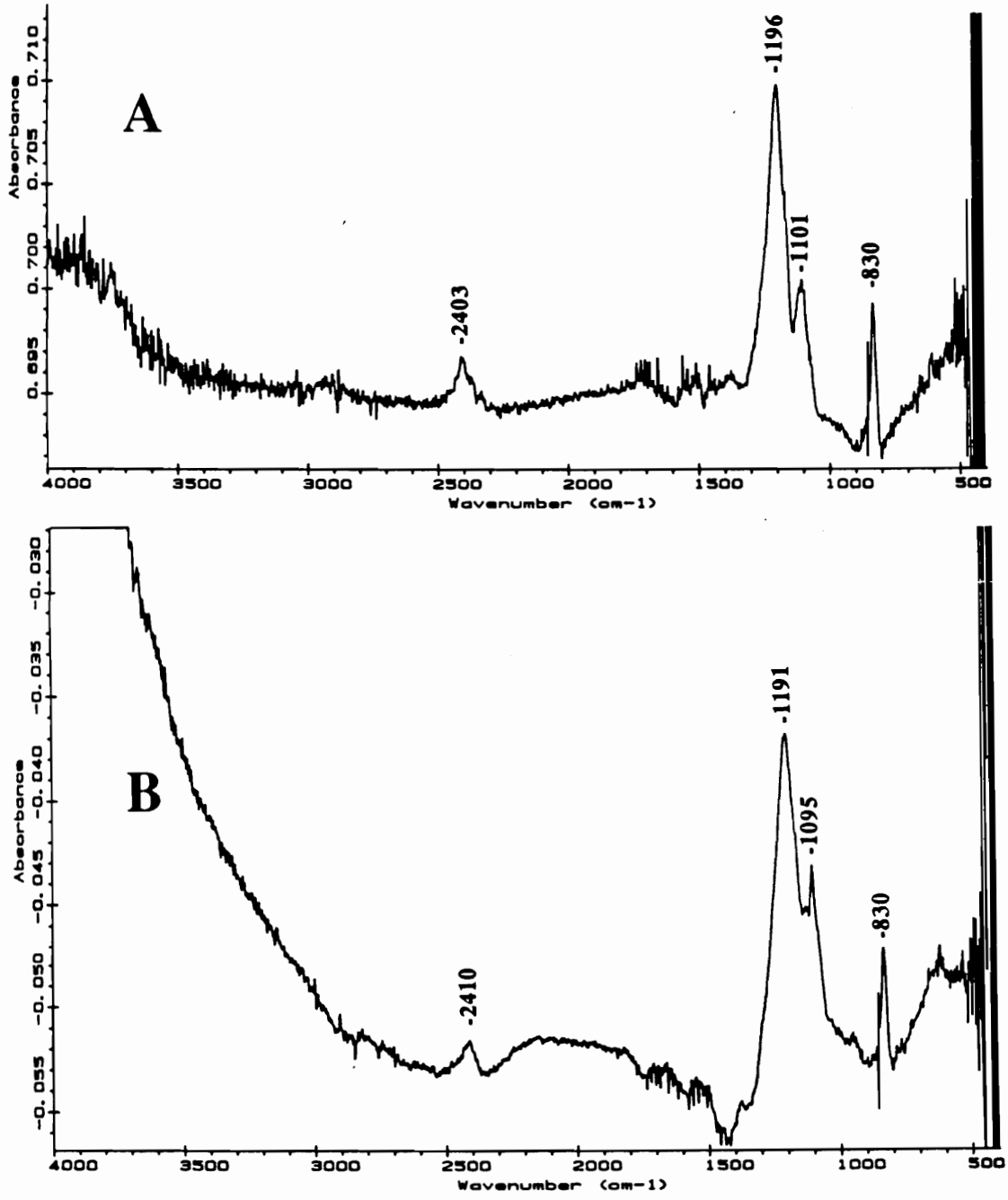

Figure 47. Reflection-absorption spectra of a phenol film on aluminum cast from a 10.0 g/100 ml phenol/methylene chloride solution.

A. No treatment. Film thickness 7.6 nm.

B. After washing with methylene chloride for 15 min. Film thickness 6.6 nm.

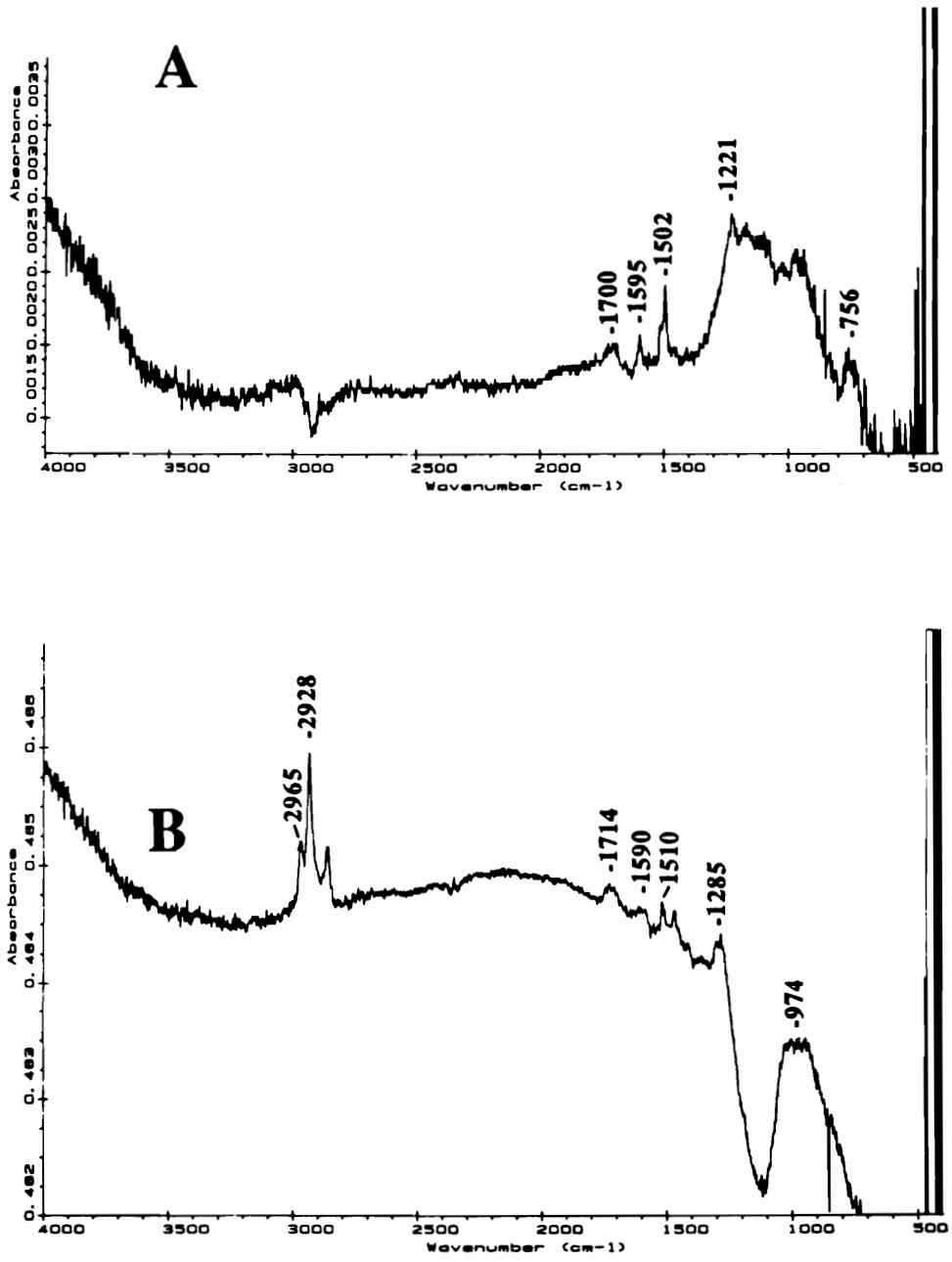

Figure 48. Reflection-absorption spectra of a phenol film on gold cast from a 10.0 g/100 ml phenol/methylene chloride solution.

A. No treatment. Film thickness 0.8 nm.

B. After heating for 30 min at 150°C, in vacuum.

are absent. This may be due to a preferred molecular orientation, which may have a very strong influence on spectrum shape for such a thin film. Recall that the spectrum of a thick phenol film on gold shown in Figure 42 has a strong peak at 3235 cm^{-1} due to OH functionality. The spectrum taken after heating shows very significant changes when compared with that taken before heating. There are only two very small peaks which can be attributed to phenol: 1590 and 1510 cm^{-1}. The peaks at 2965, 2929 and 2857 cm^{-1} are attributed to hydrocarbon contamination. Figure 49A presents the spectrum of a clean gold surface heated for 30 min at 150°C in vacuum. Absorption peaks attributed to hydrocarbon contamination are observed at 2960, 2928, and 2854 cm^{-1}. The FTIR results indicate that almost all phenol is desorbed during heating. The spectrum of the phenol film on gold heated for 30 min at 150°C, after washing with methylene chloride for 15 min. is shown in Figure 49B. The significant change produced by washing is a strong decrease in intensity for peaks attributed to hydrocarbon contamination (2965, 2928, and 2857 cm^{-1}), indicating that most of the contamination was removed by washing. The FTIR results show that the bond between phenol and gold is weak. A thin layer of phenol which remains adsorbed on gold at room temperature is desorbed by heating. The heating does not produce the desorption of the phenol films deposited on aluminum.

The comparison of the results obtained in this research for the phenol/alkaline cleaned aluminum system with those for other phenol/aluminum systems reported in literature [84-88] showed that in all cases it was found that phenol is chemisorbed on the aluminum surface. The vibrational modes associated with the OH group of the phenol are absent in all types of spectra (reflection-absorption IR, transmission IR, and inelastic electron tunneling) of phenol adsorbed on aluminum. However, it seems that the approach of this work (reflection-absorption IR) offers some advantages over those those employed in ref.84-88 (IETS and transmission IR). The aluminum substrates for reflection-

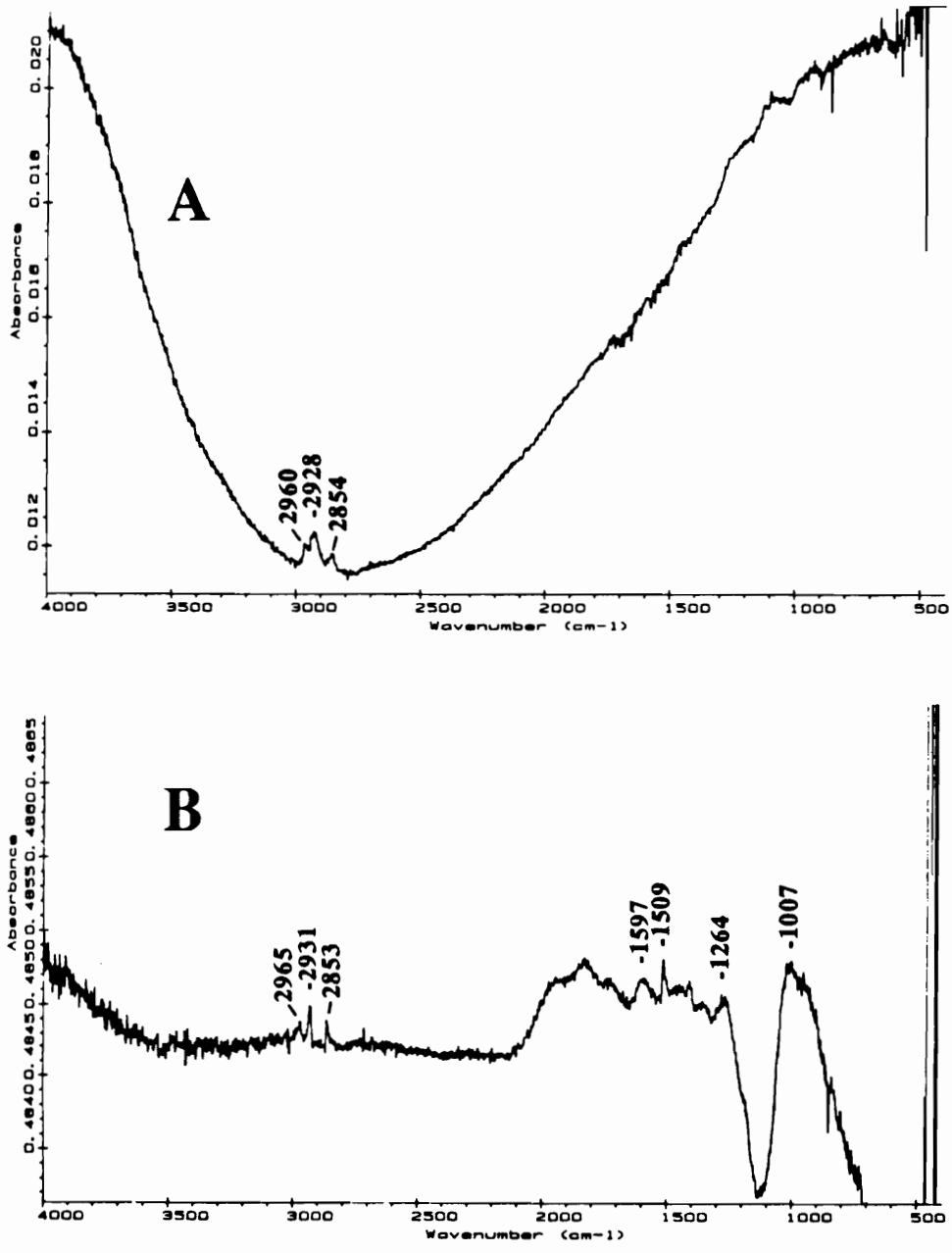

Figure 49. Reflection-absorption spectra.

A. Cleaned gold mirror heated for 30 min at 150°C in vacuum.

B. Phenol film on gold cast from a 10.0 g/100 ml phenol/methylene chloride solution, heated for 30 min at 150°C in vacuum and then washed with methylene chloride for 15 min.

absorption IR experiments were pretreated in the same way as the actual aluminum adherends. Also, in reflection-absorption spectroscopy the spectrum obtained corresponds only to the coating, while in transmission IR and IETS techniques the spectra also include the absorption bands due to substrates.

4.2.3. MDI/metal

Figures 50 and 51 present FTIR spectra for MDI films deposited on aluminum substrates from 0.025 g/100ml and 1 g/100ml MDI/methylene chloride solutions respectively, before and after heating for 30 min at 150° C in vacuum. The film thickness was estimated using the epoxy/gold reference sample whose thickness was measured by ellipsometry and the ratio of 1510 ± 2 cm^{-1} peak intensities. The peak assignments made from relevant literature are given in Table 9 [179-181, 183-187]. The fact that the spectrum taken before heating for the sample prepared from the 1 g/100ml solution is different from the one prepared from the 0.025 g/100ml solution, is explained by its much higher thickness, as indicated by its more intense peak absorbances. It was shown in 2.3.3.3. that reflectance spectra for layers of different thicknesses may be different in both shape and peak frequency. Heating reduces dramatically the thickness of the film prepared from the 1 g/100 ml solution, as indicated by the large decrease in peak absorbance. Heating does not reduce the thickness of the film prepared from the 0.025 g/100 ml MDI/methylene chloride solution. The most important change after heating is a decrease in the relative absorbance for the peak corresponding to the NCO functionality (~2280 cm^{-1}), compared to spectra taken before heating. The spectra taken after heating are practically similar for the two samples with some exceptions. The significant ones are: the relative NCO peak absorption is much lower for the thinner sample and its position is shifted to a lower wavenumber (2280 vs 2289 cm^{-1}) compared to that for the thicker sample. This may be indicative of chemical and physical interactions at the MDI/aluminum interface It is

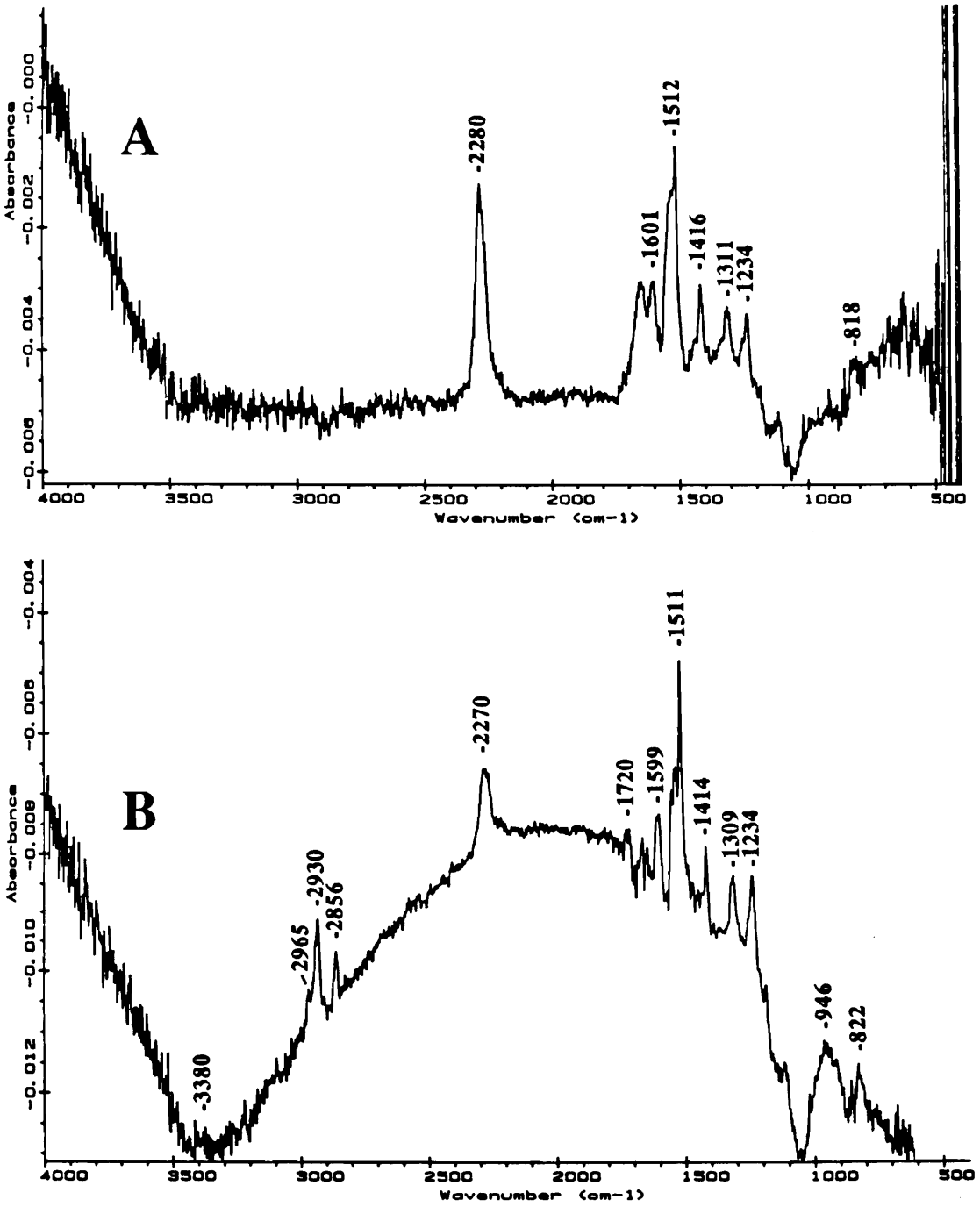

Figure 50. Reflection-absorption spectra of a MDI film on aluminum cast from a 0.025 g/100 ml MDI/methylene chloride solution.

A. No treatment. Film thickness 1.5 nm.

B. After heating for 30 min at 150°C in vacuum. Film thickness 1.5 nm.

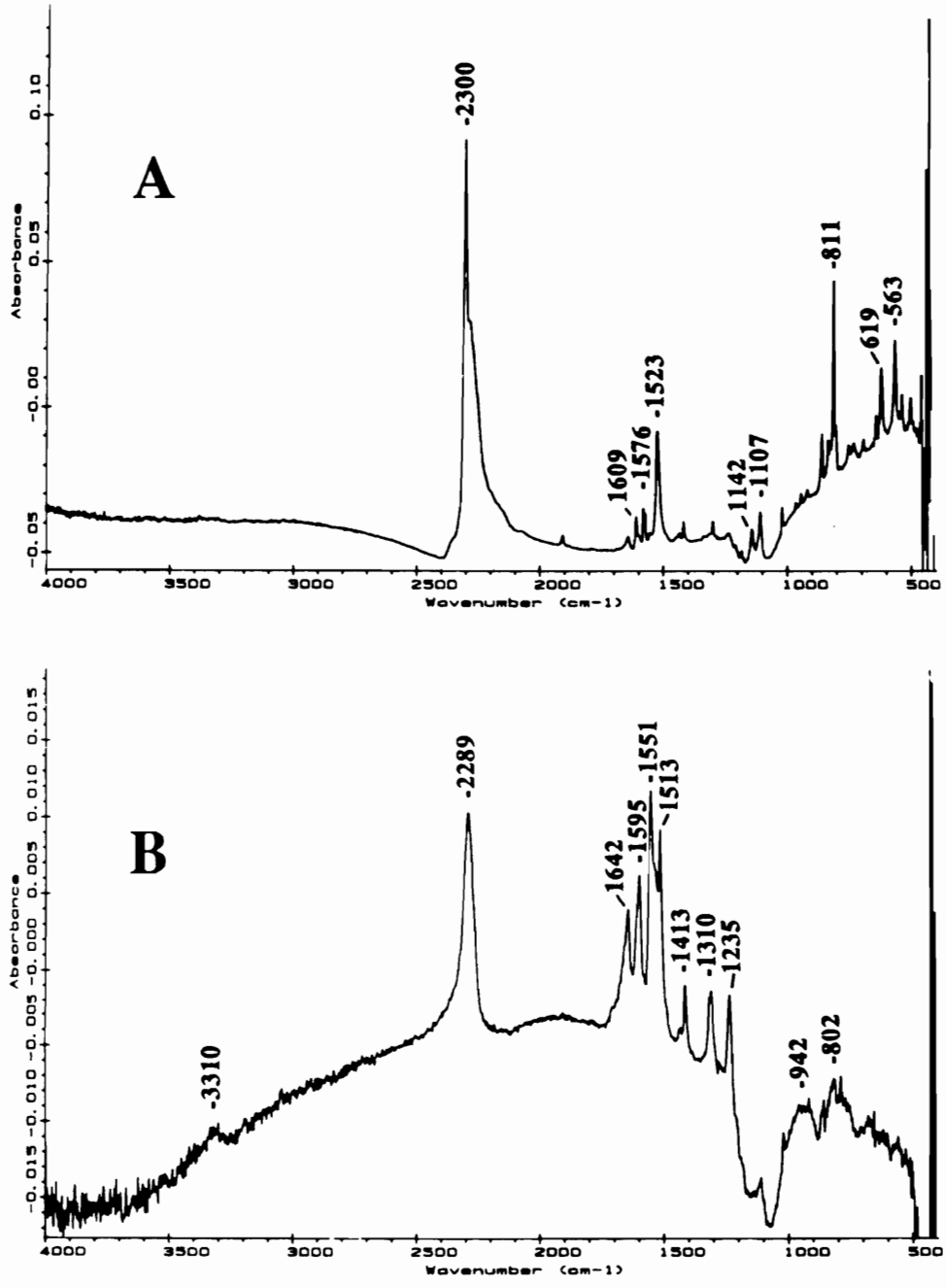

Figure 51. Reflection-absorption spectra of a MDI film on aluminum cast from a 1.0 g/100 ml MDI/methylene chloride solution.

A. No treatment. Film thickness 14.0 nm.

B. After heating for 30 min at 150°C in vacuum. Film thickness 5.3 nm.

Table 9

Peak assignments for MDI

Wavenumber, cm^{-1}	Peak assignment
2964, 2928, 2855	hydrocarbon contamination from the vacuum system
2270-2300	NCO asymetric stretch
1609, 1576, 1523	C-C ring stretch
1142, 1107	ring C-H
811	out of plane bending of p. substituted benzene ring

expected that the spectra obtained for thinner films reflect more the interfacial changes and interactions than those obtained for thicker films. It is interesting to note that the 2289 cm^{-1}/1513 cm-1 peak ratio (0.9) in the spectrum of the thicker film after heating (Figure 51) is comparable with the ratio (1.07) for the spectrum of the thinner film taken before heating shown in Figure 50. In an attempt to clarify the nature of MDI/aluminum interfacial interactions, FTIR spectra of bulk MDI were taken before and after heating for 30 min at 150°C in air (See Figure 52). The spectrum taken after heating is indentical to the spectrum before heating. No peak intensity decrease relative to the 1527 cm^{-1} was observed for the peak corresponding to NCO functionality, indicating that heating at 150°C does not alter the chemical structure of MDI.

Figure 53 shows the spectra for MDI film on aluminum prepared from 1 g/100ml MDI/methylene chloride solution, stored for about a month in a desiccator after being heated for 30 min at 150° C and for the same film after washing in methylene chloride for 15 min. The spectrum of the washed sample is similar to that determined before washing, with the exception that a much lower peak absorbance corresponding to the NCO group and a shift of this peak position to a lower wavelength from 2291 to 2280 cm^{-1} is observed. These results show that the solvent washing does not displace the MDI film from the aluminum surface. These results are indicative of a strong solvent resistant aluminum/MDI bond and suggest chemical interactions between the aluminum surface species and MDI. Considering the high reactivity of NCO groups toward OH functionality one possible reaction would be:

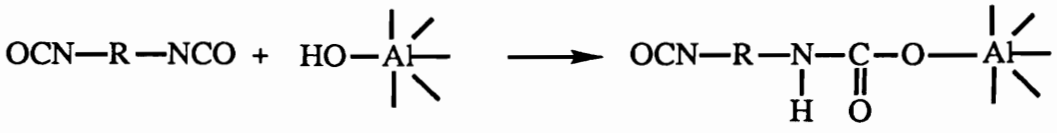

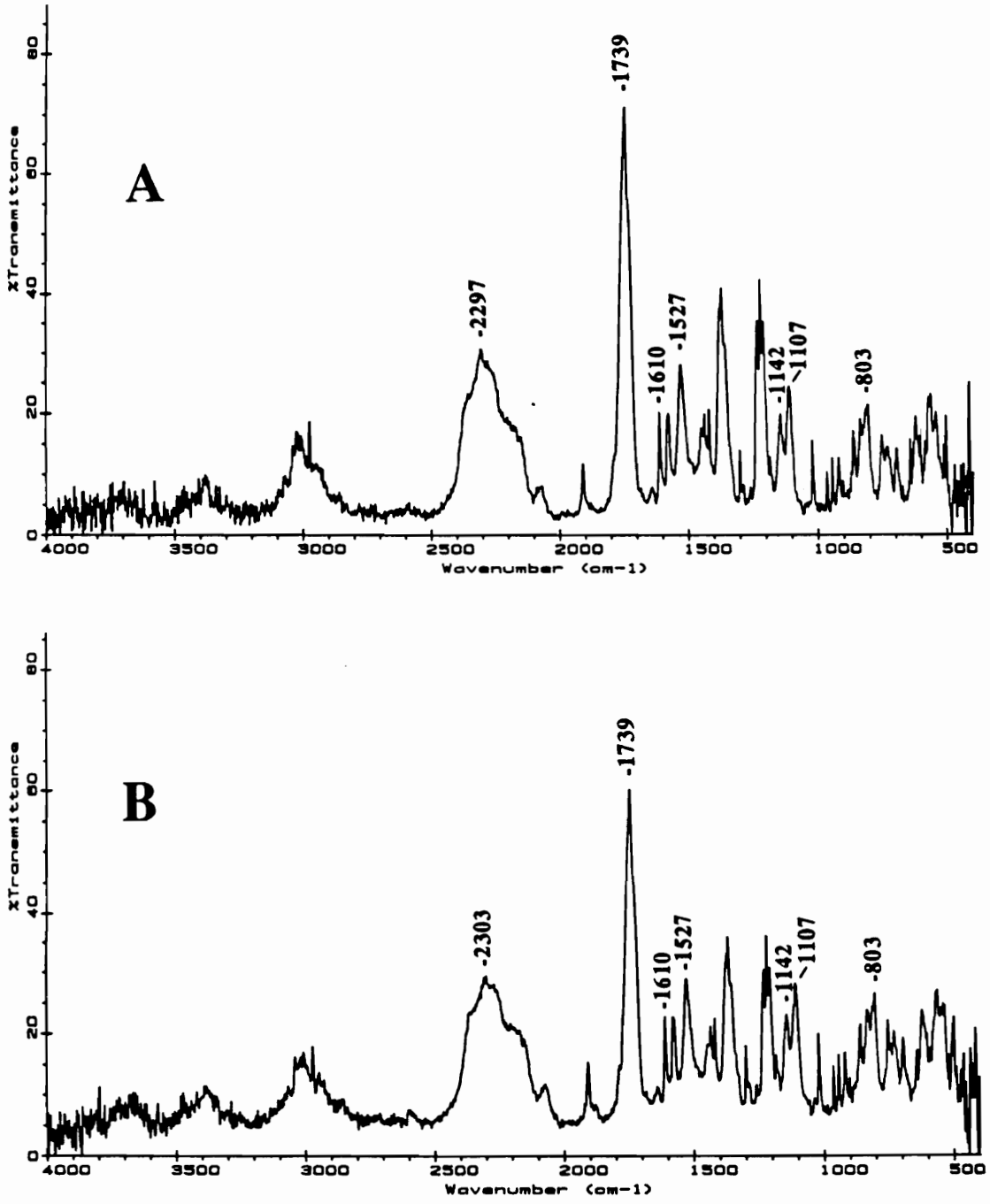

Figure 52. Photoacoustic spectra of MDI.
A. No treatment
B. After heating for 30 min at 150°C.

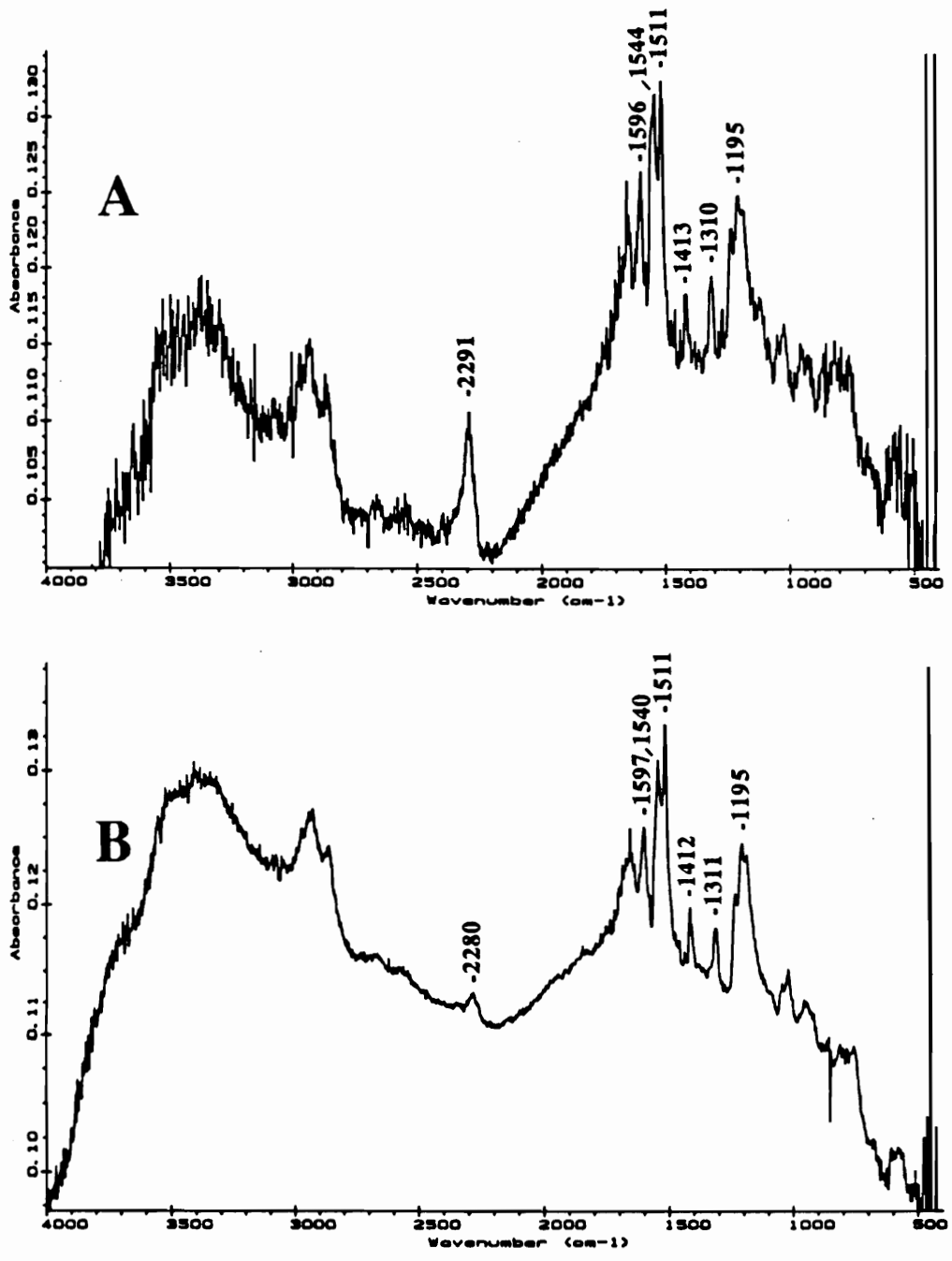

Figure 53. Reflection-absorption spectra of a MDI film on aluminum cast from a 1.0 g/100 ml MDI/methylene chloride solution heated for 30 min at 150°C in vacuum.

A. Before washing. Film thickness 6.4 nm.

B. After washing with methylene chloride for 15 min. Film thickness 5.6 nm.

Figure 54 presents the FTIR spectra for a MDI film on aluminum prepared from a 0.025 g/100 ml MDI/methylene chloride solution before and after washing with methylene chloride for 15 min. It is not possible to assess the changes regarding the peak associated with NCO functionality because of the modification in baseline position in the 2750-2350 cm^{-1} region. However, the presence of 1601, 1546, 1514, 1410, and 1237 cm^{-1} peaks in the spectrum indicates the presence of some MDI on the aluminum surface. Solvent washing removes only partially the MDI from the aluminum substrate, the estimated film thickness decreasing from 1.1nm before washing to 0.8 nm after washing. A strong decrease in the intensity of the peak associated with NCO functionality was observed after solvent washing of the heated MDI film on aluminum (see Figure 52). Other changes in the spectrum may be due to subtle changes in the background or to contamination upon exposure to air. The presence of MDI on the aluminum surface after washing with methylene chloride suggests that a strong, solvent resistant bond is established between aluminum and MDI even at room temperature.

Figure 55 shows the FTIR spectrum for a MDI film on gold prepared from a 1 g/100 ml MDI/methylene chloride solution before and after heating for 30 min at 150° C in vacuum, and Figure 56 presents the spectrum for the heated film after washing in methylene chloride for 15 min. After analyzing these spectra the significant observations are:

a) The spectra in Figure 55 are similar to the corresponding spectra for MDI films on an aluminum substrate.

b) Solvent washing produces a slight decrease in the 2276 cm^{-1} peak intensity associated with the NCO functionality and the almost complete elimination of the peaks attributed to hydrocarbon contamination (2965, 2930, and 2856 cm^{-1}). The film thickness remains the same ~0.6 nm. These results show that solvent washing does not remove the

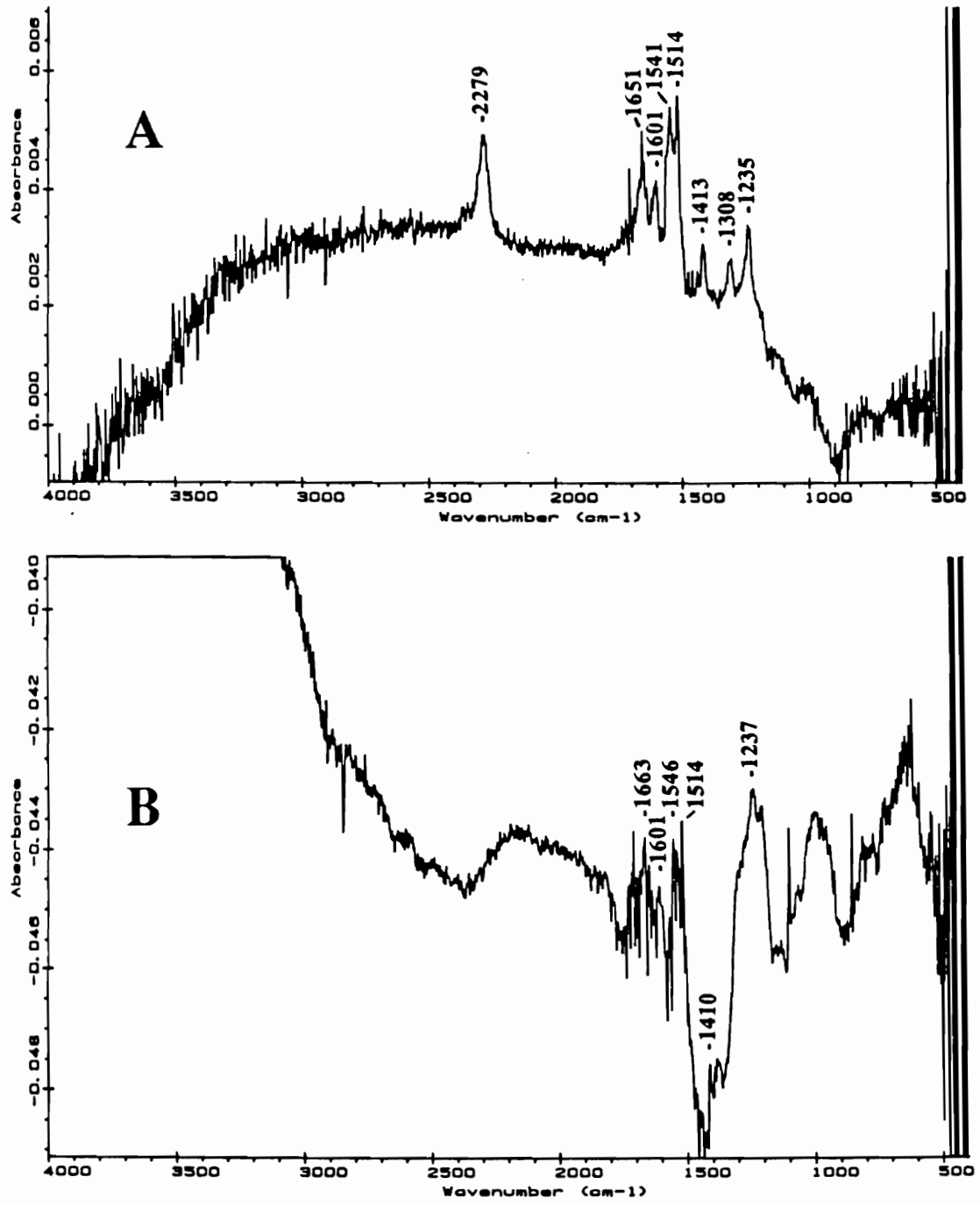

Figure 54. Reflection-absorption spectra of a MDI film on aluminum cast from a 0.025 g/100 ml MDI/methylene chloride solution.

A. Before washing. Film thickness 1.1 nm.

B. After washing with methylene chloride for 15 min. Film thickness 0.8 nm.

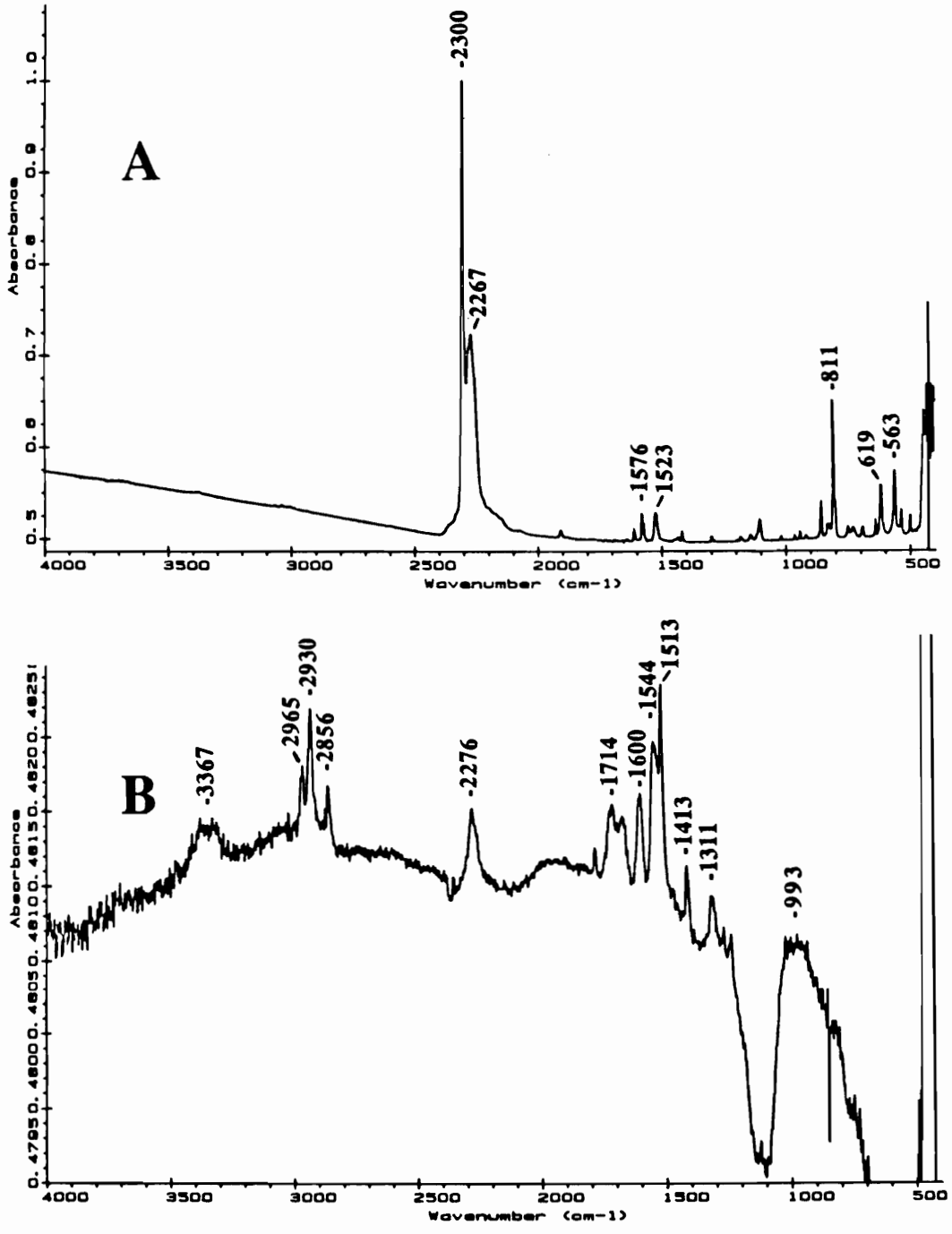

Figure 55. Reflection-absorption spectra of a MDI film on gold cast from a 1.0 g/100 ml MDI/methylene chloride solution.

A. No treatment. Film thickness 14.2 nm.

B. After heating for 30 min at 150°C in vacuum. Film thickness 0.5 nm.

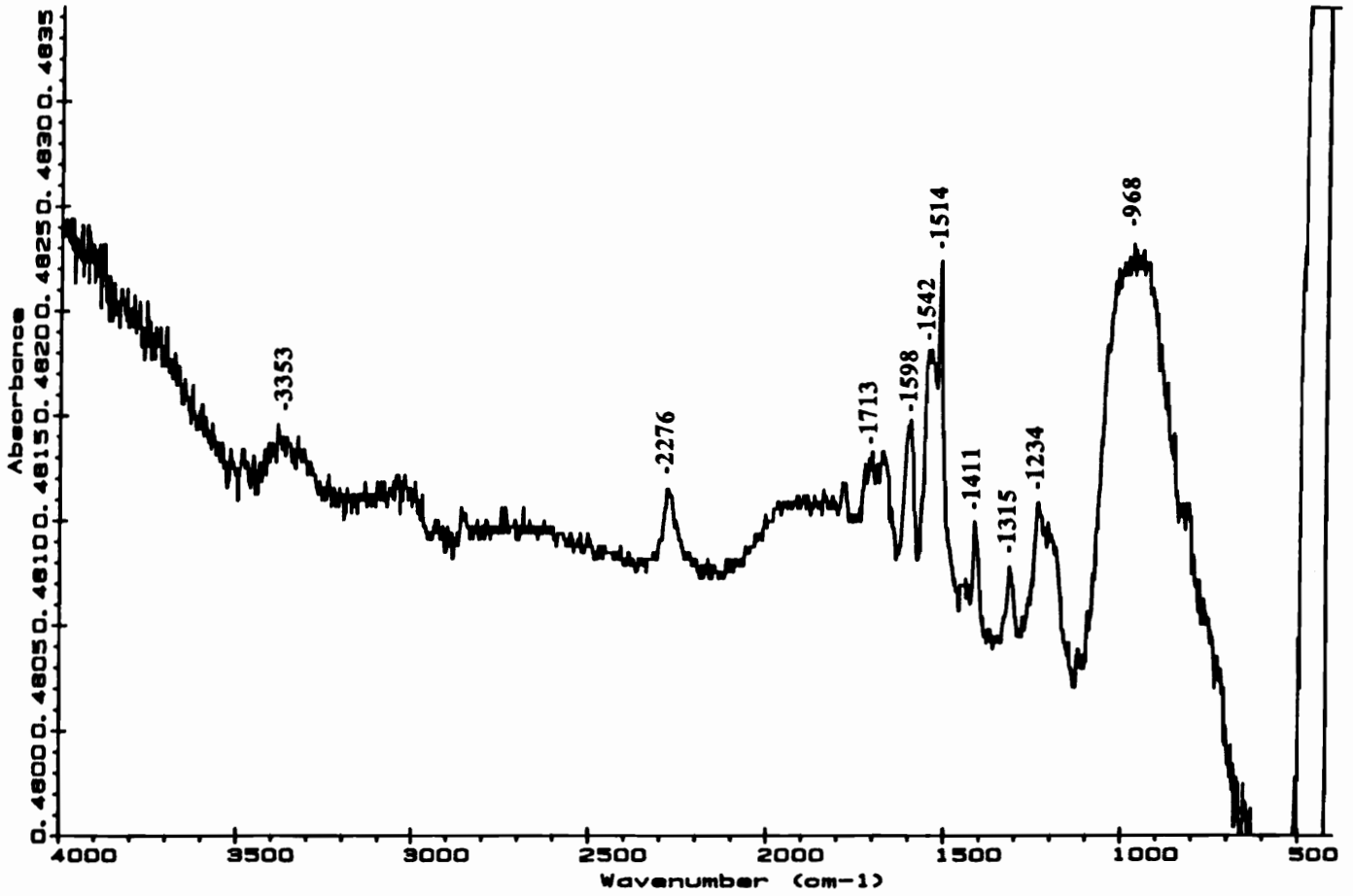

Figure 56. Reflection-absorption spectra of a MDI film on gold cast from a 1.0 g/100 ml MDI/methylene chloride solution heated for 30 min at 150°C in vacuum and then washed with methylene chloride for 15 min. Film thickness 0.6 nm.

MDI film from the gold substrate, suggesting a strong MDI/gold interaction. However, the thickness of the MDI film on gold after heating is much lower (0.5 nm) compared to thickness of the MDI film on aluminum after heating (5.3 nm).

The results of the present research indicate the existence of primer/aluminum chemical interactions for all three systems investigated: epoxy/aluminum, phenol/aluminum, and MDI/aluminum. Also it was shown that all three model compounds investigated, DGEBA, phenol, and MDI are strongly attached to the surface of alkaline cleaned aluminum even before curing. This is expected to improve the durability of adhesive bonds when primers based on these compounds are used. The aluminum adherends were pretreated exactly in the same way as the actual aluminum adherends used to prepare the adhesive bonds. Thus, the primer/aluminum interfaces investigated are almost identical with those found in the adhesive bonds used in the durability studies presented below. This allows for a better understanding of the role of primer/substrate interactions on the durability of adhesive bonds. It should be mentioned that in very few studies of primer or adhesive/metal interactions, was the metal substrate treated in the same way as the metal adherend in the adhesive bonds.

4.3. Durability tests

4.3.1. Phase a-SMC/urethane/ELPO steel samples

4.3.1.1. Failure results

4.3.1.1.1. Reference samples

Failure mode and force are controlled by the temperature at which the specimens are tested. Initial testing of as prepared lap shear, wedge, and butt torsion samples was carried out at different temperatures in the range 25°to 93°C to determine the test temperature conditions at which samples failed via a mixed mode process. Mixed mode failure was

desired to provide a set of test conditions where equal probability for adhesive or cohesive or substrate (delamination) failure occurred. These mixed mode results are reference data against which failure force and failure mode are to be compared for testing of specimens following environmental exposure.

Table 10 shows the failure results for all three types of sample geometry at the selected test temperatures. For lap shear samples a test temperature of 82°C was selected, since at this temperature a reasonable distribution of failure modes (32D/46A/22C) among the samples occurred. In addition, extensive laboratory test results are available from previous studies, and thus, a reliable reference data base exists. Cohesive failure was not observed for wedge samples. The temperature of 72°C was selected as the test temperature for wedge samples, because the distribution of delamination and adhesive failure modes is about equal (51D/49A). The modes of failure for butt torsion samples are almost exclusively delamination and adhesive failure. Cohesive failure was observed only in a small proportion of the tests at higher temperatures (72C and 82°C). The test temperature of 38°C was selected, because the distribution of delamination and adhesive mode failures was more constant among the samples, while the proportion of the delamination failure mode is still substantial (27%). For all samples the adhesive portion of the failure mode took place entirely at the adhesive/SMC interface.

4.3.1.1.2. Environmental cycle

For samples exposed to the environmental cycle, the failure results summarized in Tables 11 and 12 show that:

a) All unloaded samples survived the test and their residual strength (T) was, within the limits of precision, similar to the strength measured for the reference specimens (R) shown in Table 9: lap shear 277 ± 43 lbs (T) vs 270 ± 30 lbs (R), wedge 104 ± 15 lbs (T)

Table 10.
Failure Results. As Prepared Phase α-SMC/Treated Steel Samples Tested in Instron

Type of Sample	Test Temperature ℃	Failure Force, lbs* (Failure Moment, lb x ft)**	Failure Mode %D	%A	%C
Lap Shear	82	270 ± 30	32	46	22
Wedge	72	110 ± 10	51	49	0
Butt Torsion	38	67 ± 21	27	73	0

* For lap shear and wedge samples
** For butt torsion samples

Table 11.
Failure Results. Phase α-SMC/Urethane/ELPO Steel Samples.
Environmental Cycle. (Samples Which Survived the Test)

Duration of Cycle	Load	Type of Sample	Number of Samples Tested	Number of Samples Which Survived the Test	Average Failure Force, lbs* (Average Failure Moment, lb x ft **)	Average Failure Mode %D	%A	%C
7 Days	No Load	Lap Shear	5	5	277 ± 43	5	75	20
		Wedge	5	5	104 ± 15	39	61	-
		Butt Torsion	5	5	84 ± 3	46	54	-
	50% Load	Lap Shear	10	7	263 ± 42	1	63	36
		Wedge	10	5	100 ± 10	46	54	-
		Butt Torsion	5	-	--	-	-	-
21 Days	50% Load	Lap Shear	5	-	--	-	-	-
		Wedge	5	3	77 ± 16	47	53	-
	20% Load	Butt Torsion	5	-	--	-	-	-

* For lap shear and wedge samples
** For butt torsion samples

Table 12.

Failure Results. Phase α-SMC/Urethane/ELPO Steel Samples.
Environmental Cycle. (Samples Which Failed During the Test)

Duration of Cycle	Load	Type of Sample	Number of Samples Tested	Which Failed the Test	Time to Failure h - hours d - days	Average Failure Mode %D	%A	%C
7 Days	No Load	Lap Shear	5	-	--	-	-	-
		Wedge	5	-	--	-	-	-
		Butt Torsion	5	-	--	-	-	-
	50% Load	Lap Shear	10	3	1d, 3d, 4d	4	96	-
		Wedge	10	5	1d (three), 2d, 3d	7	93	-
		Butt Torsion	5	5	1d (all five)	5	83	12
21 Days	50% Load	Lap Shear	5	5	1d (four), 2d	5	95	-
		Wedge	5	2	1d, 17d	-	100	-
	20% Load	Butt Torsion	5	5	1d, 2d (two), 3d, 8d	4	61	35

vs 110 ± 10 lbs (R), and butt torsion 84 ± 3 lb x ft (T) vs 67 ± 21 lb x ft (R). The strengths are considered similar if there is an overlap in the ranges of values.

b) The application of a load produced failure of some samples during the environmental cycle. A very important observation is that all failures in the environmental cycle occurred while samples were in the 82°C (180°F) dry air condition. Thirty percent of the loaded lap shear samples, 50% of the loaded wedge samples, and all butt torsion samples exposed for up to seven days failed during the test. The residual strength for the samples which survived the test was similar to the reference strength (Table 10): lap shear 263 ± 42 lbs (T) vs 270± 30 lbs (R) and wedge 100 ± 10 lbs (T) vs 110 ± 10 lbs (R). All loaded lap shear samples and 40% of the loaded wedge samples exposed for up to 21 days failed during the exposure. The residual strength for the wedge samples which survived the test was lower than the strength of the reference samples (see table 10): 77± 16 lbs (T) vs 110 ± 10 lbs (R). All butt torsion samples, loaded either at 50% or at 20% of the ultimate failure force, failed during the test. The increase in load from 20% to 50% of the ultimate failure moment decreases the average time to failure for butt torsion samples from 3 days to 1 day indicating the significance of the load level on durability.

c) The most important observation regarding the failure mode is that adhesive failure occurred only at the adhesive/SMC interface for all samples. Exposure to the environmental cycle alters the failure mode for the unloaded lap shear and wedge samples so that a greater portion of failure occurs adhesively compared with the reference samples (Table 9): lap shear 5D/75A/20C (T) vs 32D/46A/22C (R) and wedge 39D/61A (T) vs 51D/49A (R). For the unloaded butt torsion samples the proportion of delamination failure was higher, 46%, for the exposed samples compared to the reference sample, 27%, (Table 10).

Important differences were observed regarding the mode of failure among the loaded samples which survived the test and then were tested in the Instron. For lap shear samples practically no delamination was observed. This failure mode was unlike that of the reference samples (Table 10): 1D/63A/36C(T) vs 32D/46A/22C(R). For wedge samples, the failure mode was equivalent to that for reference samples: 46D/54A (T) vs 51D/49A (R). The failure modes were arbitrarly considered similar or equivalent if the values were within the limit ± 15%. The failure mode for loaded lap shear and wedge samples which failed during exposure was almost entirely adhesive (93-100%), the remainder (7-0 %) being failure in the SMC substrate (delamination). No cohesive failure occurred for these samples. For the loaded butt torsion samples the failure mode was partially cohesive for samples under 20% load (4D/61A/35C) and for samples under 50% load (5D/83A/12C), while no cohesive failure was observed for reference samples: 27D/73A (Table 10) or for unloaded samples exposed to the environmental cycle: 46D/54A.

A significant result is that application of load not only induces failure during the cycle for all types of samples, but leads to a greater fraction of adhesive failure for all samples that failed during the test.

d) The failure results indicate that butt torsion samples are more sensitive to the environmental durability scheme, than the lap shear and wedge samples. Sensitive samples are desirable in order to reduce the duration of accelerated durability tests. The butt torsion samples failed faster and in a higher proportion upon exposure to the environmental cycle even at a lower level of stress. For the lap shear and wedge samples the application of load coupled with environmental exposure seems to weaken primarily the adhesive/SMC interface, with failure occurring during exposure almost entirely by adhesive failure. For butt torsion samples the application of load to samples exposed to the environmental cycle produces some cohesive failure which is not observed for the unloaded samples or for the

reference samples. This indicates the weakening of the adhesive due to the particular state of stress existing in the loaded butt torsion samples. It was observed for butt torsion samples that the adhesive exhibited condiderably more plastic deformation when subjected to stress than lap shear and wedge samples. For lap shear samples there are stress concentrations near the adhesive/adherend interface (See 2.2.5.2). The finite stress analysis of loaded phase α-SMC/epoxy/ELPO steel wedge samples showed stress concentrations at the adhesive/adherend interface, with higher stresses at the adhesive/SMC side [188]. The variation of stress through the adhesive layer thickness and across the width of the joint is minimized for butt torsion samples (105). The stress concentration at the outer radius of the butt torsion samples may produce yielding and microdamaging of the adhesive through the whole thickness in that region. This damaged region provides starting points for crack initiation and leads to an irreversibly weaker adhesive and to a higher possibility of cohesive failure during the test or in the Instron test.

4.3.1.1.3. 49°C (120°F)/Static test

The finding that test samples failed only during the 82°C (180°F)/dry air portion of the environmental cycle, prompted a more detailed investigation of sample durability under fixed conditions of temperature and humidity. The durability of samples at moderate temperatures was investigated by testing lap shear and wedge samples stressed at 50% of ultimate failure load and butt torsion samples stressed at 20% of the ultimate failure load at 49°C (120°F) in dry air and 49°C (120°F) in 85% RH for up to thirty days. Failure results for these samples are collected in Tables 13 and 14. Upon examination of the results in the tables the following observations can be made:

a) All loaded lap shear and wedge samples maintained at 49°C in dry air survived the test, and their residual strength was comparable to the reference strength (Table 10): lap

Table 13.

Failure Results. Phase α-SMC/Urethane/ELPO Steel Samples.
49°C (120°F), 30 Days. (Samples Which Survived the Test)

Humidity	Load	Type of Sample	Number of Samples Tested	Which Survived the Test	Average Failure Force, lbs* (Average Failure Moment, lb x ft **)	Average Failure Mode %D	%A	%C
Dry Air	50% Load	Lap Shear	5	5	323 ± 30	14	66	20
		Wedge	5	5	110 ± 7	50	50	-
	20% Load	Butt Torsion	5	-	--	-	-	-
85% RH	50% Load	Lap Shear	5	5	247 ± 45	19	78	3
		Wedge#	5	5	77 ± 23	43	57	-
	20% Load	Butt Torsion	5	-	--	-	-	-

* For lap shear and wedge samples
** For butt torsion samples
# All samples developed cracks during the test

Table 14

Failure Results. Phase α-SMC/Urethane/ELPO Steel Samples.
49°C (120°F), 30 Days. (Samples Which Failed During the Test).

Humidity	Load	Type of Sample	Number of Samples Tested	Number of Samples Which Failed During the Test	Time to Failure h - hours d - days	Average Failure Mode %D	%A	%C
Dry Air	50% Load	Lap Shear	5	-	--	-	-	-
		Wedge	5	-	--	-	-	-
	20% Load	Butt Torsion	5	5	1h, 19h, 2d, 15d, 21d	35	30	35
85% RH	50% Load	Lap Shear	5	-	--	-	-	-
		Wedge	5	-	--	-	-	-
	20% Load	Butt Torsion	5	5	19h, 41h, 62h (two), 2d	14	37	49

shear 323 ± 30 lbs (T) vs 270 ± 30 lbs (R) and wedge 110 ± 7 lbs (T) vs 110 ± 10 lbs (R). All loaded butt torsion samples failed during testing at 49°C (120°F) in dry air.

b) All lap shear and wedge samples survived exposure to 49°C at 85% RH. Their residual strength was significantly lower than the residual strength of the samples tested at 49°C/dry air conditions: lap shear 247 ± 45 lbs (85% RH) vs 323 ± 30 lbs (dry air) and wedge 77 ± 23 lbs (85% RH) vs 110 ± 7 lbs (dry air). All butt torsion samples investigated at 49°C in 85% RH failed during the test. The average time to failure was lower than for the samples maintained at 49°C in dry air: 1.9 days (85% RH) vs 7.8 days (dry air).

c) Adhesive failure took place at the adhesive/SMC interface. For the exposed lap shear samples a greater fraction of adhesive failure and a lower proportion of delamination of SMC occurred compared with reference samples (Table 10): 14D/66A/20C (49°C/dry air) and 19D/78A/3C (49°C/100% RH) vs 32D/44A/22C (R). For lap shear samples studied at 49°C in 85% RH, the proportion of cohesive failure was insignificant. The failure mode for wedge samples was similar to that of the reference samples given in Table 10: 50D/50A (49°C/dry air) and 43D/57A (49°C/85% RH) vs 51D/49A (R). For butt torsion samples the failure mode was mixed, a large proportion of the failure mode being cohesive, 35D/30A/35C (49°C/dry air) and 14D/37A/49C (49°C/85% RH), while no cohesive failure was observed for the reference samples: 27D/73A.

The most significant result for these samples is that at moderate temperatures the lap shear and wedge samples survived a relatively long time, even under harsh conditions of stress and humidity, while the butt torsion samples in the same environmental conditions failed faster, even at much lower levels of stress. Exposure to humidity reduces significantly the residual strength and the time to failure compared with exposure to dry conditions. It was shown in 4.1. that both the polyurethane adhesive and the phase α-

SMC absorb water during exposure to high humidity. It is reasonable to suggest that water absorption produced when the samples are exposed to high humidity weakens both the adhesive and the SMC material and consequently decreases adhesive bond durability. Both the polyurethane adhesive and the SMC polyester matrix are polymeric materials whose mechanical properties and integrity can be deteriorated by the combined action of water and heat. The deterioration process can be physical or chemical in nature. Polyurethanes are sensitive to moisture due to the urethane linkage [90]. Also, polyesters are prone to hydrolysis [189]. So the adhesive and composite matrix hydrolysis may take place during environmental exposure, reducing their strength. Water absorbtion produces the lowering of glass transition of polymers and decreases the modulus and strength[190, 191]. For example, Brewis et al. [192] found that for an epoxy adhesive the absorption of 1.9 % water reduced the modulus by 43 % and the yield strength by 16 % when compared with the dry adhesive. Also moisture absorption may induce adhesive and composite matrix swelling and generate internal stresses [193].

4.3.1.1.4. 60°C (140°F)/Static test

The investigation of sample durability under fixed conditions of temperature and humidity was continued by testing samples at higher temperatures: 60°C and 82°C.

In Table 15 are shown the failure results for unloaded samples exposed at 60°C in dry air and at 60°C in 85% RH for 7 days. Tables 16 and 17 summarize the failure results for lap shear and wedge samples under 50% load and butt torsion samples under 20% load investigated at 60°C in dry air or at 60°C in 85% RH for up to 7 days and for lap shear and wedge samples under 50% load tested at 60°C in 85% RH for up to 30 days. For the seven day test, both wedge samples loaded in constant displacement (CD) and wedge samples

Table 15.

Failure Results. Phase α-SMC/Urethane/ELPO Steel Samples.
No Load. 60°C (140°F), 7 Days. (Samples Which Survived the Test)

Humidity	Type of Sample	Number of Samples Tested	Number of Samples Which Survived the Test	Average Failure Force, lbs* (Average Failure Moment, lb x ft **)	Average Failure Mode %D	%A	%C
Dry Air	Lap Shear	5	5	304 ± 58	7	93	-
	Wedge	5	5	95 ± 12	37	63	-
	Butt Torsion	4	4	95 ± 15	64	36	-
85% RH	Lap Shear	5	5	266 ± 28	10	90	-
	Wedge	5	5	91 ± 8	33	67	-
	Butt Torsion	5	5	77 ± 21	24	51	25

* For lap shear and wedge samples
** For butt torsion samples

Table 16.

Failure Results. Phase α-SMC/Urethane/ELPO Steel Samples.
60°C (140°F). (Samples Which Survived the Test)

Duration of Cycle	Humidity	Load	Type of Sample	Number of Samples Tested	Number of Samples Which Survived the Test	Average Failure Force, lbs* (Average Failure Moment, lb x ft **)	Average Failure Mode %D	%A	%C
7 Days	Dry Air	50% Load	Lap Shear	5	4	341 ± 25	30	70	-
			Wedge+	5	4	101 ± 15	51	49	-
			Wedge++	5	2	104 ± 3	45	55	-
		20% Load	Butt Torsion	5	-	--	-	-	-
	85% RH	50% Load	Lap Shear	5	2	216 ± 11	12	38	50
			Wedge+	5	4	68 ± 32	32	68	-
			Wedge++	5	5	86 ± 8	28	72	-
		20% Load	Butt Torsion	5	-	--	-	-	-
30 Days	85% RH	50% Load	Lap Shear	5	-	--	-	-	-
			Wedge+	5	2	94 ± 24	43	57	-

* For lap shear and wedge samples
** For butt torsion samples
+ Constant displacement loaded samples
++ Constant load

Table 17.

Failure Results. Phase α-SMC/Urethane/ELPO Steel Samples.
60°C (140°F). (Samples Which Failed During the Test)

Duration of Cycle	Humidity	Load	Type of Sample	Number of Samples Tested	Number of Samples Which Failed During the Test	Time to Failure h - hours d - days	Average Failure Mode %D	%A	%C
7 Days	Dry Air	50% Load	Lap Shear	5	1	17h	10	90	-
			Wedge+	5	1	4h	3	97	-
			Wedge++	5	3	15h, 4d, 7d	4	96	-
		20% Load	Butt Torsion	5	5	1d, 2d, 4d, 7d (2)	4	77	19
	85% RH	50 % Load	Lap Shear	5	3	4h, 16h, 1d	12	88	-
			Wedge+	5	1	2h	5	95	-
			Wedge++	5	-	--	-	-	-
		20% Load	Butt Torsion	5	5	15h, 2d (2), 3d (2)	2	63	35
30 Days	85% RH	50% Load	Lap Shear	5	5	4h, 15h, 2d (2), 9d	15	85	-
			Wedge+	5	3	13d, 23d, 28d	1	99	-

* For lap shear and wedge samples
** For butt torsion samples
+ Constant displacement loaded samples
++ Constant load

loaded in constant load mode (CL) were employed. Examination of the data presented in Tables 15-17 shows the following:

a) All unloaded samples studied at 60°C in dry air survived the test and their residual strength was similar to the strength of the reference samples (Table 10): lap shear 304 ± 58 lbs (T) vs 270 ±30 lbs (R), wedge 95 ± 12 lbs (T) vs 110 ± 10 lbs (R) and butt torsion 95 ± 15 lb x ft (T) vs 67 ± 21 lb x ft (R). These results indicate that exposure at 60° C alone does not the degrade the adhesive bonds, i.e., samples did not fail during exposure and no decrease in the residual strength was found.

b) Some loaded lap shear and wedge samples and all loaded butt torsion samples failed when tested at 60°C in dry air for 7 days. The residual strength for the samples which survived the test was higher than the reference strength for lap shear specimens (Table 10): 341 ± 25 lbs (T) vs 270 ± 30 lbs (R) but similar to the reference strength for wedge samples (Table 10): 101 ± 15 lbs (CD) and 104 ± 3 lbs (CL) vs 110 ± 10 lbs (T).

c) All unloaded samples investigated at 60°C in 85% RH survived the test and their residual strength was similar to the reference strength for lap shear and butt torsion samples (Table 10): lap shear 266 ± 28 lbs (T) vs 270 ± 30 lbs (R) and butt torsion 77 ± 21 lb x ft (T) vs 67 ± 21 lb x ft (R). For wedge specimens the residual strength was somewhat lower than the reference strength (Table 10) 91 ± 8 lbs (T) vs 110 ± 10 lbs (R).

d) Some loaded lap shear and wedge samples and all loaded butt torsion samples failed during exposure at 60°C in 85% RH for up to 7 days. The residual strength for the samples which survived the test was significantly lower than that of the reference samples (Table 10): lap shear 216 ± 11 lbs (T) vs 270 ± 30 lbs (R) and wedge 68 ± 32 lbs (CD) and 86 ±8 lbs (CL) vs 110 ± 10 lbs (T)

A higher proportion (60%) of loaded lap shear samples failed during exposure to 85% RH (60%) than in dry air (20%). Surprisingly, all wedge samples loaded in the constant load

mode and tested at 85% RH survived the test, while 60% of those maintained in dry air failed during the test. The average failure time for butt torsion samples exposed to humidity was 2.1 days while for samples exposed to dry air conditions the average time to failure was 4.2 days.

e) The increase in the time of exposure at 60°C in 85% RH from 7 days to 30 days increased the proportion of samples which failed during testing: lap shear from 60% to 100% and wedge from 20% to 60%. For the wedge samples which survived the test the residual strength was similar to the reference strength (Table 10): 94 ± 24 lbs (T) vs 110 ± 10 lbs (R).

f) All adhesive failure took place at the adhesive/SMC interface. Generally the failure mode for lap shear samples was a mixture of delamination (7-30%) and adhesive failure (93-70%). For loaded lap shear samples tested at 60°C and 85% RH and which failed in the Instron test, the failure mode was principally cohesive (12D/38A/50C). The wedge samples which survived exposure at 60°C in dry air or at 60°C in 85% RH and were then tested in the Instron, failed by a mixture of delamination (28-51%) and adhesive failure (72-49%); the failure mode being relatively close to that of the reference samples (51D/49A) given in Table 10. For wedge samples which failed during testing at 60°C in dry air or at 60°C in 85% RH, the failure mode was almost entirely adhesive (1-5% D, 99-95% A). For unloaded butt torsion samples, exposure to 85% RH shifts the failure mode distribution to a higher proportion of adhesive failure from 64D/36A for samples exposed to dry air to 24D/51A/25C for samples exposed to 85% RH. The butt torsion samples failed during testing by adhesive failure (63-77%). However, a significant portion of the failure mode was cohesive (35-19%).

g) The increase in the test temperature from 49°C to 60°C had a significant influence on the durability results. While all lap shear and wedge samples maintained at

49°C in 85% RH survived the thirty day tests, all lap shear samples and 60% of wedge samples studied at 60°C in 85% RH failed during the thirty day test. In both tests all butt torsion samples failed during the exposure, proving to be more sensitive to conditions of stress than the other two types of samples.

4.3.1.1.5. 82°C (180°F)/Static test

The finding that test samples failed only during the 82°C (180°F)/dry air portion of the environmental cycle prompted a more detailed investigation of sample durability at higher temperature. Tables 18 and 19 present the failure results for samples tested at 82°C (180°F) in dry air for up to 7 days. The results in Table 18 and 19 reveal that:

a) All lap shear and wedge samples under 20% load survived exposure at 82°C in dry air. Their residual strength was comparable to that for the reference samples (Table 10): lap shear 291 ± 20 lbs (T) vs 270 ± 30 lbs (R) and wedge samples 99 ± 13 lbs (T) vs 110 ± 10 (R). All butt torsion samples under 20% load failed during testing at 82 °C in dry air.

b) The increase in load from 20% to 50% induced failure of all lap shear and wedge specimens with the exception of two wedge specimens investigated at 82°C in 85% RH. For these, the residual strength was significantly lower than the reference strength (Table 9): 85 ± 1 lbs (T) vs 110 ± 10 lbs (R)

c) For lap shear samples the failure mode was a mixture of adhesive failure (77-99%) and delamination (23-1%). For wedge samples under 20% load and tested in dry air, the failure mode was close to that for reference samples (Table 10) 41D/59A (T) vs 51D/49A (R). For wedge samples under 50% load which survived the 82°C and 85% RH exposure, a greater fraction of adhesive failure (78%) was noted. The wedge samples under 50% load failed during exposure mostly by adhesive failure (80-91%) both in dry air

Table 18.

Failure Results. Phase α-SMC/Urethane/ELPO Steel Samples.
82°C (180°F), 7 Days. (Samples Which Survived the Test)

Humidity	Load	Type of Sample	Number of Samples Tested	Which Survived the Test	Average Failure Force, lbs* (Average Failure Moment, lb x ft **)	Average Failure Mode %D	%A	%C
Dry Air	20% Load	Lap Shear	5	5	291 ± 20	10	90	-
		Wedge	5	5	99 ± 13	41	59	-
		Butt Torsion	5	-	--	-	-	-
	50% Load	Lap Shear	5	-	--	-	-	-
		Wedge	5	-	--	-	-	-
85% RH	50% Load	Lap Shear	5	-	--	-	-	-
		Wedge	5	2	85 ± 1	22	78	-

* For lap shear and wedge samples
** For butt torsion samples

Table 19

Failure Results. Phase α-SMC/Urethane/ELPO Steel Samples.
82°C (180°F), 7 Days. (Samples Which Failed During the Test)

Humidity	Load	Type of Sample	Number of Samples Tested	Number of Samples Which Failed During the Test	Time to Failure h - hours d - days	Average Failure Mode %D	%A	%C
Dry Air	20% Load	Lap Shear	5	-	--	-	-	-
		Wedge	5	-	--	-	-	-
		Butt Torsion	5	5	2h, 2d (3), 5d	4	60	36
	50% Load	Lap Shear	5	5	7h (3), 1d, 6d	23	77	-
		Wedge	5	5	7h (4), 3d	20	80	-
85% RH	50% Load	Lap Shear	5	5	4h (4), 1d	1	99	-
		Wedge	5	3	4h (2), 8h	9	91	-

and in 85% RH. The butt torsion samples failed largely by adhesive failure (60%), while a significant proportion of the failure mode was cohesive (36%).

d) These results show clearly that exposure to high temperatures in combination with a high level of loading has a severe effect on durability for phase α-SMC/urethane /ELPO steel test specimens. Almost all lap shear and wedge samples under 50% load failed during investigation at 82°C in a short time, while all lap shear and wedge samples under the same conditions of load and temperature survived the 30 day test at 49°C (see Tables 13 and 14). This can be explained by the effect of temperature on mechanical properties of polymeric materials. Both the polyurethane adhesive and the SMC being polymeric materials have a time-dependent behavior and can display creep deformation, stress relaxation and delayed failure when subjected to long-time loading. This time - dependent behavior is accelerated by an increase in temperature [3, 194]. Consequently, with incresing temperature the compliance increases and the failure of the material takes place faster [3, 195]. As the temperature increases the strength of polymeric materials decreases [196, 197]. It was found that increasing temperature reduces both the strength of the adhesive [198, 199] and the strength of the adhesive bond [200].

4.3.1.1.6. -30°C/Static test

To inquire about the durability of samples at low temperatures, lap shear and wedge specimens were stressed at 50% of the ultimate failure load and maintained at -30°C (-22°F) for 7 days. The failure results are summarized in Table 20.

. All samples survived the test. The residual strengths were similar to the reference strengths given in Table 10: lap shear 264 ± 40 lbs (T) vs 270 ± 30 lbs (R) and wedge 90 ± 15 lbs (T) vs 110 ± 10 lbs (R). The failure mode shows a shift toward a greater proportion of adhesive failure for both types of samples: lap shear 25D/75A (T) vs 32D/56A/22C (R)

Table 20.

Failure Results. Phase α-SMC/Urethane/ELPO Steel Samples.
50% Load, - 30 °C, 7 Days.

Type of Sample	Number of Samples Tested	Which Survived the Test	Average Failure Force, lbs*	Average Failure Mode		
				%D	%A	%C
Lap Shear	5	5	264 ± 40	25	75	-
Wedge	5	5	90 ± 15	35	65	-

* All samples survived the test

and wedge 35D/75A (T) vs 51D/49A (R). These results indicate that exposure to low temperatures does not degrade the adhesive bonds, i.e., samples do not fail during exposure and no decrease in the residual strength was found. The increase in the fraction of adhesive failure may be due to a preferential weakening of the interphase region under load. It was shown before that for lap shear and wedge samples there are high stress concentrations at the adhesive/adherend interface.

4.3.1.2. Surface characterization

In addition to the durability tests, characterization measurements for failed specimens were completed to identify the mode of failure. For all three specimen configurations and all durability tests, XPS and SEM measurements were carried out for portions of the failure surface that exhibited "adhesive" failure. Considering that for all samples, failure occurred only at the SMC-adhesive side of the bond, this means that the XPS and SEM studies were performed for portions of failed surfaces where failure occurred at the SMC/adhesive interface.

In order to illustrate the findings for phase α-SMC/urethane/ELPO steel samples, the XPS and SEM results for the following tests will be presented:

a) Testing in the Instron. No load. No environment. Lap shear samples.

b) 50% load, environmental cycle, 21 days. Wedge samples.

c) 50% load, 60°C (140°F), 7 days. Wedge samples.

d) 20% load, 60°C (140°F), 7 days. Butt torsion samples

The SEM and XPS results for reference surfaces involved in a phase α-SMC/urethane/ELPO steel adhesive bond will be presented first. These results serve as reference data to be used as an aid in the identification of the failure mode for test samples. Figure 57 shows the scanning electron micrographs for as received SMC and primed SMC.

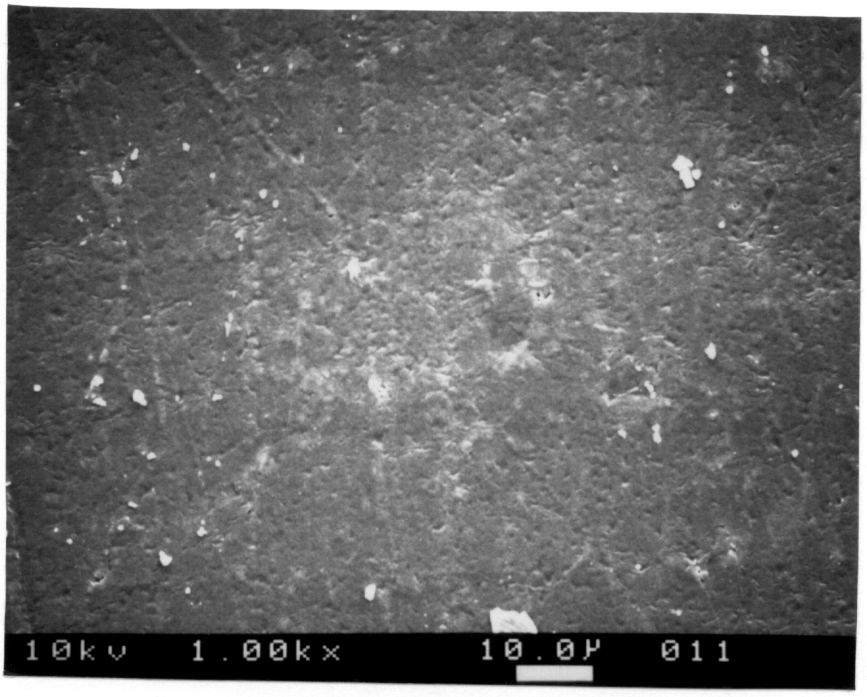

As received phase α–SMC

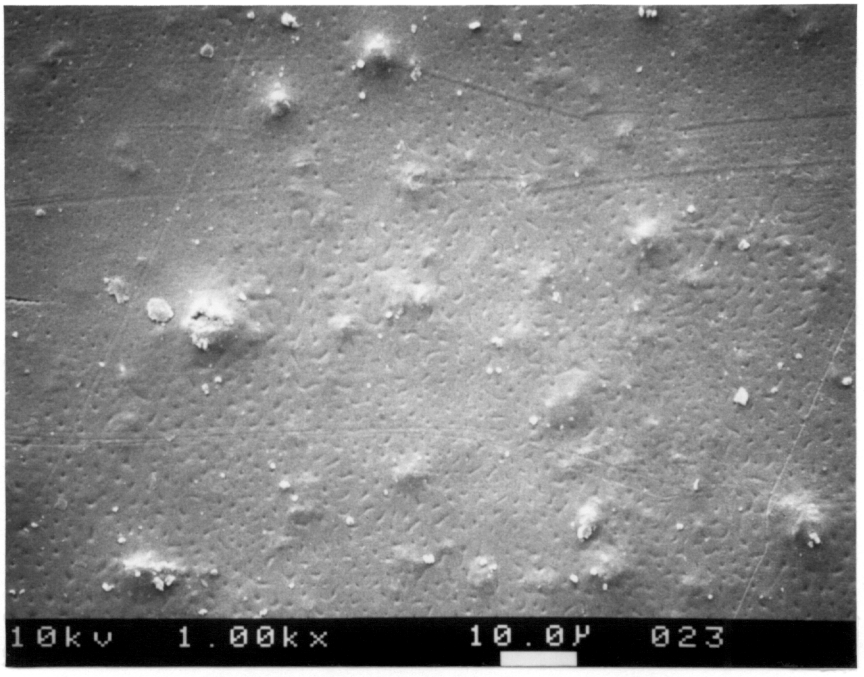

Disocyanate primed phase α–SMC

Figure 57. SEM results for reference surfaces.

The surface of as received SMC is relatively smooth, while some small mounds are observed on the primed SMC surface. In Table 21 are presented the XPS results (atomic concentration) for as received phase α-SMC, split phase α-SMC, adhesive film, split adhesive, and primed SMC surfaces. The split phase α-SMC surface was prepared by splitting a 15 x 17 mm as received SMC sample. The cut surface was measured. The split adhesive surface was prepared by removing a thin layer from the surface of an adhesive film. The primed phase α-SMC sample was prepared by priming the SMC surface with Pliogrip 6036 primer. Figure 58 shows the C 1s spectra for as received phase α-SMC, split phase α-SMC, primed SMC, and adhesive film surfaces. In Figures 59 and 60 are presented C 1s spectra, synthesized using the individual component spectra, corresponding to a limited number of combinations from the whole variety of mixed failed surfaces which could result during testing. The C ls spectra of the failed surfaces will be compared with C 1s spectra from Figures 58, 59, and 60 and in correlation with the atomic concentration results and the SEM results will be used to aid in determining the nature of the failed surfaces.

Selected scanning electron micrographs presented in Figures 61-64 for the failed adhesive side show rough surfaces with regions of smooth surface and areas where particulate materials are present. Examination of the scanning electron micrographs for the failed SMC side surfaces reveals a non-smooth surface containing a significant fraction of nodular features with smaller areas of smooth features (SMC surface). These results taken together indicate that so called "adhesive" failure is, in reality, a mixture of near surface debonding of the SMC and interfacial adhesive failure. In such a process near surface SMC material appears to be the weak link in the bonded system so that when failure occurs, outer SMC material appears on the adhesive side of the failed specimen. No fiber

Table 21

XPS Results for Reference Surfaces

(Atomic %)

	As Received Phase α–SMC	Split Phase α-SMC	Urethane Adhesive Film	Split Urethane Adhesive	Diisocyanate Primed Phase α–SMC
C	82.8	75.9	68.8	56.8	74.8
O	14.2	21.7	26.4	31.2	19.0
N	<0.1	<0.1	2.90	2.65	5.41
Si	0.42	0.27	1.35	5.67	0.59
Zn	0.38	0.22	<0.1	<0.1	<0.1
Ca	0.30	0.39	<0.1	<0.1	<0.1
Mg	1.09	0.97	0.52	1.97	<0.1
Al	0.76	0.47	<0.1	1.70	<0.1

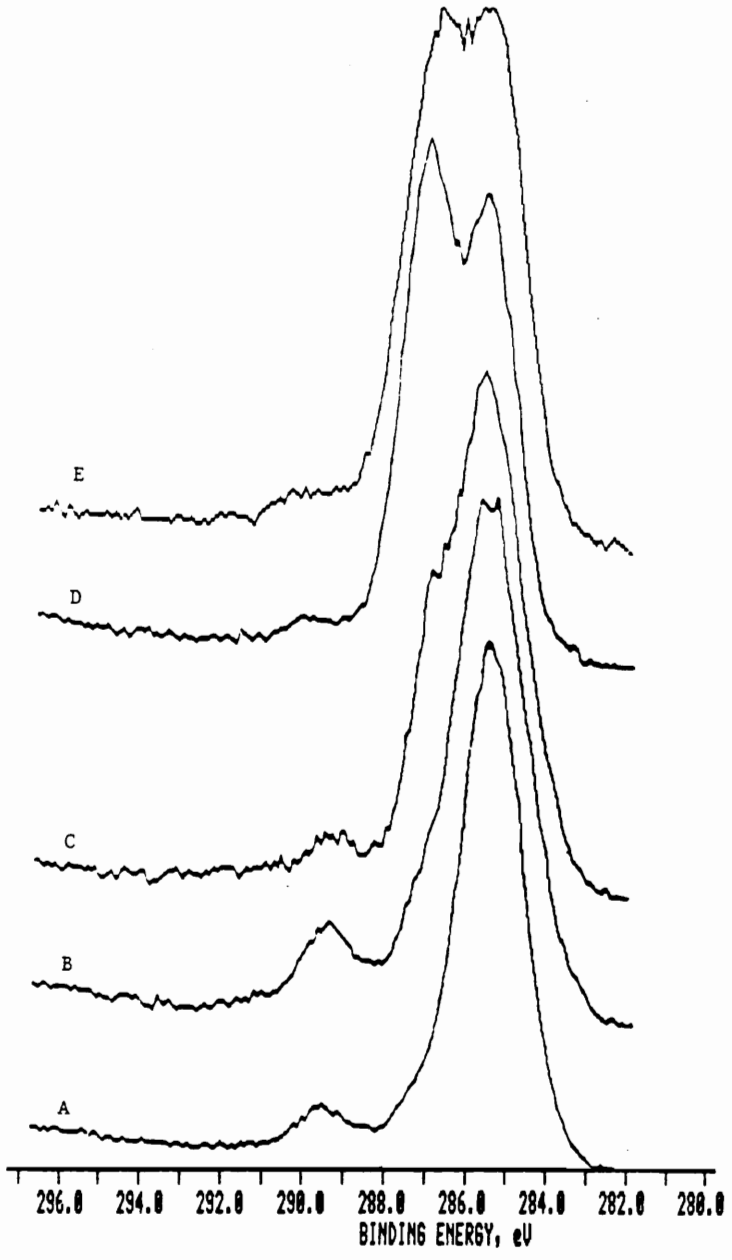

Figure 58. C 1s spectra for reference samples.

A. As received phase α-SMC
B. Split phase α-SMC
C. Primed phase α-SMC
D. Polyurethane adhesive film
E. Split polyurethane adhesive

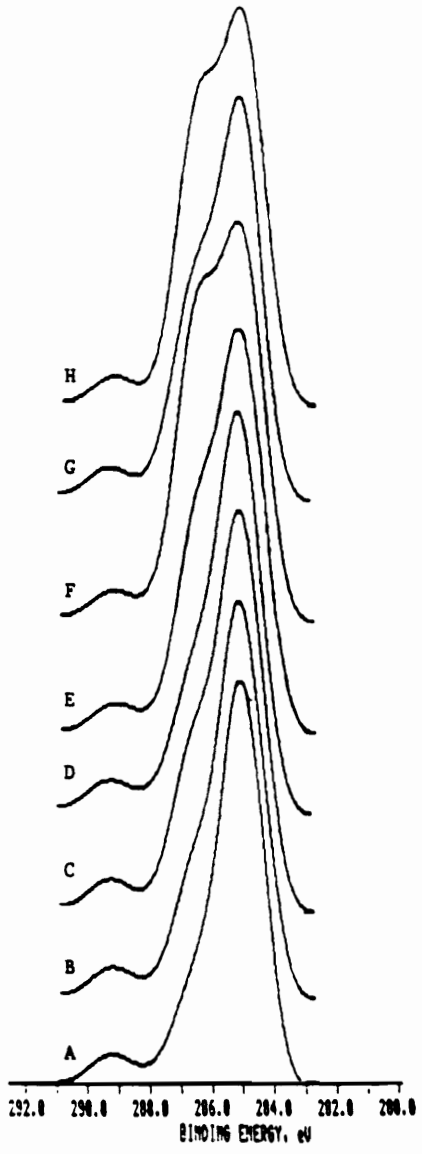

Figure 59. Synthesized C 1s spectra for mixed surfaces.

A. 75% as received phase α-SMC, 25% primed phase α-SMC
B. 50% as received phase α-SMC, 50% primed phase α-SMC
C. 25% as received phase α-SMC, 75% primed phase α-SMC
D. 75% as received phase α-SMC, 25% adhesive film
E. 50% as received phase α-SMC, 50% adhesive film
F. 25% as received phase α-SMC, 75% adhesive film
G. 33% as received phase α-SMC, 33% primed phase α-SMC, 33% adhesive film
H. 50% primed phase α-SMC, 50% adhesive film

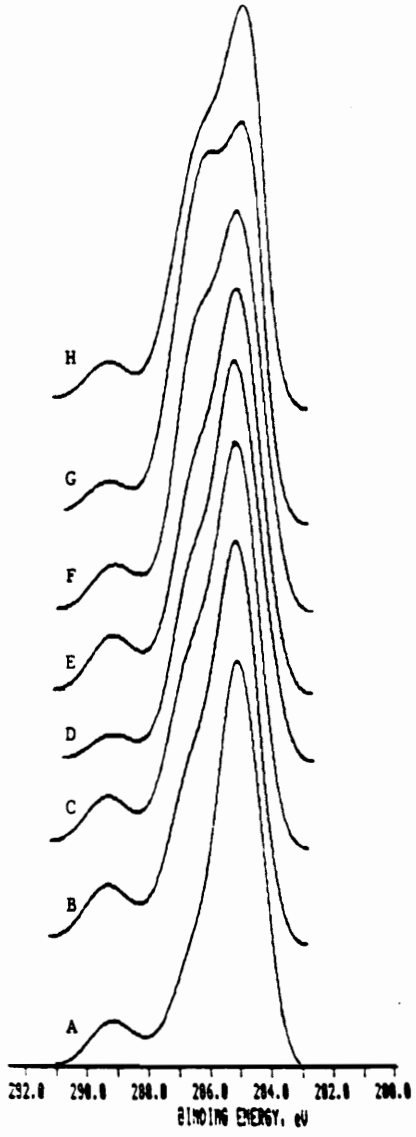

Figure 60. Synthesized C 1s spectra for mixed surfaces.

A. 75% split phase α-SMC, 25% primed phase α-SMC
B. 50% split phase α-SMC, 50% primed phase α-SMC
C. 25% split phase α-SMC, 75% primed phase α-SMC
D. 75% split phase α-SMC, 25% adhesive film
E. 50% split phase α-SMC, 50% adhesive film
F. 50% primed phase α-SMC, 50% adhesive film
G. 25% split phase α-SMC, 75% adhesive film
H. 33% split phase α-SMC, 33% primed phase α-SMC, 33% adhesive film

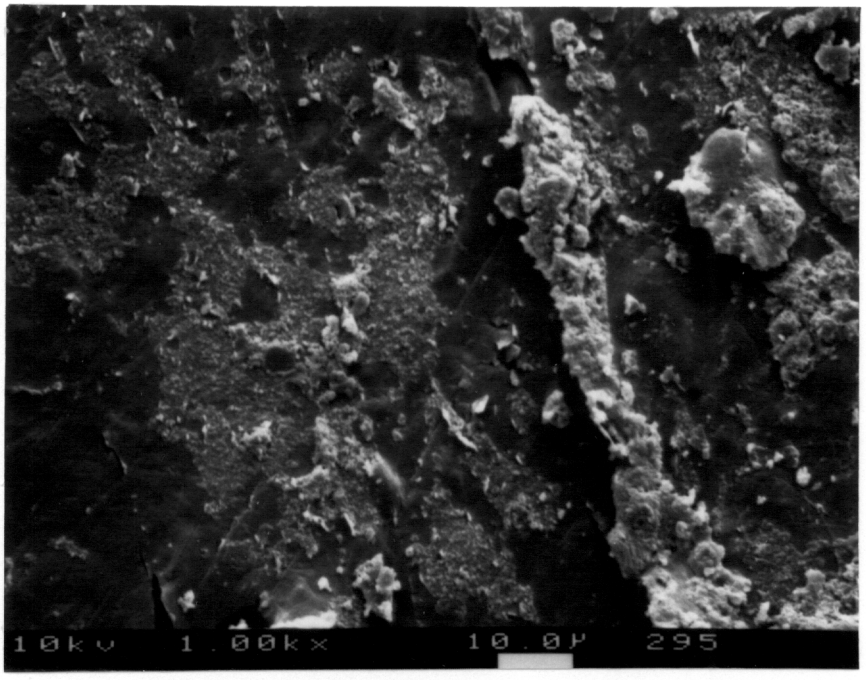

Adhesive side

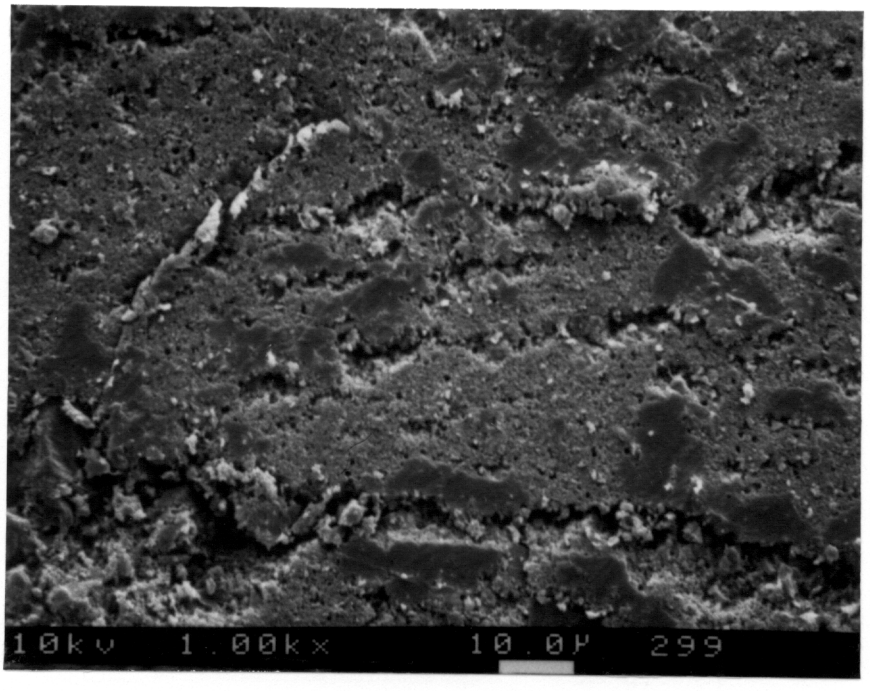

SMC side

Figure 61. SEM results. Phase α-SMC/urethane/ELPO steel lap shear specimens. No load, no environmental conditioning. Instron failure.

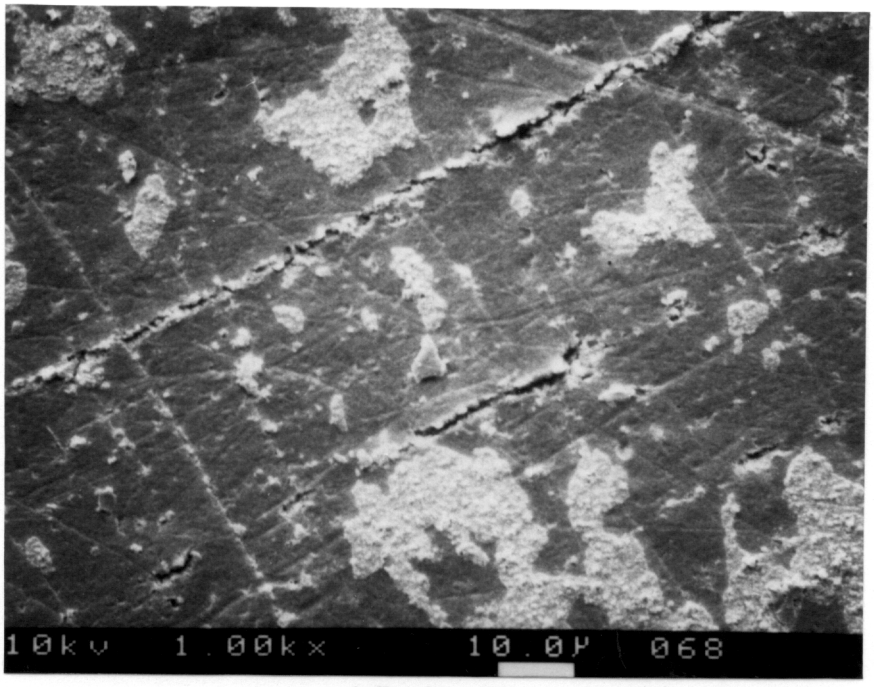

Adhesive side

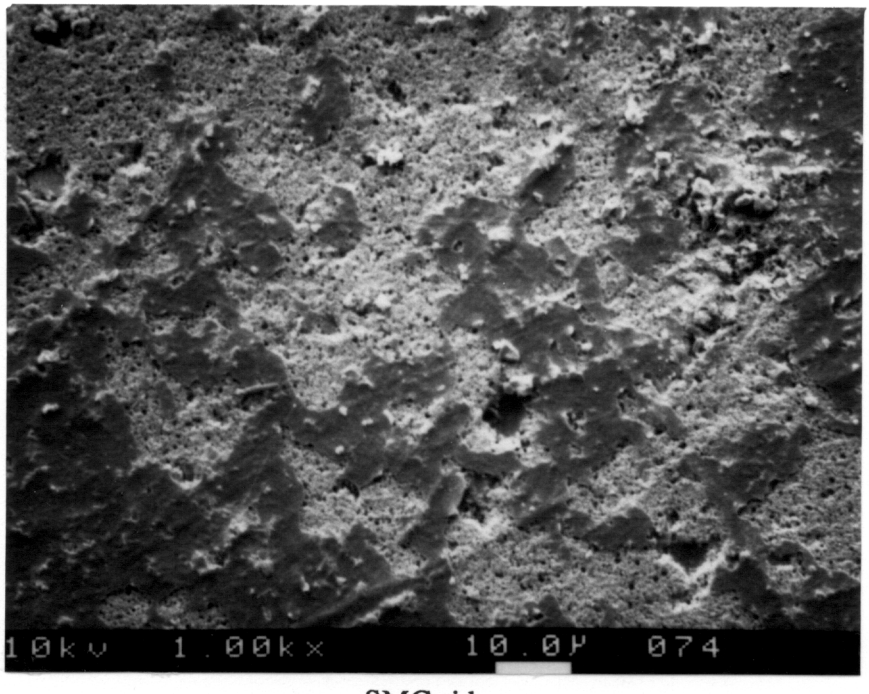

SMC side

Figure 62. SEM results. Phase α-SMC/urethane/ELPO steel wedge specimens. 50% load, environmental cycle, 21 days. Instron failure.

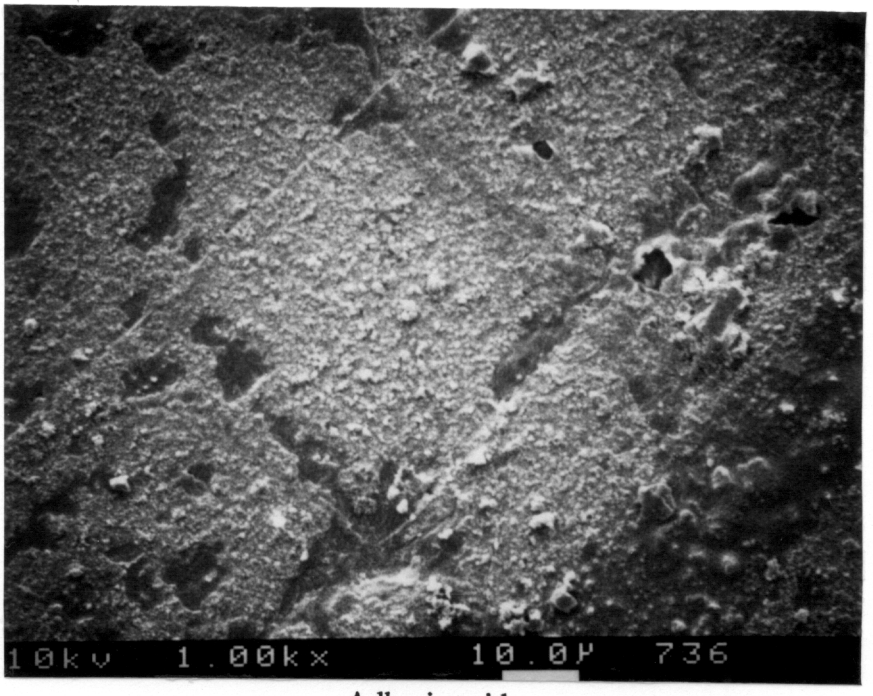

Adhesive side

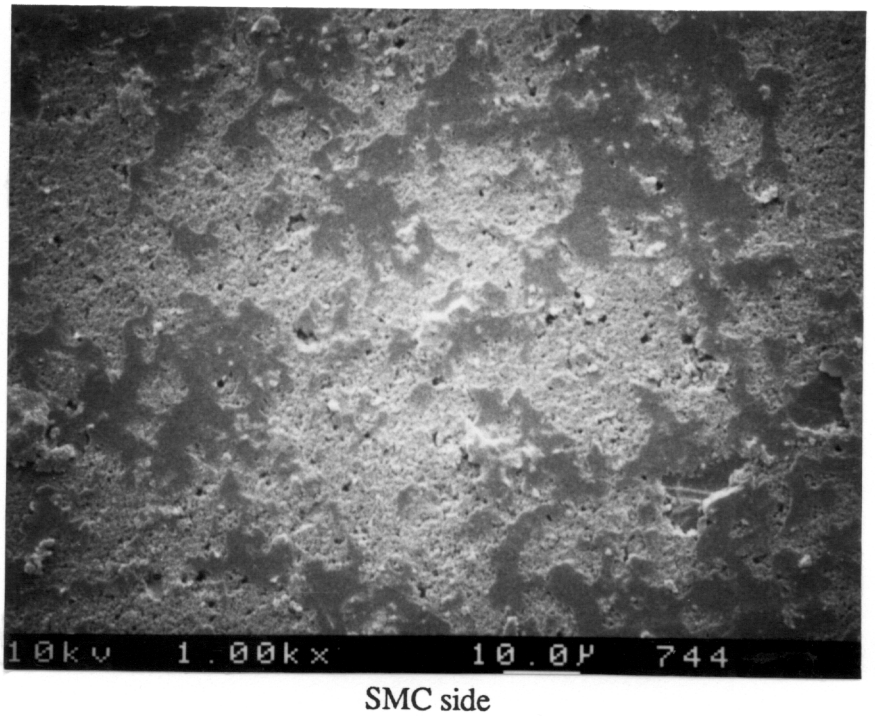

SMC side

Figure 63. SEM results. Phase α-SMC/urethane/ELPO steel wedge specimens. 50% load, 60°C (140°F), 85% RH, 7 days. Test failure.

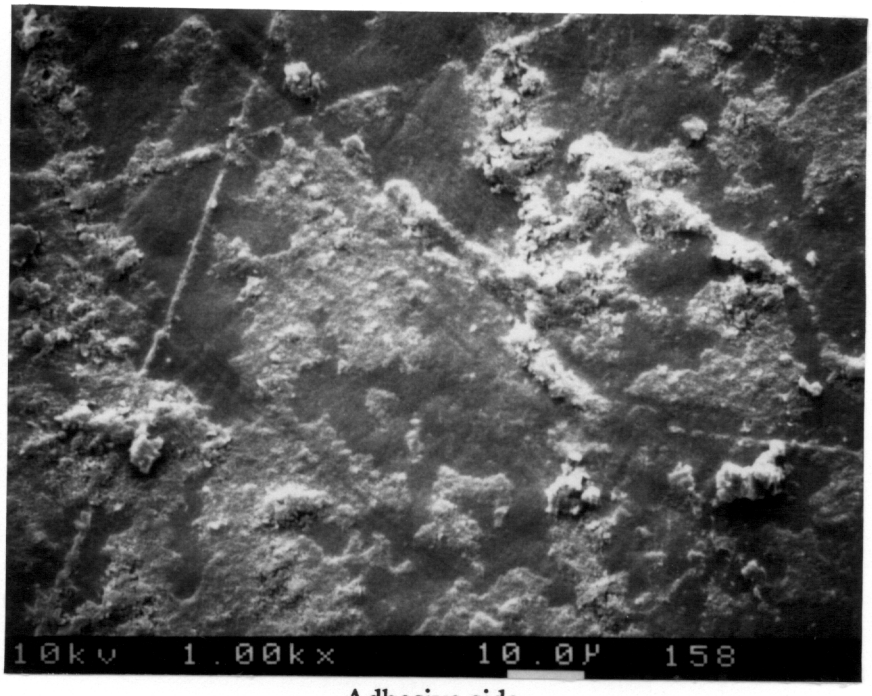

Adhesive side

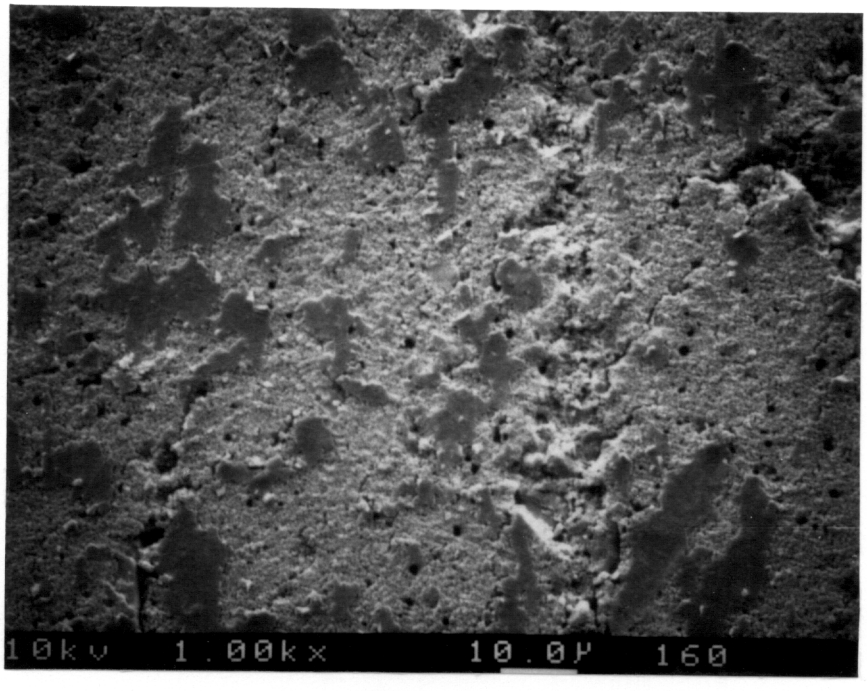

SMC side

Figure 64. SEM results. Phase α-SMC/urethane/ELPO steel butt torsion specimens. 20% load, 60°C (140°F), 85% RH, 7 days. Test failure.

or filler material is detected on either failed surface. Thus it is clear that "deep" debonding of the SMC, i.e., delamination, does not occur.

The XPS characterization results for the failed surfaces presented in Table 22 and in Figure 65 (C 1s spectra) support the SEM findings. Table 22 shows that the SMC side surfaces contain nitrogen and some adhesive side surfaces contain calcium. The surface of a pure adhesive film does not contain calcium and the non-primed SMC surface does not contain nitrogen. Thus, the detection of calcium (>0.1%) on the adhesive side failure surface suggests the presence of SMC constituents. The detection of nitrogen (>0.1%) on the SMC surface indicates the presence of adhesive and/or primer. The percentage of nitrogen on the adhesive side surfaces varies between 0.90 and 4.01 %. The calcium content on the adhesive side surfaces is lower than that for the SMC side surfaces.

Figure 65 shows the C ls spectra of failed adhesive and SMC-side surfaces. C 1s spectral features associated with $-CO_2R$ (BE 289.1 eV), >C=O (BE 288 eV), -COR/-NCO (BE 286.5 eV), and CH_n (BE 285 eV) chemical functionalities are found in each spectrum. For all samples the C ls spectra of the adhesive side do not resemble that of pure adhesive They are similar to the synthesized spectra corresponding to mixtures of as received or split phase α-SMC and primed phase α-SMC surfaces or to mixtures of as received or split phase α-SMC, primed phase α-SMC and adhesive film surfaces shown in Figures 58 and 59. For example, the C ls adhesive side spectrum of the as prepared lap shear sample (Figure 65A) is similar to the synthesized C ls spectrum (Figure 60B) corresponding to a mixture of split phase α-SMC (50%) and primed phase α-SMC (50%). The C ls adhesive side spectrum of the butt torsion samples tested at 60°C and 85% RH (Figure 65D) is very similar to the C ls spectrum corresponding to a mixture of split phase α-SMC (33.3%), primed phase α-SMC (33.3%) and adhesive film (33.3%) shown in

Table 22.
XPS Results (Atomic %). Phase α-SMC/Urethane/ELPO Steel Samples.

	No Load, No Environmental Conditioning		50% Load Environmental Cycle 21 Days		50% Load 60°C, 85%RH 7 Days		20% Load 60°C, 85%RH 7 Days	
	Lap Shear*		Wedge*		Wedge**		Butt Torsion**	
	Adh. Side	SMC Side	Adh. Side	SMC Side	Adh. Side	SMC Side	Adh. Side	SMC Side
C	72.9	76.6	73.1	84.4	74.9	79.0	73.9	80.9
O	23.0	19.6	21.0	15.5	21.0	17.4	23.2	16.4
N	1.88	1.07	4.01	0.90	2.80	0.95	2.67	0.92
Si	0.85	0.70	1.03	0.26	0.81	0.46	0.14	<0.1
Zn	<0.1	<0.1	<0.1	<0.1	<0.1	<0.1	<0.1	<0.1
Ca	0.29	0.97	<0.1	0.19	0.26	1.00	<0.1	0.61
Mg	0.56	0.65	0.50	0.27	0.34	0.66	<0.1	0.71
Al	0.56	0.42	0.33	<0.1	0.40	0.56	<0.1	0.49

* Instron test failure
** Test failure

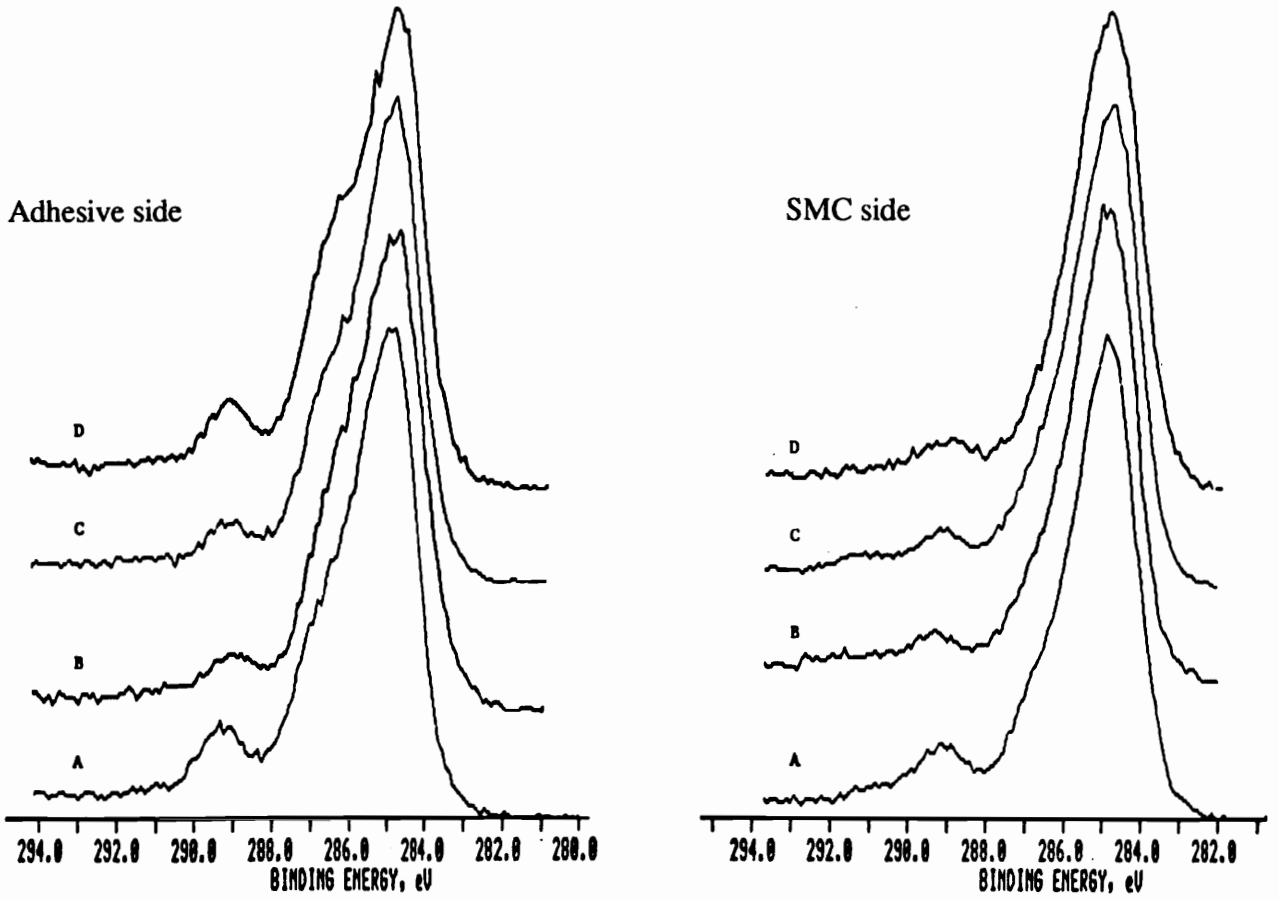

Figure 65. C 1s spectra. Phase α-SMC/urethane/ELPO steel samples.

A. No load. No environmental conditioning. Lap shear specimens.
B. 50% load, environmental cycle, 21 days. Wedge specimens. Instron test failure.
C. 50% load, 60°C, 85% RH, 7 days. Wedge specimens. Test failure.
D. 20% load, 60°C, 85% RH, 7 days. Butt torsion specimens. Test failure.

Figure 60H. These results indicate that besides primer and SMC constituents, some adhesive is present on the failed adhesive side surface for these samples.

The following results suggest that most of the nitrogen found on the adhesive side surfaces may be attributed to the primer transferred from the SMC side and that these surfaces are composed of a complex mixture of primer, SMC constituents with little or no adhesive.

a) The C ls spectra for failed adhesive side surfaces are unlike (less feature associated with -COR/-NCO functionalities) the adhesive film surface and they are intermediate between those of primed phase α-SMC and as received or split phase α-SMC surfaces or they are similar to synthesized spectra corresponding to mixtures of as received or split SMC, primed phase α-SMC, and adhesive film surfaces.

b) The adhesive side surfaces are covered to a large extent by phase α-SMC constituents (as observed by SEM), but the nitrogen concentrations in most cases are close to that of the adhesive film surface, ie, between 1.88% and 4.01%. This indicates that adhesive side surfaces which are not covered by phase α-SMC constituents have a nitrogen concentration much higher than that of the adhesive film surface. This higher nitrogen concentration can be explained by primer on the adhesive surfaces which are not covered by SMC.

Because adhesive and primer contain equivalent nitrogens it is not possible to confirm unequivocally that either adhesive and/or primer is present on the failed surfaces. To answer the question as to whether primer or adhesive or both are present, a primer containing an additional heteroatom such as phosphorus (as in phosphate-containing primers) could be employed.

Table 22 shows that the SMC side surfaces contain small amounts of nitrogen (0.32%-1.07%). The concentrations are smaller than those found on the primed SMC

surface (5.41%) or in the adhesive film surface (2.90%), shown in Table 21. The C ls spectra for the SMC side surfaces shown in Figure 65 resemble that of the split SMC (Figure 58) suggesting that nitrogen on the SMC side surface comes mostly from primer and not from adhesive. Otherwise, for this amount of nitrogen (~1%), the feature associated with -COR/-NCO chemical functionality would be more accentuated. Also, the SEM results (Figures 61-64) did not shown any material attributable to adhesive on the SMC side surface. The presence of only a small amount of nitrogen on the SMC side surface suggests that some primer remained on the SMC surface.

Some general observations can be made after analyzing the resulting for phase α-SMC/urethane/ELPO steel samples exposed to various environmental conditions.

a) The most important observation is that no adhesive failure took place at the steel/adhesive side. All the visually observed adhesive failure took place at the SMC/adhesive side, and the failure is primarily near surface debonding at the SMC-primer-adhesive interface. The correlation of XPS and SEM results shows that primer and some of the very upper layer of the SMC surface is transferred to the adhesive side. There is little or no adhesive on the SMC side, and the adhesive side surface contains primer and SMC constituents. These results clearly indicate that the surface layer of the SMC material constitutes a weak part of the diisocyanate primed phase α-SMC/urethane/ELPO steel adhesive bond. This can be explained by the presence of a high concentration of low-profile additive in the near surface of SMC (see 2.1.2). For Ashland's phase α-SMC material the low profile additive was determined to be predominantly poly(ethylene adipate) and poly(propylene adipate) with M_W= 29,000 and M_W/M_n = 1.5 [201]. The low profile additive is a low Tg thermoplastic polymer which is expected to be weaker and more sensitive to temperature and moisture than the crosslinked polyester which is the main polymeric component of bulk SMC.

b) For exposure time up to 30 days, the combinations of high load and high temperatures are particularly damaging. Exposure to humidity usually reduces the residual strength for samples which survive the tests and increases the proportion of the samples which fail during the test. Increasing the temperature increases the percentage of samples which failed during exposure. Also, an increase in the level of applied stress increases the number of samples which failed during the durability test.

c) The butt torsion specimens failed in a higher proportion and faster during tests even at a much lower load compared to the other two types of samples. This shows the importance of the mode of loading in durability studies and the necessity to use a variety of specimen geometries with different loading modes to obtain a more realistic assessment of durability. These results clearly indicate that for the design of more durable SMC/urethane/ELPO steel structures, the butt torsion configuration (mode III of loading) should be avoided.

d) The influence of the stress, temperature, and humidity on the mode of failure is difficult to rationalize because these factors affect both types of polymeric materials: the adhesive and the composite matrix. With the exception of butt torsion samples exposed at 49°C which failed largely by cohesive failure, samples failed adhesively in the near surface of SMC during the tests. This indicates that the upper layer of the SMC is particularly sensitive upon exposure to environmental conditioning. Noticeable is the significant proportion of cohesive failure for butt torsion samples that failed during exposure (12-49%) and for unloaded butt torsion samples maintained at 60°C/85% RH that failed in the Instron (25 %). No cohesive failure was observed for the other butt torsion samples tested in the Instron.

Based on the results obtained with phase a-SMC/urethane/ELPO steel samples, the following test conditions were selected for all other SMC/adhesive/metal systems to obtain rapid results for short time durability testing (7 days):

- temperature: 60°C

- stress level: 0 % and 50 % for lap shear and wedge samples; 0 % and 20 % for butt torsion samples;

- humidity: laboratory dry air (3 - 10 % RH) and 85 % RH.

4.3.2. Phase α-SMC/urethane/phase α-SMC samples

Table 23 presents the failure results for these samples. The Instron test temperature was 82°C. Examination of the results shows:

a) All loaded samples tested at 60°C in dry air survived the test. The residual strength was similar to that of the reference samples 175 ± 36 lbs (T) vs 163 ± 20 lbs (R)

b) One of five loaded samples studied at 60°C and 85% RH failed during the test. The residual strength of the samples which survived the test was significantly lower than the reference strength 119 ± 2 lbs (T) vs 163 ± 20 lbs (R)

c) The failure mode was a mixture of delamination and adhesive failure, with delamination dominating. Exposure to humidity alters the failure mode to include a higher proportion of adhesive failure 61D/39A (T (Instron failure)) and 55D/45A (T (Test failure)) vs 88D/12A (R).

The data indicate that exposure to humidity in combination with stress and temperature has a significant influence on this type of bond even at short exposure times. The test conditions induce failure during exposure, reduce the residual strength, and alter the failure mode.

Table 23.

Failure Results. Phase α-SMC/Urethane/Phase α-SMC Lap Shear Samples.
50% Load, 60°C (140°F), 7 days.

Humidity	Number of Samples	Samples Which Survived the Test					Samples Which Failed During the Test				
		Number of Samples	Average Failure Force, lbs	Average Failure Mode %D	%a	%C	Number of Samples	Time to Failure h-hours d-days	Average Failure Mode %D	%A	%C
As Prepared Samples. No Load. Room Temperature	5	5	163 ± 20	88	12	-	-	--	-	-	-
Dry Air	5	5	175 ± 36	92	8	-	-	--	-	-	-
85% RH	5	4	119 ± 2	61	39	-	1	3.6d	55	45	-

4.3.3. ELPO steel/urethane/ELPO steel samples

The failure results presented in Table 24 reveal that:

a) All samples exposed at 82°C in dry air for 14 days or at 60°C in 85% RH for 25 days survived the test. The residual strength for samples studied at 82°C in dry air was higher than the reference strength 460 ± 52 lbs (T) vs 352 ± 33 lbs (R), while the residual strength for samples tested at 60°C in 85% RH was similar to the reference strength 370 ± 68 lbs (T) vs 353 ± 33 lbs (R). The Instron test temperature was 82°C.

b) The failure mode was 100% cohesive for all samples. The data indicate that for this type of adhesive bond the adhesive is the weak link in the system and that the steel/ELPO primer and ELPO primer/adhesive bonds are stronger and more durable. The adhesion between ELPO primer and the corrosion-resistant phosphated steel is generally very good [59]. Due to their similar surface energies most adhesives will wet the ELPO primer [60]. This may explain the good ELPO primer/adhesive bond. Also it was found that the presence of ELPO primer reduced the stress concentration along the ELPO primer/adhesive/interface.

4.3.4. Polyurea/urethane/ELPO steel samples

Table 25 presents the failure results for as prepared samples tested in the Instron and for lap shear samples under 50% load and butt torsion samples under 20% load exposed to 82°C in dry air for up to 7 days. All samples failed in a short time during the test. The most important observation is that the failure mode is entirely cohesive indicating that the adhesive is the weakest link in this bond. The polyurea/adhesive bond proved to be strong even in the absence of any polyurea surface treatment. This behavior is unlike the SMC/adhesive bond performance.

Table 24.
Failure Results. ELPO Steel/Urethane/ELPO Steel Samples.
50% Load*.

Temperature	Humidity	Duration of Cycle	Number of Samples Tested	Number of Samples Which Survived the Test	Average Failure Force, lbs	Average Failure Mode %D	%A	%C
As Prepared Samples. No Load. Room Temperature.			5	5	352 ± 33	-	-	100
60°C	85% RH	14 Days	5	5	370 ± 68	-	-	100
82°C	Dry Air	25 Days	5	5	460 ± 52	-	-	100

+ All samples survived the test

* The load was 50 % of ultimate failure force for phase α-SMC/urethane/ELPO steel samples

Table 25.
A. Failure Results. As Prepared Polyurea/Urethane/ELPO Steel Samples Tested in Instron.

Temperature of Testing	Type of Sample	Number of Samples Tested	Average Failure Force, lbs* Failure Moment, lb x ft**	Average Failure Mode %D	%A	%C
62°C	Lap Shear	5	337 ± 37	-	-	100
82°C		5	224 ± 39	-	-	100
62°C	Butt Torsion	5	24 ± 10	-	-	100
82°C		5	20 ± 4	-	-	100

* For lap shear samples
** For butt torsion samples

B. Failure Results. Polyurea/Urethane/ELPO Steel Samples+.
82°C (180°F), Dry Air, 7 Days.

Load	Type of Sample	Number of Samples Tested	Which Failed During Test	Time to Failure h-hours, d-days	Average Failure Mode %D	%A	%C
50% Load	Lap Shear	5	5	3h (4), 15h	-	-	100
20% Load	Butt Torsion	5	5	7h, 10h (2), 1d (2)	-	-	100

\+ All samples failed during the test

4.3.5. Budd SMC/urethane/ELPO steel samples

4.3.5.1. Failure results

To investigate the influence of the adhesive type on the durability, tests were performed with the system Budd SMC/adhesive/ELPO steel using urethane and epoxy adhesives. These adhesives are of special interest in the automotive industry for bonding SMC. The effects of specimen geometry, temperature, humidity and stress on durability were studied.

Tables 26-28 present the failure results for Budd SMC/urethane/ELPO steel test specimens. The Instron test temperature was 82°C for lap shear specimens and 60°C for wedge and butt torsion samples. Failure of the steel adherends occurred for some wedge samples tested in the Instron. Because of this, some tests were duplicated and the steel adherends were reinforced before being tested in the Instron. The most important observations regarding the failure results are:

a) For the unloaded lap shear samples exposed at 60°C in dry air, the residual strength was higher than the reference strength for lap shear samples: 293 ± 48 lbs (T) vs 223 ± 15 (R).

b) All loaded lap shear samples tested at 60°C in dry air survived the test. Twenty five percent of the loaded wedge samples, 20% of the butt torsion samples loaded at 10% of the ultimate failure moment, and all butt torsion samples loaded at 20% of the ultimate failure moment failed during investigation at 60°C in dry air. The residual strength of the samples which survived the exposure was equivalent to the reference strength: lap shear 250 ± 32 lbs (T) vs 223 ± 15 lbs (R), wedge (with unreinforced adherend): 35 lbs (T) vs 32 ± 6.3 lbs (R), and butt torsion 30 ± 5.8 lb x ft (T) vs 24 ± 1.2 lb x ft (R).

c) All unloaded samples maintained at 60°C and 85% RH survived the test. Exposure at 60°C and 85% RH produced a slight decrease in residual strength for the lap

Table 26.
Failure Results. Budd SMC/Urethane/ELPO Steel Samples.
60°C (140°F), 7 Days. (Samples Which Survived the Test)

Humidity	Load	Type of Sample	Number of Samples Tested	Number of Samples Which Survived the Test	Average Failure Force, lbs* (Average Failure Moment, lb x ft **)	Average Failure Mode %D	%A	%C
As Prepared Samples	No Load	Lap Shear	5	5	223 ± 15	-	-	100
		Wedge	5	5	32 ± 6.3	64	5	31
Room Temperature		Butt Torsion	5	5	24 ± 1.2	-	29	71
Dry Air	No Load	Lap Shear	4	4	293 ± 48	-	5	95
		Wedge	10	5+	36 ± 11	9	5	86
				5++	47 ± 3.0	33	-	67
	50% Load	Lap Shear	10	10	250 ± 32	-	-	100
		Wedge	12	2	35 ± 0	29	-	71
				5+	33 ± 4.2	9	-	91
				2++	43 ± 3.5	50	-	50
	10% Load	Butt Torsion	5	4	30 ± 5.8	-	58	42
	20% Load		5	-	--	-	-	-

All wedge samples were loaded in constant load mode
* For lap shear and wedge samples
** For butt torsion samples
+ The metal adherend bent during the Instron test;
++ The metal adherend was reinforced to avoid bending

Table 27.
Failure Results. Budd SMC/Urethane/ELPO Steel Samples.
60°C (140°F), 7 Days. (Samples Which Survived the Test)

Humidity	Load	Type of Sample	Number of Samples Tested	Number of Samples Which Survived the Test	Average Failure Force, lbs* (Average Failure Moment, lb x ft **)	Average Failure Mode %D	%A	%C
85% RH	No Load	Lap Shear	4	4	199 ± 6	-	9	91
		Wedge	10	5+	32 ± 1.0	-	-	100
				5++	45 ± 2.0	40	4	56
	50% Load	Lap Shear	10	7	242 ± 30	-	-	100
		Wedge	8	1+	35 ± 0	-	-	100
				2++	40 ± 0.7	50	41	9
	10% Load	Butt Torsion	5	4	25 ± 2.0	1	59	40
	20% Load	Butt Torsion	5	-	--	-	-	-

All wedge samples were loaded in constant load mode
* For lap shear and wedge samples
** For butt torsion samples
+ The metal adherend bent during the Instron test;
++ The metal adherend was reinforced to avoid bending

Table 28
Failure Results. Budd SMC/Urethane/ELPO Steel Samples.
60°C (140°F), 7 Days. (Samples Which Failed During the Test)

Humidity	Load	Type of Sample	Number of Samples Tested	Which Failed During the Test	Time to Failure h - hours d - days	Average Failure Mode %D	%A	%C
As Prepared Samples Room Temperature	No Load	Lap Shear	5	-	--	-	-	-
		Wedge	5	-	--	-	-	-
		Butt Torsion	5	-	--	-	-	-
Dry Air	No Load	Lap Shear	4	-	--	-	-	-
		Wedge	10	-	--	-	-	-
	50% Load	Lap Shear	10	-	--	-	-	-
		Wedge	12	3	4d, 5d, 6d	3	1	96
	10% Load	Butt Torsion	5	1	24h	15	80	5
	20% Load	Butt Torsion	5	5	3h (2), 8h(3)	-	52	48
85% RH	No Load	Lap Shear	4	-	--	-	-	-
		Wedge	10	-	--	-	-	-
	50% Load	Lap Shear	10	3	41h (3)	-	-	100
		Wedge	8	5	6h, 22h (2), 28h, 4d	4	1	95
	10% Load	Butt Torsion	5	1	22h	5	15	80
	20% Load	Butt Torsion	5	5	2h (2), 8h (3)	-	62	38

shear samples when compared with their reference strength 199 ± 6 lbs (T) vs 223 ± 15 lbs (R).

d) For loaded samples, environmental conditioning at 60°C and 85% RH resulted in an increase in the proportion of samples which failed during the test compared to that at 60°C in dry air. The increase for lap shear samples was 0% to 30% and for wedge samples 20% to 62%. For wedge samples testing at 60°C and 85% RH decreased the time to failure compared to that at 60° in dry air(DA) from 5 days (DA) to 1.5 days (85% RH). For loaded butt torsion samples studied at 60°C in 85% RH the fraction of samples that failed during the test remained the same as for samples investigated at 60°C in dry air: 20% for samples under 10% load and 100% for samples under 20% load. For samples which survived the test, the failure force is equivalent to that for as prepared samples: lap shear 242 ± 30 lbs (T) vs 223 ± 15 lbs (R), and butt torsion 25 ± 2.0 lb x ft (T) vs 24 ± 1.2 lb x ft (R).

e) For wedge samples tested in the Instron after reinforcing the steel adherend

- the residual strength for loaded samples (L) maintained at 60°C in dry air is similar to that of unloaded samples (U) tested under the same conditions: 43 ± 3.5 lbs (L) vs 47 ± 3.0 lbs (U).

- environmental conditioning of unloaded samples at 60°C in 85% RH (H) did not lower the residual strength compared with exposure at 60°C in dry air (DA): 45 ± 2.0 lbs (H) vs 47 ± 3.0 lbs (DA)

- the residual strength for loaded samples tested at 60°C and 85% RH (H) is equivalent to that of loaded samples studied at 60°C in dry air (DA): 40 ± 0.7 lbs (H) vs 43 ± 3.5 lbs (DA).

f) All lap shear samples failed cohesively near the adhesive/steel interface. The failure mode was almost entirely cohesive for wedge samples that failed during the tests.

The wedge samples for which the steel adherend failed during the Instron test were disregarded. For the other wedge samples that failed in the Instron test, the failure was generally mixed, delamination of SMC and cohesive failure. The loaded wedge samples exposed to 60°C and 85% RH failed almost entirely by a mixture of adhesive failure and SMC delamination. For butt torsion samples, generally, a mixed adhesive and cohesive failure was observed, with adhesive failure taking place largely at the the ELPO primer/adhesive interface.

4.3.5.2. Surface characterization

Surface analysis measurements were carried out for the adhesive failure regions both for samples which failed at the adhesive/steel interface and at the adhesive/SMC interface. Representative results are given in Table 29 (atomic concentrations) and in Figures 66a and 66b (C 1s spectra) for loaded butt torsion samples tested at 60°C in 85% RH which failed during exposure at the ELPO steel/adhesive interface and for loaded butt torsion samples investigated at 60°C in dry air which failed during the exposure at the adhesive/SMC interface. For the samples which failed at the adhesive/steel interface two types of specimens were obtained: one specimen was primarily steel and the other adhesive. The following results suggest that true adhesive failure occurred at the treated steel/adhesive interface, the two failed surfaces can be characterized as almost pure treated steel and adhesive surfaces, respectively.

a) The atomic concentrations for C, O, and N for the failed ELPO steel side surface (Table 29) are close (within the limits of ± 15%) to those of the non-bonded ELPO steel surface. The atomic concentrations for C, O, N, Si, and Mg for the failed adhesive side surface are in agreement (within the limits of ± 15%) with those for the adhesive film shown in Table 21.

Table 29.
XPS Results (Atomic %). Budd SMC/Urethane/ELPO Steel Butt Torsion Samples.
20% Load, 60°C (140°F), 7 Days. Test Failure.

Element	ELPO Steel	As Received Budd SMC	Scratched Budd SMC	Primed Budd SMC	85% RH* Adhesive Side	85% RH* Steel Side	Dry Air** Adhesive Side	Dry Air** SMC Side
C	62.1	83.1	63.8	77.5	68.4	59.8	69.9	63.2
O	28.0	15.8	30.0	14.6	24.8	29.1	24.0	28.6
N	2.87	0.52	<0.1	7.59	3.41	3.23	1.90	1.38
Si	5.31	0.11	0.85	0.25	1.89	4.48	1.77	1.68
Zn	-	0.10	<0.1	<0.1	<0.1	<0.1	<0.1	<0.1
Ca	-	0.25	5.35	<0.1	<0.1	0.11	0.86	3.64
Mg	1.76	<0.1	<0.1	<0.1	0.78	1.66	0.89	1.14
Al	-	0.17	<0.1	<0.1	0.67	1.66	0.76	0.44

* Failure at the adhesive/steel interface
** Failure at the adhesive/SMC inteface

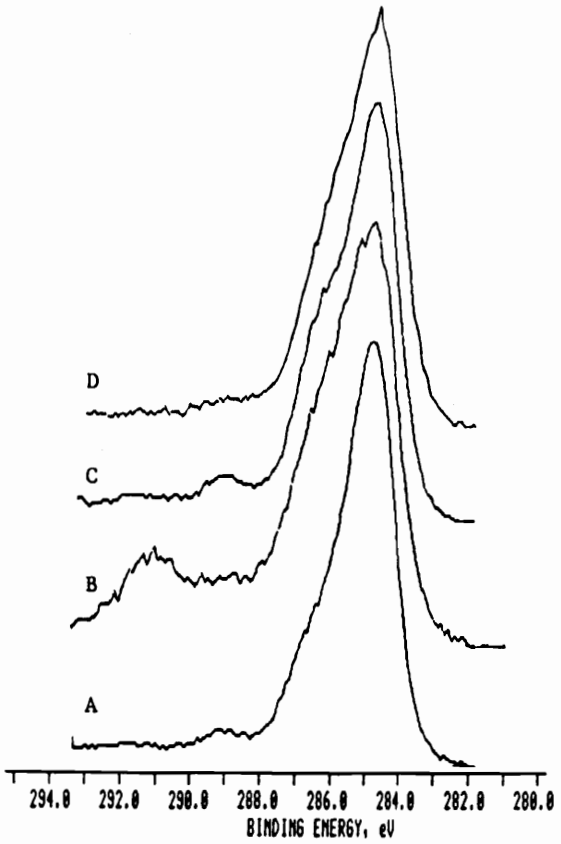

Figure 66a. C 1s spectra for reference surfaces.

A. As received Budd SMC
B. Scratched Budd SMC
C. Primed Budd SMC
D. ELPO steel

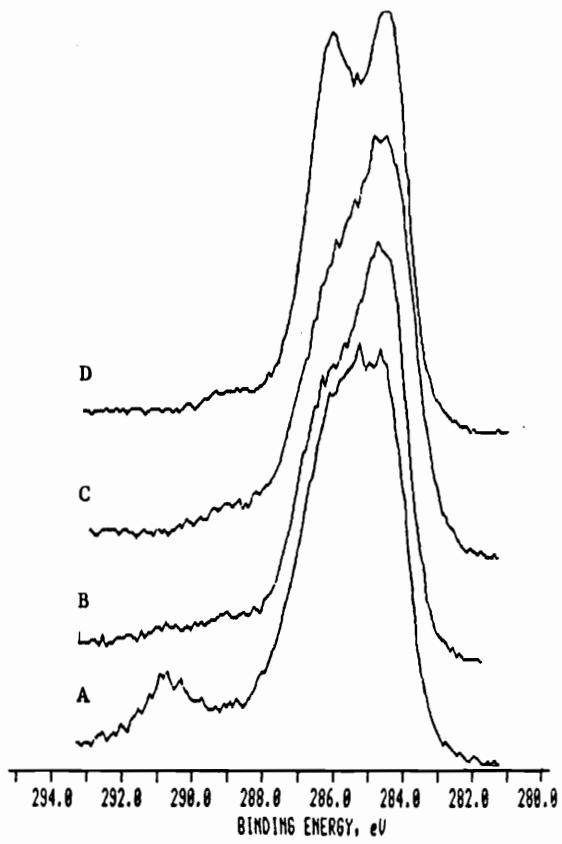

Figure 66b. C 1s spectra for failed Budd SMC/urethane/ELPO steel butt torsion specimens. 20% load, 60°C (140°F), 7 days.

A, B: Dry air. Test failure at the SMC/adhesive interface. A: SMC side, B: Adhesive side.
C, D: 85% RH. Test failure at the adhesive/steel interface. C: Steel side, D: Adhesive side.

b) The C 1s spectrum for the adhesive side surface (Figure 66bD) is equivalent to the C 1s spectrum of the adhesive film (Figure 58D). The C 1s spectrum for the ELPO steel side (Figure 66bC) resembles that of the treated steel surface (Figure 66aD) with the exception of an increased spectral feature associated with -COR/-NCO chemical functionality. The presence of NCO may indicate the presence of some adhesive (at least 10%) on the steel side surface.

c) The SEM results (Figure 67) show that both failed surfaces are smooth and unfractured.

Some samples failed at the adhesive/Budd SMC interface. The SEM results for these samples (Figure 68) reveal rough surfaces for both failed sides. The SEM results for as received Budd SMC (Figure 69) show a smooth surface, while those for Budd SMC scratched with a knife reveal a fractured structure of the bulk material. These results indicate that the visually determined "adhesive" failure is in reality near-surface debonding and the outer SMC material appears on the adhesive side of the failed surface.

The SEM results are confirmed by the XPS measurements (Table 29). The adhesive side surface contains calcium. The adhesive film surface does not contain calcium (see Table 21). The detection of calcium on the adhesive side surface indicates the presence of SMC constituents. Also the atomic concentrations of C, O, and Si on the failed adhesive side are close (within the limits of ± 15%) to those for the SMC side. The calcium content of the SMC side (3.64%) is much higher than that of the adhesive side (0.86%). The C 1s spectrum for the failed adhesive side surface, shown in Figure 66bB, does not resemble that of the adhesive film (see Figure 58D). The nitrogen concentration on the SMC side surface is only 1.38% compared with 7.59% for primed Budd SMC. This suggests that little primer is present on the SMC surface. The correlation of XPS and SEM results shows that primer and the upper layer of the SMC surface are transferred to the adhesive

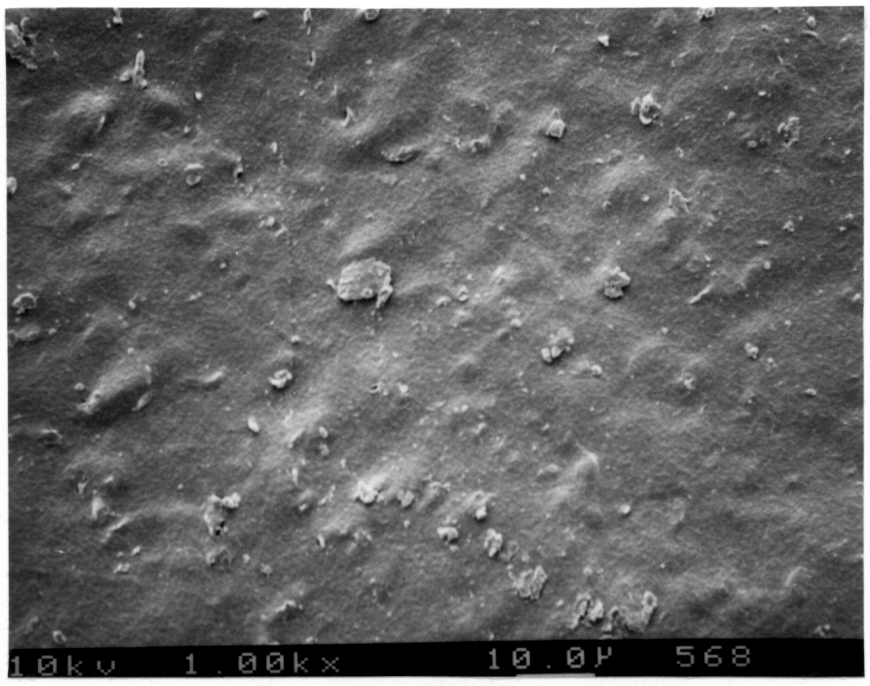

Adhesive side

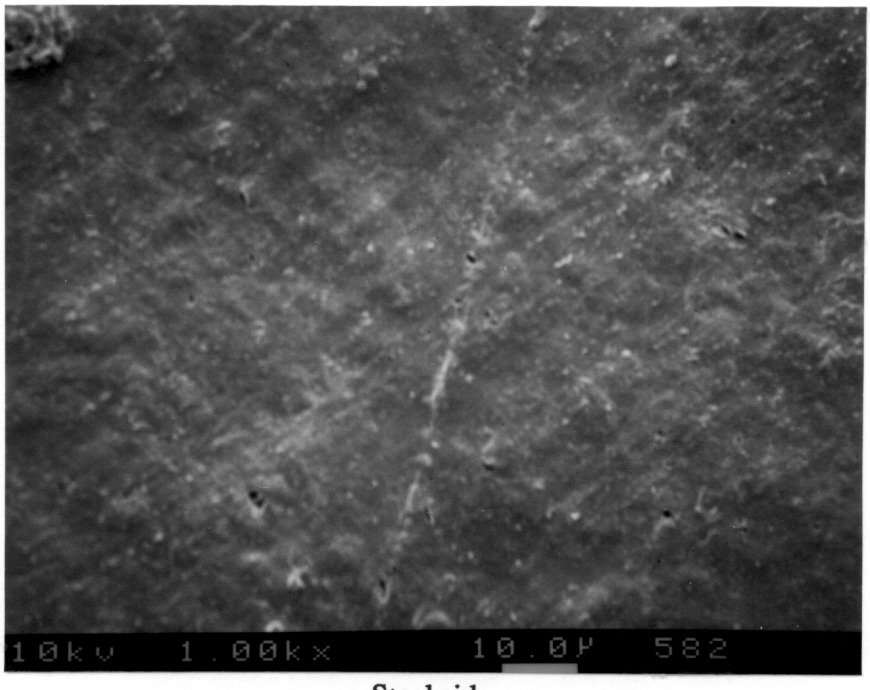

Steel side

Figure 67. SEM results. Budd SMC/urethane/ELPO steel butt torsion specimens. 20% load, 60°C (140°F), 85% RH. Test failure at the adhesive/ELPO steel interface.

Adhesive side

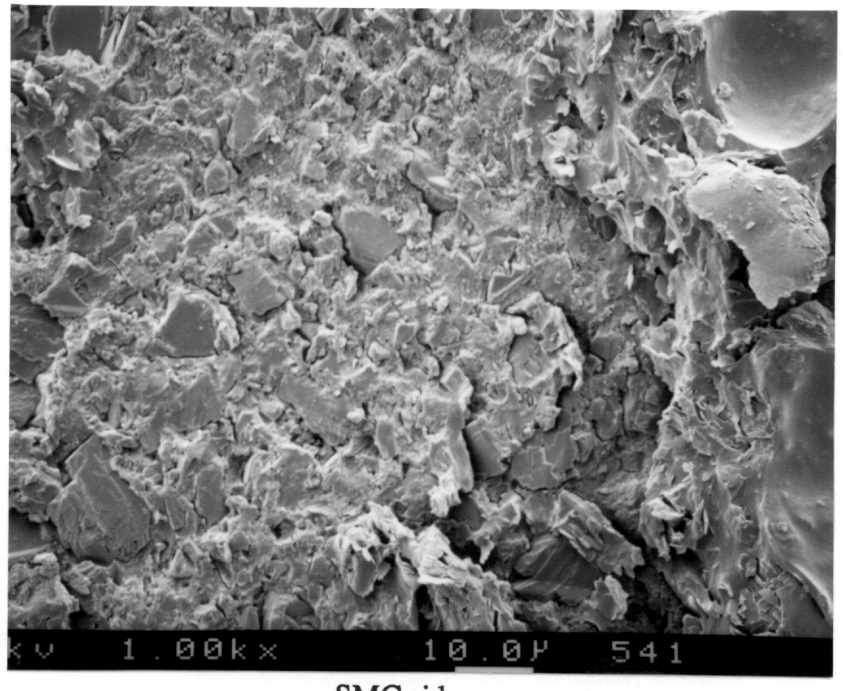

SMC side

Figure 68. SEM results. Budd SMC/urethane/ELPO steel butt torsion specimens. 20% load, 60°C (140°F), dry air. Test failure at the adhesive/SMC interface.

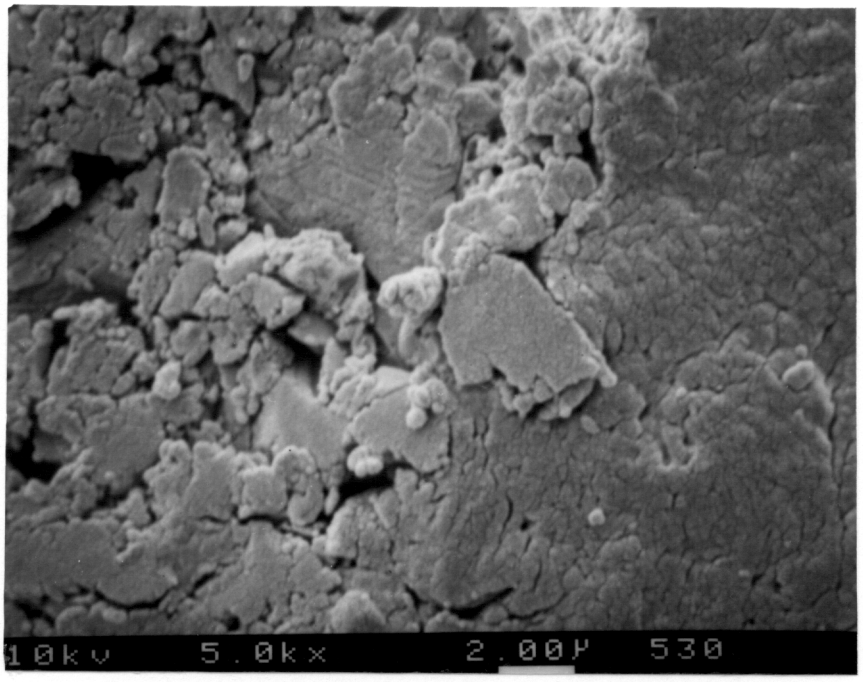

Scratched Budd SMC

As received Budd SMC

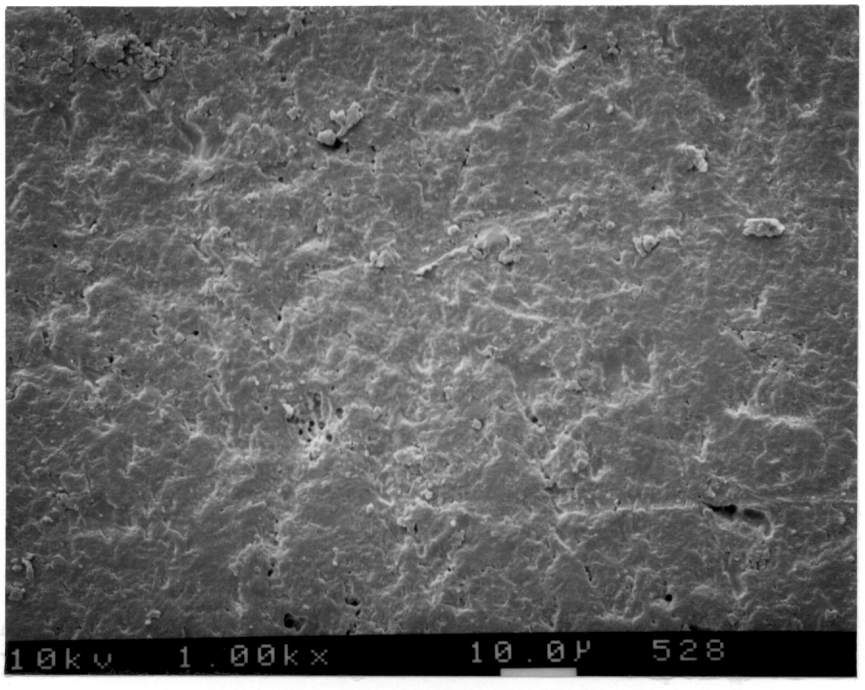

As received Budd SMC

Figure 69. SEM results for reference surfaces.

side during failure. There is no adhesive on the SMC side and the adhesive side surface contained primer and SMC constituents. The results obtained indicate that the upper layer of the SMC material is a weak part of the Budd SMC/urethane/ELPO bond. This can be explained by the presence of a high concentration of low profile additive on the SMC surface (see 4.3.1.2). The low profile additive used in the Budd SMC formulation is expected to be a low T_g thermoplastic polymer as in the case of phase α–SMC.

4.3.6. Budd SMC/epoxy/ELPO steel samples

4.3.6.1. Failure results

The failure results presented in Tables 30 and 31 reveal the following:

a) For lap shear and butt torsion samples, the reference strengths of epoxy bonded samples are greater than those for samples bonded with urethane adhesive (Table 26): lap shear 360 ± 19 lbs (epoxy) vs 223 ± 15 lbs (urethane) and butt torsion 71 ± 1.3 lb x ft (epoxy) vs 24 ± 1.2 lb x ft (urethane). For wedge samples the relative values were 26 ± 6.0 lbs (epoxy) vs 32 ± 6.3 lbs (urethane).

b) The residual strengths of samples tested at 60°C in dry air may be compared with the reference strengths. The values increase for lap shear samples 445 ± 23 lbs (T) vs 360 ± 19 lbs (R) and are similar for wedge 33 ± 5.0 lbs (T) vs 26 ± 6.0 lbs (R) and butt torsion samples 70 ± 7.8 lb x ft (T) vs 71 ± 1.3 lb x ft (R).

c) The application of load for samples investigated at 60°C in dry air produced failure of 20% of the wedge samples and 20% of the butt torsion samples. All the other samples survived the test. The residual strength was higher than the reference strength for lap shear samples 450 ± 13 lbs (T) vs 360 ± 19 lbs (R), similar for wedge samples 33 ±

Table 30.
Failure Results. Budd SMC/Epoxy/ELPO Steel Samples.
60°C (140°F), 7 Days. (Samples Which Survived the Test)

Humidity	Load	Type of Sample	Number of Samples Tested	Which Survived the Test	Average Failure Force, lbs* (Average Failure Moment, lb x ft **)	Average Failure Mode %D	%A	%C
As Prepared Samples Room Temperature	No Load	Lap Shear	5	5	360 ± 19	-	-	100
		Wedge	5	5	26 ± 6.0	38	59	3
		Butt Torsion	5	5	71 ± 1.3	46	-	54
Dry Air	No Load	Lap Shear	5	5	445 ± 23	100	-	-
		Wedge	5	5	33 ± 5.0	52	29	19
		Butt torsion	5	5	70 ± 7.8	33	2	65
	50% Load	Lap Shear	5	5	450 ± 13	92	8	-
		Wedge	5	4	33 ± 4.0	58	27	15
	20% Load	Butt Torsion	5	4	63 ± 1.3	12	-	88
85% RH	No Load	Lap Shear	5	5	360 ± 17	40 -	25	35
		Wedge	5	5	37 ± 3.0	62	15	23
		Butt torsion	5	5	72 ± 1.2	45	18	37
	35% Load	Lap Shear	5	4	294 ± 52	-	18	82
	50% Load	Lap Shear	5	4	307 ± 41	2	44	54
	50% Load	Wedge	5	3	33 ± 3.5	71	24	5
	20% Load	Butt Torsion	5	-	--	-	-	-

All wedge samples were loaded in constant load mode
* For lap shear and wedge samples
** For butt torsion samples

Table 31
Failure Results. Budd SMC/Epoxy/ELPO Steel Samples.
60°C (140°F), 7 Days. (Samples Which Failed During the Test)

Humidity	Load	Type of Sample	Number of Samples Tested	Which Failed During the Test	Time to Failure h - hours d - days	Average Failure Mode %D	%A	%C
As Prepared Samples Room Temperature	No Load	Lap Shear	5	-	--	-	-	-
		Wedge	5	-	--	-	-	-
		Butt Torsion	5	-	--	-	-	-
Dry Air	No Load	Lap Shear	5	-	--	-	-	-
		Wedge	5	-	--	-	-	-
		Butt Torsion	5	-	--	-	-	-
	50% Load	Lap Shear	5	-	--	-	-	-
		Wedge	5	1	6h	75	25	-
	20% Load	Butt Torsion	5	1	41h	35	65	-
85% RH	No Load	Lap Shear	5	-	--	-	-	-
		Wedge	5	-	--	-	-	-
		Butt Torsion	5	-	--	-	-	-
	35% Load	Lap Shear	5	1	7d	50	50	-
	50% Load	Lap Shear	5	1	6.5d	15	80	5
	50% Load	Wedge	5	2	22h, 4d	48	50	2
	20% Load	Butt Torsion	5	5	20h, 43h (3), 55h	10	34	56

All wedge samples were loaded in constant load mode

4.0 lbs (T) vs 26 ± 6.0 lbs (R), and lower for butt torsion samples 63 ± 1.3 (T) lb x ft vs 71 ± 1.3 lb x ft (R).

The decrease in residual strength for butt torsion samples may be due to microdamaging of the adhesive under stress and temperature. The application of stress during the durability tests can produce the rupture of intrinsic bonds and initiate micro-cracks in highly localized areas of stress concentration or can enlarge the defects already existing in the adhesive. These phenomena are detrimental to the cohesive strength of the adhesive and implicitly for the strength of the adhesive bond. Previous experiments showed that butt torsion samples were more sensitive to stress and temperature than the other two types of samples.

d) Exposure of unloaded samples at 60°C and 85% RH did not induce failure of samples during the test and did not lower their residual strength. The comparative failure forces (moment) were: lap shear 360 ± 16 lbs (T) vs 360 ± 19 lbs (R), wedge samples 37 ± 3.0 (T) vs 26 ± 6 lbs (R), and butt torsion 72 ± 1.2 lb x ft (T) vs 71 ± 1.3 lb x ft (R).

e) Exposure of loaded samples at 60°C in 85% RH increased the proportion of samples that failed during the test compared to environmental exposure at 60°C in dry air. For lap shear samples the percent of failure changes from 0% to 20%, for wedge samples from 20% to 40%, and for butt torsion from 20% to 100%. For samples which survived the test, the failure force was equivalent to the reference sample strength: lap shear 307 ± 41 lbs (T) vs 360 ± 19 lbs (R), and wedge 33 ± 3.5 lbs (T) vs 26 ± 6.0 lbs (R). The residual strength behavior of the lap shear samples maintained at 60°C in dry air (DA) was similar to that for samples prepared with urethane adhesive. The failure strengths were higher than that for samples tested at 60°C in 85% RH (HA): 445 ± 23 lbs (DA) vs 360 ± 17 lbs (85% RH) for the unloaded samples and 450 ± 13 lbs (DA) vs 294 ± 52 lbs (85% RH) for the loaded samples.

f) The failure mode was mixed for wedge and butt torsion specimens. Exposure to stress and environmental conditions produces changes in the failure mode. The failure mode for as prepared lap shear samples tested in the Instron was 100% cohesive on the adhesive/steel side of the specimen. The lap shear samples tested at 60°C in dry air failed almost entirely by delamination, while for samples studied at 60°C in 85% RH, the proportion of adhesive failure was significant (18-80%). For as prepared wedge samples that were tested in the Instron, the failure mode was only delamination and adhesive failure at the SMC/adhesive interface. For some exposed wedge samples a portion of the failure mode was cohesive (15-23%). The failure mode for butt torsion specimens was only delamination and cohesive for as prepared samples and for samples exposed to dry air. Some adhesive failure (18-34%) was noted for samples exposed to high relative humidity. Adhesive failure for lap shear and butt torsion samples occurs primarily at the adhesive/SMC interface. Some adhesive failure took place at the steel surface where the steel-primer (surface treated coating) was transferred to the adhesive side at failure. For the wedge samples, adhesive failure took place only at the adhesive/SMC interface.

g) Samples prepared with epoxy adhesive (Tables 30 and 31) gave better durability results than those prepared with urethane adhesive (Tables 26-28) for all specimen configurations. All butt torsion samples, prepared with polyurethane adhesive, tested at 60°C in dry air, and loaded at 20% of the ultimate failure moment, failed during the test in a short time (6h) while only 20% of the samples prepared with epoxy adhesive failed during the test. At 60°C in 85% RH, the proportion of loaded samples prepared with urethane adhesive which failed during the tests was higher than for similar samples prepared with epoxy adhesives: lap shear 30% vs 20% and wedge 63% vs 40%.

The average time to failure was longer for loaded samples prepared with epoxy adhesive investigated at 60°C in 85% RH compared with samples prepared with urethane

adhesive: lap shear 7 vs 1.7 days, wedge 2.5 vs 1.5 days, and butt torsion 1.6 vs 0.25 days. The better durability for samples prepared with epoxy adhesive may be explained by the higher cohesive strength of the epoxy adhesive. The tensile strength of the epoxy adhesive is 3435 psi vs 1000 psi for the polyurethane adhesive [202]. Also it is known that the polyurethanes are not resistant to hydrolysis [43, 90]. A higher moisture absorbtion rate was observed for the polyurethane adhesive than for the epoxy adhesive (See 4.1.), indicating a faster loss of properties upon exposure to humidity.

4.3.6.2. Surface characterization

The SEM results for loaded wedge samples that failed during the testing at 60°C and 85% RH are presented in Figure 70. The visually determined mode of failure was adhesive at the adhesive/SMC interface. However, the SEM results reveal rough fractured surfaces for both failed sides. The SEM results for an as received Budd SMC surface (Figure 69) show a smooth surface, while those for Budd SMC scratched with a knife reveal a rough structure of the bulk material. The SEM results indicate that failure did not take place exactly at the adhesive/SMC interface, at least a partial near-surface debonding of SMC occurred at failure. Fragments similar to those on the scratched Budd SMC are observed on failed surfaces.

The XPS results for the same surfaces presented in Table 32 show that the failed adhesive side surface contains calcium while the adhesive film surface does not (Table 21). The presence of calcium on the failed adhesive surface indicates the presence of SMC constituents. The nitrogen concentration on the failed adhesive surface (1.29%) is higher than for as received Budd SMC (0.52%) or for scratched Budd SMC (0.17%). The higher nitrogen concentration suggests that some adhesive is present on the failed adhesive surface and that the failure surface consists of a mixture of adhesive and SMC components. For

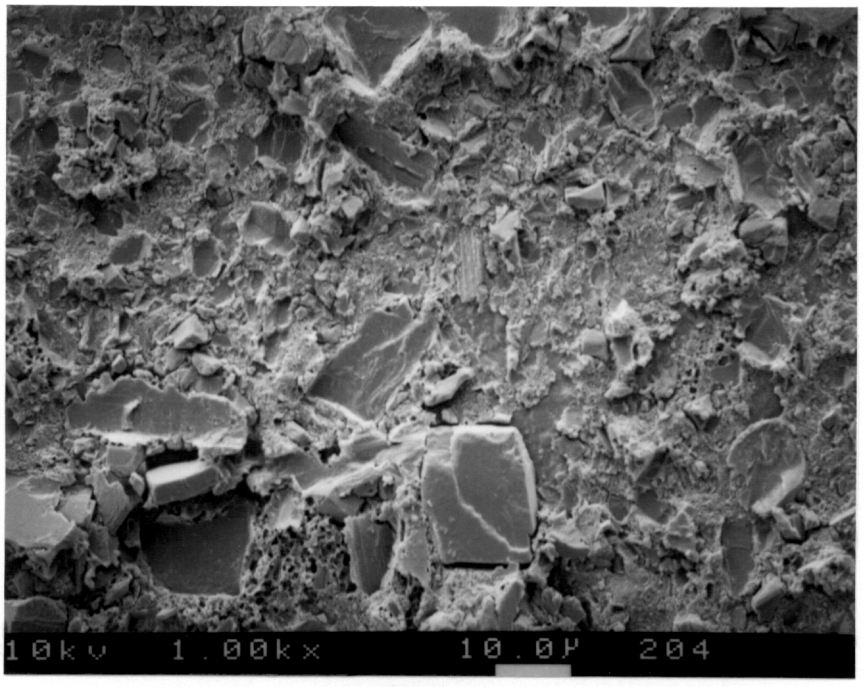

Adhesive side

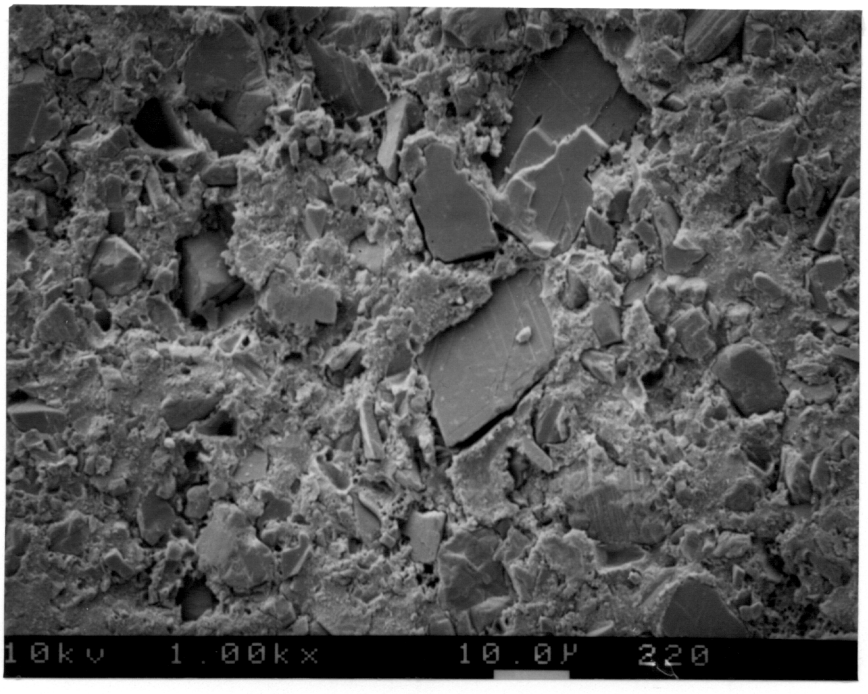

SMC side

Figure 70. SEM results. Budd SMC/epoxy/ELPO steel wedge samples. 50% load, 60°C (140°F), 85% RH, 7 days. Test failure at the adhesive/SMC interface.

Table 32.
XPS Results (Atomic %). Budd SMC/Epoxy/ELPO Steel Samples.
60°C (140°F), 7 Days.

						Lap Shear No Load **+ 85% RH		Wedge 50% Load*++ 85% RH	
Element	Epoxy Adhesive Film	Scratched Epoxy Adhesive	As Received Budd SMC	Scratched ELPO Steel	ELPO Steel	Adhesive Side	Steel Side	Adhesive Side	SMC Side
C	68.7	34.7	83.0	64.9	62.1	74.1	70.2	78.7	70.8
O	20.1	41.5	15.9	28.9	28.0	22.2	24.1	18.5	23.7
N	5.32	1.66	0.52	0.17	2.87	2.05	2.03	1.29	0.88
Si	3.63	12.7	0.15	0.92	5.31	0.88	1.85	<0.1	0.19
Mg	1.34	5.37	<0.1	0.12	1.76	<0.1	0.61	<0.1	0.49
Al	0.92	4.00	<0.1	0.16	<0.1	0.47	0.72	0.16	0.21
Ca	<0.1	<0.1	0.27	4.87	<0.1	<0.1	<0.1	0.97	3.76
Others (Zn, Ti, Fe)	<0.1	<0.1	<0.1	<0.1	<0.1	0.28	0.47	<0.1	<0.1

* Failure at the Adhesive/SMC Interface
** Failure at the Steel Surface
\+ Failure in the Instron Test
++ Failure During the Test

the failed SMC side surfaces, the nitrogen concentration (0.93% and 0.88% for lap shear and wedge, respectively) is higher than the value for as received Budd SMC (0.52%) or scratched Budd SMC (0.17%) indicating the presence of some adhesive on the failed SMC side surface.

The C 1s spectra for the same surfaces are shown in Figure 71. The spectrum for failed adhesive side (Figure 71 A) is similar to that of the epoxy adhesive scratched with a knife (Figure 72E), indicating that the adhesive side surface is composed mostly of adhesive components.

The C 1s spectra for the failed SMC side surface (Figure 71B) and for scratched Budd SMC have a spectral feature at high binding energy (~291 eV) not found in other spectra in Figures 71 and 72. This indicates that the failed SMC side surface is composed mostly of SMC components.

The SEM and XPS results taken together indicate that what appears macroscopically to be adhesive failure, microscopically, is a mixture of near surface debonding of SMC and fracture of the upper layer of the adhesive. Upon failure the mode is such that both failed side surfaces are composed of a mixture of adhesive and SMC components in different proportions.

For the samples which failed at the steel surface, the XPS results indicate that failure took place in the primer applied to steel. The atomic concentrations for both adhesive and steel sides given in Table 22 are similar. No iron is present on the failed steel surface. Also the C 1 spectra for the adhesive and steel side surfaces given in Figure 71 (C,D) are similar.

4.3.7. Phase α-SMC/urethane/aluminum samples

The experimental matrix was selected to investigate the influence of the following

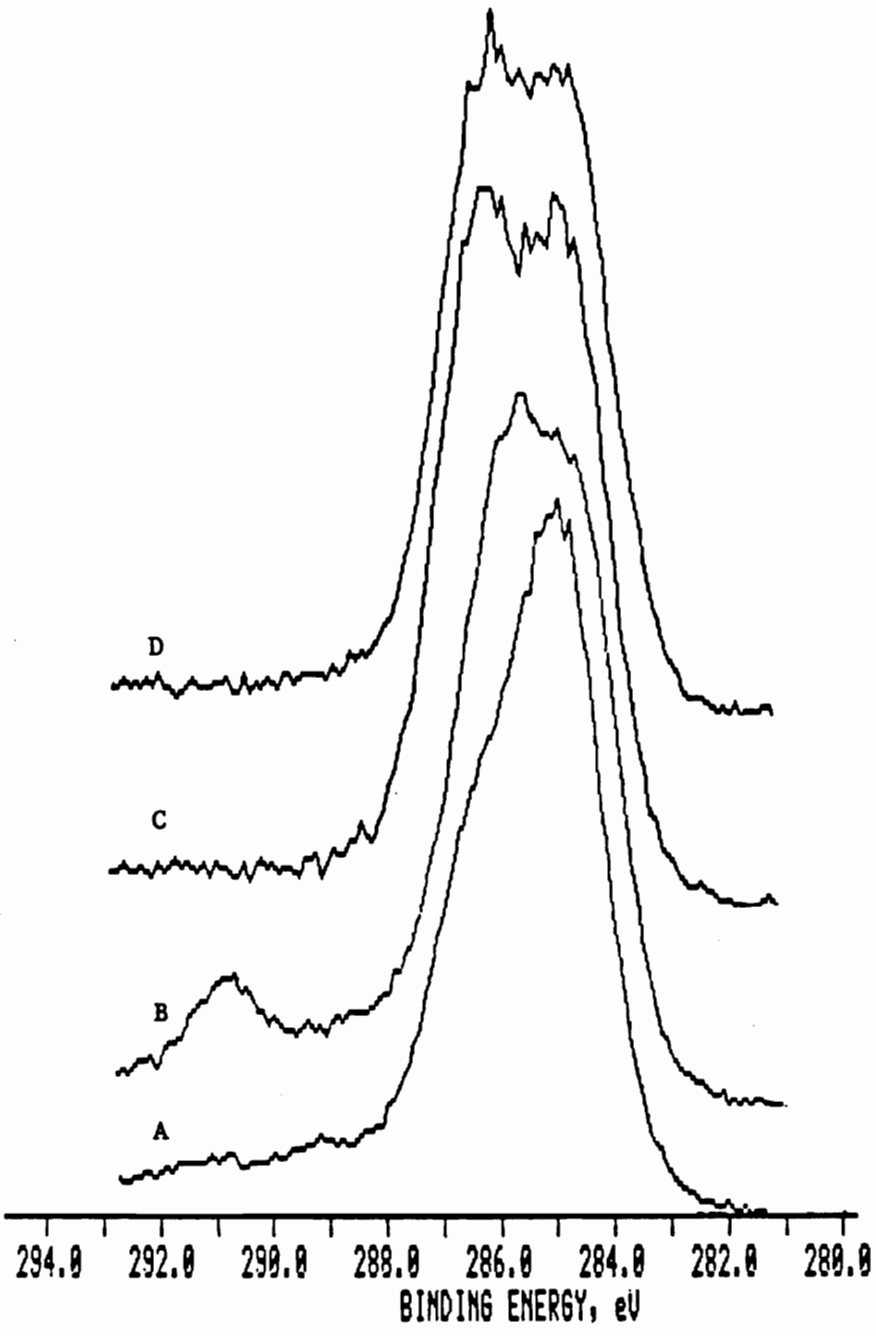

Figure 71. C 1s spectra. Budd SMC/epoxy/ELPO steel specimens, 60°C (140°F), 85% RH, 7 days.

A, B: 50% load. Wedge specimens. Test failure at the adhesive/SMC interface. A: Adhesive side, B: SMC side

C, D: No load. Lap shear specimens. Instron failure at the steel/primer interface. C: Adhesive side., D: Steel side.

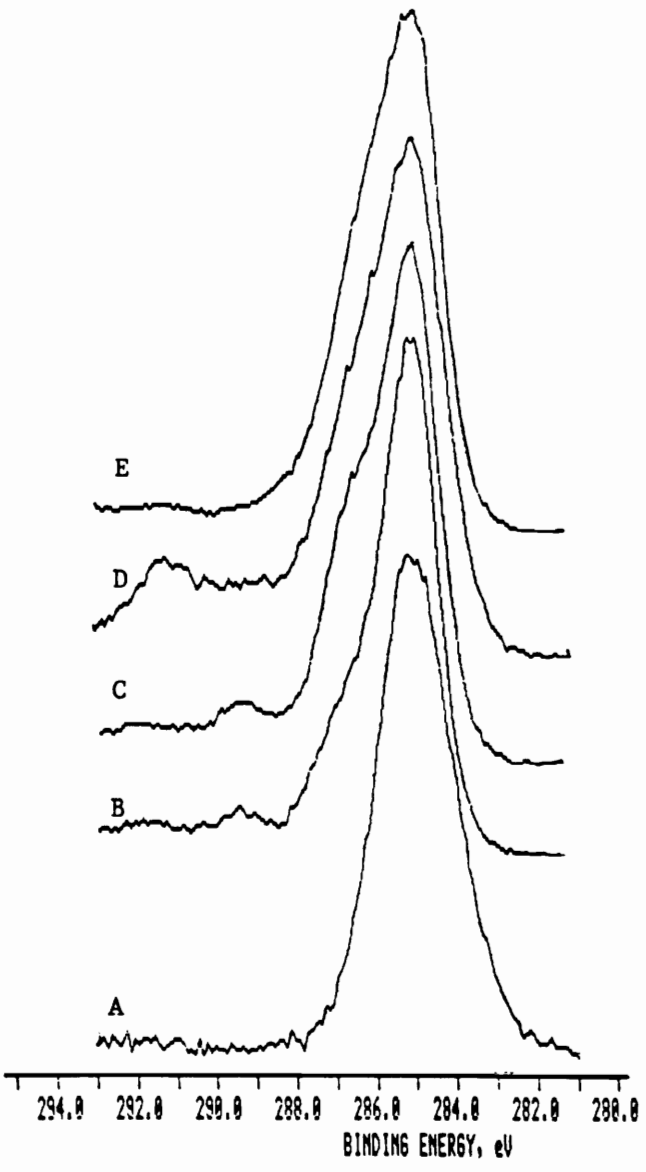

Figure 72. C 1s spectra for reference surfaces.

A. ELPO steel
B. As received Budd SMC
C. Scratched Budd SMC
D. Epoxy adhesive film
E. Scratched epoxy adhesive

factors on the durability of phase α-SMC/urethane/aluminum adhesive bonds: temperature, humidity, stress, adherend surface pretreatment, bondline thickness, and adherend thickness. The results are grouped according to the type of aluminum surface pretreatment and are presented and discussed in the order of aggressiveness of the pretreatment toward the aluminum surface (tendency of material removal). The Instron test temperature was 82°C for lap shear and 60° C for wedge and butt torsion samples.

4.3.7.1. Phase α-SMC/urethane/CH_2Cl_2 cleaned, phenolic, or epoxy primed aluminum samples

4.3.7.1.1. Failure results

The failure results for these samples are presented in Table 33. The failure mode for as prepared samples (unexposed to stress and environmental conditioning and tested in the Instron) was almost entirely cohesive. With the exception of one sample prepared with epoxy primed aluminum which failed in two days, all other samples exposed to stress, temperature, and humidity failed in a very short time (0.5 - 2 h). The failure mode was largely adhesive at the aluminum/adhesive interface. The adhesively failed surface of the metal side had the appearance of bare aluminum. It appears that all the primer applied on the aluminum adherend before bonding is transferred to the adhesive side at failure.

4.3.7.1.2. Surface characterization

The SEM results for samples prepared with phenolic primed aluminum and with epoxy primed aluminum exposed to stress, temperature, and humidity which failed adhesively during the test are shown in Figures 73 and 74. The surface texture of the failed aluminum side surfaces is identical with that for solvent cleaned aluminum (Figure 73). No fragmented or patches of material which could be attributed to adhesive and/or primer were

Table 33

Failure Results. Phase α-SMC/Urethane/Solvent Cleaned, Phenolic or Epoxy Primed Aluminum Lap Shear Samples.
60°C (140°F), 85% RH, 7 Days.

		Samples Which Survived the Test						Samples Which Failed During the Test				
Load	Type of Primer	Number of Samples	Number of Samples	Average Failure Force, lbs	Average Failure Mode %D	%A	%C	Number of Samples	Time to Failure h-hours d-days (no. samples)	Average Failure Mode %D	%A	%C
As Prepared Samples No Load R.T.	Phenolic	5	5	267 ± 47	-	6	94	-	--	-	-	-
	Epoxy	5	5	256 ± 12	-	-	100	-	--	-	-	-
50% Load	Phenolic	5	-	-	-	-	-	5	0.5h (4) 2h (1) 0	1	79	20
	Epoxy	5	-	-	-	-	-	5	0.5h (2) 1.5h (2) 2d	46	43	11

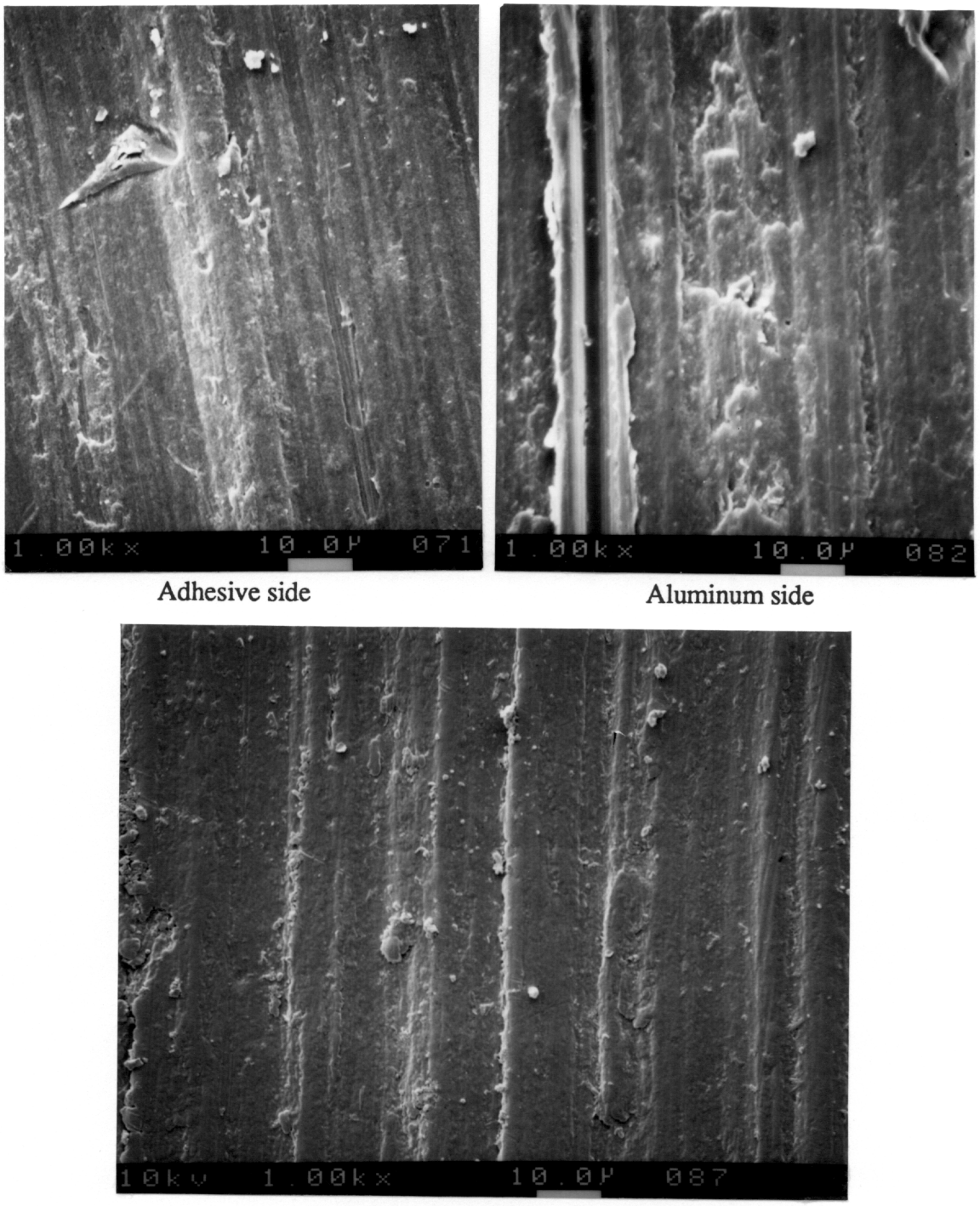

Figure 73. SEM results. Phase α-SMC/urethane/solvent cleaned phenolic primed aluminum lap shear specimens. 50% load, 60°C (140°F), 85% RH, 7 days. Test failure at the adhesive/aluminum interface.

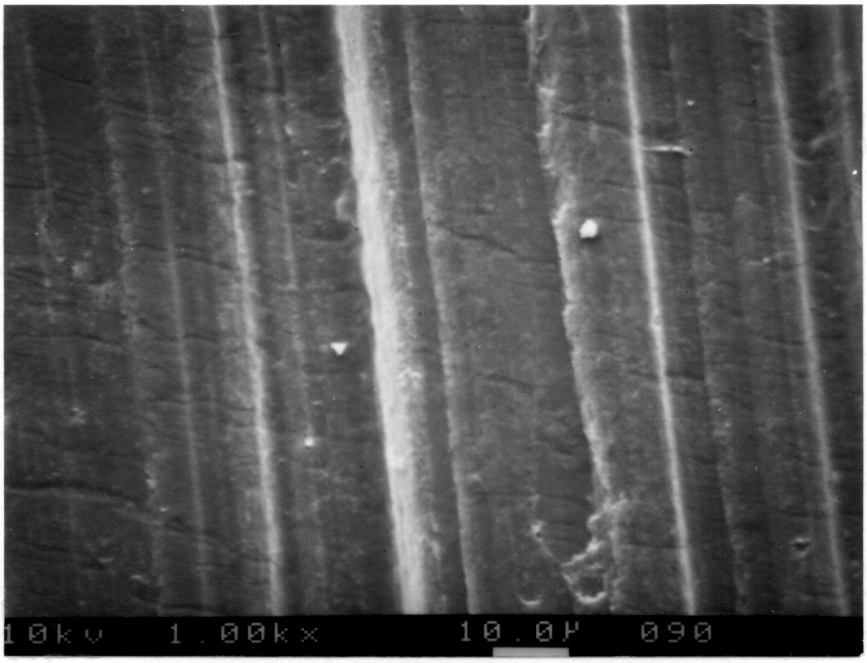

Adhesive side

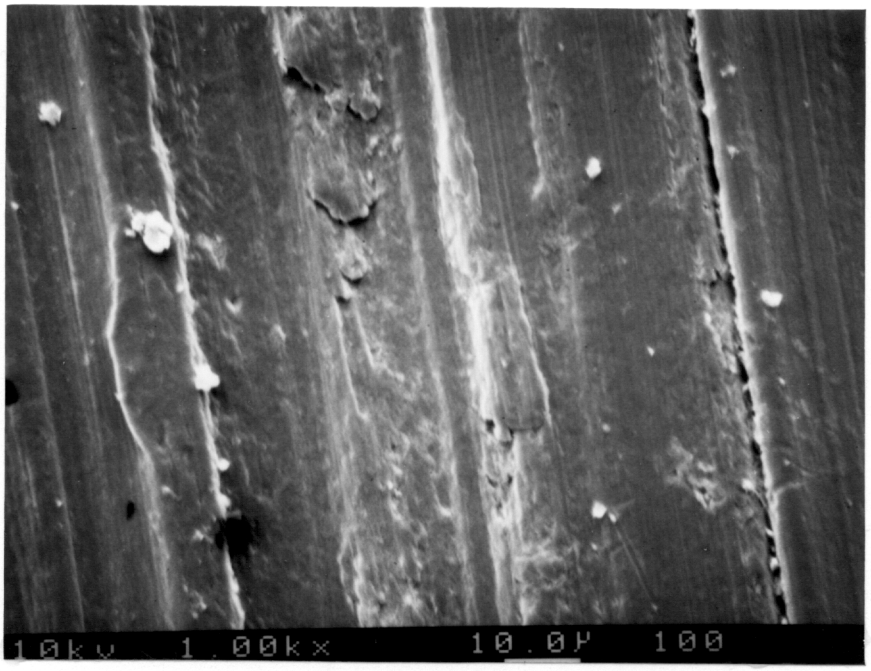

Aluminum side

Figure 74. SEM results. Phase α-SMC/urethane/solvent cleaned epoxy primed aluminum lap shear specimens. 50% load, 60°C (140°F), 85% RH, 7 days. Test failure at the adhesive/aluminum interface.

observed on the failed aluminum surface. The surface texture of the adhesive failure side surfaces is a replica of the aluminum side surface.

The XPS results for the same failed surfaces are presented in Table 34 and Figure 75 (C 1s spectra). Samples prepared with aluminum adherends primed with phenolic primer showed aluminum (1.91%) and magnesium (0.72%) on the failed adhesive side surface. The result suggests a transfer of material from aluminum to the adhesive side at failure. The primer film does not contain aluminum or magnesium. A higher concentration of nitrogen (1.32 vs 0.65%) and silicon (1.05 vs 0.30%) on the aluminum failed side compared with the solvent cleaned aluminum surface, suggests a transfer of material from the primer to aluminum at failure.

With the exception of a broad spectral feature associated with -COR functionality (BE = 286.5 eV), and a different shape for the high binding energy region, the C 1s spectrum of the failed aluminum side surface (Figure 75 C) is close to that for the non-bonded solvent cleaned aluminum (Figure 75 A). The shape of the C 1s spectrum for the failed adhesive side surface (Figure 75 B) is equivalent to that of the phenolic primer film (Figure 75 D). The SEM and XPS results indicate that for samples prepared with phenolic primed aluminum adherends exposed to stress and environmental conditioning, the visually observed adhesive failure is a true adhesive failure at the aluminum/phenolic primer interface.

For specimens prepared with epoxy primed aluminum the nitrogen concentration on the aluminum failed surface is 2.42% compared to 0.65% nitrogen on the solvent cleaned aluminum surface. This indicates that some primer remains on the aluminum side surface at failure. Some aluminum (1.88%) is present on the failed adhesive side surface which suggests a transfer of material from aluminum to the adhesive side. The epoxy primer film surface does not contain aluminum.

Table 34.

XPS Results (Atomic %). Phase α-SMC/Urethane/Solvent Cleaned, Phenolic, or Epoxy Primed Aluminum Lap Shear Samples.
50% Load, 60°C (140°F), 85% RH.

					Phenolic Primer*		Epoxy Primer*	
Element	As received Aluminum	CH_2Cl_2 Cleaned Aluminum	Phenolic Primer Film	Epoxy Primer Film	Adhesive Side	Aluminum Side	Adhesive Side	Aluminum Side
C	46.6	36.8	78.7	80.3	67.8	42.9	65.1	36.0
O	36.6	41.0	20.5	15.7	25.6	38.6	25.7	41.6
N	0.80	0.65	0.29	3.20	1.34	1.32	4.07	2.42
Si	0.57	0.30	0.54	0.68	0.80	1.05	0.99	1.81
Mg	6.80	10.6	<0.1	<0.1	0.72	3.77	0.31	3.13
Al	7.30	8.60	<0.1	<0.1	1.91	9.50	1.88	12.0
Others (S, Cl)	1.33	2.0	<0.1	0.14	0.83	2.86	2.00	3.04

* Failure during the test

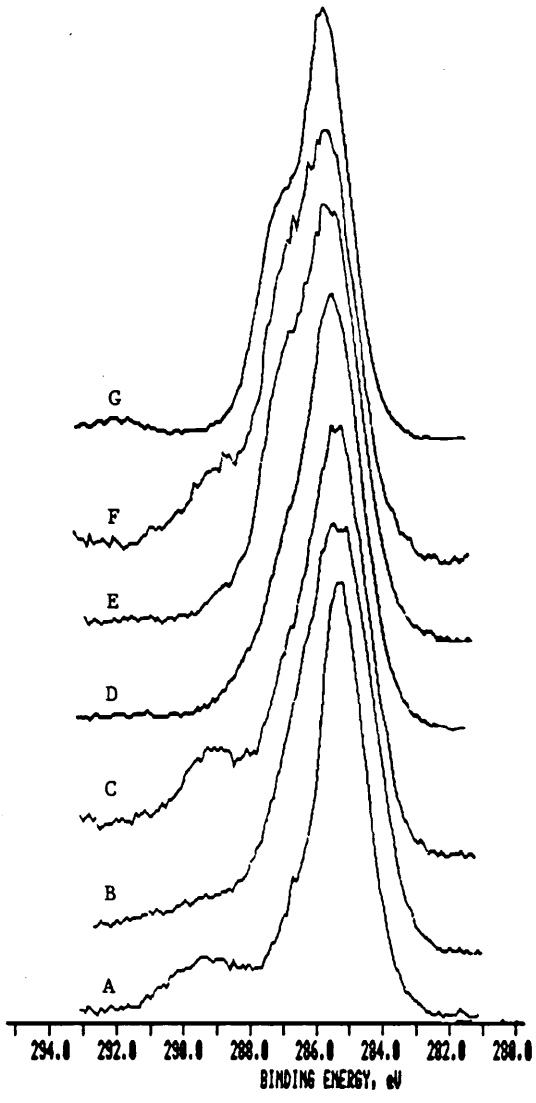

Figure 75. C 1s spectra. Phase α-SMC/urethane/CH_2Cl_2 cleaned primed lap shear specimens. 50% load, 60°C (140°F), 85% RH, 7 days.

A: CH_2Cl_2 cleaned aluminum

B, C: Phase α-SMC/urethane/CH_2Cl_2 cleaned phenolic primed aluminum specimens. Failure at the adhesive/aluminum interface. B: Adhesive side, C: Aluminum side

D: Phenolic primer film

E, F: Phase α-SMC/urethane/CH_2Cl_2 cleaned epoxy primed aluminum specimens. Failure at the adhesive/aluminum interface. E: Adhesive side, F: Aluminum side

G: Epoxy primer film

The spectrum for the failed adhesive side (Figure 75E) resembles that of the epoxy primer film (Figure 75 G). Both have a relatively strong shoulder at BE = 286.8 eV. The spectrum for the failed aluminum side (Figure 75 F) is unlike that for solvent cleaned aluminum. The shape resembles that of the failed adhesive side (Figure 75 E) except for the presence of a spectral feature at BE = 289.0 eV, which may be attributed to contamination left on the aluminum surface after solvent cleaning.

The XPS results suggest that for samples prepared with epoxy primed aluminum exposed to stress, temperature and humidity, the visually determined adhesive failure took place largely in the primer layer. However the SEM results for the aluminum side surface (Figure 74) do not show any feature attributable to primer (fragmented material or patches) on this surface. The corroboration of the XPS and SEM results leads to the suggestion that a film rather than fragments of primer are present on the failed aluminum side surface.

The failure results presented above show that for the system phase α-SMC/ urethane/primed aluminum, solvent cleaning of aluminum does not provide durable bonds upon exposure to stress, temperature, and humidity, in spite of the reasonably good strength displayed by the as prepared samples which were tested in the Instron.

The reference failure strength, 267 lbs, for phase α-SMC/ urethane/ phenolic primed aluminum, and 256 lbs for phase α-SMC/urethane/epoxy primed aluminum samples are similar to the value, 267 lbs, measured for phase α-SMC/ urethane/treated steel samples (Table 10). The change in the failure mode from almost entirely cohesive for as prepared samples tested in the Instron to largely adhesive failure at the aluminum surface for samples that failed during exposure to stress and environmental conditioning, suggests that the aluminum/primer bond is the weak link in the system.

It is suggested that inadequate primer-aluminum interaction results from the fact that solvent cleaning usually does not remove all the dirt and impurities existing on the surface

of as received metals [203, 204]. The XPS results for solvent cleaned aluminum (SCAl) and as received aluminum (ARAl), Table 34, show that the nitrogen concentration decreases from 0.80% (ARAl) to 0.65 % (SCAl) and the silicon concentration decreases from 0.57% (ARAl) to 0.30% (SCAl) upon solvent cleaning. The aluminum concentration increases from 7.30 % (ARAl) to 8.60 % (SCAl) and the magnesium concentration increases from 6.80 % (ARAl) to 10.60 % (SCAl). These results suggest that impurities existing on as received aluminum are only partially removed by CH_2Cl_2 cleaning.

A layer of contaminants will therefore remain on the aluminum surface after cleaning and will be in direct contact with the primer after priming. The bond between aluminum and the primer may be weakened faster than all other links in the system, upon exposure to stress, humidity, and temperature. Another type of cleaning must be used to obtain better bond durability. Alkaline cleaning was selected as a potentially useful method.

4.3.7.2. Phase α-SMC/urethane/alkaline cleaned unprimed aluminum samples

4.3.7.2.1. Failure results

Table 35 summarizes the failure results. A very important observation is that all samples failed adhesively at the aluminum/adhesive interface and/or cohesively. Sixty percent of the loaded samples tested at 60°C in dry air failed during the test in a very short time (1h). The residual strength of the samples which survived the test (T) was equivalent to the reference (R) sample strength: 172 ± 33 lbs (T) vs 180 ± 27 lbs (R). All unloaded samples investigated at 60°C and 85% RH survived the test, and the residual strength was similar to the reference sample strength 152 ± 56 (T) vs 180 ± 27 lbs (R). All loaded samples maintained at 60°C and 85% RH failed in a very short time (1h).

Table 35

Failure Results. Phase α-SMC/Urethane/Alkaline Cleaned, Unprimed Aluminum Lap Shear Samples.
60°C (140°F), 7 Days.

		Samples Which Survived the Test						Samples Failed During the Test				
Humidity	Load	Number of Samples Tested	Number of Samples	Average Failure Force, lbs	Average Failure Mode %D	%A	%C	Number of Samples	Time to Failure h-hours d-days (no.)	Average Failure Mode %D	%A	%C
As Prepared Samples Room Temperature	No Load	5	5	180 ± 27	-	45	55	-	--	-	-	-
Dry Air	No Load	5	5	190 ± 54	-	66	34	-	--	-	-	-
	50% Load	5	2	172 ± 33	-	68	32	3	1h (3)	-	72	28
85% RH	No Load	5	5	152 ± 56	-	98	2	-	--	-	-	-
	50% Load	5	-	-	-	-	-	5	1h (5)	-	70	30

4.3.7.2.2. Surface characterization

Representative XPS results are given in Table 36 and in Figure 76. The atomic concentrations for the failed aluminum surface are in agreement with the results for alkaline cleaned aluminum. Some nitrogen is found on the failed aluminum surface indicating the presence of some adhesive. Nitrogen is not found on alkaline cleaned aluminum. The C ls spectrum for the failed aluminum surface (Figure 76B) is similar to that of alkaline cleaned aluminum (Figure 76A) with the exception of a small shoulder at 286.5 eV which is attributed to the presence of some adhesive on the failed aluminum. The atomic concentrations for the failed adhesive surface are similar to that for the adhesive film (Table 21). Also the C 1s spectrum for the failed adhesive surface (Figure 76C) is representative of the adhesive film (Figure 58C). The XPS results indicate that the failure was almost pure adhesive failure at the aluminum/adhesive interface. These results are also confirmed by SEM.

The scanning electron micrographs in Figure 77 reveal depressions in the alkaline cleaned aluminum and in the failed aluminum surface and raised features on the failed adhesive surface. The failed adhesive surface is a replica of the failed aluminum surface which is similar to the alkaline cleaned aluminum surface. The absence of definite features which could be attributed to adhesive (fragmented material or patches) on the failed aluminum surface indicates that a film of adhesive rather than fragments of adhesive may be present on this surface. Similar results were obtained for samples tested at 60°C in 85% RH.

Table 36.

XPS Results (Atomic %). Phase α-SMC/Urethane/Alkaline Cleaned Aluminum Lap Shear Samples.
50% Load, 60°C (140°F), Dry Air, 7 Days.

	Failed Surfaces				
Element	Alkaline Cleaned Aluminum	Aluminum Side	Adhesive Side	Urethane Adhesive film	Split Urethane Adhesive
C	12.5	22.1	73.7	68.8	56.8
O	58.4	54.3	23.8	26.4	31.2
N	<0.1	0.86	1.65	2.90	2.65
Si	<0.1	0.44	0.27	1.35	5.67
Ca	<0.1	<0.1	<0.1	<0.1	<0.1
Mg	<0.1	<0.1	<0.1	0.52	1.97
Al	28.9	17.3	0.58	<0.1	1.70
Others (Zn, Cl)	<0.1	0.80	<0.1	<0.1	<0.1

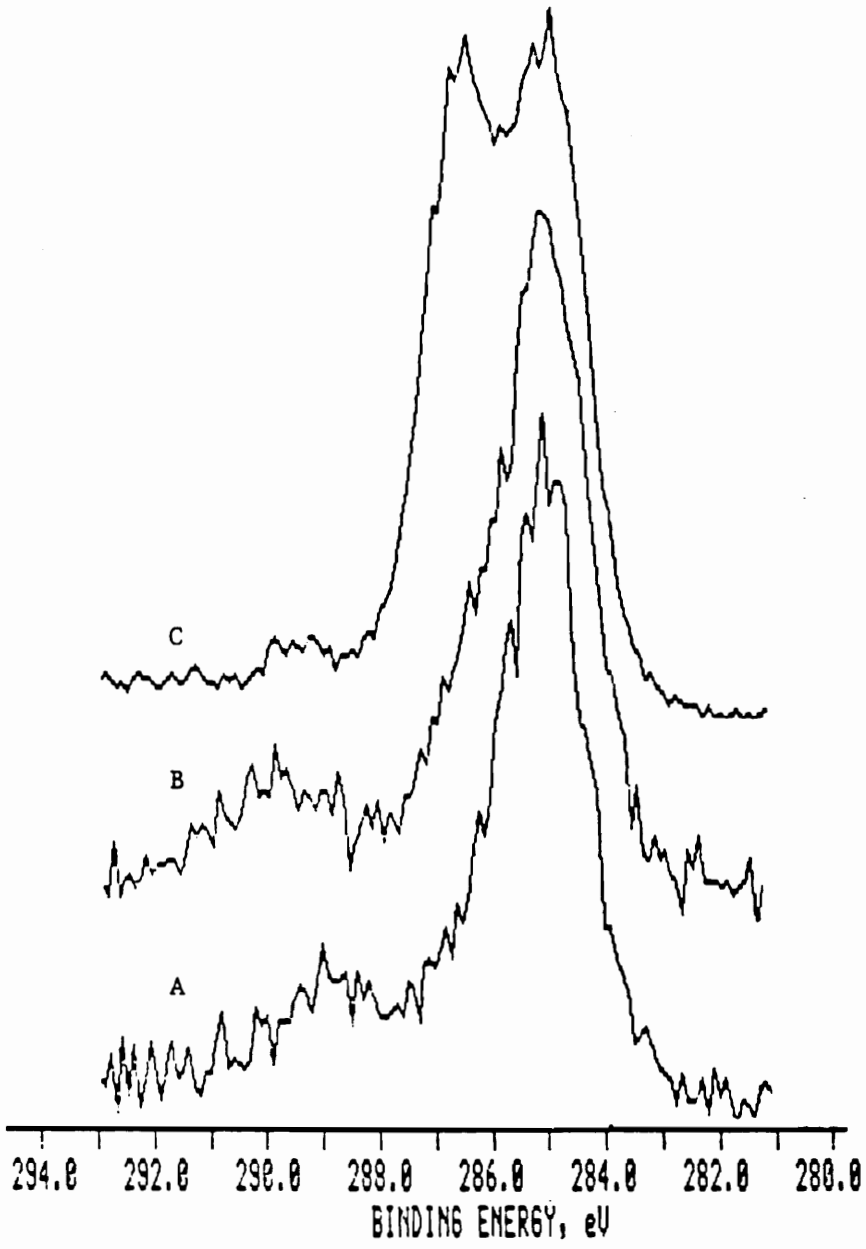

Figure 76. C 1s spectra.

A: Alkaline cleaned aluminum.

B, C: Phase α-SMC/urethane/alkaline cleaned aluminum lap shear specimens. 50% load, 60°C (140°F), dry air, 7 days. Instron failure. B: Aluminum side, C: Adhesive side.

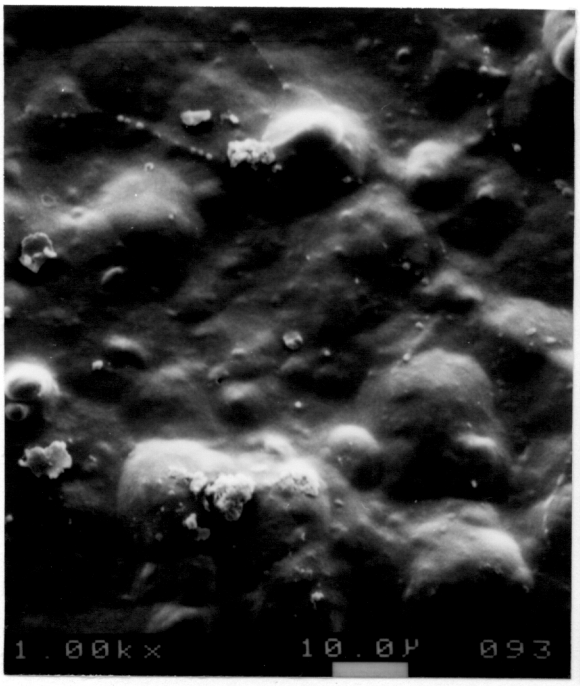

Adhesive side

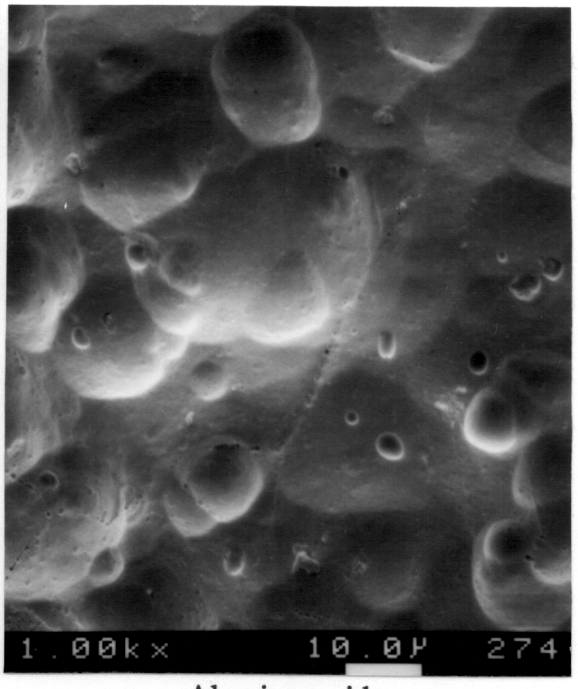

Aluminum side

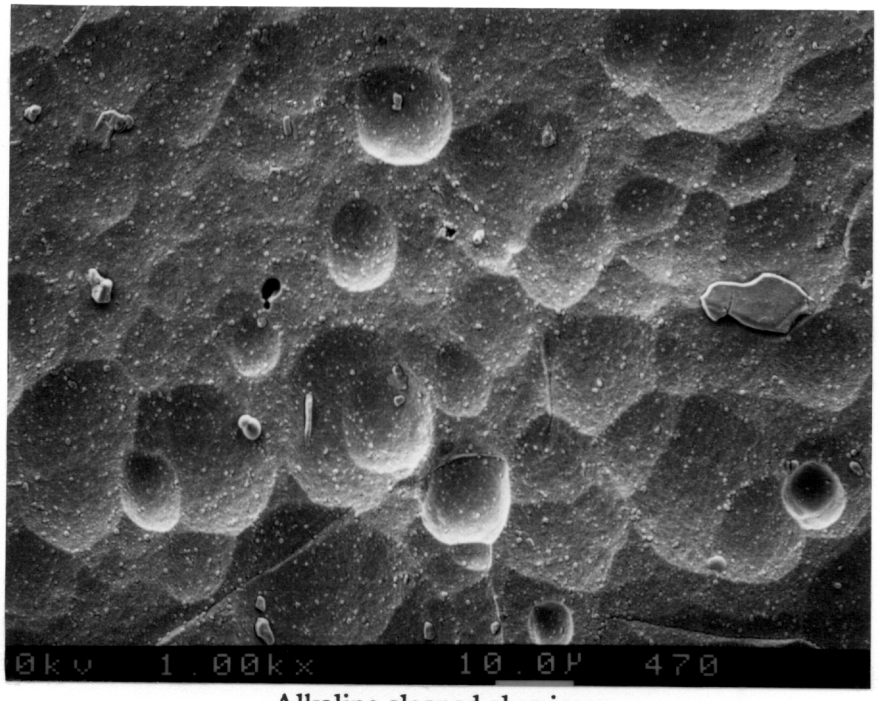

Alkaline cleaned aluminum

Figure 77. SEM results. Phase α-SMC/urethane/alkaline cleaned aluminum lap shear specimens. 50% load, 60°C (140°F), dry air, 7 days. Instron failure.

4.3.7.3. Phase α-SMC/urethane/alkaline cleaned diisocyanate primed aluminum samples

4.3.7.3.1. Failure Results

Examination of the failure results summarized in Tables 37 and 38 indicates that:

a) All unloaded samples tested at 60°C in dry air survived the test. The residual strengths were similar to those for the reference samples: lap shear 220 ± 41 lbs (T) vs 197 ± 43 lbs (R), wedge 30 ± 2.3 lbs (T) vs 30 ± 4.4 lbs (R), and butt torsion 31 ± 7.8 lb x ft vs 31 ± 4.7 lb x ft (R).

b) Twenty percent of the loaded lap shear samples and 87% of the loaded butt torsion samples failed during environmental conditioning at 60°C in dry air. The residual strengths for the samples which survived the test were comparable to the reference strengths: lap shear 211 ± 38 lbs (T) vs 197 ± 43 lbs (R), wedge 32 ± 5.6 lbs (T) vs 30 ± 4.4 lbs (R), and butt torsion 27 lb x ft (T) vs 31 ± 4.7 lb x ft (R). An improved durability for samples prepared with diisocyanate primed aluminum over samples prepared with unprimed aluminum (Table 35) was observed in dry air conditions. Upon exposure to 60°C in dry air, only 20% of loaded lap shear samples prepared with diisocyanate primed aluminum failed during the test, versus 60% of samples prepared with unprimed aluminum. Also, the time to failure was longer for samples prepared with diisocyante primed aluminum (2.5 days), than for samples preparared with unprimed aluminum (1 hr).

c) All unloaded samples tested at 60°C and 85% RH survived the test. The residual strengths were similar to the reference strengths: lap shear 163 ±47 lbs (T) vs 197 ± 43 lbs (R) and wedge samples 34 ± 3.4 lbs (T) vs 30 ± 4.4 lbs (R). The failure moment was significantly lower for butt torsion samples 15 ± 4.6 lb x ft (T) vs 31 ± 4.7 lb x ft (R).

d) All loaded lap shear and butt torsion, and 22 % of wedge specimens failed during environmental conditioning at 60°C and 85% RH in a very short time. The average

Table 37.

Failure Results. Phase α-SMC/Urethane/Alkaline Cleaned Diisocyanate Primed Aluminum Samples. 60°C (140°F), 7 Days. (Samples Which Survived the Test)

Humidity	Load	Type of Sample	Number of Samples Tested	Which Survived the Test	Average Failure Force, lbs* (Average Failure Moment, lb x ft **)	Average Failure Mode %D	%A	%C
As Prepared Samples Room Temperature	No Load	Lap Shear	10	10	197 ± 43	-	60	40
		Wedge	10	10	30 ± 4.4	41	59	-
		Butt Torsion	10	10	31 ± 4.7	7	53	40
Dry Air	No Load	Lap Shear	10	10	220 ± 41	-	85	15
		Wedge	5	5	30 ± 2.3	55	45	-
		Butt torsion	5	5	31 ± 7.8	-	82	16
	50% Load	Lap Shear	10	8	211 ± 38	-	73	27
		Wedge	5	5	32 ± 5.6	36	64	-
	20% Load	Butt Torsion	8	1	27	-	85	15
85% RH	No Load	Lap Shear	10	10	163 ± 47	-	93	7
		Wedge	9	9	34 ± 3.4	42	58	-
		Butt torsion	8	8	15 ± 4.6	-	100	-
	50% Load	Lap Shear	10	-	--	-	-	-
		Wedge	9	7	25 ± 7.4	31	69	-
	20% Load	Butt Torsion	10	-	--	-	-	-

All wedge samples were loaded in constant load mode
* For lap shear and wedge samples
** For butt torsion samples

Table 38

Failure Results. Phase α-SMC/Urethane/Alkaline Cleaned Diisocyanate Primed Aluminum Samples. 60°C (140°F), 7 Days. (Samples Which Failed During the Test)

Humidity	Load	Type of Sample	Number of Samples Tested	Number of Samples Which Failed During the Test	Time to Failure h - hours d - days	Average Failure Mode %D	%A	%C
As Prepared Samples Room Temperature	No Load	Lap Shear	10	-	--	-	-	-
		Wedge	10	-	--	-	-	-
		Butt Torsion	10	-	--	-	-	-
Dry Air	No Load	Lap Shear	10	-	--	-	-	-
		Wedge	5	-	--	-	-	-
		Butt Torsion	5	-	--	-	-	-
	50% Load	Lap Shear	10	2	5h, 5d	-	90	10
		Wedge	5	-	--	-	-	-
	20% Load	Butt Torsion	8	7	5h, 8h, 1d (4), 2d	7	55	38
85% RH	No Load	Lap Shear	10	-	--	-	-	-
		Wedge	9	-	--	-	-	-
		Butt Torsion	8	-	--	-	-	-
	50% Load	Lap Shear	10	10	1h (10)	-	83	17
		Wedge	9	2	4d, 7d	-	100	-
	20% Load	Butt Torsion	10	10	1h (2), 5h (5), 8h (3)	-	67	33

time to failure for samples investigated at 85% RH (H) was shorter than for the samples exposed to dry air (DA): lap shear 1h (H) vs 2.5 days (DA) and butt torsion 5h (H) vs 20h (DA). For the wedge samples which survived the test, the residual strength was similar to the reference strength 25 ± 7.4 lbs (T) vs 31 ± 4.7 lbs (R). The results for loaded lap shear samples conditioned at 60°C and 85% RH are similar to those obtained for samples prepared with unprimed aluminum adherends tested under the same conditions (Table 35). All samples failed in a short time (1h) during exposure indicating that the use of the diisocyante primer does not improve durability in humid conditions.

e) For lap shear samples the failure mode was a mixture of adhesive (60-93%) and cohesive failure (40-7%). All the adhesive portion of the failure mode took place at the aluminum/primer interface. Wedge samples failed in the Instron test by a mixture of delamination (31-55%) and adhesive (69-45%) failure. For wedge samples tested in dry air, the adhesive portion of the failure took place at the SMC/adhesive interface, while for samples maintained at 85% RH some adhesive failure took place at the aluminum/primer interface. For wedge samples which failed during exposure the failure was 100% adhesive at the aluminum/adhesive interface. The failure mode for butt torsion samples was principally adhesive and cohesive. Little delamination was observed for samples tested in dry air. The adhesive portion of the failure mode took place mostly at the aluminum/primer interface. For samples maintained at 85% RH, adhesive failure occurred only at the aluminum/primer interface. The results show that environmental conditioning in humid conditions has a significant influence on durability for this system. Increases were observed in the proportion of samples which failed during exposure and shifts in the failure mode to a higher proportion of adhesive failure at the aluminum/primer interface were noted.

4.3.7.3.2. Surface Characterization

Surface analysis measurements were carried out for the adhesive failure regions both for samples which failed at the adhesive/aluminum side and for samples which failed at the adhesive/SMC side. XPS results for representative samples are presented in Table 39 and in Figure 78 (C 1s spectra). Nitrogen is noted on all failed surfaces. For samples which failed at the adhesive/aluminum side the detection of nitrogen on the aluminum side surface indicates the presence of adhesive or primer on this surface. The following results suggest that the failure occurred at the aluminum/primer interface and that most of the primer appeared on the adhesive side.

a) The nitrogen concentration on the aluminum side surfaces is less than 1% compared with 6.72% on non-bonded diisocyanate primed aluminum.

b) The nitrogen concentration on the adhesive side surfaces is 7.89 % (dry air) and 9.56% (85 % RH) compared with 2.90% on the adhesive film (Table 21).

c) The shapes of C ls spectra for the adhesive side surfaces (Figure 78B and 78F) are not representative of the adhesive (Figure 58D). The spectra resemble the C ls spectrum for primed aluminum (Figure 78G).

d) The color of the aluminum side surface is white, while that of the adhesive side is green-yellow. (The adhesive is green and the primer is yellow).

e) Scanning electron micrographs for representative failed surfaces are shown in Figures 79 and 80. The SEM micrographs in Figure 79 show depressions in the aluminum side surfaces and raised features on the adhesive failed surfaces. No definitive features that can be attributed to adhesive are noted on failed aluminum surfaces. For the samples which failed at the adhesive/SMC interface, the SEM results (Figure 80) indicate that the visually observed adhesive failure is actually a mixture of near surface debonding of the SMC and interfacial adhesive failure. Some of the outer layer of SMC is found on the adhesive side.

Table 39.

XPS Results (Atomic %). Phase α-SMC/Urethane/Alkaline Cleaned Diisocyanate Primed Aluminum Samples 50% Load, 60°C (140°F), 7 Days.

		Dry air				85% RH	
		Lap Shear**		Wedge*		Wedge**	
Element	Diisocyanate Primed Aluminum	Adhesive Side	Aluminum Side	Adhesive Side	SMC Side	Adhesive Side	Aluminum Side
C	79.0	74.8	21.5	78.2	82.5	77.4	17.7
O	14.1	16.7	55.9	17.4	15.0	12.9	55.0
N	6.72	7.89	0.81	3.86	0.66	9.26	0.86
Si	<0.1	0.21	0.46	0.23	0.83	<0.1	0.89
Ca	<0.1	<0.1	<0.1	<0.1	<0.1	<0.1	<0.1
Mg	<0.1	<0.1	<0.1	0.37	0.21	<0.1	0.48
Al	<0.1	<0.1	20.4	<0.1	0.40	0.22	24.17
Others (Zn, Cl)	0.25	0.34	0.95	<0.1	<0.1	<0.1	0.88

* Failure at the adhesive/SMC interface

** Failure at the adhesive/aluminum interface

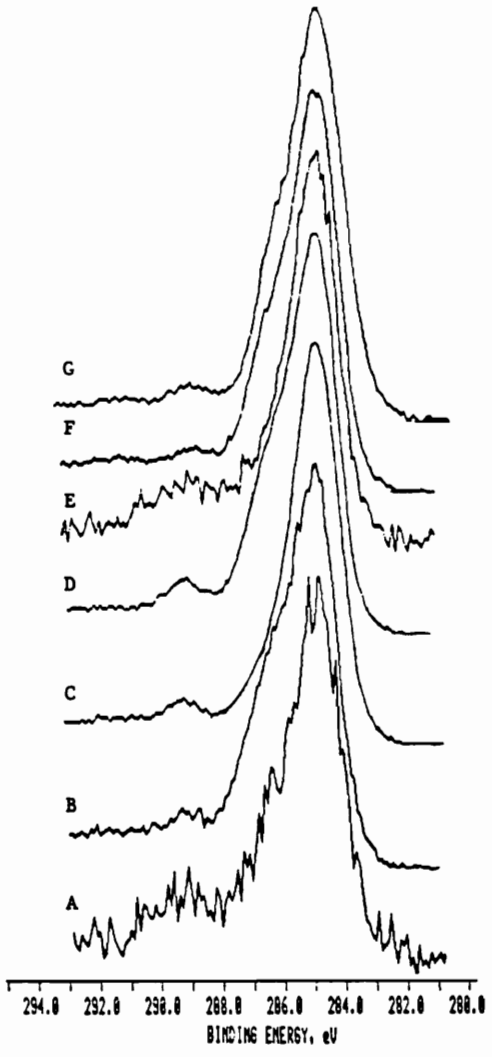

Figure 78. Phase α-SMC/urethane/alkaline cleaned diisocyanate primed aluminum specimens. 50% load, 60°C (140°F), 7 days.

A, B: Dry air. Lap shear specimens. Test failure at the adhesive/aluminum interface. A: Aluminum side, B: Adhesive side.
C, D: Dry air. Wedge specimens. Instron failure at the adhesive/SMC interface. C: SMC side, D: Adhesive side.
E, F: 85% RH. Wedge specimens. Test failure at the adhesive/aluminum interface. E: Aluminum side, F: Adhesive side.
G: Diisocyanate primed aluminum.

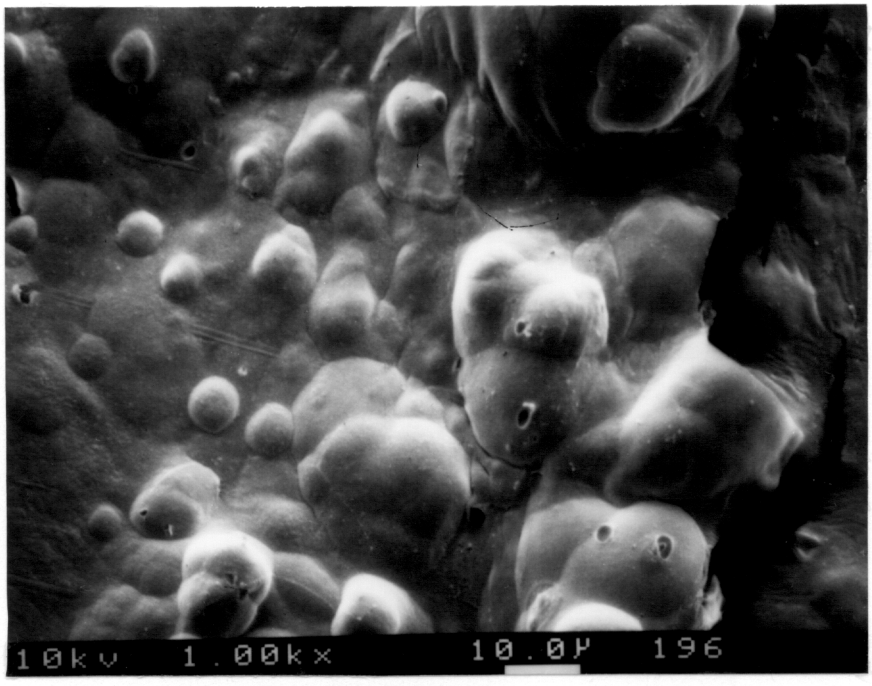

Adhesive side

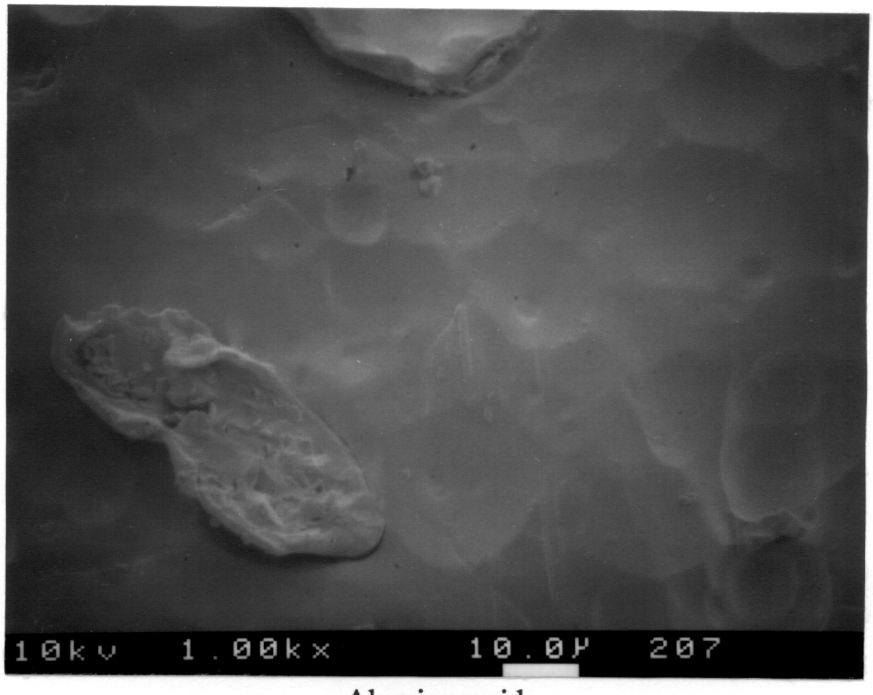

Aluminum side

Figure 79. SEM results. Phase α-SMC/urethane/alkaline cleaned diisocyanate primed aluminum lap shear specimens. 50% load, 60°C (140°F), dry air, 7 days. Test failure at the adhesive/aluminum interface.

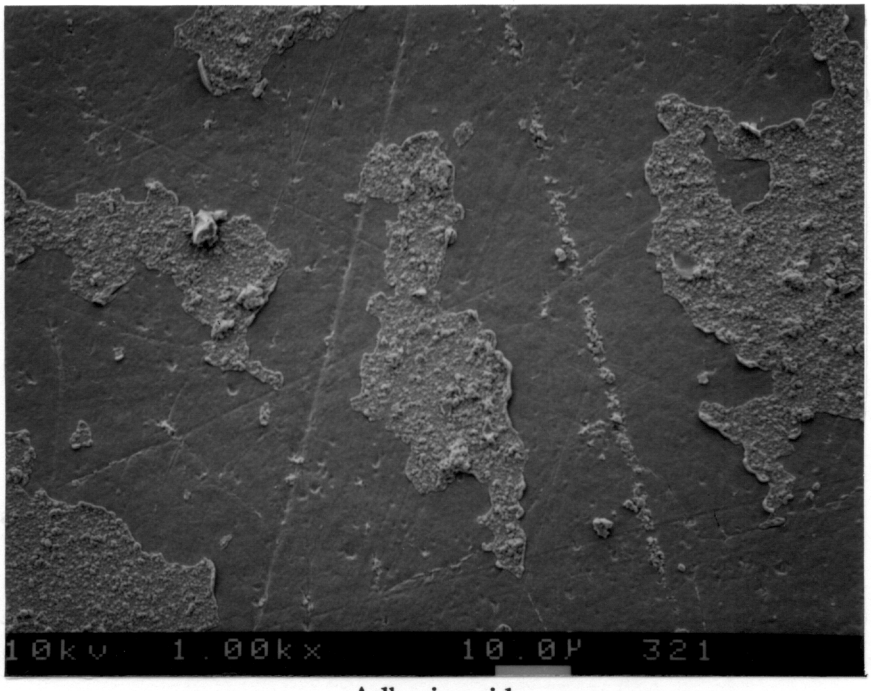

Adhesive side

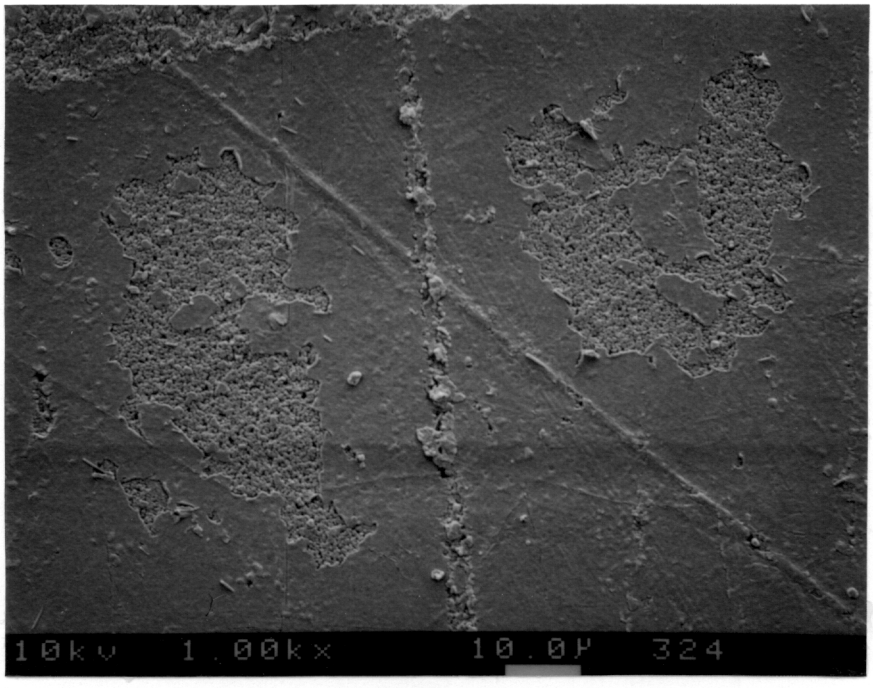

SMC side

Figure 80. SEM results. Phase α-SMC/urethane/alkaline cleaned diisocyanate primed aluminum wedge specimens. 50% load, 60°C (140°F), dry air, 7 days. Instron failure at the adhesive/SMC interface.

The XPS results confirm the SEM findings. Little nitrogen (0.66%) was found on the SMC side surface indicating that little primer is left on this surface. The shape of the C ls spectrum for the SMC side surface (78C) is very close to that of as received SMC (Figure 58A). These results suggest that SMC constituents only are present on the SMC side surface. The XPS results for the adhesive side surfaces: a nitrogen concentration of 3.86% and a C ls spectrum (Figure 78D) intermediate between that of as received SMC (Figure 58A) and primed SMC (Figure 58C) indicate that the failed SMC surface is composed of a mixture of primer and SMC. Almost all the primer and some of the outer layer of the SMC surface appear on the adhesive surface after failure.

The failure results can be explained considering the processes which may take place at the MDI/aluminum interface. The aluminum surface contains hydroxyl groups (See 2.2.3.4). Upon application of the primer, interactions take place between the primer and the aluminum surface, possibly including physisorption and chemical reactions. Considering that the diisocyanate-based primer contains -NCO groups, there are opportunties for chemical reactions between primer and the aluminum oxide surface. The FTIR studies of MDI treated aluminum presented in section 4.2.3 strongly suggest that there is a chemical interaction between the aluminum surface species and MDI, producing a strong aluminum/MDI bond resistant to solvent treatments. A possible chemical reaction would be formation of an urethane bond:

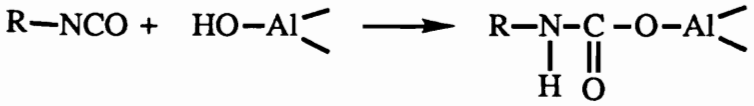

An aluminum/primer chemical interaction may explain the beneficial effect on durability in dry air conditions upon diisocyanate priming. However -NCO functionality and the urethane bond are both sensitive to water. Exposure to moisture may produce hydrolysis

of aluminum/primer chemical bonds. Application of a high load accelerates moisture attack [107] and the samples exposed to high humidity may fail much faster than those maintained in dry air under the same conditions of loading and temperature.

One possible hydrolysis reaction is:

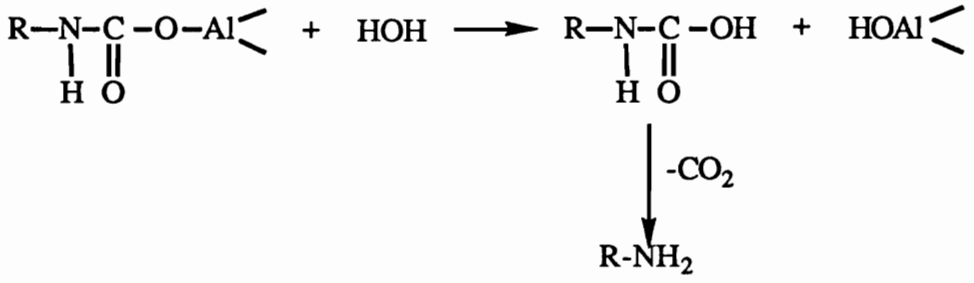

4.3.7.4. Phase α-SMC/urethane/alkaline cleaned phenolic primed aluminum samples

4.3.7.4.1. Failure results

Examination of the failure results summarized in Tables 40 and 41 shows:

a) All unloaded samples exposed to 60°C in dry air survived the test and their residual strength (T) was similar to the strength of the reference specimens (R): lap shear 327 ± 19 lbs (T) vs 286 ± 54 lbs (R) and wedge 35 ± 1.3 lbs (T) vs 36 ± 4.5 lbs (R), but higher for butt torsion samples 41 ± 8 lb x ft (T) vs 27 ± 3.5 lb x ft (R).

b) All loaded samples tested at 60°C in dry air survived the test. The residual strength was comparable to the reference strength: lap shear 298 ± 20 lbs (T) vs 286 ± 54 lbs (R); wedge 35 ± 5.0 lbs (T) vs 36 ± 4.5 lbs (R), and higher for butt torsion samples 43 ± 6.8 lb x ft (T) vs 27 ± 3.5 lb x ft (R).

c) All unloaded samples conditioned at 60°C in 85% RH survived the test and the residual strength was, within the limits of precision, similar to the strength of the reference samples: lap shear 237 ± 26 lbs (T) vs 286 ± 54 lbs (R), wedge 37 ± 3 lbs (T) vs 36 ± 4.5 lbs (R), and butt torsion 29 ± 2.6 lb x ft (T) vs 27 ± 3.5 lb x ft (R).

Table 40.

Failure Results. Phase α-SMC/Urethane/Alkaline Cleaned Phenolic Primed Aluminum Samples. 60°C (140°F), 7 Days. (Samples Which Survived the Test)

Humidity	Load	Type of Sample	Number of Samples Tested	Number of Samples Which Survived the Test	Average Failure Force, lbs* (Average Failure Moment, lb x ft **)	Average Failure Mode %D	%A	%C
As Prepared Samples Room Temperature	No Load	Lap Shear	7	7	286 ± 54	39	4	57
		Wedge	5	5	36 ± 4.5	63	37	-
		Butt Torsion	5	5	27 ± 3.5	4	30	66
Dry Air	No Load	Lap Shear	5	5	327 ± 19	79	1	20
		Wedge	5	5	35 ± 1.3	75	25	3
		Butt torsion	5	5	41 ± 8.0	61	30	9
	50% Load	Lap Shear	5	5	298 ± 20	38	23	39
		Wedge	5	5	35 ± 5.0	79	16	5
	20% Load	Butt Torsion	5	5	43 ± 6.8	46	24	30
85% RH	No Load	Lap Shear	5	5	237 ± 26	13	9	78
		Wedge	5	5	37 ± 3.0	65	35	-
		Butt torsion	5	5	29 ± 2.6	16	42	42
	50% Load	Lap Shear	15	8	266 ± 40	32	15	53
		Wedge	10	10	37 ± 5.6	69	31	-
		Wedge+	5	5	36 ± 2.2	29	45	26
	20% Load	Butt Torsion	10	-	--	-	-	-

All wedge samples were loaded in constant load mode

* For lap shear and wedge samples; ** For butt torsion samples

\+ Samples exposed for 21 days

Table 41

Failure Results. Phase α-SMC/Urethane/Alkaline Cleaned Phenolic Primed Samples. 60°C (140°F), 7 Days. (Samples Which Failed During the Test)

Humidity	Load	Type of Sample	Number of Samples Tested	Which Failed During the Test	Time to Failure h - hours d - days	Average Failure Mode %D	%A	%C
As Prepared Samples Room Temperature	No Load	Lap Shear	7	-	--	-	-	-
		Wedge	5	-	--	-	-	-
		Butt Torsion	5	-	--	-	-	-
Dry Air	No Load	Lap Shear	5	-	--	-	-	-
		Wedge	5	-	--	-	-	-
		Butt Torsion	5	-	--	-	-	-
	50% Load	Lap Shear	5	-	--	-	-	-
		Wedge	5	-	--	-	-	-
	20% Load	Butt Torsion	5	-	--	-	-	-
85% RH	No Load	Lap Shear	5	-	--	-	-	-
		Wedge	5	-	--	-	-	-
		Butt Torsion	5	-	--	-	-	-
	50% Load	Lap Shear	15	7	3h (2), 8h, 12h, 3d (2), 5d	46	39	15
		Wedge	10	-	--	-	-	-
		Wedge+	5	-	--	-	-	-
	20% Load	Butt Torsion	10	10	4h, 7h (2), 9h 1d (5), 2d	12	11	77

All wedge samples were loaded in constant load mode

* For lap shear and wedge samples; ** For butt torsion samples

\+ Samples exposed for 21 days

d) Forty seven percent of the loaded lap shear and all loaded butt torsion samples studied at 60°C and 85% RH failed during the test, while all samples tested under the same conditions of stress and temperature in dry air survived the test.

The residual strength for lap shear samples which survived the test was similar to the reference strength 266 ± 40 lbs (T) vs 286 ± 54 lbs (R). For lap shear samples the residual strength tended to be higher than the reference strength for samples exposed to dry air conditions and lower than the reference strength for samples exposed to 85% RH. However, statistically they are equivalent. All loaded wedge samples tested at 60°C and 85% RH survived the test. The increase in exposure from 7 days to 21 days did not induce failure during the test and did not lower the residual strength: 36 ± 2.2 lbs (21 day test) and 37 ± 5.6 lbs (7 day test) vs 36 ± 4.5 lbs for the reference strength.

e) The most significant finding is that all adhesive failures occurred at the SMC/adhesive interface. Lap shear samples failed mostly by cohesive failure and delamination of SMC with the cohesive portion of failure taking place near the aluminum surface. The failure mode for all wedge samples tested for 7 days was a mixture of adhesive failure at the adhesive/SMC interface and SMC delamination. For the loaded wedge samples investigated at 60°C and 85% RH for 21 days, the failure mode included a significant proportion (26%) of cohesive failure near the SMC/adhesive interface indicating weakening of the adhesive under longer exposure to humidity, temperature and stress. The deterioration of adhesive under these conditions may be due to hydrolysis or to physical aging. Probably, physical aging in the form of cracking or crazing is the main cause for weakening of the adhesive [107]. For butt torsion samples mixed mode failure occurred with a large proportion of cohesive failure taking place near the aluminum/adhesive interface.

4.3.7.4.2. Surface characterization

Selected XPS results are presented in Table 42 for loaded lap shear specimens tested at 60°C in dry air that failed in the Instron test on the aluminum/adhesive side of the specimen. Results are also presented for loaded lap shear specimens investigated at 60°C and 85% RH that failed adhesively during the test at the SMC/adhesive interface. The C 1s spectra are shown in Figure 81. All failed surfaces contain nitrogen at different concentrations. For samples which failed at the aluminum/adhesive side, the atomic concentrations and the C 1s spectra for both the adhesive side (Figure 81D) and the aluminum side (Figure 81E) are similar to those for split adhesive (see Table 21 and Figure 58E). The SEM results for the same samples (Figure 82) reveal identical rough surfaces, attributed to fractured adhesive, for both failed aluminum and adhesive side surfaces. The surface analysis results show that the failure is entirely cohesive. Similar results were obtained for samples that failed at the aluminum/adhesive side when tested at 85% RH.

For the samples which failed at the SMC/adhesive interface, the SEM results (Figure 83) indicate that the visually observed adhesive failure is more accurately regarded as a mixture of near-surface debonding of the SMC and interfacial adhesive failure. Some of the SMC outer layer surface appears on the adhesive side. The XPS results (Table 42) and C 1s spectra (Figure 81) confirm the SEM results. The nitrogen concentration on the failed SMC side surface is 3.37% while that on primed SMC is 5.41% (Table 21). The spectrum for the SMC side (81B) is close to the synthesized spectrum corresponding to a mixture of primed SMC surface (75%) and as received SMC surface (25%), see Figure 59C. The XPS results suggest that a mixture of primer and SMC constituents is present on the SMC side surface after failure.

The nitrogen concentration on the failed adhesive side is 4.45% while that for the adhesive film is 2.90 % (Table 21). The C 1s spectrum (Figure 81C) is equivalent to that

Table 42.

XPS Results (Atomic %). Phase α-SMC/Urethane/Alkaline Cleaned Phenolic Primed Aluminum Samples. 50% Load, 60°C (140°F), 7 Days.

		Dry Air Lap Shear*+		85% RH Lap Shear**++	
Element	Phenolic Primer	Adhesive Side	Aluminum Side	Adhesive Side	SMC Side
C	81.3	56.3	53.6	75.0	78.9
O	17.6	31.1	32.7	19.6	17.2
N	0.65	2.98	2.47	4.45	3.37
Si	<0.1	5.65	6.35	0.58	0.30
Al	0.29	1.35	1.71	<0.1	<0.1
Others (Mg, Zn, Cl)	0.11	2.62	3.17	0.40	0.30

* Failure in the Instron test
** Failure during the test
\+ Cohesive failure near the aluminum/adhesive interface
++ Failure at the SMC/adhesive interface

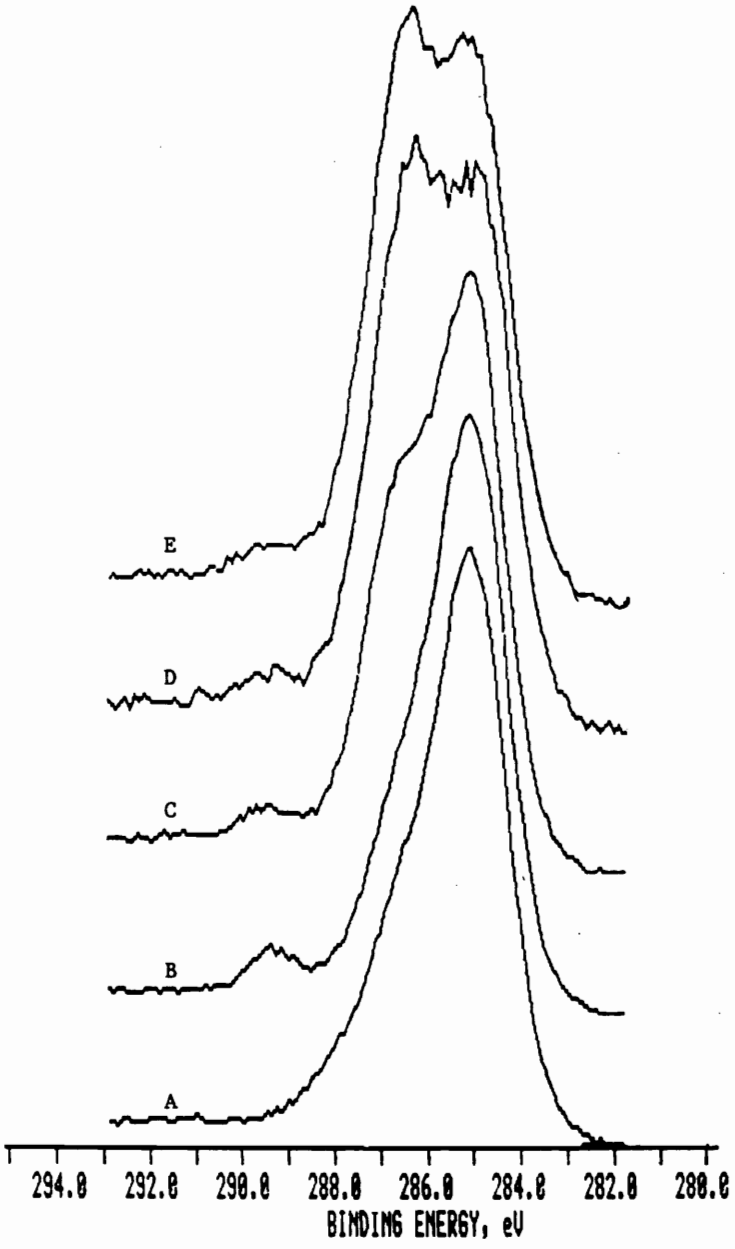

Figure 81. C 1s spectra. Phase α-SMC/urethane/alkaline cleaned phenolic primed aluminum specimens. 50% load, 60°C (140°F), 7 days.

A: Alkaline cleaned phenolic primed aluminum
B, C: 85% RH. Lap shear specimens. Instron failure at the adhesive/SMC interface. B: SMC side, C: Adhesive side
D, E: Dry air. Lap shear specimens. Instron failure: Cohesively, near the adhesive/aluminum interface. D: Aluminum side, E: Adhesive side.

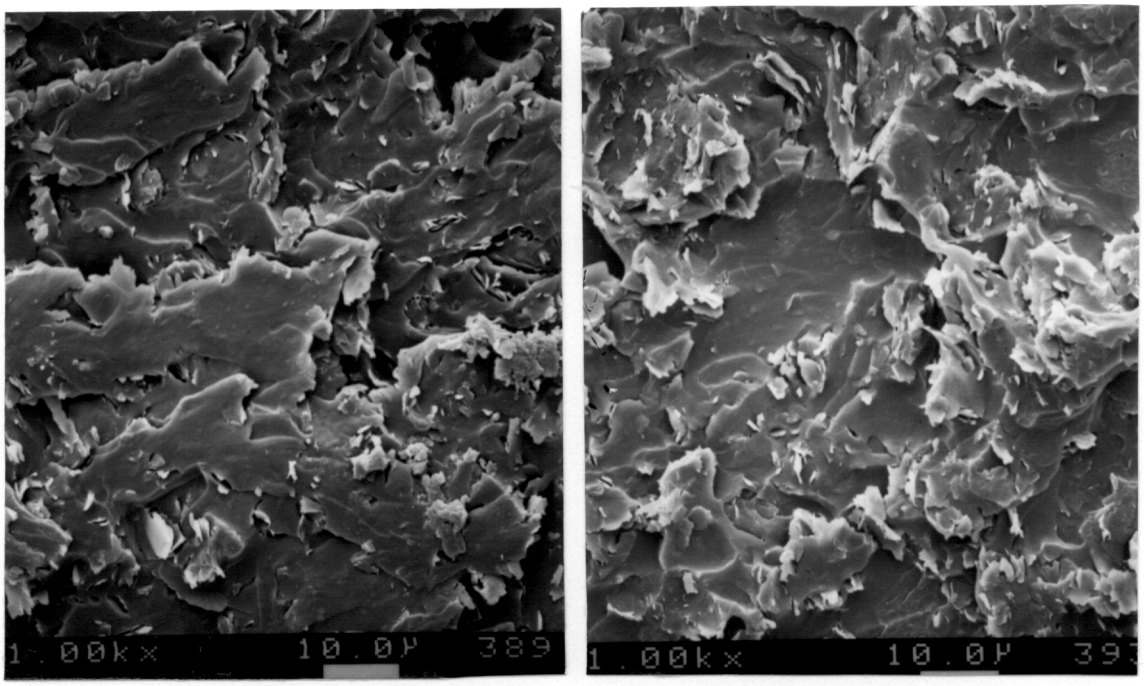

Adhesive side

Aluminum side

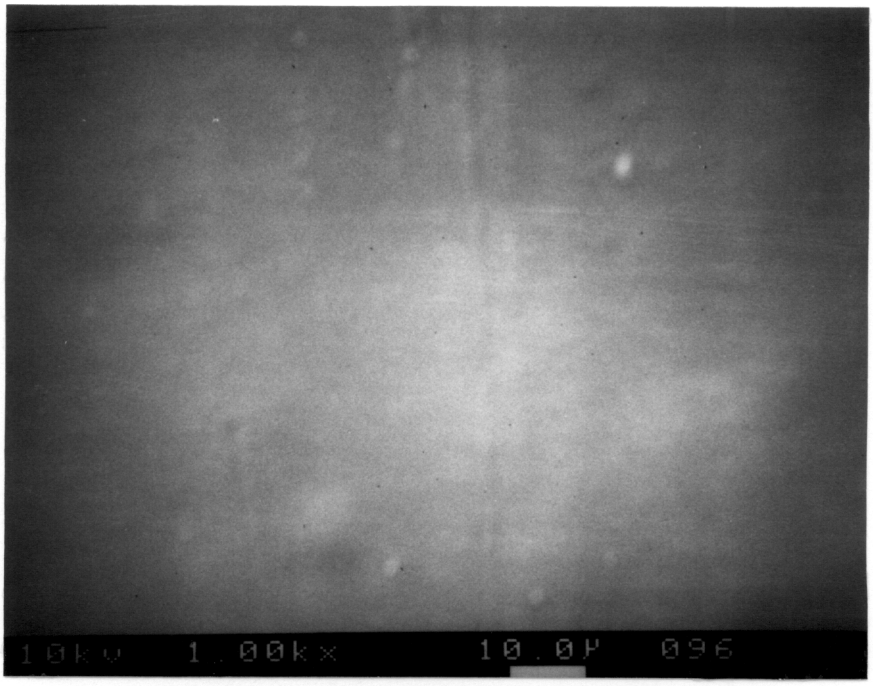

Alkaline cleaned phenolic primed aluminum

Figure 82. SEM results. Phase α-SMC/urethane/alkaline cleaned phenolic primed aluminum lap shear specimens. 50% load, 60°C (140°F), dry air, 7 days. Instron failure: Cohesively near the adhesive/aluminum interface.

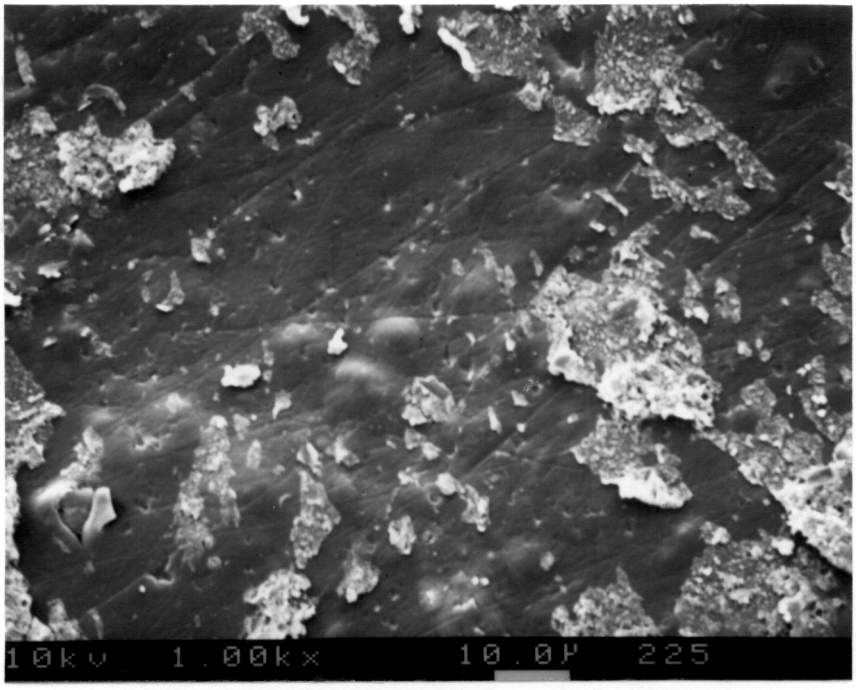

Adhesive side

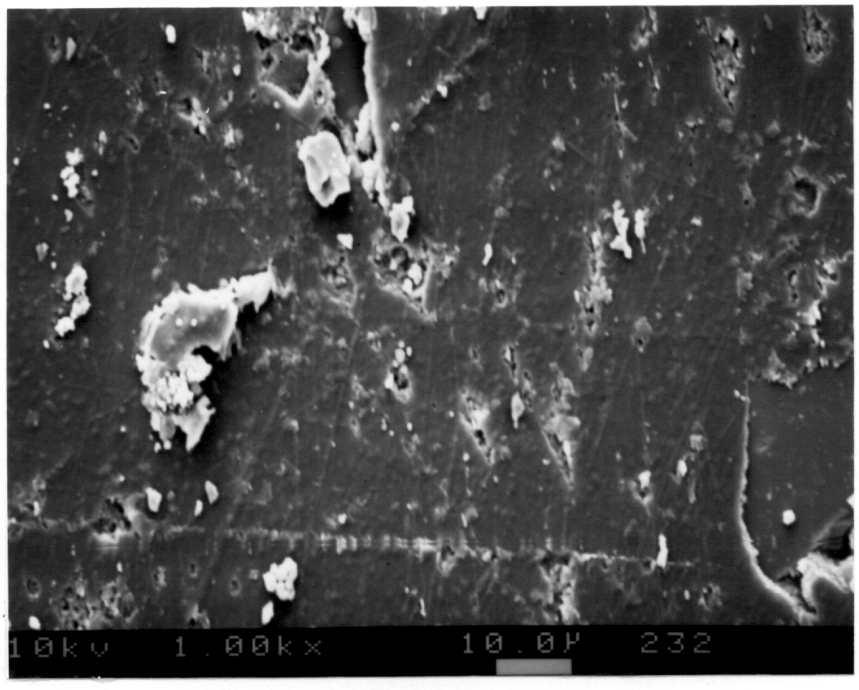

SMC side

Figure 83. SEM results. Phase α-SMC/urethane/alkaline cleaned phenolic primed aluminum lap shear specimens. 50% load, 60°C (140°F), 85% RH, 7 days. Test failure at the adhesive/SMC interface.

of primed SMC (Figure 58C), both having a relatively strong spectral feature associated with -COR/-NCO functionality (BE = 286.8). These results indicate that the adhesive side surface is composed mostly of primer transferred from the SMC surface at failure. Similar results were obtained for samples that failed adhesively at the SMC/adhesive interface when tested under dry air conditions.

The results obtained show a very important increase in durability for samples prepared with alkaline cleaned-phenolic primed aluminum when compared with samples prepared with solvent cleaned-diisocyanate primed aluminum; alkaline cleaned-unprimed aluminum; or alkaline cleaned-diisocyanate primed aluminum. These results are summarized below.

Percentage of Loaded Samples That Failed During the Test

Sample/ Treatment	Solvent Cleaned Primed Aluminum		Alkaline Cleaned Unprimed Aluminum		Alkaline Cleaned Diisocyanate Primed Aluminum		Alkaline Cleaned Phenolic Primed Aluminum	
	DA	HA	DA	HA	DA	HA	DA	HA
Lap Shear 50% Load	NM	100	60	100	20	100	0	47
Wedge 50% Load	NM	NM	NM	NM	0	22	0	0
Butt Torsion 20% Load	NM	NM	NM	NM	88	100	0	100

NM = not measured
DA =dry air
HA =humid air (85% RH)

A lower proportion of samples prepared with phenolic primed aluminum failed during the tests than for the other type of samples. The time to failure for samples prepared with alkaline cleaned phenolic primed was longer than for the other types of samples. These results are due to a more durable aluminum/primer bond, no adhesive failure took place at the aluminum surface. For the other types of samples, the aluminum/primer or

aluminum/adhesive bond proved to be much less durable under exposure to stress, temperature, and humidity, and the mode of failure was mostly adhesive at the aluminum surface. The good durability for phenolic primed aluminum specimens can be explained by the strong interaction between phenolic resin and surface aluminum oxides. The phenolic resins contain hydroxyl groups which are among the few polar groups which actually contribute the bond durability [75]. In the phenolic primer used in this research the presence of -OH groups is indicated by the shoulder at BE = 286.5 eV in the C 1s spectrum (See Figure 81A) corresponding to -COR carbon species.

The hydroxyl group can interact strongly with oxides over a wide IEPS (isoelectric point of the surface) range [75]. It was reported that chemical reactions occur between phenol or phenol-based compounds, and aluminum surface species (See 2.2.3.4.). Also, reflection absorption FTIR studies of phenol films on aluminum presented in 4.2.2, indicate chemical interactions between phenol and alkaline cleaned aluminum surface species. A possible chemical reaction between a phenolic resin and aluminum surface species would be:

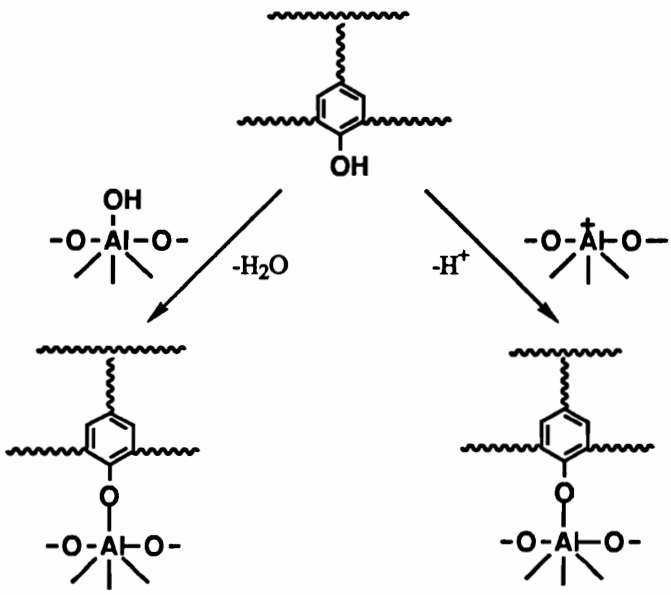

There is also opportunity for hydrogen bonding between phenol groups of the phenolic resins and aluminum surface species.

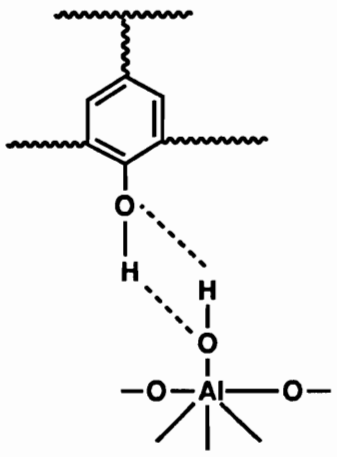

The strong, durable aluminum/phenolic primer bond may be due to both chemical reactions and hydrogen bonding between components of the phenolic primer and aluminum surface species.

4.3.7.5. Phase α-SMC/urethane/alkaline cleaned epoxy primed aluminum samples

4.3.7.5.1. Failure results

Examination of the failure results presented in Table 43 and 44 reveals that:

a) All unloaded samples maintained at 60°C in dry air survived the test and the residual strength was similar to the strength of reference samples: lap shear 273 ± 22 lbs (T) vs 244 ± 15 lbs (R), wedge 39 ± 4.0 lbs (T) vs 38 ± 3.0 lbs (R), and butt torsion 38 ± 6.5 lb x ft (T) vs 33 ± 2.3 lb x ft (R).

b) All loaded lap shear and wedge samples, but only 20% of the loaded butt torsion samples investigated at 60°C in dry air survived the test. For lap shear samples, the residual strength was higher than their reference sample strength 331 ± 23 lbs (T) vs 244 ±

Table 43.

Failure Results. Phase α-SMC/Urethane/Alkaline Cleaned Epoxy Primed Aluminum Samples. 60°C (140°F), 7 Days. (Samples Which Survived the Test)

Humidity	Load	Type of Sample	Number of Samples Tested	Number of Samples Which Survived the Test	Average Failure Force, lbs* (Average Failure Moment, lb x ft **)	Average Failure Mode %D	%A	%C
As Prepared Samples Room Temperature	No Load	Lap Shear	7	7	244 ± 15	38	10	52
		Wedge	5	5	38 ± 3.0	85	15	-
		Butt Torsion	5	5	33 ± 2.3	22	9	69
Dry Air	No Load	Lap Shear	5	5	273 ± 22	12	4	84
		Wedge	5	5	39 ± 4.0	67	31	2
		Butt torsion	5	5	38 ± 6.5	48	23	29
	50% Load	Lap Shear	5	5	331 ± 23	74	6	20
		Wedge	5	5	35 ± 1.7	67	30	3
	20% Load	Butt Torsion	5	1	38	20	25	55
85% RH	No Load	Lap Shear	5	5	235 ± 27	3	-	97
		Wedge	5	5	40 ± 2.0	68	30	2
		Butt torsion	5	5	30 ± 2.8	13	23	64
	50% Load	Lap Shear	10	5	244 ± 29	13	9	78
		Wedge	10	10	33 ± 4.2	54	43	3
		Wedge+	5	5	32 ± 3.5	27	46	27
	20% Load	Butt Torsion	10	-	--	-	-	-

All wedge samples were loaded in constant load mode

* For lap shear and wedge samples; ** For butt torsion samples

\+ Samples exposed for 21 days

Table 44

Failure Results. Phase α-SMC/Urethane/Alkaline Cleaned Epoxy Primed Aluminum Samples. 60°C (140°F), 7 Days. (Samples Which Failed During the Test)

Humidity	Load	Type of Sample	Number of Samples Tested	Number of Samples Which Failed During the Test	Time to Failure h - hours d - days	Average Failure Mode %D	%A	%C
As Prepared Samples Room Temperature	No Load	Lap Shear	7	-	--	-	-	-
		Wedge	5	-	--	-	-	-
		Butt Torsion	5	-	--	-	-	-
Dry Air	No Load	Lap Shear	5	-	--	-	-	-
		Wedge	5	-	--	-	-	-
		Butt Torsion	5	-	--	-	-	-
	50% Load	Lap Shear	5	-	--	-	-	-
		Wedge	5	-	--	-	-	-
	20% Load	Butt Torsion	5	4	1d, 2d, 3d, 4d	15	12	73
85% RH	No Load	Lap Shear	5	-	--	-	-	-
		Wedge	5	-	--	-	-	-
		Butt Torsion	5	-	--	-	-	-
	50% Load	Lap Shear	10	5	1d, 2.5d, 3.5d, 6d, 7d	79	21	-
		Wedge	10	-	--	-	-	-
		Wedge+	5	-	--	-	-	-
	20% Load	Butt Torsion	10	10	4h (6), 9h, 18h (3)	21	19	60

All wedge samples were loaded in constant load mode

* For lap shear and wedge samples; ** For butt torsion samples

+ Samples exposed for 21 days

15 lbs (R). The residual strength for the other two types of samples which survived the test compares with the reference sample strength: wedge 35 ± 1.7 lbs (T) vs 38 ± 3.0 lbs (R), and butt torsion 38 lb x ft (T) vs 33 ± 2.3 lb x ft (R).

c) All unloaded samples tested at 60°C in 85% RH survived the test. For all types of samples the residual strength was similar to the strength of the reference samples: lap shear 235 ± 27 lbs (T) vs 244 ± 15 lbs (R), wedge 40 ± 2.0 lbs (T) vs 38 ± 3.0 lbs (R) and butt torsion 30 ± 2.8 lb x ft (T) vs 33 ± 2.3 lb x ft (R).

d) For the loaded samples, environmental conditioning at 60°C and 85% RH increased the proportion of samples which failed during the test compared to exposure at 60°C in dry air. For lap shear samples the proportion that failed increased from 0% to 50% and for butt torsion specimens from 80 to 100%. All wedge samples survived the test. The residual strength of the samples which survived the test was comparable with the reference sample strength: lap shear 244 ± 29 lbs (T) vs 244 ± 15 lbs (R), wedge 33 ± 4.2 lbs (7 day exposure) and 32 ± 4.2 lbs (21 day exposure) vs 38 ± 3 lbs (R). For loaded wedge samples the increase in the exposure time from 7 days to 21 days did not induce failure of samples during the test and did not decrease the residual strength.

e) For the samples prepared with alkaline cleaned-epoxy primed aluminum, all the adhesive portion of the failure mode took place at the SMC/adhesive interface. No adhesive failure was observed at the aluminum/adhesive interface. For lap shear samples, the failure mode was mostly cohesive and delamination of SMC. Cohesive failure occurred near the aluminum/adhesive interface. A small portion of the failure mode was adhesive at the SMC/adhesive interface. Generally, the failure mode for wedge samples was a mixture of SMC delamination and adhesive failure at the SMC/adhesive interface. For loaded wedge samples investigated at 60°C and 85% RH for 21 days, the failure mode included also 27% cohesive failure at the SMC/adhesive interface, indicating a weakening of the

adhesive at longer exposure times. The failure mode for butt torsion samples was mixed. Cohesive failure dominated and took place mostly near the aluminium/adhesive interface.

4.3.7.5.2. Surface characterization

Surface analysis measurements were carried out for samples which failed adhesively at the adhesive/SMC interface and for samples which failed near the aluminum/adhesive interface for which the failure mode was difficult to determine visually. Representative XPS results are given in Table 45. C 1s spectra are given in Figure 84 for loaded lap shear specimens tested at 60°C in dry air which failed cohesively in the Instron test near the aluminium/adhesive interface and for loaded wedge samples exposed at 60°C in dry air which failed in the Instron test at the adhesive/SMC interface.

For the lap shear samples that failed cohesively near the aluminum/adhesive interface the atomic concentrations (Table 45) and the C 1s spectra (Figures 84D and 84E) are similar to those of the split adhesive (see Table 21 and Figure 58E) for both adhesive and aluminum failed sides. These results indicate that both surfaces are identical demonstrating that the failure mode is entirely cohesive.

The SEM results for these surfaces shown in Figure 85 confirm the XPS findings. Both failed sides have identical rough surfaces attributed to fractured adhesive. Similar results were obtained for samples which failed near the aluminum/adhesive interface but tested under different conditions (85% RH).

For loaded wedge samples investigated at 60°C in dry air that failed adhesively at the SMC/adhesive interface, the SEM results shown in Figure 86 indicate that adhesive failure is a mixture of interfacial adhesive failure and near-surface debonding of SMC. Some of the SMC upper layer is noted on the adhesive side. The findings are confirmed by the XPS results presented in Table 45 and in Figure 84 (C 1s spectra). The nitrogen

Table 45.

XPS Results (Atomic %). Phase α-SMC/Urethane/Alkaline Cleaned Epoxy Primed Aluminum Samples.
50% Load, 60°C (140°F), Dry Air, 7 Days.
Failure in the Instron Test.

		Lap Shear*		Wedge**	
Element	Epoxy Primer	Adhesive Side	Aluminum Side	Adhesive Side	SMC Side
C	65.7	51.3	48.4	80.1	82.8
O	28.0	37.2	38.4	16.0	14.9
N	2.51	2.96	2.71	3.70	1.06
Si	2.22	5.01	6.05	0.20	0.44
Al	1.56	1.42	1.55	<0.1	0.47
Others (Mg, Zn, Cl)	<0.1	2.11	2.84	<0.1	0.42

* Cohesive failure near the aluminum/adhesive interface
** Failure at the SMC/adhesive interface

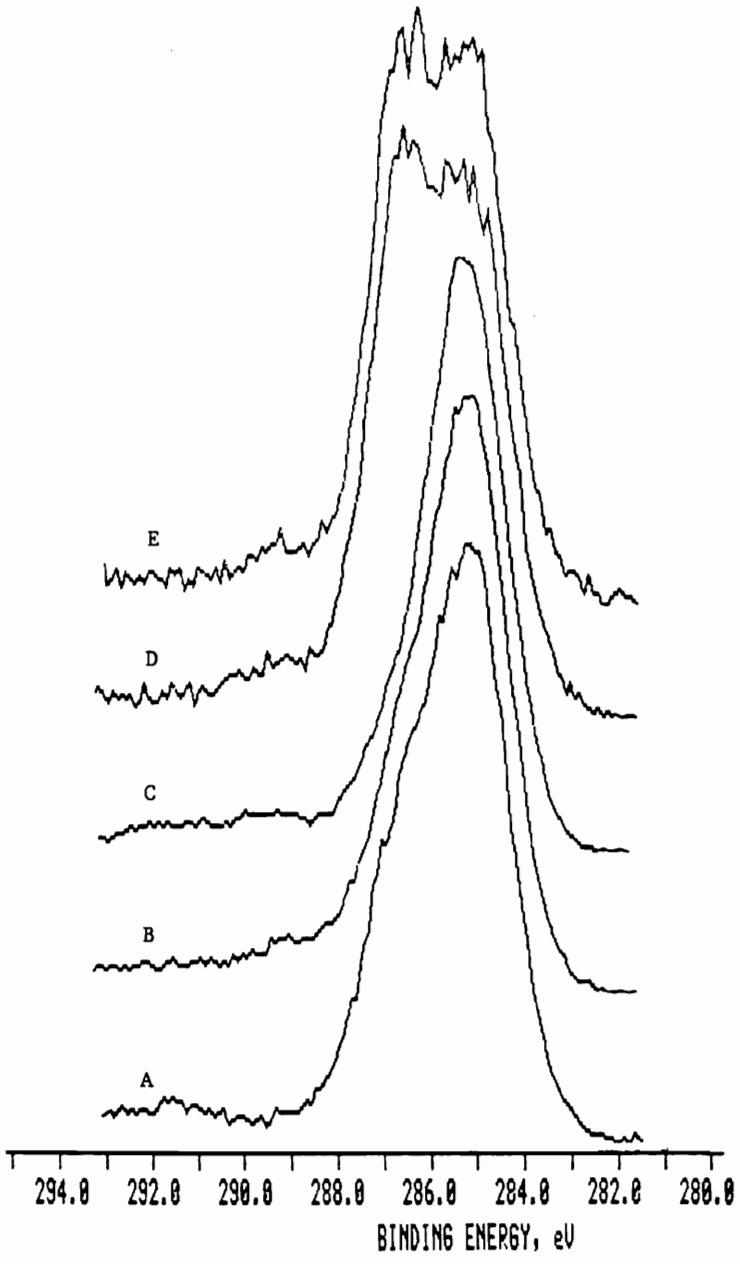

Figure 84. C 1s spectra. Phase α-SMC/urethane/alkaline cleaned epoxy primed aluminum specimens. 50% load, 60°C (140°F), dry air, 7 days.

A: Alkaline cleaned epoxy primed aluminum
B, C: Wedge specimens. Instron failure at the adhesive/SMC interface. B: Adhesive side, C: SMC side
D, E: Lap shear specimens. Instron failure: Cohesively, near the adhesive/aluminum interface. D: Adhesive side, E: SMC side.

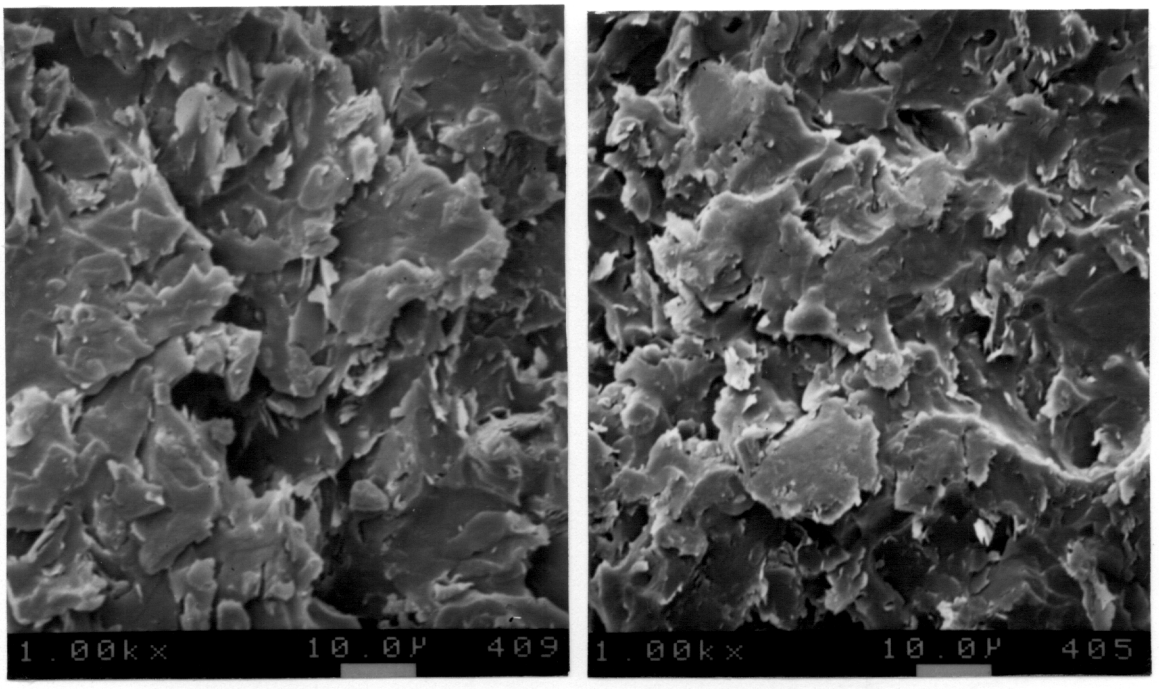

Adhesive side

Aluminum side

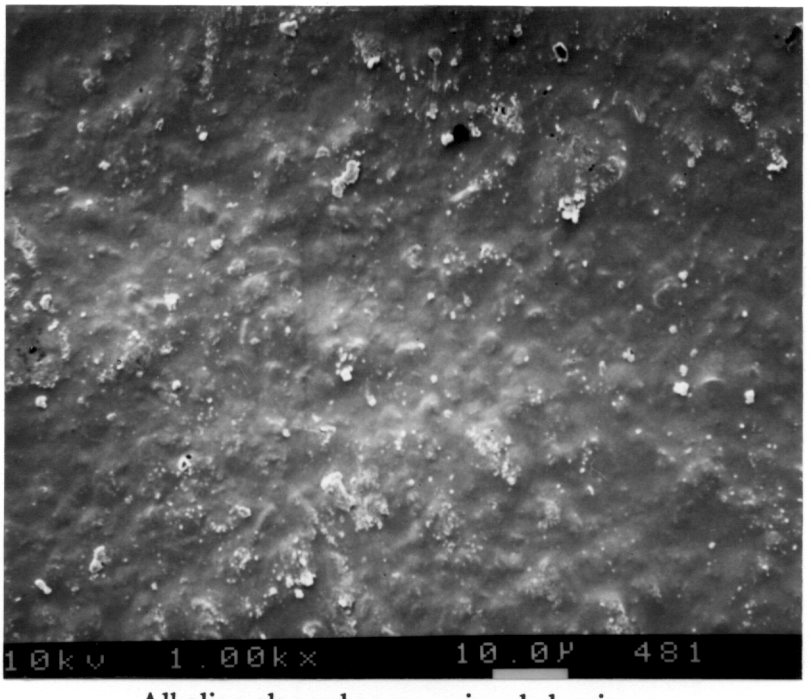

Alkaline cleaned epoxy primed aluminum

Figure 85. SEM results. Phase α-SMC/urethane/alkaline cleaned epoxy primed aluminum lap shear specimens. 50% load, 60°C (140°F), dry air, 7 days. Instron failure: Cohesively near the adhesive/aluminum interface.

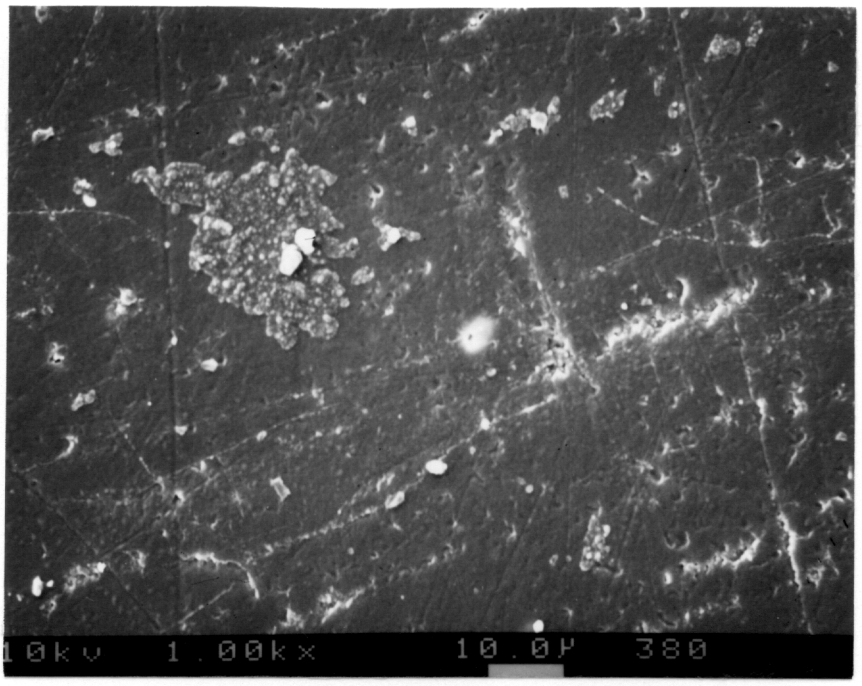

Adhesive side

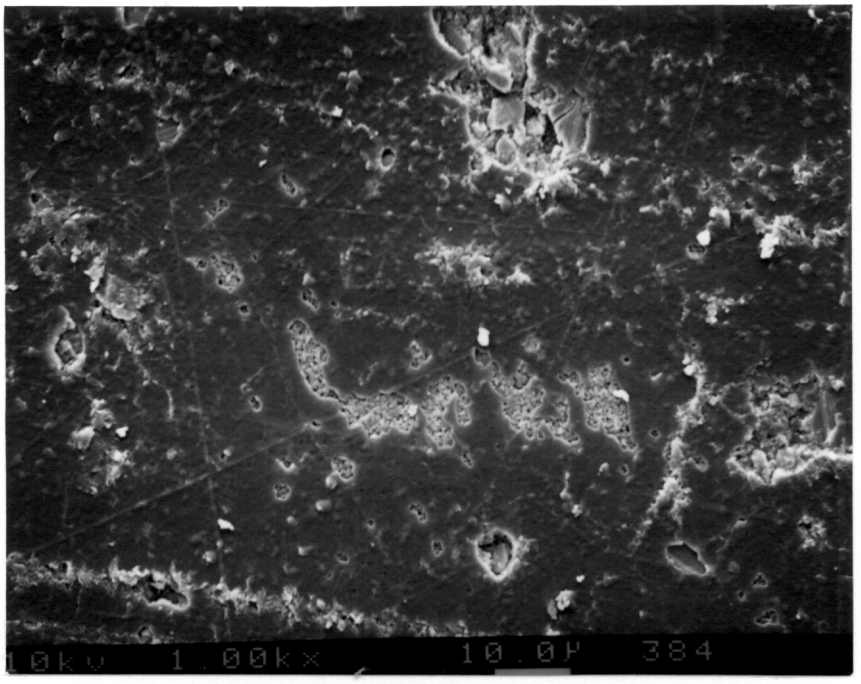

SMC side

Figure 86. SEM results. Phase α-SMC/urethane/alkaline cleaned epoxy primed wedge specimens. 50% load, 60°C (140°F), dry air, 7 days. Instron failure at the adhesive/SMC interface.

concentration on the SMC side surface is 1.06% while that on primed SMC is 5.41% (Table 21). The C 1s spectrum for the SMC side (Figure 84C) is similar to that for as received SMC shown in Figure 58A. The nitrogen concentration on the failed adhesive side (3.70%) is close to that of the adhesive film, 2.90% (Table 21), but the C 1s spectrum (Figure 84B) for the adhesive side does not resemble that of the adhesive (Figure 58D). The spectrum is close to that of the synthesized spectrum corresponding to a mixture of as received SMC surface (50%) and primed SMC surface (50%) shown in Figure 59B. The XPS and SEM results taken together reveal that primer and some SMC components appear on the adhesive side. Little primer remains on the SMC surface. Thus failure occurs at the primer - SMC interface. Similar surface analysis results were obtained for samples tested at 60°C in 85% RH, where failure occurred at the SMC/adhesive interface.

As for the samples prepared with alkaline cleaned-phenolic primed aluminum, the aluminum/primer bond was durable; no failure occurred at the aluminum/primer interface. The cured epoxy resin contains hydroxyl groups which offer ample opportunities for hydrogen bonding to the aluminum oxide surface. It was shown that hydrogen bonds involving hydroxyl groups are less susceptable to water attack than those involving other polar groups, which are less favored in competition with water molecules [75]. The FTIR study of DGEBA films on alkaline cleaned aluminum discussed in 4.2.1 showed that the aluminum surface species interact chemically with DGEBA upon heating. Also, chemical interactions of epoxy resins with various metallic substrates have been previously reported in the literature (see 2.2.3.4). The formation of chemical bonds between primer and substrate is of importance for bond durability. For example, Gettings et al. [205], working with silane primers and epoxy/steel adhesive bonds, found that the environmental resistance of the adhesive bonds increases only when primer/steel chemical interfacial bonds are formed. Based on the findings in this work it may be concluded that the durable

aluminum/epoxy-based primer bond is due to chemical interactions and hydrogen bonds established between aluminum surface species and epoxy resin at curing.

Except for the durability results obtained for butt torsion samples tested at 60°C in dry air, the failure results for samples prepared with epoxy primed aluminum and phenolic primed aluminum were similar. However, the samples prepared with alkaline cleaned-epoxy primed aluminum showed a somewhat lower durability compared to the findings for alkaline cleaned-phenolic primed aluminum. Eighty percent of the loaded butt torsion samples prepared with alkaline cleaned-epoxy primed aluminum, tested at 60°C in dry air, failed during the test. All butt torsion samples prepared with alkaline cleaned-phenolic primed aluminum tested under the same conditions survived the test.

4.3.7.6. Phase α-SMC/urethane/alkaline cleaned epoxy primed aluminum; 1.25 mm bondline thickness.

4.3.7.6.1. Failure results

To determine the influence of bond thickness on durability in the phase α-SMC/urethane/aluminum system, samples with a 1.25 mm thick bond were prepared and tested under the same conditions as those used for samples prepared with a 3.5 mm thick bond. Examination of the failure results presented in Tables 46 and 47 shows:

a) For as prepared samples the failure force (moment) for these samples was higher for the lap shear samples 382 ± 32 lbs (1.25 mm) vs 244 ± 15 lbs (3.5 mm) and similar for wedge samples 37 ± 3.7 lbs (1.25 mm) vs 38 ± 3.0 lbs (3.5 mm), and butt torsion specimens 34 ± 2.5 lb x ft (1.25 mm) vs 33 ± 2.3 lb x ft (3.5 mm) compared with the results obtained for samples with a 3.5 mm thick bond (See Tables 43 and 44).

b) For unloaded samples testing at 60°C in dry air did not lower the residual strengths. The bond strengths were similar to the reference strengths: lap shear 400 ± 33

Table 46.

Failure Results. Phase α-SMC/Urethane/Alkaline Cleaned Epoxy Primed Aluminum Samples.
1.25 mm Bond Thickness.
60°C (140°F), 7 Days. (Samples Which Survived the Test)

Humidity	Load	Type of Sample	Number of Samples Tested	Number of Samples Which Survived the Test	Average Failure Force, lbs* (Average Failure Moment, lb x ft **)	Average Failure Mode %D	%A	%C
As Prepared Samples Room Temperature	No Load	Lap Shear	4	4	382 ± 32	-	34	64
		Wedge	5	5	37 ± 3.7	34	66	-
		Butt Torsion	5	5	34 ± 2.5	29	61	10
Dry Air	No Load	Lap Shear	5	5	400 ± 33	6	71	23
		Wedge	5	5	32 ± 4.4	39	60	1
		Butt torsion	5	5	40 ± 6.2	60	14	26
	35% Load	Lap Shear	5	5	424 ± 36	8	92	-
	50% Load	Wedge	5	4	30 ± 7.4	41	39	20
	20% Load	Butt Torsion	5	-	--	-	-	-
85% RH	No Load	Lap Shear	5	5	279 ± 40	-	62	38
		Wedge	5	5	27 ± 4.2	7	58	35
		Butt torsion	5	5	24 ± 5.0	33	33	34
	50% Load	Lap Shear	4	-	--	-	-	-
	35% Load	Lap Shear	5	4	259 ± 6.0	4	96	-
	50% Load	Wedge+	5	4	26 ± 7.5	21	70	9
	20% Load	Butt Torsion	5	-	--	-	-	-

All wedge samples were loaded in constant load mode
* For lap shear and wedge samples; ** For butt torsion samples
+ Samples exposed for 21 days

Table 47

Failure Results. Phase α-SMC/Urethane/Alkaline Cleaned Epoxy Primed Aluminum Samples.
1.25 mm Bond Thickness.
60°C (140°F), 7 Days. (Samples Which Failed During the Test)

Humidity	Load	Type of Sample	Number of Samples Tested	Which Failed During the Test	Time to Failure h - hours d - days	Average Failure Mode %D	%A	%C
As Prepared Samples Room Temperature	No Load	Lap Shear	4	-	--	-	-	-
		Wedge	5	-	--	-	-	-
		Butt Torsion	5	-	--	-	-	-
Dry Air	No Load	Lap Shear	5	-	--	-	-	-
		Wedge	5	-	--	-	-	-
		Butt Torsion	5	-	--	-	-	-
	35% Load	Lap Shear	5	-	--	-	-	-
	50% Load	Wedge+	5	1	17h	-	100	-
	20% Load	Butt Torsion	5	5	6h (2), 29h (3)	12	59	29
85% RH	No Load	Lap Shear	5	-	--	-	-	-
		Wedge	5	-	--	-	-	-
		Butt Torsion	5	-	--	-	-	-
	50% Load	Lap Shear	4	4	1h (2), 3h, 7h	16	53	31
	35% Load	Lap Shear	5	1	5d	-	40	60
	50% Load	Wedge+	5	1	5h	4	96	-
	20% Load	Butt Torsion	5	5	6h (3), 19h, 42h	30	53	17

All wedge samples were loaded in constant load mode

+ Samples exposed for 21 days

lbs (T) vs 382 ± 32 lbs (R), wedge 32 ± 4.4 lbs (T) vs 37 ± 3.7 lbs (R), and butt torsion 40 ± 6.2 lb x ft (T) vs 34 ± 2.5 lb x ft (R).

c) Of the loaded samples investigated at 60°C in dry air, all lap shear samples survived the test, and 20% of the wedge and all butt torsion samples failed during the test. For the samples which survived the test, the residual strength was equivalent to the reference sample failure stress: lap shear 424 ± 36 lbs (T) vs 382 ± 32 lbs (R) and wedge 30 ± 7.4 lbs (T) vs 37 ± 3.7 lbs (R).

d) All unloaded samples maintained at 60°C and 85% RH survived the test, but the residual strength for all types of samples was lower than for the reference strength: lap shear 279 ± 40 lbs (T) vs 382 ± 32 lbs (R), wedge 27 ± 4.2 lbs (T) vs 37 ± 3.7 lbs (R), and butt torsion 24 ± 5.0 lb x ft (T) vs 34 ± 2.5 lb x ft (R).

e) Exposure at 60°C and 85% RH induced failure of some loaded samples during the test. All lap shear samples loaded at 50% failed in a very short time (1 to 7 h); 20% of the lap shear samples loaded at 35%, 20% of the wedge samples, and all butt torsion samples failed during the test. The residual strength for the samples which survived the test was lower than the reference strength: lap shear 259 ± 6 lbs (T) vs 382 ± 32 lbs (R), and wedge 26 ± 7.5 lbs (T) vs 37 ± 3.7 lbs (R).

f) Generally the failure mode was mixed for all specimen geometries. All adhesive failures took place at the SMC/adhesive interface. Diisocyanate primer is detected visually on a large proportion of the adhesively failed SMC side surfaces, suggesting that failure took place in the primer or at the primer/adhesive interface. All cohesive failures took place on the aluminum/adhesive side of the specimen; a thin layer of adhesive remained on the aluminum side surface after failure. Of interest is the change in failure for lap shear samples upon exposure to stress. For the loaded samples which survived the test, the

failure mode was almost entirely (>90%) adhesive. For the other lap shear samples the failure mode was generally a mixture of adhesive and cohesive failure.

The comparison of the failure results for samples with 1.25 mm or 3.5 mm bond thickness (see Tables 43 and 44) shows that the thicker bonded samples displayed better durability properties. All 1.25 mm bond lap shear samples under 50% load maintained at 60°C and 85% RH failed in one to seven hours (see Tables 46 and 47), while only 50% of the 3.5 mm bond lap shear samples exposed to the same conditions failed during the test, and the time to failure was longer. Also all 1.25 mm bond-loaded butt torsion samples investigated at 60°C in dry air failed during the test in a relatively short time, 6 to 29 hours, while only 80% of the 3.5 mm bond butt torsion samples failed during the test. The time to failure for those samples not enduring the test was one to four days. The decrease in adhesive thickness also changed the failure mode distribution. A substantial increase in the proportion of adhesive failure mode for all three types of samples was found: the adhesive range of the proportion of adhesive failure for lap shear samples with 3.5 mm thick bond was 0-10%, while for samples with 1.25 mm thick bond, the proportion was in the range 34-96%.

A possible explanation for the better durability of samples prepared with thicker bonds is that the increase in thickness reduces the rigidity of the adhesive layer, allows more plastic deformation, and improves the stress distributions in the bond (more uniformly distributed stresses and lower stress concentrations). The increase in the adhesive portion of the failure mode may be due also to an increase in stress concentration at the SMC/adhesive interface with the decrease in the bondline thickness.

4.3.7.6.2. Surface characterization

Surface analysis measurements were carried out for adhesively failed sample

surfaces where diisocyanate primer remained on the SMC surface and where the diisocyanate primer was transferred to the adhesive side. Representative XPS results are given in Table 48 for loaded wedge samples investigated at 60°C and 85% RH, which failed in the Instron test; for as prepared butt torsion samples tested in the Instron; and for loaded butt torsion samples exposed to 60°C in 85% RH, which failed during the test. Figure 87 shows the C 1s spectra for loaded wedge samples tested at 60°C and 85% RH which failed in the Instron test. For the samples where primer remained on the SMC, the atomic concentrations for the adhesive side surfaces are close to those for the adhesive film given in Table 21. Carbon 1s spectra for these surfaces are similar to those for the adhesive (Figure 58D); a representative spectrum is shown in Figure 87D. These results indicate that the failed adhesive side surfaces are composed almost entirely of adhesive material. The atomic concentrations for the SMC side surface are equal to those for primed SMC (Table 21). The C 1s spectrum for this surface (Figure 87C) is similar to that for primed SMC as shown in Figure 58C. The spectra exhibit a relatively strong spectral feature associated with -COR/-NCO functionality (BE = 286.8), a characteristic of a primed SMC surface. The XPS results suggest that the failed SMC surfaces are covered with primer.

The SEM photomicrographs for these samples, presented in Figure 88, show that both failed surfaces (adhesive and SMC) are relatively smooth indicating that the failure took place adhesively at the primer/adhesive interface without fracture either of SMC or adhesive. The SEM results confirm the XPS findings presented before, showing a complete separation of primer from the adhesive at failure. Similar results were obtained for samples tested under other conditions (dry air) when the diisocyanate primer remained on the SMC surface at failure.

Surface analysis measurements were carried out also for adhesively failed surfaces

Table 48
XPS Results (Atomic %)
Phase α-SMC/Urethane/Alkaline Cleaned Epoxy Primed Aluminum Samples.
1.25 mm Bond Thickness. 60°C (140°F).

	Wedge 50% Load. 85% RH++				Butt Torsion 20% Load. 85% RH+		As Prepared Samples++	
Element	Adhesive* Side	SMC* Side	Adhesive** Side	SMC** Side	Adhesive* Side	SMC* Side	Adhesive** Side	SMC** Side
C	71.4	75.3	77.0	87.8	71.2	73.5	77.5	81.3
O	22.7	19.0	17.5	11.1	23.0	19.8	19.1	15.9
N	3.44	4.31	3.68	0.77	3.52	5.37	2.25	1.14
Si	1.38	0.72	0.85	<0.1	1.22	0.80	0.32	<0.1
Al	0.50	<0.1	0.18	0.22	0.51	0.21	<0.1	0.30
Others (Zn, Ca)	0.58	0.67	0.79	0.11	0.55	0.32	0.83	1.36

* The primer remained on SMC
** The primer was transfered to the adhesive
+ Failure during the test
++ Failure in the Instron test

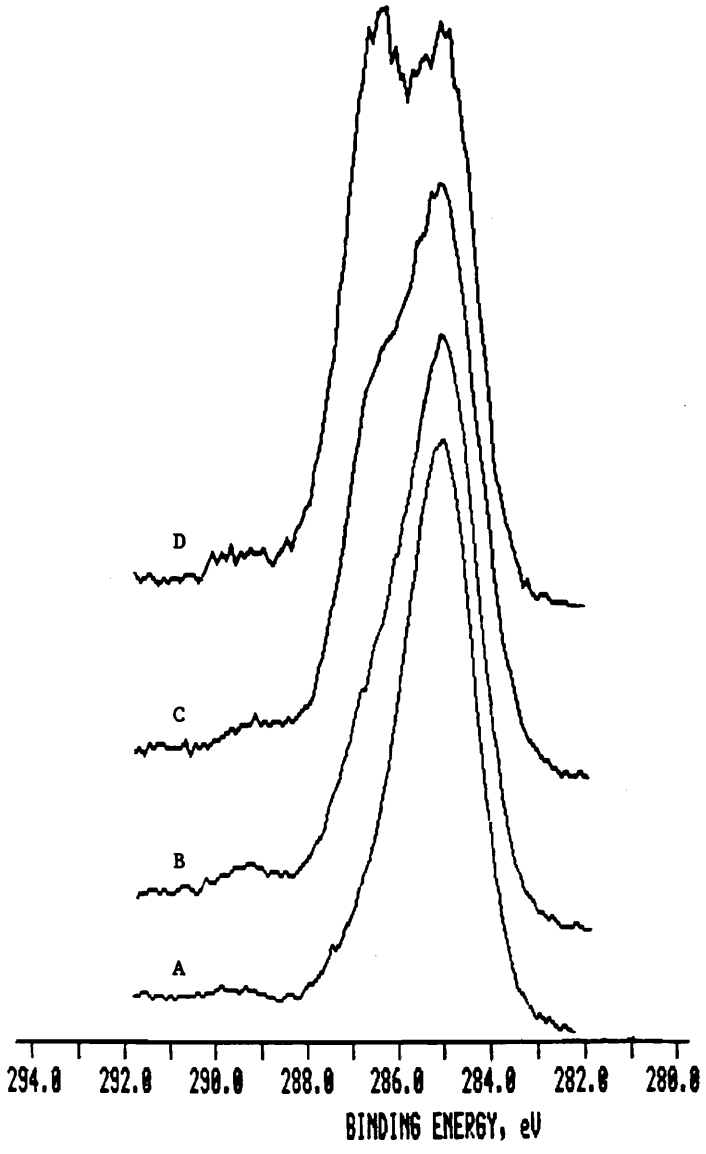

Figure 87. C 1s spectra. Phase α-SMC/urethane/alkaline cleaned epoxy primed aluminum wedge specimens. 1.25 mm thick bond. 50% load, 60°C (140°F), 85% RH, 21 days.
A, B: Instron failure at the SMC/primer interface. A: SMC side, B: Adhesive side.
C, D: Instron failure at the adhesive/primer interface. C: SMC side, D: Adhesive side.

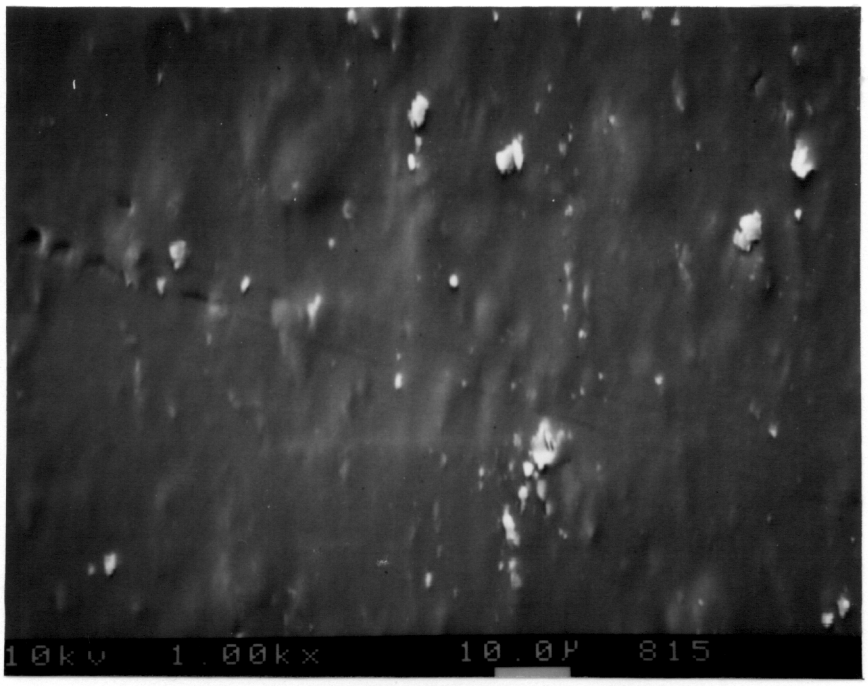

Adhesive side

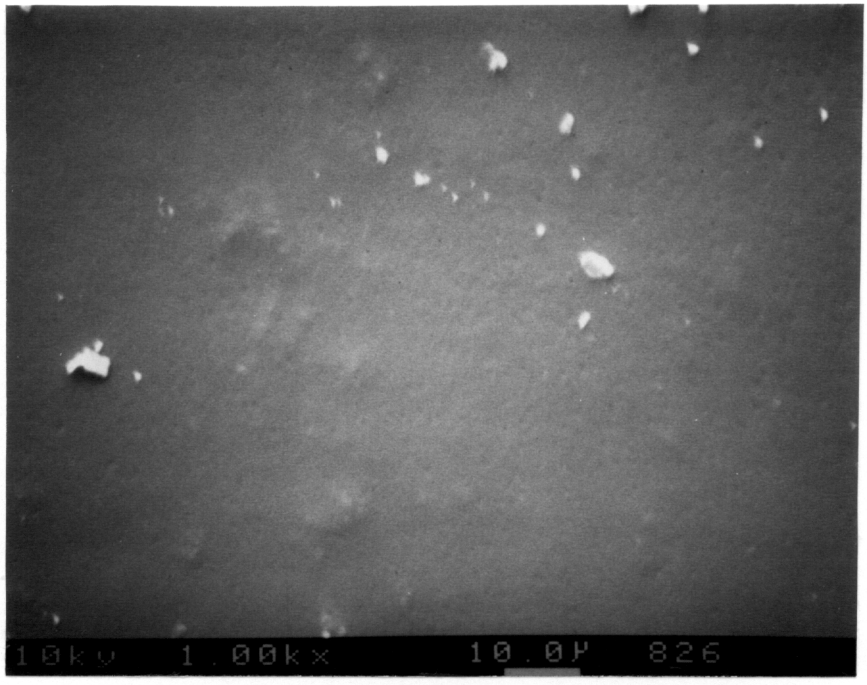

SMC side

Figure 88. SEM results. Phase α-SMC/urethane/alkaline cleaned epoxy primed aluminum wedge specimens. 1.25 mm thick bond. 50% load, 60°C (140°F), 85% RH, 21 days. Instron failure at the adhesive/primer interface.

where it was determined visually that primer was transferred from SMC to the adhesive at failure. For example, the SEM results for loaded wedge samples studied at 60°C and 85% RH which failed in the Instron test (Figure 89) show that the failure is in reality a mixture of near surface debonding of SMC and adhesive failure at the SMC/primer interface.These findings are confirmed by the XPS results. The nitrogen concentration for the failed SMC side surface (Table 48) is low (0.77%) compared with a value of 5.41% found on the primed SMC surface (Table 21). This comparison indicates a low proportion of primer on the SMC surface. The C 1s spectrum of the SMC side surface (Figure 87A) is similar to that of as received SMC (Figure 58A). The XPS results indicate that only SMC constituents are present on the SMC side surface. For the adhesive side surface the nitrogen concentration (Table 48) is ~3.7%. The C 1s spectrum (Figure 87B) appears most nearly equivalent to the synthesized C 1s spectrum corresponding to a mixture of primed SMC surface (75%) and as received SMC surface (25%) shown in Figure 59C. The results indicate that the adhesive failed surfaces are composed of a mixture of primer and SMC.

4.3.7.7. Phase α-SMC/urethane/alkaline cleaned epoxy primed aluminum, lap shear samples; 0.200" thick SMC adherend

These samples were prepared and tested to investigate the influence of SMC adherend thickness on the durability of phase α-SMC/urethane/aluminum lap shear specimens. The SMC adherend thickness was increased from 0.100" to 0.200", increasing also the stress concentration at the aluminum/adhesive interface.

The failure results presented in Table 49 reveal the following:

a) For these samples the reference failure strength was similar to that for samples prepared with 0.100" thick SMC adherends; 229 ± 12 lbs (0.200") vs 244 ± 15 lbs (0.100").

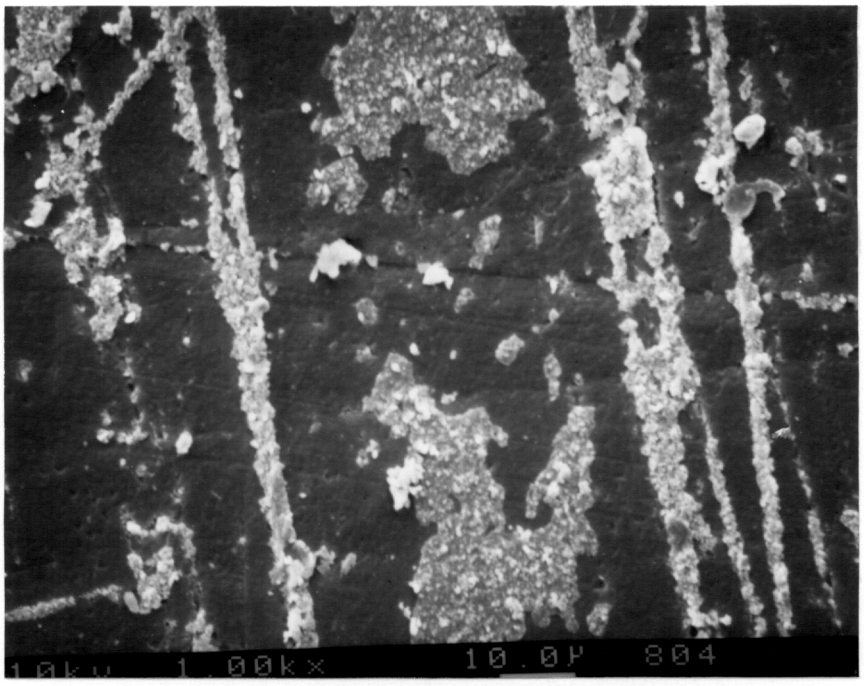

Adhesive side

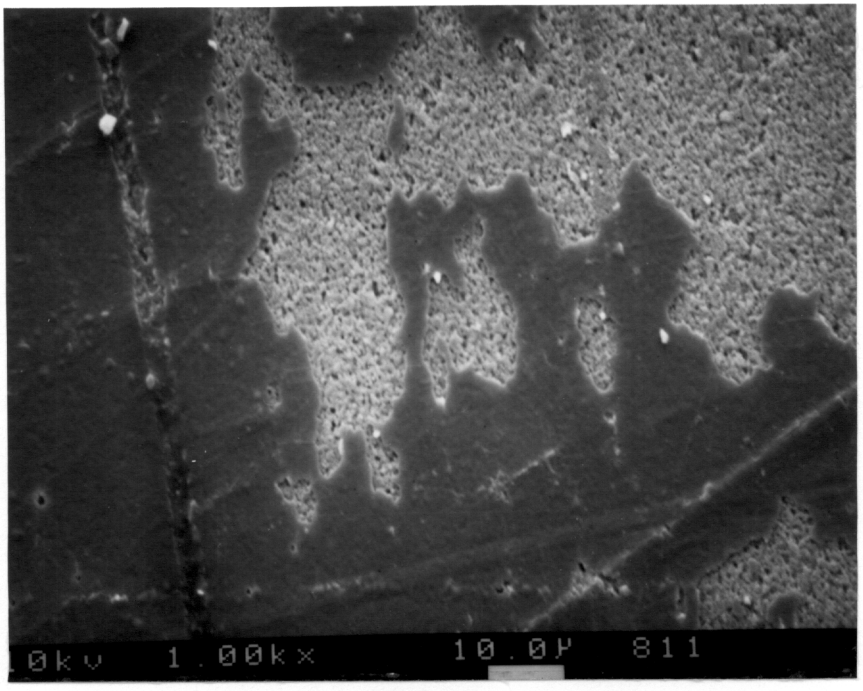

SMC side

Figure 89. SEM results. Phase α-SMC/urethane/alkaline cleaned epoxy primed aluminum wedge specimens. 1.25 mm thick bond. 50% load, 60°C (140°F), 85% RH, 21 days. Instron failure at the SMC/primer interface.

Table 49

Failure Results. Phase α-SMC/Urethane/Alkaline Cleaned Epoxy Primed Aluminum Samples
0.200" Thick SMC Adherend.
60°C (140°F), 7 Days.

		Samples Which Survived the Test						Samples Failed During the Test				
Humidity	Load	Number of Samples Tested	Number of Samples	Average Failure Force, lbs* (Average Failure Moment lbxft)**	Average Failure Mode %D	%A	%C	Number of Samples	Time to Failure h-hours d-days (no samples)	Average Failure Mode %D	%A	%C
As Prepared Samples Room Temperature	No Load	5	5	229 ± 12	-	-	100	-	--	-	-	-
Dry Air	No Load	5	5	317 ± 20	-	-	100	-	--	-	-	-
	50% Load	5	5	281 ± 7	-	-	100	-	--	-	-	-
85% RH	No Load	5	5	213 ± 9	-	-	100	-	--	-	-	-
	50% Load	5	3	193 ± 18	-	-	100	2	4d, 7d	22	9	69

Note: All samples failed in Instron cohesively near the Al/adhesive interface. Two samples failed during exposure at SMC/adhesive interface.

b) The residual strength for unloaded samples maintained at 60°C in dry air was higher than the reference sample strength 317 ± 20 lbs (T) vs 229 ± 12 lbs (R).

c) All loaded samples tested at 60°C in dry air survived the test. The residual strength was higher than that for the reference samples 281 ± 7 lbs (T) vs 229 ± 12 lbs (R).

d) All unloaded samples maintained at 60°C in 85% RH survived the test. The residual strength was approximately equal to the strength for the reference specimens: 213 ± 9 lbs (T) vs 229 ± 12 lbs (R).

e) Forty percent of the loaded samples studied at 60°C in 85% RH failed during the test. The residual strength of the samples which survived the test was somewhat lower than the reference strength 193 ± 18 lbs (T) vs 229 ± 12 lbs (R).

f) The failure results for these samples are similar to those for samples prepared with 0.100" thick SMC adherends (see Tables 43 and 44). However, the failure mode is dissimilar. For samples prepared with 0.100" thick SMC adherends the failure mode was mixed: delamination of SMC and cohesive. The failure mode was 100% cohesive at the aluminum/adhesive interface for samples prepared with 0.200" thick SMC adherends, with the exception of the two loaded samples that failed during investigation at 60°C and 85% RH. The two loaded samples failed by a mixed mode: delamination of SMC and cohesive, at the SMC/adhesive interface. This difference in the mode of failure may be explained by the change in stress distribution upon increasing the stiffness of the SMC adherend. The increased stiffness produces an increase in the load carried by aluminum.

4.3.7.8. Alkaline cleaned epoxy primed aluminum/urethane/alkaline cleaned epoxy primed aluminum lap shear samples

Examination of failure results presented in Table 50 shows that:

a) Forty percent of the samples exposed to 60°C failed during the test . The residual strengh of the samples which survived the test was similar to the reference

Table 50
Failure Results. Alkaline Cleaned Epoxy Primed Aluminum/Urethane/Alkaline Cleaned Epoxy Primed Aluminum Lap Shear Samples.
50% Load, 60°C (140°F), 7 Days.

		Samples Which Survived the Test						Samples Failed During the Test				
Humidity	Load	Number of Samples Tested	Number of Samples	Average Failure Force, lbs* (Average Failure Moment lbxft)**	Average Failure Mode %D	%A	%C	Number of Samples	Time to Failure h-hours d-days (no samples)	Average Failure Mode %D	%A	%C
As Prepared Samples Room Temperature	No Load	5	5	333 ± 24	-	-	100	-	--	-	-	-
Dry Air	50% Load	5	3	340 ± 34	-	-	100	2	13h (2)	-	-	100
85% RH	50%Load	5	5	338 ± 12	-	-	100	2	3h, 43h	-	-	100

strength: 340 ± 34 lbs (T) vs 333 ± 24 lbs (R)

b) Forty percent of the samples tested at 60°C and 85% RH failed during the test. The residual strength of the samples which survived the exposure was close to the failure force for reference samples: 340 ± 34 lbs (T) vs 333 ± 24 lbs(R)

c) The failure mode for all samples was 100% cohesive for all samples These results clearly show that the adhesive is the weakest link in this bond.

5. SUMMARY AND CONCLUSIONS

For phase α-SMC/urethane/ELPO steel samples the most significant finding is that failure does not occur at the ELPO steel/adhesive interface or at the steel/ELPO primer interface but occurs only at the SMC/adhesive interface or cohesively. All adhesive failures occur at the SMC/adhesive interface. What appeared visually to be adhesive failure is in reality a mixture of interfacial adhesive failure and near surface SMC debonding. The near surface SMC material and the thin layer of primer on the SMC surface appear to be the weak links in the bonded systems, so when the visually determined adhesive failure occurs, most of the primer and more or less all of the upper layer of the SMC material are transferred to the adhesive side. This is explained by the presence of a high concentration of low-profile additive in the near surface of SMC, a fact that is expected to reduce its resistance to temperature and humidity when compared with the bulk SMC which is composed mainly of crosslinked polyester. This finding is more significant when the results obtained for other systems are considered. For ELPO steel/urethane/ELPO steel samples no failure occurred during exposure to severe conditions of temperature and humidity; no decrease in residual strength was found after exposure, and the failure was 100% cohesive. The failure mode was also 100% cohesive for all polyurea/ELPO steel samples. This shows that in the absence of the upper layer of SMC material, the adhesive becomes the weak link in the system, and that the steel /ELPO primer bond is strong and durable.

The results obtained suggest that in order to improve the durability of the phase α-SMC/urethane/ELPO steel adhesive bonds increasing the strength of the upper layer of the SMC material is crucial.

The exposure to low temperatures and to a salt solution does not have any significant effect on the time of failure for phase α-SMC/urethane/ELPO steel samples.

The metal surface pretreatment is very important for the durability of aluminum/composite adhesive bonds. The quality of the aluminum surface pretreatment and implicitly the bond durability depends both on the quality of metal cleaning and on the proper selection of the primer. The two types of cleaning used, solvent cleaning and alkaline cleaning created metal surfaces with different properties as shown by the XPS and SEM results. After solvent cleaning, a layer of contaminants still remains on the metal surface indicated by the presence of nitrogen and silicon on this surface. Alkaline cleaning removes all dirt, impurities, and the old oxide layer, creating a new, clean oxide layer on the aluminum surface, as evidenced by the high aluminum content on this surface. The use of solvent cleaned aluminum adherends primed with epoxy or phenolic primer gave poor durability results, the failure mode being mostly adhesive at the aluminum surface. This indicates a weak aluminum/primer bond which is also explained by the presence of contaminants on the aluminum surface after solvent cleaning. The impurities hinder the establishment of strong primer/aluminum bonds. The samples prepared with alkaline cleaned unprimed aluminum also displayed poor durability. The use of alkaline cleaned diisocyanate primed aluminum adherends improved durability only in dry air conditions but not in 85% RH. A considerable improvement in durability under all conditions was obtained by priming alkaline cleaned aluminum adherends with epoxy or phenolic primers.

For samples prepared with alkaline cleaned unprimed aluminum or with alkaline cleaned diisocyanate primed aluminum exposed to environmental conditioning, the failure mode was mostly adhesive at the aluminum surface indicating a weak bond between aluminum and primer or aluminum and adhesive for these samples. For the specimens prepared with alkaline cleaned epoxy or phenolic primed aluminum, no adhesive failure at the aluminum surface was observed. This shows a strong and stable bond between the alkaline cleaned aluminum and the epoxy or phenolic primers.

The reflection-absorption infrared studies indicated chemical interactions between identical or similar compounds existing in the primers used (DGEBA, phenol , and MDI) and alkaline cleaned aluminum surface species.

The strong and durable phenolic primer/aluminum and epoxy primer/aluminum bonds are attributed to the existence of chemical and hydrogen bonds between components of phenolic and epoxy resins and aluminum surface species. Much weaker diisocyanate primer/aluminum bonds can be explained by the high susceptibility of the -NCO functionality to water. The presence of water can rapidly weaken bonds formed at the primer/aluminum interface.

An increase in bond thickness from 1.25 mm to 3.5 mm proved to be beneficial for adhesive bond durability for phase α-SMC/urethane/alkaline cleaned epoxy primed aluminum samples. Greater durability may be due to a more uniform distribution of stress in the thicker bonds. The increase in stiffness of the SMC adherend in phase α-SMC/urethane/alkaline cleaned epoxy primed aluminum lap shear samples did not change significantly the failure results, but the mode of failure was altered. Even if the stress concentration at the aluminum side increased, the failure took place cohesively, the aluminum/primer bond proved to be durable.

Exposure for seven days to a moderate temparature (60°C) alone did not not reduce the residual strength of the adhesive bonds. For lap shear samples, exposure to 60°C usually tended to increase the residual strength.

The application of load induced failure of some samples exposed at temperatures of 50-80°C, indicating that the stress loading is a significant factor in bond durability.

Butt torsion samples proved to be more sensitive to stress and temperature than the lap shear or wedge samples. They failed faster and in higher proportion than the other two types of samples when exposed to the same conditions of temperature and humidity under a

lower level of stress. This shows the important role of the manner of sample loading on adhesive bond durability. The combination of high levels of loading and high temperatures has a severe effect on durability even for short times of exposure.

Humidity had a detrimental effect on the metal/SMC adhesive bonds producing an increase in the proportion of loaded samples which failed during exposure and a decrease in the time to failure. The residual strength for the lap shear samples exposed to 85% RH tends to be lower than that for samples exposed to dry air conditions.

The type of adhesive also plays a role in bond durability. For the system Budd SMC/ELPO steel, an epoxy adhesive gave better durability than a polyurethane adhesive. This finding can be explained by the higher cohesive strength, lower moisture absorption rate, and higher resistance to hydrolysis for the epoxy adhesive.

Although the adhesive bond durability problem is complex due to the great number of parameters involved, using the short-time methods developed in this research, it was possible to determine the influence of the most important of the parameters intervening in the durability of metal/SMC adhesive bonds. The results from this work may be helpful in the proper selection of adherend surface pretreatments and in the design of bond configurations. It should be mentioned also that the durability results for the system SMC/urethane/alkaline cleaned epoxy or phenolic primed aluminum were similar to those for the system SMC/urethane/ELPO steel which is already used in the automobile industry. Also, the simplicity of the aluminum pretreatments used in this research, compared with those used in the aerospace industry, makes them suitable for high volume production. All these indicate, from an adhesion point of view, the feasibility of replacing steel with aluminum in the manufacturing of load carrying-metal structures. The results obtained in these accelerated laboratory tests, in combination with service data, should prove useful in making predictions about the durability of the system studied.

6. REFERENCES

1. D. McCosh, Popular Science, 234, 115 (1989).

2. A. J Kinloch, "Introduction" in Durability of Structural Adhesives, A. J.Kinloch, ed., Chapter 1, Applied Science Publishers, New York , 1983.

3. A. Liechti, W. S. Johnson, and D. A. Dillard "Experimentally Strength of Adhesively Bonded Joints" in Joining Fiber-Reinforced Composites, F. L. Mattews, ed., Chapter 4, Elsevier Applied Publishers, London 1987.

4. S. R. Hartshorn, "The Durability of Structural Adhesive Joints" in Structural Adhesives, S. R. Hartshorn, ed.,Chapter 8, Plenum Press, New York, 1986.

5. Ching-Chih Lee, Polym. Eng. Sci., 29, 1051 (1989).

6. R. Burns, Polyester Molding Compounds, Marcel Dekker, Inc., New York, 1982, pp 8.

7. S. Newman and D. G. Fesko, Polymer Composites, 5, 88 (1987).

8. J. Y Yadhav and S. W. Kantor, Encyclopedia of Polymer Science, vol.12, H. F. Mark and J. I. Kroschwitz , eds., John Wiley & Sons, New York, 1988, pp 274.

9 R. Burns, Polyester Molding Compounds, Marcel Dekker, Inc., New York, 1982, pp. 62.

10. R. Burns, Polyester Molding Compounds, Marcel Dekker, Inc., New York, 1982, pp. 181.

11. C. B. Bucknall, P. Davies, and I. K. Partrige, Polymer, 26, 109 (1985).

12. G. D. Cheever, J. Coat. Technol., 50, 36 (1978).

13 G. D. Cheever, J. Coat. Technol., 58, 37 (1986).

14 R. Burns, Polyester Molding Compounds, Marcel Dekker, Inc., New York, 1982, pp. 307.

15. F. L. Mattews, "Introduction" in Joining Fiber-Reinforced Composites, F. L. Mattews ed., Chapter 1, Elsevier Applied Publishers, London 1987.

16. S. Wu, Polymer Interface and Adhesion, Marcel Dekker, Inc., New York, 1982, pp 359.

17. S. Wu, Polymer Interface and Adhesion, Marcel Dekker, Inc., New York, 1982, pp 434.

18. J. D. Venables, J. Mater. Sci. 19, 2431 (1984).

19. S. S. Voyutskii, Autohesion and Adhesion of High Polymers, V. Vakula, ed., Interscience, New York, 1963, pp 140.

20. N. S. Korenevskaya, V. V. Lavrentyev, S. M. Yagnyatinskaya, V. G. Raevskii, and S. S. Voyutskii, Polym. Sci. U. S. S. R., 8, 1372 (1966).

21. N. H. Sung, Polym. Eng.Sci., 19, 810 (1979).

22. A. J. Kinloch, Adhesion and Adhesives:Science and Technology, Chapman and Hall, London, 1987, pp 72.

23. W. C. Wake, Adhesion and Formulation of Adhesives, Applied Science Publishers, London, 1989, pp 74 and 86.

24. A. J. Kinloch, Adhesion and Adhesives:Science and Technology, Chapman and Hall, London, 1987, pp 73.

25 B. V. Deryaguin and V. P. Smilga, Adhesion, Fundamentals and Practice. McLaren and Son, London, 1969, pp 152.

26. B. V. Deryaguin, Research, 8, 70 (1955).

27. H. Krupp, J. Adhes., 4, 83 (1972).

28. H. Krupp, J. Adhes., 5, 269 (1973).

29. A. J. Kinloch, Adhesion and Adhesives:Science and Technology, Chapman and Hall, New York, 1987, pp 78.

30. W. C. Wake, Adhesion and Formulation of Adhesives, Applied Science Publishers, London, 1989, pp 92.

31. A. D. Roberts, Adhesion 1, K. W. Allen, ed., Applied Science Publishers, London, 1977, pp 207.

32. A. J. Kinloch, Adhesion and Adhesives:Science and Technology, Chapman and Hall, New York, 1987, pp 76.

33. F. M. Fowkes, Encyclopedia of Polymer Science, Supplement Volume, H. F. Mark and J. I. Kroschwitz , eds., John Wiley & Sons, New York, 1989, pp 1.

34. F. M. Fowkes, D. O. Tischler, L. A. Lannigan, C. D. Ademu-John, and M.J. Halliwell J. Polym. Sci., Polym. Chem. Ed., 22, 547 (1984).

35. F. M. Fowkes, J. Adhes., 4, 155 (1972).

36. W. C. Wake, Recent Advances in Adhesion, L. H. Lee, ed., Gordon and Breach, New York, 1973, pp. 285.

37. I. E. Klein, J. Sharon, A. E. Yaniv, H. Dodiuk and D. Katz, Int. J. Adhes. Adhes., 3, 159 (1983).

38. M. Gettings and A. J. Kinloch, J. Mater. Sci., 12, 2511 (1977).

39. A. J. Kinloch, Adhesion and Adhesives:Science and Technology, Chapman and Hall, London, 1987, pp. 101.

40. S. Wu, Polymer Interface and Adhesion, Marcel Dekker, Inc., New York, 1982, pp. 279.

41. A. J. Kinloch, Adhesion and Adhesives:Science and Technology, Chapman and Hall, London, 1987, pp. 103-121.

42. A. J. Kinloch, Adhesion and Adhesives:Science and Technology, Chapman and Hall, London, 1987, pp. 123.

43. W. A. Lees, Int. J. Adhes. Adhes. 4, 171 (1986).

44. S. V. Hoa and D. Feldman, Polymer Composites, 3, 48 (1982).

45. J. G. Dillard and I. M. Spinu, J Adhes., 31, 147 (1990).

46. J. D. Minford, "Adhesive-Joining Aluminum to Engineering Plastics" in Physiochemical Aspects of Polymer Surfaces, K. L. Mittal ed., Plenum Press, New York, 1983, pp. 1139.

47. J. G. Dillard, T. F. Cromer, and C. E. Burtoff, J. Adhes., 26, 181 (1988).

48. J. Newbould and K. T. Schroeder, "Infrared Laser Surface Treatment of Sheet Molding Compound (SMC)", Research Publication GMR-5902, General Motors Research Laboratories, Warren, MI, 1987.

49. K. Y. Chihara and E. Melby, US Patent 4745018, 1988.

50. J. Newbould, "The Effect of Surface Preparation on the Adhesive Properties of Sheet Molding Compound (SMC)", Research Publication GMR-6449, General Motors Research Laboratories, Warren, MI, 1988.

51. B. R. Bonazza, "Adhesive Bonding of Polyethylene Sulfide Thermoplastic Composites, "Technical Sessions of the 45th Annual Conference, Composite Institute, Washington, DC, Feb. 1990, The Composite Institute of the Society of the Plastic Industry, Inc., 1990.

52. D. J. D. Moyer and J. P. Wightman, Surf. Interface Anal., 17, 457 (1991).

53. A. J. Kinloch, Adhesion and Adhesives:Science and Technology, Chapman and Hall, London, 1987, pp 139.

54. A. J. Kinloch, Adhesion and Adhesives:Science and Technology, Chapman and Hall, London, 1987, pp 140.

55. W. Brockmann, "Steel Adherends" in Durability of Structurall Adhesives, A. J. Kinloch, ed., Chapter 7, Applied Science Publishers, New York ,1983.

56. J. Kinloch, Adhesion and Adhesives:Science and Technology, Chapman and Hall, London, 1987, pp 145.

57. R.T. Foister, "Adhesive Bonding to Galvanized Steel II. Substrate Chemistry, Morphology, and Bond Failure Analysis", Research Publication GMR-5711, General Motors Research Laboratories, Warren, MI, 1987.

58. R.T. Foister, and K. J. Schroeder, "Adhesive Bonding to Galvanized SteeI. I. Lap Shear Strengths and Environmental Durability", Research Publication GMR-5702 General Motors Research Laboratories, Warren, MI, 1987.

59. P. E. Pierce, J. Coat. Technol., 53, 52 (1981).

60. R. T. Foister, R. K. Gray, and P. A. Madsen, J.Adhes. 24, 17 (1987).

61. D. Schmueser, N. L. Johnson, and R. T. Foister, J. Adhes., 24, 47 (1987).

62. K. W. Allen, C. Y. T. Chan, and K. B. Armstrong, Int. J. Adhes. Adhes., 2, 239 (1981).

63. J. A. Bishop, E. K. Sim, G. E. Thompson, and G. C. Wood, "Effects of Environment on Bonded Aluminum Joints: An Examination by Electron Microscopy" in Adhesion 13, K.W. Allen, ed., Chapter 13, Elsevier Applied Science, New York, 1988.

64. A. J. Kinloch, Adhesion and Adhesives:Science and Technology, Chapman and Hall, London, 1987, pp 150.

65. T. S. Sun, J. M. Chen, J. D. Venables, and R.L. Hopping, Appl. Surf. Sci., 1, 202 (1978).

66. G. D. Davis and J. D. Venables,"Surface and Interfacial Analysis"in Durability of Structural Adhesives, A. J. Kinloch, ed., Chapter 2, Applied Science Publishers, New York , 1983.

67. D. Moth, "Factors Affecting Pretreatment Design to Optimise Adhesive Bonding in Aluminum" in Adhesion 14, K.W. Allen, ed.,Chapter 2, Elsevier Applied Science, New York, 1989.

68. J. D. Venables, D. K. McNamara, J. M. Chen, T. S. Sun, and R. L. Hopping, Appl. Surf. Sci., 3, 88 (1979).

69. R.J. Davies and A. J. Kinloch "The Surface Characterization and Adhesive Bonding of Aluminum"in Adhesion 13, K.W. Allen, ed., Chapter 2, Elsevier Applied Science. New York, 1988.

70. D. M. Brewis, "Aluminum Adherends" in Durability of Structural Adhesives, A. J. Kinloch, ed., Chapter 2, Applied Science Publishers, New York, 1983.

71. J. A. Bishop, E. K. Sim, G. E. Thompson, and G. C. Wood, J. Adhes., 26, 237 (1988).

72. W. Brockmann, O. -D. Hennemann, H. Kollek, and C.Matz, Int. J. Adhes. Adhes., 6, 115 (1986).

73 H. Ishida, "The Role of Interface on Adhesion of Coatings and Compsites" in Proceedings of the14th Annual Meeting of the Adhesion Society, Clearwater, FL, 1991, pp. 106.

74. L. T. Drzal, The Role of the Polymer-Substrate Interface in Structural Adhesion, AFML-TR-77-129 (1977).

75. J. C. Bolger, "Acid Base Interactions Between Oxide Surfaces and Polar Organic Compounds" in Adhesive Aspects of Polymeric Coatings, K. L. Mittal, ed., Plenum Press, New York, 1983, pp. 3.

76. J. B. Peri, J. Phys. Chem., 69, 220 (1965).

77 K. Wefers and C. Misra, "Oxides and Hydroxides of Aluminum", Alcoa Technical Paper No. 19, Revised, Alcoa Laboratories, 1987.

78. H. Kollek, Int. J. Adhes. Adhes., 5, 75 (1985).

79. S Affrossmann, N. M. D. Brown, R. A. Pethrick, V. K. Sharma, and R. J. Turner, Appl. Surf Sci. 16, 469 (1983).

80. N. M. D. Brown, R. J. Turner, S. Affrossmann, I. R. Dunkin, R. A. Pethrick, and C.J. Shields, Spectrochem. Acta, 40B, 847 (1985).

81. J. Comyn, C. C. Horley, D. P. Oxley, R. G. Pritchard, and J. L. Tegg, J. Adhes. 12, 171 (1981).

82. J. Nigro and H. Ishida, J. Appl. Polym. Sci., 38, 2191 (1981).

83. S. Yoshida and H. Ishida, J. Adhes., 16, 217 (1984).

84. I. I. Shabalin, E. A. Kiva, Yu. V. Churkin, L. A. Rusanova, and M. F. Mazitov, Kinet. Kataliz., 15, 1540 (1974).

85. D. R. Taylor and K. H. Ludlum, J. Phys. Chem., 76, 2882 (1972).

86. B. F. Lewis, W. M. Bowser, J. L. Horn Jr.,T. Luu, and W. H. Weinberg, J. Vac. Sci. Technol., 11, 262 (1974).

87. I. W. N. Morris, N. M. D. Brown, and D. G. Walmsley, J. Chem. Phys., 66, 3952 (1977).

88 N. M. D. Brown, B. J. Meenan, S. Affrossmann, R. A. Pethrick, and B. Thomson, Surf. Interface Anal. 10, 184 (1987).

89. A. J. Kinloch, "Rubber-Toughened Thermosetting Polymers" in Structural Adhesives Developments in Resins and Primers, A. J. Kinloch, ed., Elsevier Applied Science Publishers, New York, 1986, pp.142.

90. W. C. Wake, Adhesion and Formulation of Adhesives, Applied Science Publishers, London, 1989, pp 215.

91. A. J. Kinloch, Adhesion and Adhesives:Science and Technology, Chapman and Hall, London, 1987, pp 188.

92. J. M. Miller, A Review of Standard Mechanical Test Methods for Adhesives, AL Report No 57-88-15, 1988.

93. D. B. Arnold, "Mechanical Test Methods for Aerospace Bonding" in Developments in Adhesives-2, A. J. Kinloch, ed., Applied Science Publishers, New York, 1983.

94. G. R. Anderson, S. J. Bennett, and K. L. DeVries, Analysis and Testing of Adhesive Bonds, Academic Press, New York, 1977, pp 12.

95 M. Goland and E. Reissner, J. Appl. Mech., A, 66, 17 (1944).

96. R. D. Adams, "Strength Predictions for Lap Shear Joints, Especially with Composite Adherends. A review" in Proceedings of the 35th Sagamore Army Materials Research Conference, Manchister, New Hamphshire, June 1988.

97 O. Volkersen, Luftfohrschung, 15, 41 (1938).

98 R. D. Adams, "Stress Analysis: A Finite-Element Analysis Approach" in Developments in Adhesives-2, A. J. Kinloch, ed., Applied Science Publishers, New York, 1983.

99. H. L. Groth, Int. J. Adhes. Adhes., 10, 207 (1991).

100. J. A.Marceau, Y. Moji, and J. C. McMillan, Adhesives Age, 10, 28 (1977).

101. A. J. Kinloch, Adhesion and Adhesives:Science and Technology, Chapman and Hall, London, 1987, pp 360.

102. J. Cognard, Int. J. Adhes. Adhes., 8, 93 (1988).

103. J. Cognard, Int. J. Adhes. Adhes., 6, 215 (1986).

104. J. Cognard, J. Adhes, 20, 1 (1986).

105. R. D. Adams, J. Coppendale, and N. A. Peppiat, J. Strain Anal., 13, 1 (1978).

106. A. J. Kinloch, Adhesion and Adhesives:Science and Technology, Chapman and Hall, London, 1987, pp 352.

107. A. J. Kinloch, Adhesion and Adhesives:Science and Technology, Chapman and Hall, London, 1987, pp 339.

108. A. J. Kinloch, Adhesion and Adhesives:Science and Technology, Chapman and Hall, London, 1987, pp 351.

109. J. Comyn "Kinetics and Mechanism of Environmental Attack" in Durability of Structural Adhesives, A. J. Kinloch, ed., Chapter 2, Applied Science Publishers, New York, 1983.

110. A. J. Kinloch, J. Mater. Sci., 17, 617 (1982).

111. R. A. Gledhill and A. J. Kinloch, J. Adhes., 6, 315 (1974).

112. A. J. Kinloch, Adhesion and Adhesives: Science and Technology, Chapman and Hall, London, 1987, p 366-377.

113. A. J. Kinloch, J. Adhes., 10, 193 (1979).

114. A. J. Kinloch, L. S. Welch, and H. E. Bishop, J. Adhes., 16, 165 (1984).

115. J. Cognard, J. Adhes., 26, 155 (1988).

116. R. A. Gledhill, A. J. Kinloch, and S. J. Shaw J. Adhes., 11, 3 (1980).

117. J. Comyn, "A Review of Certain Recent Work on the Durability of Aluminum Alloy Bonded with Epoxy and Phenolic Adhesives", Proceedings of the 35th Sagamore Army Material Research Conference, Manchester, New Hampshire, USA, June 1988.

118. A. J. Kinloch, Adhesion and Adhesives: Science and Technology, Chapman and Hall, London, 1987, pp 389.

119. D. M. Brewis, J. Comyn, R. J. A. Shalash, and J. L. Tegg, Polymer, 21, 357 (1980).

120. J. D. Keenan, J. C. Seferis, and J. T. Quinlivan, J. Appl. Polym. Sci, 24, 2375 (1979).

121. J. Mijovic and K. F. Lin, J. Appl. Polym. Sci., 30, 2527 (1985).

122. M. K. Antoon and J. L. Koenig, J. Polym. Sci: Polym. Phys. Ed., 19, 197 (1981).

123. D. M. Brewis, J. Comyn, A. K. Raval, and A. J. Kinloch, Int. J. Adhes. Adhes., 10, 247 (1990).

124. J. L. Cotter, "The Durability of Structural Adhesives" in Developments in Adhesives, W. C. Wake, ed., Chapter 1, Applied Science Publishers, London, 1977, pp 1.

125. K. Nakamura, T. Ueda, S. Hosono, and T. Maruno, Int. J. Adhes. Adhes., 7, 209 (1987).

126. A. J. Kinloch, Adhesion and Adhesives: Science and Technology, Chapman and Hall, London, 1987, pp 360.

127. J. D. Minford, in Treatise on Adhesion and Adhesives, Vol. 5, Chapter., R. L. Patrick ed., Marcel Dekker, New York. 1975, p. 45.

128. P. A. Fay and A. Maddison, Int. J. Adhes. Adhes., 10, 179 (1990).

129. I. G. Zewi, F. Flashner, H. Dodiuk, and L. Drori, Int. J. Adhes. Adhes., 4, 13 (1984).

130. A. J. Kinloch, Adhesion and Adhesives: Science and Technology, Chapman and Hall, London, 1987, pp 391-394.

131. K. W. Allen, S. M. Smith, W. C. Wake, and A. O. Raalte, Int. J. Adhes. Adhes., 5, 23 (1985).

132. D. M. Brewis, J. Comyn, and J. L. Tegg, Int. J. Adhes. Adhes., 1, 35 (1980).

133. T. Smith, J. Adhes., 17, 1 (1984).

134. A. J. Kinloch, Adhesion and Adhesives: Science and Technology, Chapman and Hall, London, 1987, pp 153.

135. A. J. Kinloch, Adhesion and Adhesives: Science and Technology, Chapman and Hall, London, 1987, pp 368-371.

136. K. W. Allen and M. G. Stevens, J. Adhes., 14, 137 (1982).

137. A. R. Krause, J. W. Holubka, and W. Chun, "The Effect of Adhesive Chemistry on the Fatigue Resistance of Adhesive Bonds in Service Environment", Proceedings of the 2th Conference for Advanced Composites, Dearborn, Michigan,1986, ASM International, 1986.

138. A. J. Kinloch, H. E. Bishop, and N. R. Smart, J. Adhes., 14, 105 (1982).

139. P. Poole and J. F. Watts, Int. J. Adhes. Adhes., 5, 33 (1985).

140. J. C. McMillan, "Durability Test Methods for Aerospace Bonding" in Developments in Adhesives-2, A. J. Kinloch ed., Chapter 7, Applied Science Publishers, London, 1981.

141. A. J. Kinloch, Adhesion and Adhesives: Science and Technology, Chapman and Hall, London, 1987, pp.354.

142 A. J. Kinloch, Adhesion and Adhesives: Science and Technology, Chapman and Hall, London, 1987, pp 340.

143. W. C. Jones III, E. McCabee, R. F. Wegman, and D. W. Levi, J. Appl.Polym. Sci., 18, 555 (1974).

144. J. I. Goldstein, D. E. Newbury, D. C. Joy, C. Fiori, and E. Lifshin, Scanning Electron Microscopy and X Ray Microanalysis: A Text for Biologists, Material Scientists, and Geologists, Plenum Press, New York, 1984, p.17.

145. J. I. Goldstein, "Electron Optics" in Practical Scanning Electron Microscopy, J. J. Goldstein, and H. Yakowitz, eds., Chapter 2, Plenum Press, New York, 1975.

146. J. I. Goldstein, D. E. Newbury, D. C. Joy, C. Fiori, and E. Lifshin, Scanning Electron Microscopy and X Ray Microanalysis: A Text for Biologists, Material Scientists, and Geologists, Plenum Press, New York, 1984, p. 57.

147. J. I. Goldstein, "Electron Beam-Specimen Interaction" in Practical Scanning Electron Microscopy, J. J.Goldstein and H. Yakowitz, eds., Chapter 3, Plenum Press, New York, 1975.

148. J. I. Goldstein, D. E. Newbury, D. C. Joy, C. Fiori, and E. Lifshin, Scanning Electron Microscopy and X Ray Microanalysis: A Text for Biologists, Material Scientists, and Geologists, Plenum Press, New York, 1984, pp. 461-463.

149 C. D. Wagner, W. M. Riggs, L. E. Davis, and J. F. Moulder, Handbook of X-ray Photoelectron Spectroscopy, G. E. Mullenberg, ed., Perkin-Elmer Corporation 1979, pp. 5.

150. M. P. Seah, "Quantification of AES and XPS" in Practical Surface Analysis by Auger and Photoelectron Spectroscopy, D. Briggs and M. P. Seah, eds., John Wiley and Sons, Chapter 5, Chichester, 1983.

151. G. Gillberg, J. Adhes., 21, 129 (1987).

152. T. A. Carlson, Photoelectron and Auger Spectroscopy, Plenum Press, New York, 1975, pp. 16.

153. D. Briggs, and J. C. Riviere, "Spectral Interpretation" in Practical Surface Analysis by Auger and Photoelectron Spectroscopy, D. Briggs and M. P. Seah, eds., Chapter 3, John Wiley and Sons, Chichester, 1983.

154. C. D. Wagner, "Auger and Photoelectron Energies and the Auger Parameter. A Data Set" in Practical Surface Analysis by Auger and Photoelectron Spectroscopy, Briggs and M. P. Seah, eds., Apendix 4, John Wiley and Sons, Chichester, 1983.

155. C. S. Fadley, R. J. Baird, W. Siekhaus, T. Novakov, and S. A. L. Bergstrom, J. Elect. Spect. Rel. Phenom., 4, 93 (1974).

156. C. Battistoni, G. Mattogno, and E. Paparazzo, Surf. Interface Anal., 7, 117 (1985).

157. J. Powell, and P. E. Larson, Appl. Surf. Sci., 1, 186 (1978).

158. P. M. A. Sherwood, "Data Analysis in Photoelectron Spectroscopy" in Practical Surface Analysis by Auger and Photoelectron Spectroscopy, D. Briggs and M. P. Seah, eds., Apendix 3, John Wiley and Sons, Chichester, 1983.

159. R. M. Silverstein, G. C. Bassler, and T. C. Morrill, "Spectroscopic Identification of Organic Compounds", John Wiley and Sons, New York, 1981, p 95.

160. N. B. Calthup, L. H. Daly, S. E. Wiberley, Introduction to Infrared and Raman Spectroscopy, Academic Press, New York, 1975, p. 11.

161. R. M. Silverstein, G. C. Bassler, and T. C. Morrill, "Spectroscopic Identification of Organic Compounds", John Wiley and Sons, New York, 1981, pp. 97.

162. N. B. Calthup, L. H. Daly, S. E. Wiberley, Introduction to Infrared and Raman Spectroscopy, Academic Press, New York 1975, p. 111.

163. R. T. Graf, J. L. Koenig, and H. Ishida, "Introduction to Optics and Infrared Spectroscopic Techniques" in Fourier Transform Infrared Characterization of Polymers, H. Ishida, ed., Chapter 1, Plenum Press, New York, 1987.

164. H. Ishida, Rubber Chem. Technol., 60, 497 (1987).

165. R. W. Duerst, P. Mahmoodi, and M. D. Duerst, "IR-PAS Studies: Signal to Noise Enhancement and Depth Profile Analysis" in Fourier Transform Infrared Characterization of Polymers, H. Ishida, ed., Chapter 3, Plenum Press, New York, 1987.

166. R. G. Greenler, J. Chem. Phys., 44, 310 (1966).

167. D. L. Allara, A. Baca, and C. A. Pryde, Macromolecules, 11, 1215 (1978).

168. R. G. Greenler, R. R. Rahn, and J. P. Schwartz, J. Catal., 23, 42 (1971).

169. D. Briggs, "Applications of XPS in Polymer Technology "in Practical Surface Analysis by Auger and Photoelectron Spectroscopy, D. Briggs and M. P. Seah, eds.,Chapter 9, John Wiley and Sons, Chichester, 1983.

170. C. Burtoff, Surface Analysis of Sheet Molded Composite (SMC) Material as Related to Adhesion, Virginia Polytechnic Institute and State University, M.S. Thesis, 1986.

171. D. T. Clark, "Investigation of Polymer Surfaces By Means of ESCA " in Polymer Surfaces, D. T. Clark and W.J. Feast, eds., John Wiley & Sons, Chichester, 1971.

172. H. Lee and K. Neville, Handbook of Epoxy Resins, McGraw Hill, New York, 1967, pp. 4-29.

173. R. C. Weast and M. J. Astle, Handbook of Data on Organic Compounds, Vol.II, CRC Press Inc, Boca Raton, FL, 1985, pp. 51.

174. J. N.Cooper, The Effect of Residual Thermal Stress on the Viscoelastic Behavior of Adhesively Bonded Joints , Virginia Polytechnic Institute and State University, M.S. Thesis, 1987.

175. A. C. Loos, G. S. Springer, B. A. Sanders, and R. W. Tung, "Moisture Absorptionof Polyester-E Glass Composites" in Environmental Effects on Composite Materials, G. S. Springer, ed., Chapter 5 Technomic Publishing Co., Inc., Westport, CT, 1981.

176. S. C. Lin, B. J. Bulkin, and E. M. Pearce, J. Polym. Sci.: Polym Chem Ed., 17,312 (1979).

177. H. Lee and K. Neville, Handbook of Epoxy Resins, McGraw Hill, New York, 1967, pp. 5-8.

178. H. Lee and K. Neville, Handbook of Epoxy Resins, McGraw Hill, New York, 1967, pp. 5-32.

179. J. C. Evans, Spectrochim. Acta, 16, 1382 (1960).

180. H. D. Bust, J. C. D. Brand, and D. R. Williams , J. Molec. Spectrosc., 24, 402 (1967).

181. J. H. S. Green, D. J. Harrison, and W. Kynaston, Spectrochim. Acta, 27A, 2199 (1971).

182 J. A. Filbey and J. P. WIghtman, J. Adhes., 28, 23 (1989).

183. C. V. Stephenson, W. C. Coburn, Jr., and W. S. Wilcox, Spectrochim. Acta, 17, 933 (1961).

184. W. H. T. Davison, J. Chem. Soc., 3712 (1953).

185. R. P. Hirschman, R. N. Kniseley, and V. A. Fassel, Spectrochim. Acta, 21, 2125 (1965).

186. G. L. Carlson, Spectrochim. Acta, 20, 1781 (1964).

187. H. Hoyer, Chem. Ber., 89, 2677 (1956).

188. B. P. Self, "Finite Element Analysis of Steel/Epoxy/SMC Bonds", ASC Summer Undergraduate Research Report, Virginia Polytechnic Institute, Center for Adhesive and Sealant Science, 1990.

189. H. V. Boenig, Unsaturated Polyesters: Structure and Properties, Elsevier Applied Science Publishers, Amsterdam, 1964 pp. 99.

190. J. Comyn, "Diffusion and Adhesion"" in Polymer Permeability, J. Comyn, ed., Chapter 5, Elsevier Applied Science Publishers, 1985.

191. N. G. McGrum, C. P. Buckley, and C. B. Bucknall, Priciples of Polymer Engineering, Oxford University Press, New York, 1988, pp. 141-144, 345-347.

192. D. M. Brewis, J. Comyn, A. K. Raval, and A. J. Kinloch, Int. J. Adhes. Adhes., 10, 247 (1990).

193. G. Marom, "The Role of Water Transport In Composite Materials" in Polymer Permeability, J. Comyn, ed., Chapter 9, Elsevier Applied Science Publishers, 1985.

194. J. D. Ferry, Viscoelastic Properties of Polymers, John Wiley & Sons, New York, 1980, pp 264.

195. N. G. McGrum, C. P. Buckley, and C. B. Bucknal, Priciples of Polymer Engineering, Oxford University Press, New York, 1988, pp. 359.

196. J. M. G. Cowie, Polymers: Chemistry and Physics of Modern Materials, Intex Educational Publishers, New York, 1974, pp. 232.

197. N. G. McGrum, C. P. Buckley, and C. B. Bucknal, Priciples of Polymer Engineering, Oxford University Press, New York, 1988, pp. 174.

198. W. C. Wake, Adhesion and Formulation of Adhesives, Applied Science Publishers, London, 1982, pp. 240.

199. L. J. Hart-Smith, "Stress Analysis: A Continuum Mechanics Approach" in Developments in Adhesives-2, A. J. Kinloch , ed.,Chapter 1, Applied Science Publishers, London, 1981.

200. E. Cutts, "Laboratory Testing of Rubber to Metal Bonds" in Developments in Adhesives-2, A. J. Kinloch , ed., Chapter 10, Applied Science Publishers, London, 1981.

201. R. S. Farinato, "Adhesion and Surface Chemistry of Sheet Molding Compound" in Proceedings of the 14th Annual Meeting of the Adhesion Society, Clearwater, Fla. Feb. 1991, H. M. Clearfield, ed., The Adhesion Society, 1991.

202. T. Osiroff, Analysis of a Bonded Joint Using Bulk Adhesive Properties, Virginia Polytechnic Institute and State University, M.S. Thesis, 1988.

203. P. Albericci, "Aerospace Applications" in Durability of Structural Adhesives, A. J.Kinloch, ed., Chapter 8, Applied Science Publishers, New York , 1983.

204. A. J. Kinloch, Adhesion and Adhesives:Science and Technology, Chapman and Hall, London, 1987, pp. 141.

205. M. Gettings and A. J. Kinloch, J. Mater. Sci. , 12, 2049 (1977).

Vita

The author, Spinu Ionel, was born in Braila , Romania. Upon completition of high school he attended Jassy Polytechnic Institute and received a M. S. degree in Chemical Engineering in 1972. Between 1972 and 1978 he worked for Research Institute for Rubber and Plastics and from 1978 to 1982 for Institute for Engineering and Design for Chemical Industry, both located in Bucharest, Romania. In 1982 he came to United States and worked between 1983 and 1986 for Hysol Corporation in Pittsburg, California. In 1987 he entered the MESC program at VPI &SU to pursue a Ph. D. degree under the direction of Dr. J. G. Dillard. During his stay at Virginia Tech he received fellowships for the years 1989 and 1990 from the Center for Adhesive and Sealant Science. The author received the Ph. D. degree in the fall of 1991. He is married to Maria Spinu and has a daughter, Oana.